

IFIP AICT 530

Svetan Ratchev (Ed.)



Precision Assembly in the Digital Age

8th IFIP WG 5.5

International Precision Assembly Seminar, IPAS 2018

Chamonix, France, January 14–16, 2018

Revised Selected Papers

 Springer

Editor-in-Chief

Kai Rannenber, Goethe University Frankfurt, Germany

Editorial Board

TC 1 – Foundations of Computer Science

Jacques Sakarovitch, Télécom ParisTech, France

TC 2 – Software: Theory and Practice

Michael Goedicke, University of Duisburg-Essen, Germany

TC 3 – Education

Arthur Tatnall, Victoria University, Melbourne, Australia

TC 5 – Information Technology Applications

Erich J. Neuhold, University of Vienna, Austria

TC 6 – Communication Systems

Aiko Pras, University of Twente, Enschede, The Netherlands

TC 7 – System Modeling and Optimization

Fredi Tröltzsch, TU Berlin, Germany

TC 8 – Information Systems

Jan Pries-Heje, Roskilde University, Denmark

TC 9 – ICT and Society

David Kreps, University of Salford, Greater Manchester, UK

TC 10 – Computer Systems Technology

Ricardo Reis, Federal University of Rio Grande do Sul, Porto Alegre, Brazil

TC 11 – Security and Privacy Protection in Information Processing Systems

Steven Furnell, Plymouth University, UK

TC 12 – Artificial Intelligence

Ulrich Furbach, University of Koblenz-Landau, Germany

TC 13 – Human-Computer Interaction

Marco Winckler, University Paul Sabatier, Toulouse, France

TC 14 – Entertainment Computing

Matthias Rauterberg, Eindhoven University of Technology, The Netherlands

IFIP – The International Federation for Information Processing

IFIP was founded in 1960 under the auspices of UNESCO, following the first World Computer Congress held in Paris the previous year. A federation for societies working in information processing, IFIP's aim is two-fold: to support information processing in the countries of its members and to encourage technology transfer to developing nations. As its mission statement clearly states:

IFIP is the global non-profit federation of societies of ICT professionals that aims at achieving a worldwide professional and socially responsible development and application of information and communication technologies.

IFIP is a non-profit-making organization, run almost solely by 2500 volunteers. It operates through a number of technical committees and working groups, which organize events and publications. IFIP's events range from large international open conferences to working conferences and local seminars.

The flagship event is the IFIP World Computer Congress, at which both invited and contributed papers are presented. Contributed papers are rigorously refereed and the rejection rate is high.

As with the Congress, participation in the open conferences is open to all and papers may be invited or submitted. Again, submitted papers are stringently refereed.

The working conferences are structured differently. They are usually run by a working group and attendance is generally smaller and occasionally by invitation only. Their purpose is to create an atmosphere conducive to innovation and development. Refereeing is also rigorous and papers are subjected to extensive group discussion.

Publications arising from IFIP events vary. The papers presented at the IFIP World Computer Congress and at open conferences are published as conference proceedings, while the results of the working conferences are often published as collections of selected and edited papers.

IFIP distinguishes three types of institutional membership: Country Representative Members, Members at Large, and Associate Members. The type of organization that can apply for membership is a wide variety and includes national or international societies of individual computer scientists/ICT professionals, associations or federations of such societies, government institutions/government related organizations, national or international research institutes or consortia, universities, academies of sciences, companies, national or international associations or federations of companies.

More information about this series at <http://www.springer.com/series/6102>

Svetan Ratchev (Ed.)

Precision Assembly in the Digital Age

8th IFIP WG 5.5

International Precision Assembly Seminar, IPAS 2018

Chamonix, France, January 14–16, 2018

Revised Selected Papers

Editor

Svetan Ratchev 

University of Nottingham

Nottingham, UK

ISSN 1868-4238

ISSN 1868-422X (electronic)

IFIP Advances in Information and Communication Technology

ISBN 978-3-030-05930-9

ISBN 978-3-030-05931-6 (eBook)

<https://doi.org/10.1007/978-3-030-05931-6>

Library of Congress Control Number: 2018964127

© IFIP International Federation for Information Processing 2019

This work is subject to copyright. All rights are reserved by the Publisher, whether the whole or part of the material is concerned, specifically the rights of translation, reprinting, reuse of illustrations, recitation, broadcasting, reproduction on microfilms or in any other physical way, and transmission or information storage and retrieval, electronic adaptation, computer software, or by similar or dissimilar methodology now known or hereafter developed.

The use of general descriptive names, registered names, trademarks, service marks, etc. in this publication does not imply, even in the absence of a specific statement, that such names are exempt from the relevant protective laws and regulations and therefore free for general use.

The publisher, the authors, and the editors are safe to assume that the advice and information in this book are believed to be true and accurate at the date of publication. Neither the publisher nor the authors or the editors give a warranty, express or implied, with respect to the material contained herein or for any errors or omissions that may have been made. The publisher remains neutral with regard to jurisdictional claims in published maps and institutional affiliations.

This Springer imprint is published by the registered company Springer Nature Switzerland AG

The registered company address is: Gewerbestrasse 11, 6330 Cham, Switzerland

Preface

Assembly, as one of the traditionally most difficult processes to automate, is being transformed by the advances in informatics technologies. Technological developments such as big data analytics, intelligent and autonomous machines and systems, smart devices, and the Industrial Internet of Things (IIoT) have been identified as key for how future assembly systems are designed and deployed.

This book includes a selected set of papers presented at the 8th International Precision Assembly Seminar (IPAS 2018) held in Chamonix, France, in January 2018. The International Precision Assembly Seminar, which was first held in 2003, was conceived by the European Thematic Network Assembly-Net with the objective of providing a forum for the precision assembly community to share the latest research results, discuss new ideas in a wide range of assembly theory and practice, and demonstrate new industrial applications. Now in its eighth edition, the seminar has become a traditional biennial international event bringing together researchers in precision assembly.

With every seminar the research program has evolved to better reflect new scientific and industrial challenges. Originally started with a specific focus on micro-assembly processes and systems, the scope of the seminar now includes precision assembly topics in a wide range of product types, sizes, and volumes of manufacture. The specific focus of the 8th IPAS 2018 seminar has been greatly influenced by the recent developments in digital technologies for manufacturing and the Industry 4.0 research agenda. The contributions therefore address a number of related research topics including: machine vision and metrology for assembly operations, gripping and handling technologies, numerical methods and planning in assembly, digital technologies and Industry 4.0 applications, precision assembly methods, assembly systems and platforms, human cooperation and machine learning.

The book is structured into five chapters. Chapter 1 addresses different aspects of design and deployment of assembly systems with specific emphasis on architectures, concepts, resource planning, and scheduling. Chapter 2 critically examines some of the latest developments in human–robot interactions including novel solutions for automated disassembly, gesture-based programming, zone planning and machine vision-based robot control. Some novel assembly process methods and models for trade-off analysis in design for joining, fabrication, and assembly of piezo-ceramic fiber array transducers and cloud-based data analytics framework for assembly are presented in Chapter 3. Chapter 4 considers the impact of Industry 4.0 technologies in terms of informatics-rich metrology, low-cost IIoT-enabled smart tools, informatics-enabled assembly platforms, and impact of digital technologies for SMEs. Specific research aspects of part handling and gripping are discussed in Chapter 5, including micro-grippers design and control and methods for rigid body registration.

The seminar is sponsored by the International Federation of Information Processing (IFIP) WG 5.5 and the International Institution of Production Engineering Research (CIRP).

The organizers should like to express their gratitude to the members of the International Advisory Committee for their support and guidance and to the authors of the papers for their original contributions and enthusiastic and active participation in the seminar. My special thanks go to Professor Luis Camarinha-Matos, chair of the IFIP WG 5.5, and Professor J. W. Sutherland, chair of the STC-A of CIRP for their continuous support and encouragement. My special thanks also go to Ruth Strickland, Nancy Martin, Florence Drouvin, and Sarah Hannon-Bland from the Institute for Advanced Manufacturing of the University of Nottingham and Evelyne Roudier-Poirot from the Tourist Office of Chamonix for handling the administrative aspects of the seminar, putting the proceedings together, and managing the detailed liaison with the publishers.

November 2018

Svetan Ratchev

Organization

International Advisory Committee

M. Aurisicchio	Imperial College London, UK
D. Axinte	University of Nottingham, UK
J. Barata	UNINOVA, Portugal
M. Björkman	Linköping Institute of Technology, Sweden
D. Branson	University of Nottingham, UK
A. Delchambre	ULB, Belgium
M. Desmulliez	Heriot-Watt University, UK
M. Dickerhof	Karlsruhe Institute for Technology, Germany
S. Dimov	University of Birmingham, UK
G. Dini	University of Pisa, Italy
A. Drouot	University of Franche-Comté, France
K. Ehmann	Northwestern University, USA
I. Fassi	ITIA-CNR, Italy
P. Felli	Free University of Bozen-Bolzano, Italy
J. Jacot	EPFL, Switzerland
M. Krieger	CSEM, Switzerland
P. Lambert	ULB, Belgium
M. Lanz	Technical University of Tampere, Finland
R. Leach	University of Nottingham, UK
N. Lohse	Loughborough University, UK
P. Lutz	ENSMM, France
H. Maekawa	AIST, Japan
B. Nelson	ETH, Switzerland
M. Onori	KTH, Sweden
D. Pham	University of Birmingham, UK
M. Pillet	University of Savoie Mont Blanc, France
G. Putnik	University of Minho, Portugal
A. Raatz	Leibniz University of Hannover, Germany
K. Ridgway	University of Sheffield, UK
J. Segal	University of Nottingham, UK
W. Shen	National Research Council, Canada
M. Tichem	TU Delft, The Netherlands
T. Tolio	Milan Polytechnic, Italy

Contents

Design and Deployment of Assembly Systems

An All-in-One Robotic Platform for Hybrid Manufacturing of Large Volume Parts.	3
<i>Francesco Crivelli, Valentin Baumann, Markus Steiner, Mark D’Urso, Philipp Schmid, and Alexander Steinecker</i>	
Deployment of a Distributed Multi-Agent Architecture for Transformable Assembly.	15
<i>Jack C. Chaplin and Svetan Ratchev</i>	
Creating Resource Combinations Based on Formally Described Hardware Interfaces.	29
<i>Niko Siltala, Eeva Järvenpää, and Minna Lanz</i>	
Functional Modelling in Evolvable Assembly Systems.	40
<i>David Sanderson, Jack C. Chaplin, and Svetan Ratchev</i>	
Production and Maintenance Scheduling Supported by Genetic Algorithms.	49
<i>Duarte Alemão, Mafalda Parreira-Rocha, and José Barata</i>	
Human Robot Cooperation and Machine Vision	
A Learning Method for Automated Disassembly.	63
<i>Julius Wolff, Torge Kolditz, and Annika Raatz</i>	
Gesture-Based Robot Programming Using Microsoft Kinect.	72
<i>Sebastian Blankemeyer, Joshua Göke, Tobias Grimm, Benedikt Meier, and Annika Raatz</i>	
The Comfort Zone Concept in a Human-Robot Cooperative Task.	82
<i>Alireza Changizi and Minna Lanz</i>	
A Low-Cost Automated Fastener Painting Method Based on Machine Vision.	92
<i>Ran Zhao, Adrien Drouot, Joseph Griffin, Richard Crossley, and Svetan Ratchev</i>	

Assembly Methods and Models

A Probabilistic Approach for Trade-off Analysis of Composite Wing Structures at the Conceptual Phase of Design 103
Konstantinos Bacharoudis, Thomas Turner, Atanas Popov, and Svetan Ratchev

Precision Assembly of Optical Backplanes 114
Serena Ruggeri, Gianmauro Fontana, and Irene Fassi

Prefabrication and Automated Micro Assembly of Piezoceramic Fiber Array Transducers in Microstructured Surfaces of Sheet Metals 124
Marek Schmidt and Volker Wittsock

Towards a Cloud-Based Analytics Framework for Assembly Systems 134
German Terrazas, Lavindra de Silva, and Svetan Ratchev

Digital Technologies and Industry 4.0 Applications

Information-Rich Manufacturing Metrology 145
Richard Leach, Patrick Bointon, Xiaobing Feng, Simon Lawes, Samanta Piano, Nicola Senin, Danny Sims-Waterhouse, Petros Stavroulakis, Rong Su, Wahyudin Syam, and Matthew Thomas

Aerospace Assembly Gap Measurement Using Low Cost Smart Tools with Machine Vision 158
Richard Crossley and Svetan Ratchev

Towards Industry 4.0: The Future Automated Aircraft Assembly Demonstrator 169
Adrien Drouot, Ran Zhao, Lucas Irving, and Svetan Ratchev

Does Industry 4.0 Pose a Challenge for the SME Machine Builder? A Case Study and Reflection of Readiness for a UK SME 183
Mark Jones, Leszek Zarzycki, and Gavin Murray

Gripping and Handling Solutions in Assembly

Sliding Mode Impedance Controlled Smart Fingered Microgripper for Automated Grasp and Release Tasks at the Microscale 201
Bilal Komati, Cédric Clévy, and Philippe Lutz

Fluid Dynamics Aided Design of an Innovative Micro-Gripper 214
Gianmauro Fontana, Serena Ruggeri, Antonio Ghidoni, Alessandro Morelli, Giovanni Legnani, Adriano Maria Lezzi, and Irene Fassi

Improving Rigid-Body Registration Based on Points Affected
by Bias and Noise. 226
Marek Franaszek and Geraldine S. Cheok

Author Index 235

Design and Deployment of Assembly Systems



An All-in-One Robotic Platform for Hybrid Manufacturing of Large Volume Parts

Francesco Crivelli¹(✉), Valentin Baumann², Markus Steiner², Mark D'Urso², Philipp Schmid¹, and Alexander Steinecker¹

¹ CSEM SA, Untere Gründlistrasse 1, 6055 Alpnach Dorf, Switzerland
francesco.crivelli@csem.ch

² Hexagon Manufacturing Intelligence,
Mönchmattweg 5, 5035 Unterentfelden, Switzerland

Abstract. 3D printing offers many advantages over conventional machining and its applications in industrial manufacturing is growing. However, existing additive technologies present limitations in workspace volume, accuracy and surface quality. These limitations could be overcome by combining both additive and subtractive processes. Such hybrid approaches allow layer-by-layer construction, alternating fast and rough material deposition with machining steps, when the layer's geometry is finished. Despite its potential, the development and industrial application of hybrid machines is slow. Particularly, no systems exist for the construction of large parts. The project KRAKEN is well-situated in this context, aiming at the development of a novel, fully automated, all-in-one platform for large volume hybrid manufacturing. This powerful tool will not only combine additive with subtractive processes, but it will also include both metal and non-metal 3D printing, resulting in a completely new machine for the construction of large, multi-material parts. A control approach based on direct measurement of the end-effector position will allow a combination of large workspace (up to 20 m) and high manufacturing accuracy (tolerances < 0.3 mm, surface roughness $R_a < 0.1$ μm). This paper presents the preliminary steps toward the development of this robotic platform, focusing on the use of the real-time feedback of an absolute laser tracker to control motion and positioning of the manufacturing robot. The proposed control strategy is presented and discussed. Finally, the use of an Extended Kalman Filter to fuse the laser measurement with the robot position sensors is presented and discussed based on offline evaluation.

Keywords: Hybrid manufacturing · Large parts · Multi-material
All-in-one machine · Robotic manufacturing · Extended Kalman Filter

1 Introduction

Additive Manufacturing (AM) processes consists of constructing objects directly from their 3D model by joining material layer by layer. These approaches present interesting advantages such as rapid prototyping and design freedom, and allow very complex and enclosed structures which are otherwise highly difficult or impossible to build with traditional machining [1]. Currently, these technologies find many applications ranging

from industrial production to individual consumer. Since 2003, part production based on AM has increased from 3.9% to 34.7% of all product and service revenues [2].

Today, at the industrial level AM machines exist which are able to produce parts up to 1 m³ in polymer material (BIGREP One, Fortus 900mc, Object1000 Plus), and even bigger volumes are reachable using sand casting (ExOne Exerial, Voxeljet VX4000), clay (WASP BigDelta) or metal (Xline2000, EOS M400, SML500HL, RPM Innovation, Norks Titanium RPDTM, SCIAKY). However, as larger parts are required, current technology shows its limitations. Most available AM machines have a limited construction volume due to process requirements (e.g. powder bed), inert gas or vacuum (e.g. laser or electron beam), or safety requirements (e.g. laser containment). In the future metal-based AM is expected to exceed polymeric-based processes in market size and growth [3]. Today, several metal-based AM technologies exist, however there is a lack regarding large volume production. In addition to production volume, present AM are limited in obtainable accuracy, surface quality, and uniformity of material properties. Today, the high quality and resolution required for applications in tight-tolerance and critical conditions can be reached only with considerable increase of cost-to-build-rate ratio, or it cannot be reached at all. This is the reason why most additive manufactured parts (both metal and thermosets) require post-processing to improve quality characteristics and/or relieve residual stresses.

Both volume and accuracy limitations can be overcome by combining AM with conventional machining processes (e.g. CNC) in workstations for hybrid additive and subtractive processing (WHASP) [4]. The capability of these hybrid systems to both add and subtract material in a concurrent and optimized manner allows construction of high quality parts within a single machine as well as addressing geometrical challenges (e.g. internal and overhanging features), reducing material wastage and tooling consumption.

Hybrid machines have been a fertile research field since the mid-late 1990s [5, 6], however the commercialisation of this approaches has been slow. Particularly, no real solutions exist for constructions of large volume parts yet. Today, the development of commercial hybrid manufacturing is accelerating. In the future, reconfiguration and responsiveness are suggested to play a fundamental role in the manufacturing economy, which will move away from production lines toward single all-in-one machines able to transform raw materials into finished products. This is well aligned with the WHASP approach.

The European project KRAKEN is well-situated in this context, aiming to develop an all-in-one hybrid-manufacturing machine for customized design, production, repair, and quality control of medium and large parts [7]. In addition to different manufacturing processes, this robotic platform will allow combination of metal and non-metal structures, representing a considerable improvement with respect to the current large size products manufacturing. The project proposes a further development of the MEGAROB system, a platform for high accuracy machining of large parts (up to 20 × 6 × 3 m) developed using an industrial robot mounted on a crane [8]. Analogously to this previous project, the novelty of the proposed approach is controlling robot positioning and motion based on the direct measurement of the robot end-effector pose (i.e. position and orientation) provided in real-time by an absolute laser tracker. Including real-time measurement of the absolute end-effector pose in the motion

control loop allows compensation of the intrinsically limited absolute accuracy of both the crane and the robot. Using an absolute laser tracker has been shown to be effective in improving absolute accuracy of industrial manipulators in presence of low stiffness and unmodeled process forces [9–11]. The chosen approach will enable fulfilling both requirements of large manufacturing and tight-tolerance applications, with an affordable machine based on standard industrial components. With respect to existing machines which are constrained by limited workspace, accuracy performance, and costs that are directly dependent on mechanical components (e.g. actuated axes), this project proposes a flexible solution that can be easily adapted to desired workspace size and logistical configurations, with minor impact on functions and costs.

2 The Setup

2.1 Manufacturing Approach

The proposed machine will allow production and reparation of middle and large parts with dimensional tolerances below 0.3 mm and surface roughness below Ra 0.1 μm . The manufacturing concept is based on a layer-by-layer additive/subtractive alternating task [5, 6]. Step after step, the material deposited during the additive process is machined in order to correct geometrical characteristics. This allows high manufacturing accuracy, also for large parts up to 20 m, as well as releasing the stress in the 3D printed structures. Furthermore, this approach enables construction of complex geometries and enclosed structure that are not feasible with existing conventional methods.

The layer by layer approach will include a geometry inspection step, where the actual execution of the manufacturing task and the accuracy of the constructed part are monitored in an automated manner using a high-resolution metrology device (T-SCAN, Sect. 2.3) mounted on the robot end-effector. This allows direct identification and immediate reparation of eventual errors and deviations from the desired accuracy. Such in-process intervention prevents a full part to be rejected and, consequently, dramatically reduces wasted time and material. A concluding grinding and polishing step allows production of final parts with high quality surfaces (roughness < Ra 0.1 μm).

The robot control system is based on an absolute laser tracker providing measurement of the robot end-effector's absolute pose (Cartesian position and orientation) in real-time. The direct measurement of the end-effector pose is used in the control-loop in order to compensate positioning and motion errors and achieve the desired high geometrical accuracy. Furthermore, the laser tracker will be used to automatize robot calibration processes as well as the identification of geometrical characteristics and localization of cell components and manufacturing workspace.

2.2 Robotic Platform

The machine is based on the same robotic structure developed in [5], which consists in an industrial 6 degrees-of-freedom (DoF) anthropomorphic manipulator (NJ130, Comau S. p. A., TO, I) mounted upside down on a three-axes overhead crane (Fig. 1).



Fig. 1. Prototype system with CSEM control and Leica tracking system (installation at AITIIP, Zaragoza, Spain).

The crane structure measures $24 \times 6 \times 5$ m and allows a workspace of approximately 22 m length, 4 m width, and 2 m height. The two horizontal axes are driven by motors and brakes directly acting on the moving wheels of the crane. The vertical axis moves the robot up and down using an actuated rack and pinion system, guided through two sliders, and supported by four electrically controlled pneumatic cylinders. The crane motion is controlled in open-loop and no external position sensors are used.

The robot supports payload up to 130 kg, has a maximum horizontal reach of 2.980 m allowing flexible and effective handling of the different tools required for hybrid manufacturing process. With a repeatability of 0.07 mm, the robot guarantees the high positioning accuracy required for tight-tolerances applications and high-quality manufacturing.

2.3 Absolute Laser Tracker

The Leica Absolute Tracker AT960 is a robust, all-in-one laser tracker offering high-speed dynamic measurement as standard. It is a complete solution for 6 DoF probing, scanning and automated inspection as well as reflector measurement (Fig. 2).

The AT960 features wireless communication and a battery operation option. The Absolute Interferometer (AIFM) enables accurate high-speed measurement (Table 1) to a moving target while the PowerLock function ensures an interrupted beam is instantly re-established without user intervention, reducing operator workload and training requirements. Intuitive touch-screen controls minimize the potential for user error,

saving time, effort and money. Check and compensation architecture means basic adjustments can be made in the field, while robust design guarantees on-specification operations with minimal calibration and servicing.

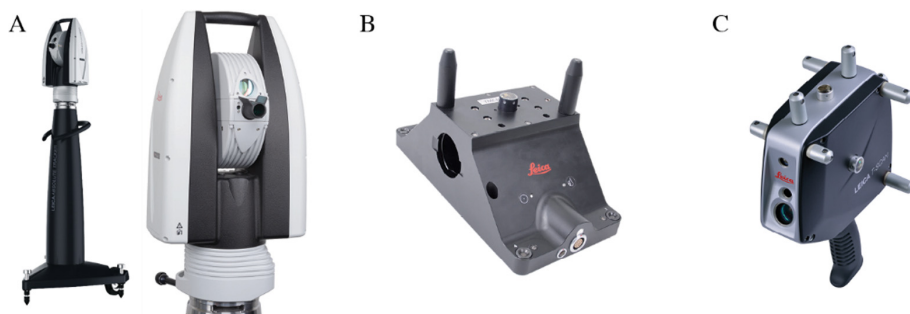


Fig. 2. (A) Leica Absolute Laser Tracker AT960. (B) T-MAC. (C) T-SCAN.

Table 1. Accuracy of the Leica Absolute Laser Tracker AT960 and related accessories.

Accuracy values	
Reflector*	$U_{(x,y,z)} = \pm 15 \mu\text{m} + 6 \mu\text{m/m}$
AIFM Absolute Distance Performance	$\pm 0.5 \mu\text{m/m}$
Absolute Angular Performance	$\pm 15 \mu\text{m} + 6 \mu\text{m/m}$
Dynamic Lock-on	$\pm 10 \mu\text{m}$
Orient to Gravity (OTG)	$U_{z(\text{OTG})} = \pm 15 \mu\text{m} + 8 \mu\text{m/m}$
Leica T-Scan 5	$U_L = \pm 60 \mu\text{m}/210\,000 \text{ points/s}$
Leica T-Mac**	$15 \mu\text{m} + 6 \mu\text{m/m}$
Typical Rotation Accuracy	$\pm 0.01^\circ$
Accuracy of Timestamp	$< 5 \mu\text{s}$

*All accuracies specified as Maximum Permissible Errors (MPE) and calculated per ASME B89.4.19-2006 and ISO10360-10:2016 using precision Leica 1.5" Red Ring Reflectors at up to 60 m distance unless otherwise noted.

**All accuracies specified as Maximum Permissible Errors (MPE). Typical results are half of MPE.

Real-Time Interface. When combined with the Real-Time Feature Pack, the Leica Absolute Tracker AT960 evolves into a laser tracker solution that meets the deterministic measurement data-delivery requirements of high-end automated installations. Built on the industry-proven EtherCAT protocol, it enables the delivery of 6 DoF measurement data with accurate timestamps at an output rate of up to 1000 Hz. Known as 7 DoF measurement data, this enables real-time machine control even with highly-dynamic robotic setups.

The fully automated measuring system makes measurement processes more time- and cost-efficient than ever before. The process accuracy is no longer limited by the

positioning device. The unparalleled accuracies of the 6 DoF Leica Absolute Tracker AT960 can be applied to any robotic positioning system, turning it from an ordinary robot into an incredibly accurate metrology device. With a Leica T-Scan or a Leica T-Mac equipped with a tactile or optical probe mounted on a robot, the Leica Absolute Tracker AT960 is the core of a completely automatic coordinate measuring installation.

T-MAC. The Leica T-Mac (Tracker-Machine control sensor) is the next-generation 6DoF tracking device for automated applications. It answers the needs of a growing number of tracker customers who have either modified the existing Leica T-Probe for automated measurement applications or have expressed interest in doing so.

The Leica T-Mac is an off-the-shelf solution that can be custom-tailored to the needs of a specific application. For example, when needed, an interface for precise tool exchange units can be included.

T-SCAN 5. The combination of Leica T-Scan 5 and Leica Absolute Tracker offers the perfect match to ensure the capture of hundreds of millions of accurate points on virtually any surface, from highly reflective to matte black, even carbon fiber, all without any special preparation. The higher scan rates allow ideal feature recognition, smaller detail detection and much quicker scanning at an approved quality level on all surfaces and colours. The user's scanning experience is enhanced with a dual color guide light and acoustic feedback. The Leica T-Scan 5 is also best qualified for automation and robotic applications, where inspection processes can benefit from maximum laser tracking and machine performance.

2.4 System Architecture

The main software runs on a regular windows-based desktop PC and allows the user to interact with the system. This high-level software allows bidirectional communication with each system component over TPC/IP communication protocol.

The manufacturing process is divided in steps. The crane moves the robot to the working position and the robot performs the manufacturing task for the specified working position. After the task is concluded, the robot is moved to the following working position, and the same procedure is repeated until the whole part is constructed.

During each task, the crane is maintained in a stationary position and the robot is guided along the desired trajectory. The robot motion is controlled through a Comau C4G Open system. The "open" feature offered by this interface allows partial or complete modification of the standard control approach by integrating an external controller (Fig. 3). Such additional external controller has been implemented on a regular desktop PC running Linux patched with RTAI extension, which guarantees real-time execution of the control algorithms. The external controller PC is interfaced with the C4G Open unit over RTNet at a frequency of 1 kHz.

The external controller completes the control action of the standard controller in order to compensate the deviation of the robot end-effector from reference position and orientation, given in an absolute coordinate frame (Sect. 2.5). The 6D pose of the robot end-effector is measured and provided in real-time by the absolute laser tracker (Sect. 2.3) at a frequency of 1 kHz over EtherCAT.

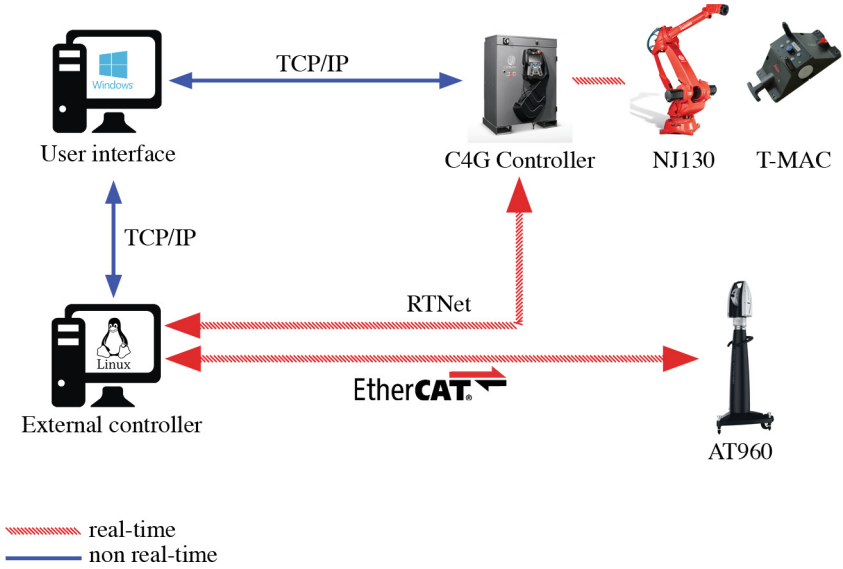


Fig. 3. System architecture.

2.5 Control Approach

The robot controller is divided in two parts: the standard Comau controller and the external controller. The Comau controller is used to move the motor on the desired trajectory given in the robot coordinate frame. The controller includes customisable velocity and acceleration profiles, payload and weight compensation, kinematic and dynamic models of the robot, as well as low level closed-loop control of the robot motors. Robot kinematic is calculated based on the Denavit-Hartenberg convention [12].

The external controller is used to compensate: the deviation of the end-effector absolute pose from the desired trajectory as well as the deviation of the robot base from its ideal pose.

The position and orientation of the robot base with respect to the global coordinate frame (A_L^R) are obtained prior to the manufacturing task through least-squares estimation [13]. However, during operation the backlash and elasticity of the crane could cause a displacement of the robot base with respect to the ideal value. The external controller estimates the actual position of the robot base and the related coordinate transformation matrix (A_R^R), based on the measured position of the robot joints, the measured Cartesian position of the end-effector, and the robot's kinematics model. The corrected pose of the robot base is then used to recalculate the reference trajectory in the actual robot coordinate frame and improve the absolute accuracy of the system.

The difference between reference and measured end-effector pose in global coordinate is transformed into the actual robot coordinate frame, transformed to the joint space through inverse kinematics and fed to a linear PID controller. The resulting value is added to the control input calculated by the Comau controller and sent to the motor controllers.

Observing the control loop of the end-effector absolute position, the Comau controller can be described as the model-based feedforward term (open-loop) and the external controller as the feedback controller term (closed-loop) (Fig. 4).

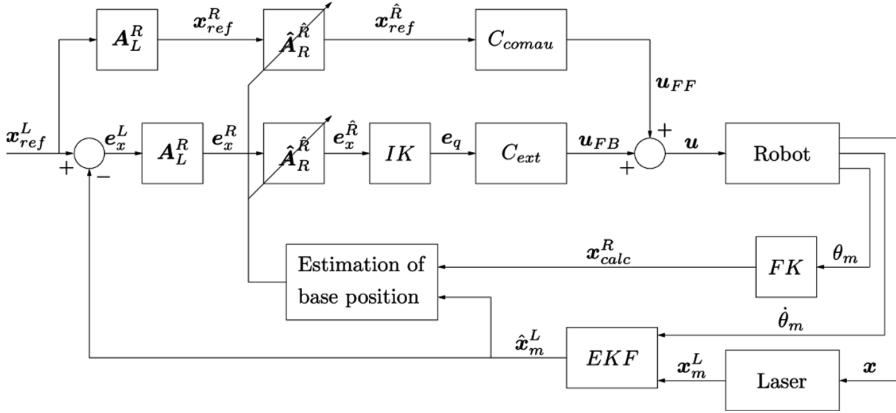


Fig. 4. Flow chart of the proposed control strategy. A_1^2 = homogeneous transformation matrix from 1 to 2; FK = forward kinematics; IK = inverse kinematics; C = controller. *Indexes:* ref = reference; m = measured; $calc$ = calculated. *Coordinate frames:* L = laser (global); R = robot; \hat{R} = robot with base displacement correction; x , \hat{x} = Cartesian space; q , θ = joint space.

An Extended Kalman Filter (EKF) [14, 15] has been implemented to improve the estimation of the Cartesian position of the robot end-effector based on the laser measurement, the speed of the robot joints, and the physical model of the system (Sect. 3.2).

3 Preliminary Results and Discussion

3.1 Control Approach

A first version of the external controller was implemented and evaluated on a reduced setup of the KRAKEN system [16]. The reduced setup includes a 6 DoF industrial manipulator (NS12-1.85, Comau S. p. A., TO, I), which is a slightly smaller version of the robot used in the original system. The robot is mounted on a linear rail, which allows testing the performance of the motion controller in presence of robot base displacement (both desired and undesired). As for the original system, the 6D pose of the robot end-effector is measured with an absolute laser tracker and the same system architecture presented in (Sect. 2.3) is used. The accuracy of the robot, calculated as the absolute position error with respect to the reference trajectory, was evaluated in both free space motion and during milling (8.5 mm depth, medium-density fiberboard wood). The tests showed that even in presence of artificial disturbance of the robot base

position (3 mm/s in random direction) the external controller allowed to keep the absolute error below 0.3 mm in free space motion and below 0.6 mm during milling [16]. The results show the feasibility of the control approach and the effectiveness of the external controller in improving the positioning and motion performance of the industrial robot (Fig. 5).

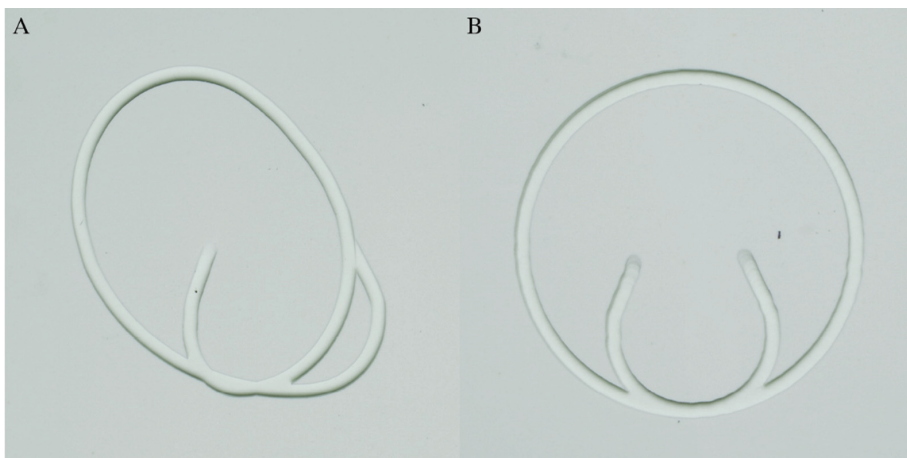


Fig. 5. Milling a circle with large disturbance in the robot base position. (A) without external controller. (B) with external controller.

However, the implemented strategy was effective only for very slow movements (15 mm/s). Differently from the controller implemented in [16], the strategy described in this paper (Sect. 2.5) will allow the external controller to directly act on the control input and not only on the reference point fed to the Comau controller. Additionally, the low-pass filters used in [16] to smooth the laser measurements have been replaced with a model based Extended Kalman Filter (Sect. 3.2). These modifications will allow an increased bandwidth of the system that could improve the robot performance also at higher speed.

3.2 Extended Kalman Filter

The control of the robot is based on the measurement of the robot's joint angular position provided by the C4G robot controller, and on the 6D pose of the robot end-effector provided by the laser tracker. While the encoders guarantee a highly precise and reliable measurement of the robot's joints position, the feedback provided by the laser tracker could present unexpected errors due to bad alignments between T-MAC (Sect. 2.3) and laser tracker, laser beam/line of sight interruptions, or highly dynamic motions. In order to increase the robustness of the system in such critical situations a Kalman Filter was implemented. The Kalman approach allows fusing multiple sensors feedback into a reliable, real-time, model-based estimation of the robot state. These methods have been widely used for multi-sensor fusion in order to enhance state

estimation and control performance of robot manipulator [17, 18]. Particularly, Kalman filters are extensively applied to estimate the robot pose in task involving robot vision and vision-aided navigation [19]. Similarly, in this project a Kalman filter allows fusing absolute position and orientation measured by the laser tracker, with position and velocities directly measured on the robot joints. The system's state vector \mathbf{x}_k includes angular position, velocity, and acceleration of the robot joints. The state transition model is assumed to be a linear second-order system with no input, driven by random acceleration rate. The measurement \mathbf{z}_k includes end-effector position and orientation expressed in quaternion, and 3D Cartesian coordinate, and robot joint angular velocity (Table 2).

Table 2. Discrete transition model.

Transition model	
$\mathbf{x}_k = \mathbf{F} \mathbf{x}_{k-1} + \mathbf{w}_k$ $\mathbf{z}_k = h(\mathbf{x}_{k-1}) + \mathbf{v}_k$	$\mathbf{x}_k = \left[\theta_1, \dots, \theta_6, \dot{\theta}_1, \dots, \dot{\theta}_6, \ddot{\theta}_1, \dots, \ddot{\theta}_6 \right]^T \in \mathbb{R}^{18}$ $\mathbf{z}_k = \left[X, Y, Z, q_1, q_2, q_3, q_4, \dot{\theta}_{1,m}, \dots, \dot{\theta}_{6,m} \right]^T \in \mathbb{R}^{13}$ $\mathbf{M} = \begin{bmatrix} 0_{6,6} & \mathbf{I}_{6,6} & 0_{6,6} \\ 0_{6,6} & 0_{6,6} & \mathbf{I}_{6,6} \\ 0_{6,6} & 0_{6,6} & 0_{6,6} \end{bmatrix}$ $\mathbf{F} = \mathbf{I} + T_s \mathbf{M} + \frac{T_s^2}{2} \mathbf{M}^2$

\mathbf{w}_k and \mathbf{v}_k are the process and observation noise with covariance matrix \mathbf{Q} and \mathbf{R} , respectively. $h(\cdot)$ is the forward kinematic function given in Cartesian position and quaternion orientation [12, 20]. While the state transition model is linear, the observation function $h(\cdot)$ is highly non-linear. Thus, an Extended Kalman Filter design was chosen, where the measurement residual is calculated using the non-linear function $h(\cdot)$, while the observation matrix \mathbf{H}_k is linearised around the current state estimation $\hat{\mathbf{x}}_{k|k-1}$ (Table 3).

Table 3. Extended Kalman filter algorithm

Prediction step	Update step
$\hat{\mathbf{x}}_{k k-1} = \mathbf{F} \hat{\mathbf{x}}_{k-1 k-1}$ $\mathbf{P}_{k k-1} = \mathbf{F} \mathbf{P}_{k-1 k-1} \mathbf{F}^T + \mathbf{Q}$	$\mathbf{H}_k = \left. \frac{\partial h}{\partial \mathbf{x}} \right _{\hat{\mathbf{x}}_{k k-1}}$ $\mathbf{K}_k = \mathbf{P}_{k k-1} \mathbf{H}_k^T (\mathbf{H}_k \mathbf{P}_{k k-1} \mathbf{H}_k^T + \mathbf{R})^{-1}$ $\mathbf{y}_k = \mathbf{z}_k - h(\hat{\mathbf{x}}_{k k-1})$ $\hat{\mathbf{x}}_{k k} = \begin{cases} \hat{\mathbf{x}}_{k k-1} + \mathbf{K}_k \mathbf{y}_k, & \text{if } \mathbf{z}_k \text{ reliable} \\ \hat{\mathbf{x}}_{k k-1}, & \text{otherwise} \end{cases}$ $\mathbf{P}_{k k} = (\mathbf{I} - \mathbf{K}_k \mathbf{H}_k) \mathbf{P}_{k k-1}$

The implemented filter has been tested offline using MATLAB (R2017a, the MathWorks Inc., Natick (MA), USA), simulating arbitrary robot motion where the ideal end-effector pose has been artificially perturbed by adding Gaussian noise and

missing data (Fig. 6). In the visualized example the 3D Cartesian deviation from respect to the ideal trajectory was reduced from 0.16(0.07) m (absolute error reported as $mean(standard\ deviation)$) to 0.07(0.03) m, while the orientation error calculated as the angle of the quaternion difference was reduced from $9.00(3.90)^\circ$ to $3.89(1.71)^\circ$. This preliminary evaluation shows how the implemented algorithm is effective and robust in significantly improving the quality of the signal even in presence of 50% of randomly distributed missing values. In the next step the performance of the implemented approach will be evaluated on the real robot.

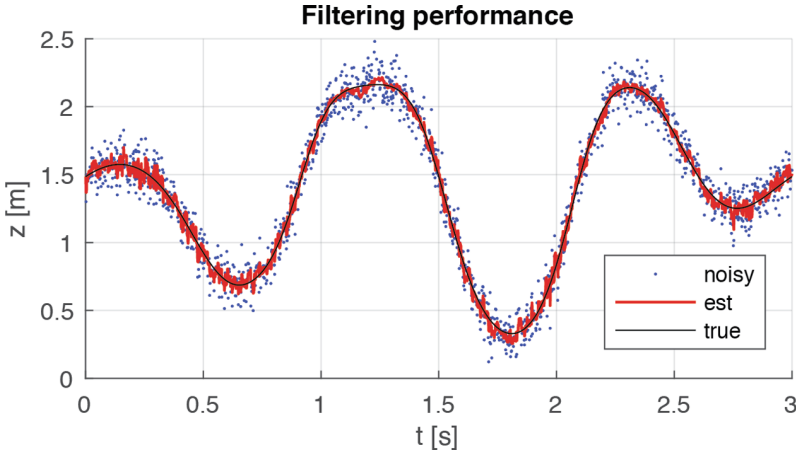


Fig. 6. EKF performance in offline evaluation. The plot visualizes end-effector z coordinate of a simulated trajectory. (*est*) shows the estimated pose calculated by the EKF for a simulated noisy measurement. The simulated measurement (*noisy*) was obtained by adding Gaussian noise and 50% of homogeneously distributed missed values to the ideal signal (*true*).

4 Conclusion and Outlook

This paper presents the preliminary steps towards the development of an all-in-one machine able to combine additive and subtractive manufacturing processes, as well as metal and non-metal material, into a novel and powerful tool which could represent a remarkable leap in industrial large volume manufacturing and prototyping.

Feasibility of the proposed approach has been proven for subtractive manufacturing and, currently, new control approaches are being investigated and tested in order to improve robot positioning and motion accuracy. Different manufacturing process will imply different control requirements: milling requires high position accuracy, finishing and polishing require constant interaction force between the tool and the part, while additive manufacturing requires constant dispenser velocity in order to guarantee homogeneous material deposition. Different control approaches are being studied and developed in order to meet those specific requirements and allow a successful integration of the desired manufacturing processes into this revolutionary hybrid manufacturing machine.

Acknowledgments. This project has received funding from the European Union’s Horizon 2020 research and innovation program under grant agreement No 723759. Their support is gratefully acknowledged.

References

1. Berman, B.: 3-D printing: The new industrial revolution. *Bus. Horiz.* **55**(2), 155–162 (2012)
2. Wohlers, T.T.: 3D printing and additive manufacturing state of the industry annual worldwide progress report. Wohlers report, Wohlers Associates (2014)
3. Allison, A., Scudamore, R.: *Additive Manufacturing: Strategic Research Agenda*. TWI, Cambridge (2014)
4. Flynn, J.M., Shokrani, A., Newman, S.T., Dhokia, V.: Hybrid additive and subtractive machine tools - research and industrial developments. *Int. J. Mach. Tools Manuf* **101**, 79–102 (2016)
5. Akula, S., Karunakaran, K.P.: Hybrid adaptive layer manufacturing: an Intelligent art of direct metal rapid tooling process. *Robot. Comput.-Integr. Manuf.* **22**(2), 113–123 (2006)
6. Karunakaran, K.P., Suryakumar, S., Pushpa, V., Akula, S.: Low cost integration of additive and subtractive processes for hybrid layered manufacturing. *Robot. Comput.-Integr. Manuf.* **26**(5), 490–499 (2010)
7. Kraken project homepage. <http://www.krakenproject.eu>. Accessed 31 Oct 2017
8. Megarob project homepage. <http://www.megarob.eu>. Accessed 31 Oct 2017
9. Shirinzadeh, B., Teoh, P.L., Tian, Y., Dalvand, M.M., Zhong, Y., Liaw, H.C.: Laser interferometry-based guidance methodology for high precision positioning of mechanisms and robots. *Robot. Comput.-Integr. Manuf.* **26**(1), 74–82 (2010)
10. Möller, C., Schmidt, H.C.: Real-Time 7DoF Pose Control of an Industrial Robotic System for Machining of Large-Scale CFRP Parts in the Aerospace Industry. Fraunhofer IFAM, Stade (2017)
11. Droll, S.: Real time path correction of a KUKA robot with optical feedback from a Leica laser tracker. Master Thesis, ETH Zurich, Zurich (2013)
12. Sciavicco, L., Siciliano, B.: *Modelling and Control of Robot Manipulators*. Springer, London (2012)
13. Veldpaus, F.E., Woltring, H.J., Dortmans, L.J.M.G.: A least-squares algorithm for the equiform transformation from spatial marker co-ordinates. *J. Biomech.* **21**(1), 45–54 (1988)
14. Jazwinski, A.H.: *Stochastic Processes and Filtering*. Dover Publications, New York (1970)
15. Julier, S.J., Uhlmann, J.K.: Unscented filtering and nonlinear estimation. *Proc. IEEE* **92**(3), 401–422 (2004)
16. Boesel, D.F., Glocker, P., Dienste, J.A., Peinado, V.: Realtime control of absolute Cartesian position of industrial robot for machining of large parts. In: *Austrian Robotics Workshop 2015*, p. 9. Klagenfurt (2015)
17. Lightcap, C.A., Banks, S.A.: An extended Kalman filter for real-time estimation and control of a rigid-link flexible-joint manipulator. *IEEE Trans. Control Syst. Technol.* **18**(1), 91–103 (2010)
18. Jassemi-Zargani, R., Neculescu, D.: Extended Kalman filter-based sensor fusion for operational space control of a robot arm. *IEEE Trans. Instrum. Meas.* **51**(6), 1279–1282 (2002)
19. Chen, S.Y.: Kalman filter for robot vision: a survey. *IEEE Trans. Industr. Electron.* **59**(11), 4409–4420 (2012)
20. Trawny, N., Roumeliotis, S.I.: Indirect Kalman filter for 3D attitude estimation. Department of Computer Science and Engineering, University of Minnesota, Minnesota (2005)



Deployment of a Distributed Multi-Agent Architecture for Transformable Assembly

Jack C. Chaplin^(✉)  and Svetan Ratchev 

Institute for Advanced Manufacturing, Advanced Manufacturing Building,
Jubilee Campus, University of Nottingham, Nottingham NG7 2GX, UK
jack.chaplin@nottingham.ac.uk

Abstract. Industry 4.0 represents a new philosophy in manufacturing systems, based on networked, intelligent, and cooperative resources. This revolution is necessary to make the cost-effective production of batch-size-of-one customised items in high-value manufacturing domains such as aerospace a reality. However, there exist large numbers of legacy production cells which generate value for enterprises which would ideally become part of a future manufacturing system, but which lack the necessary computational or networking capabilities. This is especially important in the case of small to medium enterprises, where Industry 4.0 is perceived as an expensive endeavour out of reach due to cost. There is a requirement for Industry 4.0 to be brought to existing legacy production cells in a cost effective and standards-compliant manner. This paper describes the technical implementation of an Evolvable Assembly Systems deployment onto an existing legacy manufacturing cell, describing the concepts and technical specifics of how to interface a software-based multi-agent system with real manufacturing hardware, and demonstrates how it is possible to make a transformable manufacturing cell which is compliant to the Industry 4.0 ideals in a cost-effective and expedient manner.

Keywords: Industry 4.0 · Evolvable Assembly Systems · Smart manufacturing

1 Introduction

Higher product complexity in terms of physically complex designs and assemblies with stringent tolerance requirements, demand for customer-unique customisation, and increasingly smart products with bespoke software installed at assembly-time is a significant challenge for modern and future manufacturing. Exacerbating this situation, products are changing to meet customer demands increasingly quickly, reducing the time available to develop an assembly process for a product [1].

There are numerous national and international initiatives to address the challenges of managing the data generated by such complex manufacturing processes, so more effective decisions can be made quicker. These include Industry 4.0 [2] and the Industry 4.0 reference architecture RAMI4.0 [3], and the Industrial Internet Consortium and their Industrial Internet Reference Architecture (IIRA) [4].

There is a need for distributed intelligent control that can mitigate the exponential rise in the number of communication interconnections between increasing numbers of

networked manufacturing resources and sensors, which would enable production lines to be agile in response to new product variants and robust to system failure.

In addition, with individually customised products becoming increasingly important in the manufacturing economies of high-technology, high-wage cost regions, there is a requirement to track and log data associated with every single product created, to ensure full traceability when a product has been assembled with a unique assembly strategy. This is particularly important in highly regulated domains such as aerospace, pharmaceuticals, and construction.

Many modern production systems utilise Programmable Logic Controllers (PLCs) to control manufacturing resources, and which possess the ability to exchange and process information. However, these can often only communicate via vendor-specific protocols, and program execution may be constrained to IEC 61131-3 programming languages [5], limiting the opportunity for more complex algorithms. In addition, many legacy production resources still provide value to their operators, but these may lack any computational capacity or utilise obsolete communication methods if they possess any communication methods at all. It is important that the fourth industrial revolution does not pass over small to medium enterprises (SMEs), who may have higher proportions of legacy equipment because they cannot afford to purchase expensive new resources or controllers, or lack the time and expertise to invest in manufacturing digitisation [6]. Hence, a solution must be found to include legacy resources in any smart manufacturing system in a homogeneous, simple, and low-cost way.

This requirement for an open, accessible, and low-cost solution to the digitalisation of manufacturing processes would enable the implementation of system-wide intelligence, and a strategy for sharing system-generated data to allow companies to participate in the fourth industrial revolution. The system must facilitate the dynamic checking of the manufacturability of new products to ensure the system can keep up with the increasing pace of product change, and facilitate transformable manufacturing cells able to evolve to match changing product requirements. Information on the manufacturing process must be logged to ensure traceability of product data.

There are existing architectures for distributed system-wide intelligence that tackle the above problems based on multi-agent systems [7–9]. These include the Product-Resource-Order-Staff Architecture (PROSA) [10], the Adaptive Holonic Control Architecture for Distributed Manufacturing Systems (ADACOR) [11], and Evolvable Assembly Systems (EAS) [12]. However, how these software architectures are actually deployed on to existing legacy manufacturing lines remains an open challenge.

This paper details the implementation of a technical solution for deploying a distributed multi-agent manufacturing intelligence architecture (specifically Evolvable Assembly Systems) on to an existing legacy robotic manufacturing cell which lacks inherent Industry 4.0 features. It does this in a standards-compliant, low-cost way which would be applicable to SMEs which want to take advantage of Industry 4.0 principles, but cannot risk the high expenditure required to replace existing production cells.

2 Scenario and Current Limitations

To demonstrate the approach described in this paper, we present a scenario using aerospace components on a robotic assembly cell. The cell forms part of a larger assembly line – the Future Automated Aerospace Assembly Demonstrator (FA3D) – and prepares rib components for inclusion in a wing or fuselage assembly by applying sealant and/or scanning the part with a line scanner to check part accuracy and the quality of the sealant application.

This cell has two primary challenges that must be met for which the current control method is inadequate. The first challenge is that the FA3D assembles batch-size-of-one products, where every item being assembled is unique and must be treated differently. The larger assembly line is required to produce aircraft components for high-complexity, highly-customisable, and low-volume airframes while keeping costs low, and as such each assembled airframe can be considered to be unique. Additionally, the high precisions required of the final assembly require every part to be analysed for deviations from specification, and the assembly process altered to compensate. As a result, seemingly identical components being handled in the cell must be identifiable and able to be treated differently as the quality of supply varies.

The second primary challenge for the cell is the logging of data. In highly regulated industries such as aerospace, pharmaceuticals, or construction, logging data is essential for tracing the root causes of problems, analysing data to identify problems before they occur, and providing accountability for failures. This is especially important for batch-size-of-one manufacturing, where every product is assembled in a unique manner which may be determined automatically by intelligent manufacturing systems. The data must be interrogable to understand why decisions were made in the event of failure, and to understand the behaviour of the system over time.

The demonstration cell operates on rib components for aerospace assemblies. The ribs are placed in pallets, which can then be moved around the cell. The cell utilises two ABB IRB6700-150-320 robotic arms to perform operations on the rib components. The robots are set-up in a master-slave configuration, with a single Siemens S7 1513-1 PN PLC controlling both. Each robot has a separate tool changing rack. The master robot has access to a proxy sealant applicator (to facilitate testing), and a Micro Epsilon scanCONTROL compact 2900-50/BL laser line scanner. The slave robot has access to a bespoke pallet gripper and a bespoke rib gripper, allowing it to pick up pallets or pick ribs out of pallets. To one side is a storage rack, where pallets with or without ribs can be stored and retrieved.

The cell has a loading/unloading area for loading pallets and ribs onto a conveyor system. Loaded pallets move into the slave robot's working area, allowing the pallet or rib to be picked up. The conveyor system is to be expanded to allow complete ribs in pallets to be dispatched to the second cell to be assembled in a larger aerospace assembly. The conveyor system is controlled by a Siemens SIMATIC ET 200SP Open Controller with software-based PLC functionality (Fig. 1).

The cell in its current state has several technical limitations. With the expansion to the conveyor system planned to link the cell to the wider FA3D production line, these

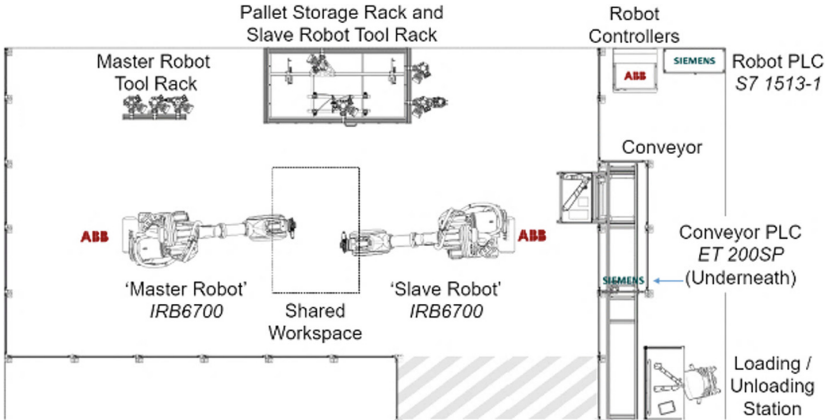


Fig. 1. (Top) Schematic layout of the demonstrator cell. (Bottom) View of the cell from in front of the storage rack, showing the two robots.

limitations must be overcome if the cell is able to contribute to high-precision, batch-size-of-one products.

The first limitation is that the demonstration cell has no networking between its components; the PLCs for the robots and for the conveyor system are not connected, and instead rely on user interfaces with which a worker can execute several pre-specified actions manually.

The second limitation is that it does not have any system-wide control that allows for automated production of parts. For batch-size-of-one products, this approach is insufficient as the worker must understand the production plan for a potentially complex part sufficiently to correctly pick the order of operations, as well as to know when to perform any manual operations such as loading/unloading parts. Additionally, with

no networking, the system cannot communicate with the wider production line, which is a significant problem if this cell is to be integrated with the FA3D.

The third limitation is that data collected by the system is transitory and not stored, which does not allow for retrospective analysis of cell performance or identification of errors. Additionally, data generated by the laser line scanner is saved as a file, which must then be manually transferred to the FA3D via USB drive. To remove this manual step, it would be preferable for data to be transferred automatically to the appropriate resources.

The fourth limitation is that the actions which can be performed by the robots and the conveyor system are fixed. The commissioning of the cell included programming the PLCs and specifying the actions performable by the robots, and changing these risks violating the safety certification of the cell necessary to have the cell open for manual worker access.

3 Enabling Technologies for Low-Cost Industry 4.0 Implementation

To address these limitations and upgrade the cell, we propose the use of technologies which directly tackle the issues of networking, system-wide intelligence, and data logging, and also mitigate the issue of fixed actions which are inherent to including legacy production cells into Industry 4.0-compliant manufacturing lines. These technologies and approaches are discussed here.

3.1 Data Distribution Services

Increasing the number of devices within manufacturing production lines, combined with a requirement for devices to talk to other devices in the line requires an exponential number of interconnects. Though service-orientated architectures are an improvement on existing point-to-point solutions, this still requires a client/server relationship. Instead, the approach taken by the Industrial Internet Consortium [4] to decouple industrial manufacturing as much as possible is the use of Data Distribution Services (DDS) [13], which is a standard administered by the Object Management Group (OMG).

DDS is a networking middleware designed to decouple the origins and consumers of data within a specified domain. Nodes in the DDS that produce data are called publishers, and publish pieces of information (called samples) to topics. A publisher can publish data without needing to know what (if any) nodes will consume this data. Nodes which consume data are called subscribers, and subscribe to topics to receive samples published there. Similarly, a subscriber can subscribe to topics without needing to know the origin node of the data.

The result is a data-driven communication system, where the most important element – the data – drives the operation of the manufacturing system. Nodes in the system do not communicate directly, but instead form a shared system context where a single canonical view of the state of the system is distributed between the nodes, and from which nodes can selectively subscribe to information relevant to them.

The lack of a communication broker, or direct interconnects between resources in the system serves two important roles in the context of a manufacturing system. Firstly, there is no single point of failure and data is replicated by the middleware between nodes (in most DDS implementations), leaving a robust system that can continue execution even if nodes fail. Secondly, with no explicit network structure, the system can be reconfigured and nodes added or removed without having to alter the networking configuration. Additionally, if the networking uses wireless methods (as with this demonstration), there is no requirement to alter the physical networking infrastructure either.

3.2 Embedded Computers

With a data-driven approach, there is no direct communication between resources in the manufacturing system. As a result, there is no single orchestrator that instructs each resource as to what to do and when to do it, in contrast to traditional monolithic architecture. Instead, each resource must be smart enough to analyse the state of the system in the shared system context and make decisions as to what to do. For this, every resource in the system requires a degree of computing power, which is not something that can be assumed for legacy systems. Neither can it be assumed that resources with computing abilities (such as those with Programmable Logic Controllers) are provided as open by their vendors and hence capable of running the necessary decision making algorithms or DDS implementation.

To solve this problem, the approach given here uses embedded computers to handle decision making and communication, as this allows for the execution of general-purpose code and use of communication standards which might not otherwise be available. This approach removes vendor-specific implementation considerations at the earliest possible stage, and transforms all control and information into homogeneous and open methods. This does require an interface between the embedded computer and the resource controller, which may be a modern PLC with interface APIs, a legacy controller with no consideration for external interfacing, or a human worker which will require a smart or wearable device to communicate information.

Embedded computers also provide local data storage capacity, and the ability to connect to larger capacity database, enabling the storage of large quantities of operational data that would otherwise be lost, which could be pre-processed and analysed at the edges of the system to extract events and filter out unneeded data.

Combined with the data distribution services, the use of embedded computer solves the challenges of networking and lost data. However, the challenges of system-level intelligence and fixed actions remain. To solve this limitation, we utilise intelligent agents.

3.3 Intelligent Agents

Each module in an Industry 4.0 enabled cell requires localised intelligence to make decisions, be context aware, and share information with the rest of the production line. These intelligences represent the production resources which carry out operations on parts in line with their capabilities.

To implement localised intelligence, we utilise Belief-Desire-Intention (BDI) [14, 15] intelligent agents (or simply ‘agents’) [7–9] which are independent, self-contained software entities which use the BDI model of planning, allowing a decoupling of the agent’s perceptions of the world, the selection of plans, and the execution of plans. These agents execute on the embedded computers, and are the interface with the wider production line, publishing and subscribing to the shared system context, and making decisions based on the state of the cell as to when to execute capabilities. Upon these agents, we implement the Evolvable Assembly Systems architecture.

4 Technical Implementation of Evolvable Assembly Systems

The three key technologies of DDS, embedded computers, and intelligent agents can be used together to create an implementation of a smart Industry 4.0-compatible manufacturing system. Combined with the data distribution services, the use of embedded computers solves the challenges of networking and lost data. However, the challenge of system-wide intelligence remains despite the use of intelligent agents – agents are a general purpose solution and not tailored to manufacturing cells. To solve this challenge, we employ Evolvable Assembly Systems.

Evolvable Assembly Systems [7, 8] is a manufacturing paradigm defining transformable, responsive production lines for effectively producing low-volume products. It focuses on the use of multiple independent and modular components to allow for rapidly reconfigurable and transformable production cells. The use of intelligent agents to execute the Evolvable Assembly System paradigm to make decisions as to what actions to perform based on the state of the system as per the shared system context satisfies the requirement for system-wide intelligence, as this enables batch-size-of-one production where each step in manufacturing is defined in a recipe. Our software implementation of EAS is detailed in [12, 16], and utilises agents to implement distributed intelligence in manufacturing systems, the automated checking of the manufacturability of submitted batch-size-of-one product recipes against the capabilities of a production cell or line, and allocation of requirements to manufacturing resources. However, the technical challenges remain of how the agents are deployed, and how the determined requirements are automatically executed on manufacturing resources. This is solved with the approach detailed in this section, resulting in a functional demonstrator of an Evolvable Assembly systems deployment.

4.1 Embedded Computers and Smart Devices

To implement our approach, we used embedded computers. A wide variety of embedded computers are available, ranging from the basic Raspberry Pi Zero W [17], to more fully featured products such as the Siemens SIMATIC IOT2000 Intelligent Gateway series [18]. The exact model used will depend on the interface requirements with the resource controller. As our implementation is hardware agnostic, a mixture of embedded computer models could be used.

In our case, the Siemens SIMATIC S7 1513-1 PN PLC and SIMATIC ET 200SP Open Controller offer interfacing via Ethernet connections, so any embedded computer

would require an Ethernet port. Our code, including BDI agents, networking middleware, and manufacturability analysis implementation described in [16], is implemented in Java so any model chosen must support this. Communication via the data-centric shared system context between nodes is also required. As the demonstrator used in this example is not physically reconfigurable, wireless networking has less merit than in other more modular reconfigurable demonstrators such as those presented in [12, 16]. However, wireless communication is important when a human worker is involved in the process as with this demonstrator, as the human will be mobile and utilising a smart device to interface with the system. Additionally, there are few models of embedded computer with two Ethernet ports (as one is required to connect to the PLC), and so wireless networking was determined as preferential over wired technologies.

To satisfy these requirements, we selected one of the most widely available single-board computers to use as our standard model of embedded computer – the Raspberry Pi 3 Model B [19]. The Raspberry Pi is globally available, low cost, open, and flexible, and features all the connectivity we require, including in-built wireless connectivity. It is powered via a micro-USB 2.5A power source.

Though more computationally powerful or more fully featured single board computers exist, the Raspberry Pi is useful as a baseline for demonstrating this approach, as a successful implementation on a Raspberry Pi would also function on other more powerful and more expensive models. These embedded computers enable the execution of intelligent agents which communicate and cooperate, giving the demonstration cell system-wide intelligence and context awareness as required.

Human workers in the production line also require interfacing to the wider system intelligence. This is achieved through the use of mobile smart devices. For now, we utilise Lenovo X260 Ultrabooks, though future work will include the deployment of the interfaces to low-cost tablet computers (Fig. 2).



Fig. 2. A legacy production resource can be considered to be advertising its capabilities via a user interface. A smart manufacturing system such as an Evolvable Assembly System wishes to instantiate these capabilities. But how can the intelligent agents actually interface with the resource?

4.2 Interfaces with Resources

The intelligent agents executing on the embedded computers and smart devices require interfaces with the resources (or human workers), enabling the requesting of capability instantiation and collection of data.

This approach suggests use of service-orientated architecture such as OPC Unified Architecture [20] where the resource advertises services (i.e. the instantiation of capabilities) and the embedded computer acts as the client to select these. However,

retrofitting these capabilities into existing production lines (such as this demonstration cell) does not necessarily allow for such idealised solutions. PLC code may have been tested and proven correct for years prior to the decision being made to include Industry 4.0 technologies, and stakeholders may not want to risk sweeping changes to PLC execution. Additionally, some legacy resources may not be able to execute OPC UA (or similar) at all. An alternative solution must be found.

As the demonstration cell was designed to be used manually, the PLCs to control the robots and to control the conveyor system both have user interfaces by which a worker can instantiate capabilities by pressing virtual buttons on a touch screen interface. Though not designed with service-orientation in mind, a user interface essentially allows the resource to advertise capabilities in the form of buttons or other UI elements, and to receive requests from a client in the form of button presses.

To leverage this indirect service orientation, the embedded computers must be able to simulate a button press on the user interface, which enables automated execution of PLC code without modifying the PLC code itself. The precise manner in which this is achieved will necessarily vary depending on the user interface and vendor in question. Presented here is the method used for both the Siemens SIMATIC S7 1513-1 PN PLC and SIMATIC ET 200SP Open Controller used for the robots and conveyor system respectively.

User interfaces for Siemens PLCs are created using SIMATIC WinCC [21]. This executes on the PLC, but in a separate memory space to the main PLC code. Buttons are created and have actions associated with them when the button is pressed; the general pattern is for a bit in memory to be set when the button is depressed and reset when the button is released. Code in the PLC checks the state of the bit associated with the button and performs actions if the bit is set. Despite both the S7 and Open Controller PLCs having different internal architectures, they both follow this pattern (with minor deviations as both were commissioned by different organisations).

S7Connector is an open source Java library for interfacing with S7 PLCs via Ethernet [22]. As the ET 200SP is based on an S7-1500 CPU, both PLCs are compatible with this approach. It allows for reading and writing values to the memory of the PLC via a Java program executing on a connected device. This permits the connected device to alter the bit that is set by pressing a button on the user interface, simulating a button press.

One limitation of this approach is that it requires knowledge of the memory location of the bit connected to the button on the user interface, which in turn means access to the original project files for the PLC. Interfacing with a user interface via an embedded computer without access to the source for the PLC program would be challenging, and other solutions may be required, such as having the resource embedded computer using its own interface on a smart device to instruct a worker to press the required button.

With the same approach, any data made available to the user interface (resource status or data generated by the line scanner for example) can be retrieved in the same manner by reading the variable which controls the UI element display. This allows the embedded computer to know what the attached resource is doing, and read (and optionally publish) data it generates.

Human workers are also perceived in Evolvable Assembly Systems as manufacturing resources, and hence require an interface between the smart device on which

code executes and the worker themselves. This takes the form of a user interface, instructing the operator what tasks to perform at a given time, and offering the user the ability to specify the completion of work (Figs. 3 and 4).

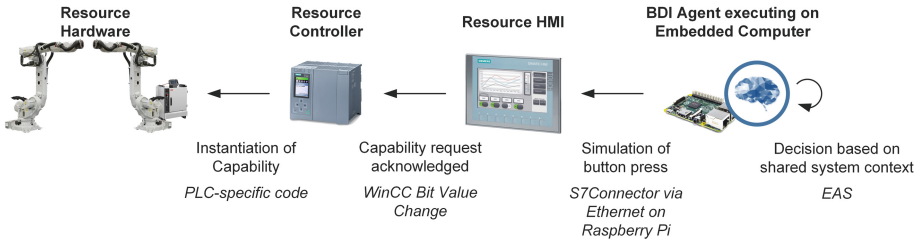


Fig. 3. The communication stack for an agent to execute a capability on a resource, using the example of the master/slave robots.

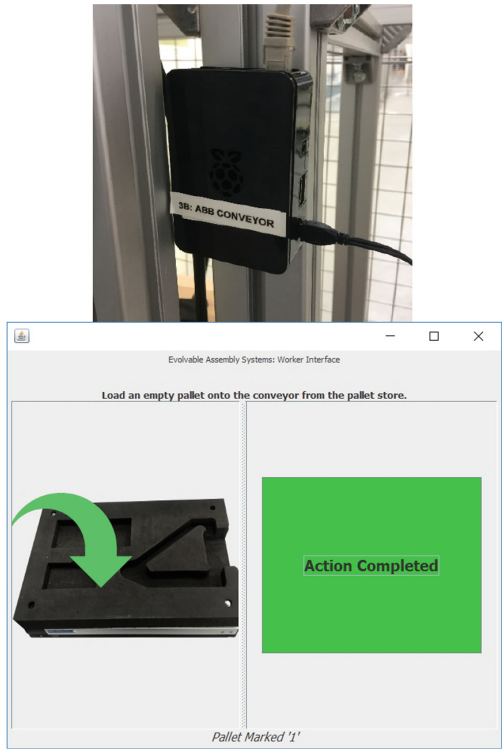


Fig. 4. (Left) A Raspberry Pi 3 Model B is networked to the conveyor PLC. (Right) A worker is instructed to load a pallet onto the conveyor system by the worker resource interface.

4.3 Networking and Data Collection

Networking resources in the production cell allows for data to be published and subscribed to via DDS and the shared system context. As the Raspberry Pi 3 Model Bs and Lenovo X260s feature built-in Wi-Fi, and as the Raspberry Pi Ethernet ports are used to interface with the PLCs, a wireless network was created using a TP-LINK TD-W8970 router. The wireless networking allows for the mobility of the human workers with laptops (and later, tablets or other smart devices), and simplifies system reconfiguration. To operate using a data-centric model, we use DDS. For this implementation, we use RTI’s Connex DDS Professional [23], which is a fully featured and compliant implementation of the OMG DDS standard [13]. It has Java libraries and native support for Raspberry Pi single board computers.

With advances in data storage and data-centric manufacturing systems, it’s now possible to store all data on a product being assembled, including a digital ‘black box’ of why decisions were made, to facilitate the tracing of errors and verification of system behaviour. We call this ProductDNA, and it includes all data generated by the involved resources, any metrology data produced including environmental data, tolerances and deviations, and system decisions made and the reasons why.

To achieve this, an additional ProductDNA agent is added to the manufacturing cell, executing on a Dell Precision 7510 laptop. This agent, like other agents in an Evolvable Assembly System, can subscribe to topics to receive data. To gather all possible data, it subscribes to all topics available using Connex DDS’ discovery service, and saves every sample to file (organised by topic) for future analysis (Fig. 5).

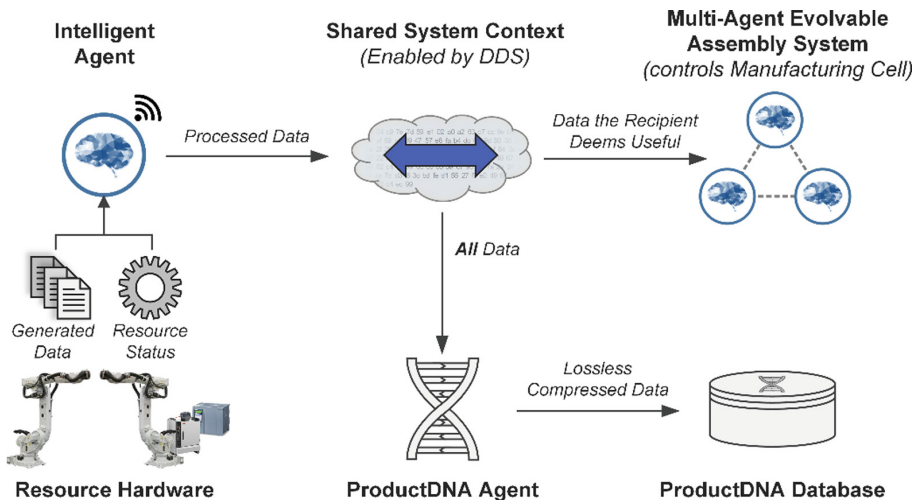


Fig. 5. Use of data in the solution. The agent (on the embedded computer) is able to retrieve information about the resource provided that information is presented on the resource user interface. This is shared (with optional pre-processing) to the shared system context, where other agents in the system can select what information they require to make optimum decisions. All data is stored by the ProductDNA agent.

4.4 Agents

Each resource in the system is controlled by an intelligent agent running on the embedded computer or smart device. We programmed agents in Java using the Java Agent Development Framework (JADE) [24, 25] which is an open source and flexible agent framework. On top of this, a BDI framework [15] was developed by which the agents reason about the demonstration cell.

The use of BDI agents has several advantages in this context. Firstly, there are strong synergies between the concept of beliefs and the use of a belief set in the BDI model, and of the use of data-centric communication, as the belief set of an agent is a subset of the shared system context representing the entire system, and the beliefs can be updated as the shared system context changes. Secondly, the BDI model decouples the storage of beliefs and the development of plans, from the execution of plans. As each agent may have a unique interface with its resource (or it may be a user interface in the case of a human worker), this simplifies the insertion of bespoke code whilst the rest of the code base remains homogenous.

The method by which the agents analyse recipes and determine how to execute capabilities to create a unique batch-size-of-one product is detailed in [16]. Users are able to submit recipes to the production line via an interface also running on the Dell laptop, which submits the recipe to the shared system context where the agents will check manufacturability and assign tasks.

5 Conclusions

This paper has presented a technical method for implementing Industry 4.0 and Evolvable Assembly Systems concepts on pre-existing legacy manufacturing cells, utilising data-centric communication, and intelligent agents executing on embedded computers which interface with their respective manufacturing resources. This method allows for a cost-effective manner in which smart manufacturing could be achieved by SMEs looking to include their production cells in the fourth industrial revolution.

One limitation of this approach is in not solving the issue of fixed actions. The use of capability topologies [10] helps mitigate the restriction of fixed actions, though does not solve the problem. The issue is inherent to the design of manufacturing cells, and in particular those not designed with maximum flexibility in mind.

Moving forwards, we aim to implement the user interfaces for human workers on smart devices such as tablet computers or smart watches, to make receiving and auctioning instructions, as well as relaying information back to the shared system context simpler. The entire demonstration cell will be integrated with the wider FA3D cell, during which the implementation will be extended to include the entire manufacturing cell, including challenges relating to interfacing with the more complex control system of the FA3D. We will also use additional models of embedded computer, including the Siemens IOT2000 [18] to experiment with system heterogeneity.

Acknowledgements. The reported research has been funded by the EPSRC grant EP/K018205/1, the support of which is gratefully acknowledged. We would also like to thank RTI for providing a license for Connex DDS Professional as part of their University Program.



References

1. Rhodes, C.: Manufacturing: statistics and policy, p. 13. House of Commons Library (2014)
2. Kagermann, H., et al.: Recommendations for implementing the strategic initiative INDUSTRIE 4.0: securing the future of German manufacturing industry; final report of the industrie 4.0 working group. Forschungsunion (2013)
3. Adolphs, P., et al.: Reference architecture model industrie 4.0 (rami4.0). VDI/VDE Society Measurement and Automatic Control (GMA) (2015)
4. Lin, S-W., et al.: The industrial internet of things volume G1: reference architecture. Industrial Internet Consortium (2017)
5. International Electrotechnical Commission: IEC 61131-3:2013 in programmable controllers - part 3: programming languages (2013)
6. Sommer, L.: Industrial revolution-industry 4.0: are German manufacturing SMEs the first victims of this revolution? *J. Ind. Eng. Manag.* **8**(5), 1512 (2015)
7. Jennings, N.R.: On agent-based software engineering. *Artif. Intell.* **117**(2), 277–296 (2000)
8. Weiss, G.: Multiagent Systems: A Modern Approach to Distributed Artificial Intelligence. MIT press, Cambridge (1999)
9. Wooldridge, M., Jennings, N.R.: Intelligent agents: theory and practice. *Knowl. Eng. Rev.* **10**(2), 115–152 (1995)
10. Van Brussel, H., et al.: Reference architecture for holonic manufacturing systems: PROSA. *Comput. Ind.* **37**(3), 255–274 (1998)
11. Barbosa, J., et al.: Dynamic self-organization in holonic multi-agent manufacturing systems: the ADACOR evolution. *Comput. Ind.* **66**, 99–111 (2015)
12. Chaplin, J., et al.: Evolvable assembly systems: a distributed architecture for intelligent manufacturing. *IFAC-PapersOnLine* **48**(3), 2065–2070 (2015)
13. Object Management Group Inc.: Data Distribution Service (DDS) Version 1.4 (2015). <http://www.omg.org/spec/DDS/1.4/>. Accessed 12 Nov 2017
14. Faccin, J., Nunes, I.: Modelling and reasoning about remediation actions in BDI agents. In: 2017 Proceedings of the 16th Conference on Autonomous Agents and MultiAgent Systems. International Foundation for Autonomous Agents and Multiagent Systems (2017)
15. Rao, A.S., Georgeff, M.P.: BDI agents: from theory to practice. In: ICMAS (1995)
16. de Silva, L., et al.: Realisability of production recipes. In: 22nd European Conference in Artificial Intelligence (ECAI 2016), The Hague, Netherlands (2016)
17. Raspberry Pi Foundation: Raspberry Pi Zero W (2017). <https://www.raspberrypi.org/products/raspberrypi-zero-w/>. Accessed 6 Dec 2017
18. Siemens AG: The intelligent gateway for industrial IoT solutions: SIMATIC IOT2000 (2017). <http://w3.siemens.com/mcms/pc-based-automation/en/industrial-iot/pages/default.aspx>. Accessed 6 Dec 2017
19. Raspberry Pi Foundation: Raspberry Pi 3 Model B (2017). <https://www.raspberrypi.org/products/raspberrypi-3-model-b/>. Accessed 7 Dec 2017
20. OPC Foundation: Unified Architecture (2016). <https://opcfoundation.org/about/opc-technologies/opc-ua/>. Accessed 5 Dec 2017

21. Siemens AG: SIMATIC WinCC V7 - maximum plant transparency and productivity (2017). <http://w3.siemens.com/mcms/human-machine-interface/en/visualization-software/scada/simatic-wincc/pages/default.aspx>. Accessed 7 Dec 2017
22. S7Connector Members: S7Connector: Java library for S7 PLCs (2016). <https://s7connector.github.io/s7connector/>. Accessed 7 Dec 2017
23. Real-Time Innovations: RTI connext DDS professional (2017). <https://www.rti.com/products/dds>. Accessed 6 Dec 2017
24. Bellifemine, F., Bergenti, F., Caire, G., Poggi, A.: Jade — a Java agent development framework. In: Bordini, R.H., Dastani, M., Dix, J., El Fallah Seghrouchni, A. (eds.) Multi-Agent Programming. MSASSO, vol. 15, pp. 125–147. Springer, Boston, MA (2005). https://doi.org/10.1007/0-387-26350-0_5
25. Bellifemine, F., Poggi, A., Rimassa, G.: JADE–A FIPA-compliant agent framework. In: Proceedings of PAAM, London (1999)



Creating Resource Combinations Based on Formally Described Hardware Interfaces

Niko Siltala^(✉) , Eeva Järvenpää , and Minna Lanz 

Laboratory of Mechanical Engineering and Industrial Systems,
Tampere University of Technology, Tampere, Finland
{niko.siltala,eeva.jarvenpaa,minna.lanz}@tut.fi

Abstract. This paper introduces the Resource Interface ontology intended to formally capture hardware interface information of production resources. It also proposes an interface matchmaking method, which uses this information to judge if two resources can be physically connected with each other. The matchmaking method works on two levels of detail, coarse and fine. The proposed Resource Interface ontology and matchmaking method can be utilised during production system design or reconfiguration by system integrators or end users. They will benefit from fast and automatic resource searches over large resource catalogues. In the end of the paper, a validation of the method is provided with a test ontology.

Keywords: Interface · Resource description
Production system reconfiguration · System design

1 Introduction

Responsiveness of manufacturing is an important strategic goal for manufacturing companies operating in a highly dynamic environment characterised by constant change. Such responsiveness and adaptivity is related to the need to reconfigure and adjust the production and corresponding production system as efficiently as possible to the required changes in processing functions, production capacity, and the dispatching of the orders. [1,2] To do this, the production system needs an inherent ability to facilitate continual and timely change in its structure and in its functional operations. Structure refers to the way in which the functional building blocks of a production system are assembled to form a holistic, interoperable system, while the term function describes the abilities of the building blocks or the production system as a whole to realise a defined purpose. [3] During system design and re-configuration, new structural configurations are built to fulfil the functional requirements set by the product. In order to achieve a feasible structural configuration, the combined resources must have compatible interfaces.

Traditionally, the system design and reconfiguration has been purely a human-driven and time consuming process, relying on the expertise and tacit knowledge of the system integrators and the end users of the system. The realisation of the requirements for fast response calls for new methods and solutions that would drastically reduce the time and effort put into planning and implementing the alterations in a factory, such as plug and play interfaces, modern information and communication technologies, simulations and new planning methods [4]. Within the past decade, there have been multiple different projects and research trying to provide computerised support for this reconfiguration planning process. Important steps towards modular assembly equipment and standardised hardware and control interfaces was made by, for example, the EU-funded project called EUPASS [5]. According to [6], the modular architecture paradigm for new production systems, which focuses on the clear functional decoupling of equipment module functionalities and the use of standardised interfaces to promote interchangeability, presents the possibility for developing automated reconfiguration methods. The currently running project ReCaM [7] aims to develop a set of integrated tools for rapid and autonomous reconfiguration of production systems. The approach relies on a unified functional description of resources, providing a foundation for rapid creation of new system configurations through capability-based matchmaking of product requirements and resource offerings.

The aim of bringing automation to the system design, re-configuration, and order dispatching requires a formal, structured representation of the product requirements as well as resource's capabilities, properties, and interfaces. For the past two decades, there has been an increasing interest in manufacturing domain on using emerging technologies such as ontologies, semantics and semantic web, to support the collaboration, interoperability and adaptation needs [8–11]. The detailed formal interface descriptions have been out of the scope of these works.

In our previous research, we have studied capability matchmaking and creation of new resource combinations, which have combined capabilities to satisfy the processing requirements of the specific product [12]. The Web Ontology Language (OWL)-based Capability Model allows such combinations to be created from the capability perspective [13]. In order to make sure that the resources can be physically connected, a formal resource interface description and associated matchmaking is also required.

The objective of this paper is to present recent development of a Resource Interface ontology that can be used for finding production resources, which can be connected together. The Resource Interface ontology shall provide a response to the following use cases: Find resources that can be connected with particular interface of a resource; Find resource combinations with connectable interfaces; and Ensure that suggested resource combinations found by an external system (e.g. capability matchmaking [12] or system designer propositions) are physically connectable. The work builds upon our existing work on formalised interface description as a part of XML-based Resource Description concept [14, 15].

The paper is organised as follows. The second chapter represents the Resource Interface ontology and its details. Next chapter illustrates the interface match-making first on coarse level, followed by fine level matchmaking. One example SPARQL query is shown. The fourth chapter shows first evaluation results through a few test cases with our test ontology. Finally, the paper ends with discussion and conclusion.

2 Interface Description

2.1 Interface Description in Resource Description Concept

The Resource Description (RD) concept formalises characteristics of production resources by creating a comprehensive description of resource's features. This description, the RD [14, 15], is then published and used to exchange information between resource provider and various systems used for production system design and execution.

One section of the RD model formalises the information defined by electro-mechanical interface standards. The interface information captured by a RD are: name, identifier (ID), category, gender, and force and torque limits of the interface; additional properties characterising the interface; and implementations of it. Each interface implementation provides its physical pose (frame origin in 3D space) and the kinematic model, if the interface is a movable one. Additionally, the RD defines the organisation that defines the interface standard, and what is the general purpose of the interface. The latter is done through link with the abstract interface model, which is a shared contract between similar kind of resources.

Only a subset of information required for the interface matchmaking is retrieved from a RD, and read into the Resource Interface ontology. This is done to collect together information from several resources and to utilise the search methods provided by ontologies.

2.2 Resource Interface Ontology

OWL is used to codify the Resource Interface ontology and for storing the actual resource instances and their interface information instances. Figure 1 shows the structural model of the Resource Interface ontology. Next, the key components of this model are described.

Class *InterfaceDefinition* is the main entry point for the Interface Model ontology. It defines an implementation of the hardware interface and links it to an interface standard (*IfStandard* with *implementsStd* object property), purpose of the interface port (*InterfacePurpose* with *hasPurpose*), a set of characterising information (*IfCharacteristic* with *hasIfCharacteristic*), set of physical interface port implementations (*IfPortImplementation* with *hasIfPortImplementation*), and *ForceAndTorqueLimit* (with *hasForceAndTorqueLimit*), which defines the maximum forces the interface can handle at different directions. In addition,

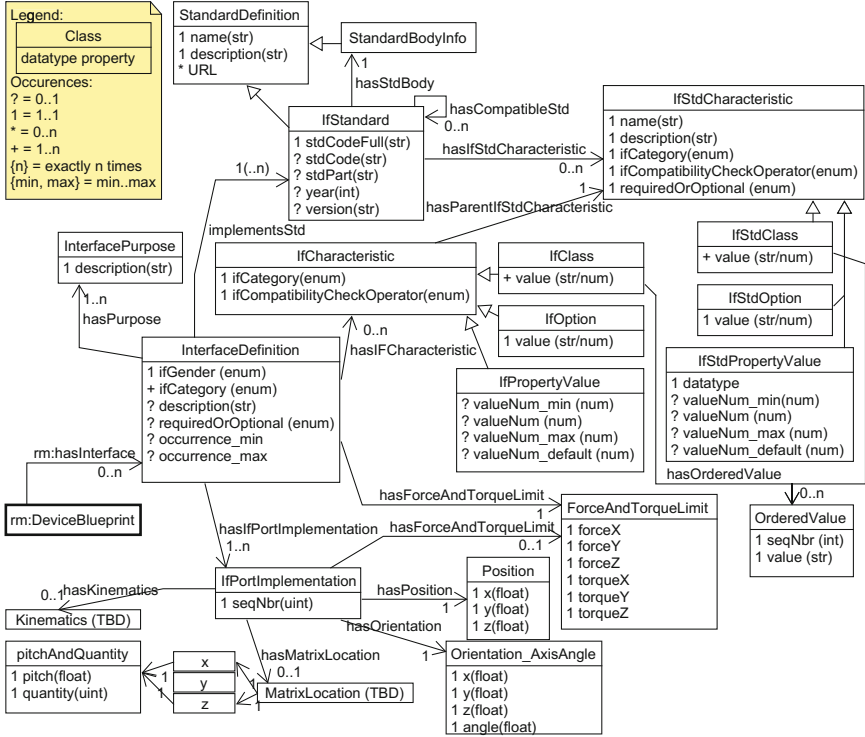


Fig. 1. Resource interface ontology

the *InterfaceDefinition* defines the gender and category of the interface implementation. Optionally it can define human readable description, and occurrence minimum and maximum, which define a range of how many occurrences of this interface implementation can exist within this resource.

First, we focus on the interface standard, because it is the primary linking factor when judging, if two interface implementations, present in two resources, can be connected together. The *IfStandard*'s property *stdCodeFull* is used as ID and primary key connecting two implementations together. Human readable name and description of each interface standard must be provided. Furthermore, the *IfStandard* can have the designation represented as elementary items. These can be stored into the corresponding properties *stdCode*, *stdPart*, and *year*. The *IfStandard* links to *StandardBodyInfo*, which groups the interface standards under a standardisation body, and to *IfStdCharacteristic*, which provides characteristics for this interface standard. Additionally, the *IfStandard* has object property *hasCompatibleStd*, which states that another interface standard can be used as compatible replacement of the other. This link is only unidirectional, and all compatibles must be explicitly stated.

The gender (*ifGender* data property) of **InterfaceDefinition** is the second linking factor and it can have one of three enumerated values - male, female, or neutral. This defines polarity of the interface, and which implementations of the same **IfStandard** can be connected together. Rules are simple - male and female or two neutrals can be connected together. Examples of setting up a gender are such as a plug is male, a socket is female and a plain flange with mounting through holes could form a neutral gender.

The *ifCategory* data property defines the category of the interface. It has six available enumerations - Mechanical, Electrical, Service, Communication, Other, and N/A (Not Available). Category is used to classify the role and purpose of the interface. Similarly *ifCategory* is used to categorise interface characteristics.

Interface characteristics formalise designations, variants, or configuration options defined in the interface standards. Examples of these are size, pneumatic supply configuration, fieldbus used, and accuracy. These characteristics are presented in two places - **IfStdCharacteristic** and **IfCharacteristic**. The difference between these two is that the former defines all values for the characteristic, which are directly coming from the standard, and the latter provide the value(s), which is(are) applicable for the interface implementation. The latter is also linked with the former through *hasParentIfStdCharacteristic* object property, that enables the name and description be given only in one place at **IfStdCharacteristic**. Both types of characteristics have three similar sorts of implementations - class, option, and property value. The interface class is used in cases where characteristic defines a finite set of predefined values, of which usually one is present in the implementation. Values can also be an ordered set, if they can be compared and set to growing order. Interface option is used in cases when there is an option, which is, or is not, present at the implementation of the interface. Only one value is bound to the option. The third is property value that is used to represent a range or a real number characterising the interface and its usage. Even the resource would have several instances of the same interface standard, but they are not sharing the same set of **IfCharacteristic**, a new **InterfaceDefinition** must be defined.

Every physical connection port (or interface) in the resource has its own **IfPortImplementation**. This defines every physical implementation of the **InterfaceDefinition**, having representation for the position and orientation of the interface in the spatial space. Additionally, it can define kinematics of the interface; matrix locations, which represent repetition of the interface such as a matrix of a threaded holes; and finally, it can refine more stricter force limits.

InterfacePurpose is used to group different interfaces and interface implementations by the overall purpose of the interface. There is a predefined set of general purposes, which are linked to interface definitions. This allows user to search for detailed interface implementations across different resources and interface standards fulfilling a specific intended purpose such as main mounting point, material transfer in, or tool interface.

Finally, a resource needs to state that it has an interface or interfaces. For example, a class **DeviceBlueprint** from the Resource Model ontology can do

this by assigning *hasInterface* object property linking it to an instance of *InterfaceDefinition*.

3 Interface Matchmaking

The interface matchmaking means in this case a process for finding out connectable and compatible production resources from the hardware interface point of view. This can be illustrated with a few use case scenarios, which utilise the Resource Interface ontology: (1) To find all resources, which can be connected with the selected resource; (2) To find all resources, which can be connected with one particular interface of the selected resource, instead of all interfaces; (3) To find all possible resource combinations, which are connectable together. This is generalised case of the first; and (4) To analyse if the connections in the proposed system layout are connectable also from the interface point of view. This has the similarities with the second case. In all previous four cases the matching can be done at two different levels of detail. The first, more coarse level (a), is to analyse only interface ID and the gender information. The second level (b) is finer and uses also the *IfCharacteristic* information and associated rules (*ifCompatibilityCheckOperator*). Section 3.1 focuses on the coarse level and Sect. 3.2 on the fine level.

3.1 Process for Comparing the Interfaces

SPARQL Protocol and RDF Query Language (SPARQL) is used to make queries to the Resource Interface ontology. At the moment these queries are executed manually with an ontology editor such as Protégé, but in the future a Software (SW) Application Program Interface (API) will be developed to run and process them in sequences, and to provide additional filtering of the results.

The following SPARQL query (Listing 1.1) is used as an example. It finds resources, which are connectable with resource X's interface Y, and query result is a listing of records of matching resources. Matching is done in this case at the coarse level i.e. using only the interface ID and gender information. Only values of X (on line 2) and Y (on line 3) are changed, when matching with another resource or interface, and the rest of the query remains the same. In the validation case, values could be: X = '*Manipulator_2-axis*' and Y = '*ISO 29262*'. Similar SPARQL queries are prepared for finding answers for other scenarios, mentioned in the beginning of the chapter.

```

1 SELECT ?fromMO ?fromIF ?fromGender ?toGender ?toIF ?toMO ?
   fromIFStdCode WHERE {
2 ?fromMO rdfs:label 'X' .
3 FILTER regex(?fromIFStdCode, 'Y', "") .
4 ?fromMO a rim:TempDeviceBlueprint ;
5   rim:hasInterface ?fromIF .
6 ?fromIF rim:implementsStd ?fromIFStd ;
7   rim:ifGender ?fromGender .

```



```

8 ?fromIFStd rim:stdCodeFull ?fromIFStdCode .
9 ?toIFStd rim:stdCodeFull ?fromIFStdCode .
10 ?toIF rim:implementsStd ?toIFStd .
11 bind(xsd:string(if(?fromGender='NEUTRAL','NEUTRAL',xsd:
    string(if(?fromGender='MALE','FEMALE','MALE'))))
    as ?toGender) .
12 ?toIF rim:ifGender ?toGender .
13 ?toMO rim:hasInterface ?toIF .
14 FILTER (?fromMO != ?toMO) . }

```

Listing 1.1. SPARQL example finding interface matches with resource X's interface Y

Listing 1.1 works as following: Line 1 starts the SPARQL query and defines what information is shown on the resulting records. Line 2 selects the named resource as a focus module (from). Line 3 uses regular expressions to look for the specific interface standard. Lines 4..8 find and select the resource(s), which are used as focus modules for the matching. Also its interface is found out. Lines 9..10 look for counter part resources implementing the same interface standard. Line 11 defines which gender is accepted for the counterpart, and lines 12..13 find and select such resources as targets (to). Finally, line 14 filters out the records connecting the focus module to itself.

3.2 Rules for Interface Characteristics

The finer level interface matching needs further information from the interface implementation, and the choices made by the resource provider. The concept of interface characteristic provides this additional information. It provides not only the IDs and values of the characteristic, but also a compatibility operator that defines how these values must relate against each other in case of a positive match. The two resources are connectable at finer level, if and only if all (mandatory) *IfCharacteristics* of an interface provide a positive match.

Each of the *IfCharacteristic* has one *ifCompatibilityCheckOperator*. This operator specifies how the values from the source resource are compared with the target resource. Table 1 defines these twelve different interface compatibility operators, and for which kind of *IfCharacteristic* types a compatibility operator can be assigned to. A mathematical formulation of the compatibility operator is represented at the end of the description.

The three *IfCharacteristic* types are source set, ordered set, and value. In case of Source set (S), values of the *IfCharacteristic* at source resource's side are compared with Target set (T), i.e. remote resource's corresponding values, according to the corresponding compatibility operator.

In case of 'Ordered set' type of *IfCharacteristics* (column Type has O in Table 1) it applies: There exist an ordered set (OS), where $OS = \{a_1, \dots, a_i, a_j, \dots, a_n\} \wedge a_i < a_j$. This set is actually defined by the interface standard and stored in *IfStdCharacteristic*. For target set (T) applies $\forall y : y \in T \wedge T \subset OS \wedge y \in OS$.

Table 1. Compatibility operators with descriptions and which interface characteristic types the operator is applicable for

Type	Compatibility Operator	Description
S,O,V	SAME.SET	The source and the target contain exactly the same set of values (or a value or a range). $\forall x : x \in S \wedge x \in T \wedge S = T$
S,O	ALL_FROM.SET	All items in the source set can be found from the target set. $\forall x : x \in S \wedge S \subseteq T$
S,O	ANY_FROM.SET	Any item(s) of the source set can be found from the target set. $\exists x : x \in S \wedge x \in T$
S,O	ONE_FROM.SET	Exactly one item from the source set can be found from the target set. Size of target set is one. $\exists x : x \in S \wedge x = T \wedge T \subset S$
O	LOWER_OR_EQUAL	Standard defines an ordered set of values. Source value is lower or equal than the target value. $\forall x : x \in S \wedge S \subset OS \wedge x \in OS \wedge x \leq y$
O	HIGHER_OR_EQUAL	Standard defines an ordered set of values. Source value is higher or equal than the target value. $\forall x : x \in S \wedge S \subset OS \wedge x \in OS \wedge x \geq y$
V	INSIDE_RANGE	Source value or range is inside the target range. $S = [a, b] \wedge a \leq b \wedge a \geq t_{min} \wedge b \leq t_{max}$
V	PART_OF_RANGE	There is an overlap between the source range (or value) and the target range (or value). $S = [a, b] \wedge a \leq b \wedge a \leq t_{max} \wedge b \geq t_{min}$
V	PART_OF_RANGE_OR_LOWER	The source range (or value) is lower than the target range (or value) or there is an overlap. $S = [a, b] \wedge a \leq b \wedge b \leq t_{max}$
V	PART_OF_RANGE_OR_HIGHER	The source range (or value) is higher than the target range (or value) or there is an overlap. $S = [a, b] \wedge a \leq b \wedge a \geq t_{min}$
V	CAPTURES_RANGE	The source range (or value) captures completely the target range (or value). $S = [a, b] \wedge a \leq b \wedge a \leq t_{min} \wedge b \geq t_{max}$
-	NO_RULE	No compatibility operator is defined for IfCharacteristic

Legend: Type of **IfCharacteristic** values { S = Set, O = Ordered Set, V = Value }

In case of ‘Value’ type of **IfCharacteristics** (column Type has V in Table 1) it applies: The target set (T) is defined such as $T = [t_{min}, t_{max}]$. Source set (S) is a range ($[a, b]$) or a single value ($a = b$).

4 Test Cases for Interface Matchmaking

The developed Resource Interface ontology is validated with a test ontology containing some representative resources. Table 2 shows these resources, which interface standard they implement, and at which gender. If the interface standard has some characteristics, these are illustrated with applied characteristic values and compatibility operator. These are discussed in the following.

Looking for a Pair for a Specific Resource – Coarse. Scenario 1.a. Various resources from Table 2 are used as parent resource, and in all cases, the exactly expected list of counter resources is found. I.e. ‘Manipulator_2-axis’ connects with all grippers, ‘BoringChuck’ with all drills, and a drill bit with ‘BoringChuck’ and ‘FingerGripper2’.

Looking for a Pair for a Specific Resource and its Particular Interface – Coarse. Scenario 2.a. Listing 1.1 is used as SPARQL query. This works as the previous one, but focuses only on one interface and provides only those matches as results.

Table 2. Resources and their interfaces in the test ontology

Resource	Interface standard	Gender	Characteristics	Comp. Operator
basePlate	PROP.BasePlate. Grooved	N	-	-
Manipulator_2-axis	ISO 29262:2011	F	Size = 20 Service = PP Service = PV	SAME_SET ANY_FROM_SET ANY_FROM_SET
	PROP.RobotBase	N	-	-
FingerGripper1	ISO 29262:2011	M	Size = 20 Service = PV	SAME_SET ANY_FROM_SET
	PROP.GripperTCP	F	-	-
FingerGripper2	ISO 29262:2011	M	Size = 25 Service = PV	SAME_SET ANY_FROM_SET
	PROP.GripperTCP	F	-	-
	SHAPE.CYLINDER	F	Diameter = [5.0, 20.0] Holding length = [5.0, 40.0]	CAPTURES_RANGE PART_OF_RANGE
FingerGripper3	ISO 29262:2011	M	Size = 25 Service = PV	SAME_SET ANY_FROM_SET
	PROP.GripperTCP	F	-	-
BoringChuck	SHAPE.CYLINDER	F	Diameter = [3.0, 16.0] Holding length = [20.0, 80.0]	CAPTURES_RANGE PART_OF_RANGE
DrillBit_1mm	SHAPE.CYLINDER	M	Diameter = 1.0 Holding length = [10.0, 30.0]	INSIDE_RANGE PART_OF_RANGE
DrillBit_12mm	SHAPE.CYLINDER	M	Diameter = 12.0 Holding length = [30.0, 70.0]	INSIDE_RANGE PART_OF_RANGE

Legend: Gender {N=Neutral, M=Male, F=Female}
 service values: {PP=Pressure-Pressure, PV=Pressure-Vacuum}

Looking for a Pair for a Specific Resource and its Particular Interface. Taking Into Account Interface Properties – Fine. Scenario 2.b. Some tested queries are ‘DrillBit_1mm’ & ‘CYLINDER’; ‘DrillBit_12mm’ & ‘CYL’; and ‘Manipulator_2-axis’ & ‘ISO 29262’. The first query does not have any matches – as expected, because the drill’s diameter is so small. The second found both ‘BoringChuck’ and ‘FingerGripper2’, with a total of four records, as all given drill bit characteristics match in this case. The result is also as expected. The third provides as a result four records – all three grippers in case of *IfCharacteristic* = ‘service’, but only ‘FingerGripper1’ in case of *IfCharacteristic* = ‘size’. Thus, some additional filtering of results is needed to judge that from these only ‘FingerGripper1’ can be connected from the interface matching point of view. This is because it is the only one conforming to all the characteristics requirements from the manipulator side. Therefore, this use case requires additional SW application to execute several SPARQL queries and filter out the final result of the interface match.

Looking for Pairing Resources from a Larger Set of Resource – Coarse. Scenario 3.a Scenario works and provides results. However, the result has every match listed twice, having each resource presented both as focus and target module. Further filtering of the result is needed.

5 Discussion and Conclusions

This paper represents the developed Resource Interface ontology and how it can be utilised for hardware interface matchmaking. In case of the interface matchmaking, the paper limits only to the proof of concept. Four test cases were defined and corresponding SPARQL queries were developed. These queries were run in our small test ontology, and they were able to sort out from the ontology the results indicating which resources are connectable together. However, the results show that further filtering and processing of the results is needed. As future work, the authors will prepare an API for getting the parametric inputs for the queries, running multiple queries in sequence, and further filtering and purifying the results.

The Resource Interface ontology will be complementing our Resource Description concept by collecting together a snippet of information from several RDs, and offering more powerful search abilities over the information. Especially important are the links where information from different resources comes together. RD remains as comprehensive information container focusing a single resource.

The proposed concept was successfully applied and it found out resources with the matching interfaces. This makes it possible to search easily, fast, and automatically for resources, which can be connected physically, from large resource catalogues. This will support system integrators and end users during system design and reconfiguration, to find out faster the working system configurations.

Acknowledgements. This research has received funding from the European Union's Horizon 2020 research and innovation programme under grant agreement No. 680759 [7].




References

1. Koren, Y., Shpitalni, M.: Design of reconfigurable manufacturing systems. *J. Manuf. Syst.* **29**(4), 130–141 (2010)
2. Wiendahl, H.-P., et al.: Changeable manufacturing - classification, design and operation. *CIRP Ann.* **56**, 783–809 (2007)
3. Rahimifard, A., Weston, R.H.: A resource-based modelling approach to support responsive manufacturing systems. *Int. J. Adv. Manuf. Technol.* **45**, 1197–1214 (2009)
4. Westkämper, E.: Factory transformability: adapting the structures of manufacturing. In: Dashchenko, A.I. (ed.) *Reconfigurable Manufacturing Systems and Transformable Factories*, pp. 371–381. Springer, Berlin (2006). https://doi.org/10.1007/3-540-29397-3_19
5. EUPASS - Evolvable Ultra-Precision Assembly SystemS - project. EU FP6, GA No 507978 (2006). http://cordis.europa.eu/project/rcn/75342_en.html. Accessed 30 Oct 2017

6. Ferreira, P., Lohse, N., Ratchev, S.: Multi-agent architecture for reconfiguration of precision modular assembly systems. In: Ratchev, S. (ed.) IPAS 2010. IAICT, vol. 315, pp. 247–254. Springer, Heidelberg (2010). https://doi.org/10.1007/978-3-642-11598-1_29
7. ReCaM - Rapid reconfiguration of flexible production systems through capability-based adaptation, auto-configuration, integrated tools for production planning - project. EU Horizon 2020, GA No 680759 (2017). <http://www.recam-project.eu/>. Accessed 30 Oct 2017
8. Ameri, F., Urbanovsky, C., McArthur, C.: A systematic approach to developing ontologies for manufacturing service modeling. In: 2012 Proceedings of the Workshop on Ontology and Semantic Web for Manufacturing, 14 p. (2012)
9. Borgo, S., Leitão, P.: Foundations for a core ontology of manufacturing. In: Sharman, R., Kishore, R., Ramesh, R. (eds.) Ontologies. ISIS, vol. 14, pp. 751–775. Springer, Boston (2007). https://doi.org/10.1007/978-0-387-37022-4_27
10. Strzelczak, S.: Towards ontology-aided manufacturing and supply chain management – a literature review. In: Umeda, S., Nakano, M., Mizuyama, H., Hibino, H., Kiritsis, D., von C, G. (eds.) APMS 2015. IAICT, vol. 460, pp. 467–475. Springer, Cham (2015). https://doi.org/10.1007/978-3-319-22759-7_54
11. Terkaj, W., Urgo, M.: Virtual factory data model to support performance evaluation of production systems. In: CEUR Workshop Proceedings, vol. 886, pp. 44–58 (2012)
12. Järvenpää, E., Siltala, N., Hylli, O., Lanz, M.: Capability matchmaking procedure to support rapid configuration and re-configuration of production systems. *Procedia Manuf.* **11**, 1053–1060 (2017)
13. Järvenpää, E., Siltala, N., Lanz, M.: Formal resource and capability descriptions supporting rapid reconfiguration of assembly systems. In: 2016 IEEE International Symposium on Assembly and Manufacturing (ISAM), pp. 120–125. IEEE (2016)
14. Siltala, N.: Formal digital description of production equipment modules for supporting system design and deployment. Ph.D. dissertation, Tampere University of Technology (2016). <http://urn.fi/URN:ISBN:978-952-15-3783-7>
15. Siltala, N., Järvenpää, E., Lanz, M.: Formal information model for representing production resources. In: Nääs, I., et al. (eds.) APMS 2016. IAICT, vol. 488, pp. 53–60. Springer, Cham (2016). https://doi.org/10.1007/978-3-319-51133-7_7



Functional Modelling in Evolvable Assembly Systems

David Sanderson¹(✉) , Jack C. Chaplin² , and Svetan Ratchev² 

¹ Centre for Aerospace Manufacturing, University of Nottingham, Easter Park, Nottingham NG7 2PX, UK

david.sanderson@nottingham.ac.uk

² Institute for Advanced Manufacturing, Advanced Manufacturing Building, Jubilee Campus, University of Nottingham, Nottingham NG7 2GX, UK
 {jack.chaplin, svetan.ratchev}@nottingham.ac.uk

Abstract. The design and reconfiguration of adaptive production systems is a key driver in modern advanced manufacturing. We summarise the use of an approach from the field of functional modelling to capture the function, behaviour, and structure of a system. This model is an integral part of the Evolvable Assembly Systems architecture, allowing the system to adapt its behaviour in response to changing product requirements. The integrated approach is illustrated with an example taken from a real EAS instantiation.

Keywords: Architecture · Evolvable assembly systems · Functional modelling
 Multi-agent systems

1 Introduction

The manufacturing industry as a whole is facing increased market unpredictability and labour costs, as well as growing consumer demand for highly personalised goods and services with a shorter time to market and increased product diversity [1]. In order to incorporate these changes, manufacturing systems have begun to take advantage of adaptive control for flexibility, resilience, and monitoring. Manufacturing companies in many sectors are therefore investigating smart, flexible, and adaptive manufacturing lines that can autonomously self-heal, self-adapt, and reconfigure in response to changing product requirements. This is typified by the ‘batch-size-of-one’ problem, wherein each product may be unique and the manufacturing system must be capable of carrying out different production processes as required by the current product.

A common approach to these problems is that of cyber-physical systems [2], often implemented as a multi-agent system [3]. One such implementation is that of the Evolvable Assembly Systems project [4] (EAS). The EAS project addresses the challenges of design and modelling of such systems with a behavioural framework based on functional modelling. This is embedded in a multi-agent cyber-physical systems architecture, allowing the system structure and behaviour to be related to intended system function, drawing on the Function-Behaviour-Structure (FBS) formalisms of Gero, Rosenman, Umeda, and others [5–11]. This provides the capability

for the system to identify when the requirement to reconfigure is triggered, and then “design the change” that implements the reconfiguration.

2 Functional Modelling and the Behavioural Approach

The modelling, design, and integration of assembly systems is primarily based on process requirements. This requires that the capabilities of a production resource are captured and can be reasoned about. There are two main ways of capturing the capabilities of a production resource: by considering the processes that the resource can perform, and by considering how their structure and behaviour relate to their intended functions. We take the second approach, based on the Function-Behaviour-Structure (FBS) formalisations developed by Gero, Rosenman, Umeda, and others in the field of functional modelling [5–11] that separate the objective structure of a system from its subjective function, and the different behaviours related to each of those. The general behavioural approach derived from functional modelling is shown in Fig. 1.

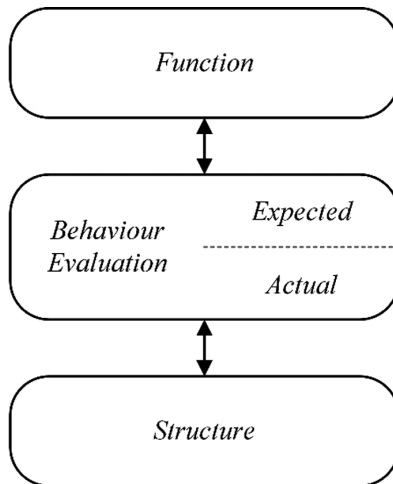


Fig. 1. Overview of the functional modelling behavioural approach

We therefore define **Function** as an abstraction of behaviour for a specific use or purpose, **Behaviour** as state transitions from input to output, and **Structure** as the physical model of the system and subsystem, and the connections between them. Describing a system in such a function-based manner allows for a decomposition to be performed for each of the various uses required at any given time. Applying this to modular and reconfigurable manufacturing systems requires the decomposition to be guided by the available modules [12, 13]. With this in mind, we can define **Function**, **Behaviour**, and **Structure** in the context of an EAS.

In any assembly system, the system **Function** is primarily to assemble a given product. Evolvable Assembly Systems however, are flexible, reconfigurable, self-

adaptive systems. This leads to a set of functions to enable that adaptivity. In any manufacturing context, there is also always a set of requirements for quality. We can therefore say that the Functions of an EAS are divided into those relating to the *product requirements*, those relating to the *adaptation requirements*, and those relating to *quality requirements*.

When discussing **Behaviour**, the most important concept is to distinguish between the *expected* behaviour required by the system Function, and the *structural* behaviour expressed by the system Structure. For each of these, there are many kinds of behaviour in the system. The behaviour type covered by previous work on FBS models could be described as *non-adaptive behaviour*. This describes the steady-state production processes carried out by the assembly system, and is often a simple sequence of actions. As we are dealing with an adaptive system, we must account both for behaviours that are *adaptive processes*, and for those that handle the *reconfiguration* of the system.

As a modular, flexible, reconfigurable manufacturing system, an EAS is a complex, context-aware, collective adaptive system of systems [14]. As such, the **Structure** of the system is composed of components, *modules*, or sub-systems, the *connections* between them, and the *state* of the system. As the structure of the system may change over time – in response to adding, removing, or re-arranging components – the system structure can be optionally divided into *configurations* from which the system can select.

The concept of system **Views** is included to formalise the requirement to describe only the aspects of a system that are relevant to the task at hand [8, 9, 15]. In existing design literature, this is included to ensure that (for example) the permittivity of light of a material is only considered if it is relevant to its purpose. In our case, we can consider the system from a variety of Views, for example focussing on process capabilities when checking for manufacturability, or focussing on the topology and connections of the system where layout is important. This allows the framework to be applied at the correct level of abstraction and complexity for each specific application.

3 Evolvable Assembly Systems

The behavioural framework described in Sect. 2 is at the core of the Evolvable Assembly Systems approach. The required set of functions is used to determine the behaviours that are expected to fulfil those functions. The structure of the system is then designed, and the actual behaviour expressed by that structure is compared to the expected behaviour. The algorithmic basis for this process of distributed behavioural evaluation is described in more detail in [16].

Each resource in the system consists of some structure and corresponding behaviour(s). Some resources also have multiple configurations. These are managed by an intelligent agent; all agents in the system communicate with each other to provide distributed control based on a joint system model that provides both operational data, and the coordination for the distributed behavioural evaluation.

3.1 Multi-agent Architecture

An agent-oriented view of the EAS architecture is shown in Fig. 2. Each resource in the system is controlled at a high level by an intelligent agent – an encapsulated piece of software that makes control decisions based on available information. EAS uses the Beliefs-Desires-Intentions agent paradigm [18], so this information is stored as beliefs, and translated into immediate intentions (plans) in order to accomplish long-term desires (goals). The intentions of the agent are executed through behaviour in the system, based on the behaviours that can be expressed by the structure of the resource that is being controlled.

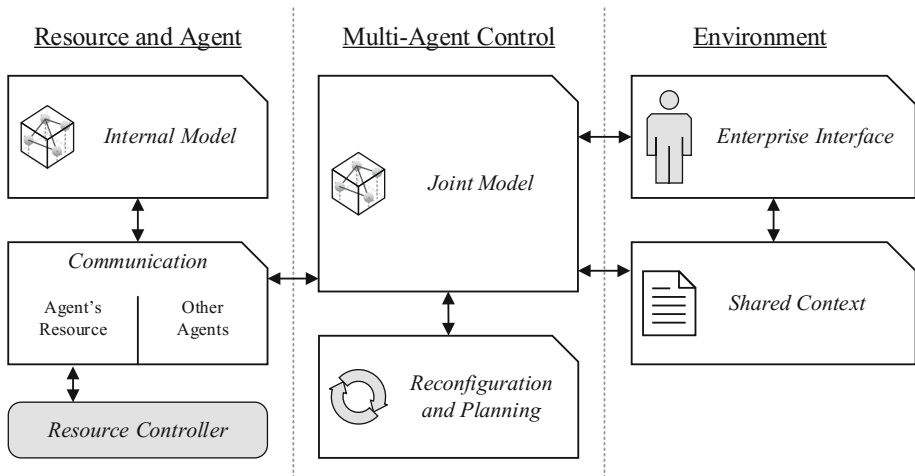


Fig. 2. An agent-oriented view of EAS architecture

Each resource in the system can be defined as a set of structures and associated behaviours using Business to Manufacturing Markup Language (B2MML) based on the ISA-95 standard [17, 18]. To enable an agent to control a resource, this description is used to generate an interface. This interface connects the agent with the PLC, controller, or similar that provides the low-level control for the resource hardware. This interface layer allows the agent core to remain the same whilst still providing control for a variety of hardware archetypes.

3.2 Shared Context

Although each agent is responsible for local control of the resource it is attached to, the collection of agents provide a distributed agent control layer for the whole production system. Communication between these agents is based on the ubiquitous sharing of contextual information.

This contextual information covers all aspects of the system. At the most fundamental level, it describes the product that is to be produced by the system, and the production capabilities of each resource in the system, as well as any “joint capabilities” resulting from combinations of resources. This is further enhanced by information

about the state of the product and system, for example the pose of a robot arm, the location of a pallet, or relevant metrology data. The context also provides a link between the EAS control system and the rest of the enterprise in which it is situated. This may include control systems for other assembly cells, or higher-level enterprise information systems. All of this information is stored in a context layer that is accessible to all agents as required. This shared context is implemented using a publish-subscribe data distribution service [19].

4 Implementation Example

This system has been implemented in a real precision assembly demonstrator (PAD, shown in Fig. 3) at the University of Nottingham. The demonstrator is designed to assemble interior hinges from the automotive industry. Each product is defined by a recipe file that indicates the *détente* force – achieved by the configuration of ball-spring pairs added to the hinge. Because each hinge produced by the system could be unique, these recipe files are a way to formalise the batch-size of one requirements in the system.



Fig. 3. The precision assembly demonstrator (PAD)

The demonstrator consists of two KUKA KR5 sixx R650 robots alongside a testing station with visual inspection and force testing equipment, connected via a linear shuttle system. Each robot has an individual working area, as does the testing station. The robots share a tool rack, giving them each access to a variety of different end effectors via an automatic tool changer. The whole system is accessible via a part loading station, where pallets of unassembled parts are loaded, and pallets with

In order to assemble the hinges, each subsystem has a number of behaviours as described in Table 2. The robots have the following pick and place behaviours: move the pallet between the shuttle system and the workspace; change end effector; match the hinge leaves; insert the hinge pin; insert a variable number of springs; insert a variable number of balls; insert the cap. The testing station has pick and place behaviours to move the product between the shuttle system and the workspace, as well as a force testing behaviour to test the détente force, and a vision testing behaviour to ensure the product is correctly assembled. The shuttle system has only one behaviour: moving from one station to another. The loading station and operator can only load parts into the system and remove parts from the system.

These behaviours are then utilised by the agent controlling the relevant resource in order to produce the product specified by the recipe file – that is, accomplish the required function inherent in the new product. Each agent may further be able to adapt some or all of the structure of its resource. In the case of our example, the shared tool rack provides a selection of end effectors. The selection of a new end effector changes both the structure and behaviour of the resource.

As the “loading station” behaviours are carried out by an operator, they are logically part of the system but do not have to be programmed into an agent – the operator only needs some way to tell the rest of the system what behaviour has been carried out.

Table 2. Behaviours available to each production module in the PAD

Module	Behaviour	Sub-behaviour (optional)	Behaviour type	
Linear shuttle	Move	To [<i>location</i>]	Adaptive	
Loading station	Load pallet		Non-adaptive	
	Unload pallet		Non-adaptive	
Robot 1 & 2	Move pallet	Shuttle → workspace	Non-adaptive	
		Workspace → shuttle	Non-adaptive	
	Change end effector	[<i>Various end effectors</i>]	Reconfiguration	
	Match hinge leaves		Adaptive	
	Insert hinge pin		Adaptive	
	Insert springs	[<i>Variable number</i>]	Adaptive	
	Insert balls	[<i>Variable number</i>]	Adaptive	
	Insert cap		Adaptive	
	Tool rack	Provide end effector		Reconfiguration
		Receive end effector		Reconfiguration
Testing station	Move pallet	Shuttle → workspace	Non-adaptive	
		Workspace → shuttle	Non-adaptive	
	Force test	[<i>Variable force</i>]	Adaptive	
	Vision test		Adaptive	

In addition to the behaviours available to each physical production module, there are a number of behaviours available to the distributed agent control layer. These behaviours are not linked to any specific production resource; they allow the system to adapt and reconfigure its own function, behaviour, and structure from a top-level.

One example of such a behaviour is reconfiguration of the control flow in response to the removal of a production module. Although the system is designed to allow the work to be shared between both robots, as the robots are identical and share a tool rack, the work can be done by a single robot. In this way, the system can select between the single robot configuration and the dual robot configuration and re-plan the sequence of production behaviours accordingly.

5 Summary and Acknowledgements

This paper has described the agent-oriented architecture of Evolvable Assembly Systems in the context of the FBS approach from function modelling. This approach allows the system to accurately model the adaptive structure and behaviour of the system, and leverage them to achieve the system functions required by the changing product requirements of a batch-size of one scenario. This approach has been demonstrated on a real demonstration cell at the University of Nottingham.

The authors gratefully acknowledge the support provided by UK EPSRC Evolvable Assembly Systems (EP/K018205/1).

References

1. Kagermann, H., Helbig, J., Hellinger, A., Wahlster, W.: Recommendations for implementing the strategic initiative INDUSTRIE 4.0: securing the future of German manufacturing industry, Final Report of the Industrie 4.0 Working Group (2013)
2. Monostori, L.: Cyber-physical production Systems: roots, expectations and R&D challenges. *Procedia CIRP* **17**, 9–13 (2014)
3. Wooldridge, M., Jennings, N.R.: Intelligent agents: theory and practice. *Knowl. Eng. Rev.* **10**, 115–152 (1995)
4. Chaplin, J.C., et al.: Evolvable assembly systems: a distributed architecture for intelligent manufacturing. *IFAC-PapersOnLine* **48**, 2065–2070 (2015)
5. Gero, J.S.: Design prototypes: a knowledge representation schema for design. *AI Mag.* **11**, 26–36 (1990)
6. Gero, J.S., Kannengiesser, U.: A function–behavior–structure ontology of processes. *AI EDAM Artif. Intell. Eng. Des. Anal. Manuf.* **21**, 379–391 (2007)
7. Rosenman, M., Gero, J.: Purpose and function in design: from the socio-cultural to the techno-physical. *Des. Stud.* **19**, 161–186 (1998)
8. Umeda, Y., Takeda, H., Tomiyama, T., Yoshikawa, H.: Function, behaviour, and structure. In: *Applications of Artificial Intelligence in Engineering V*, pp. 177–193 (1990)
9. Umeda, Y., Ishii, M., Yoshioka, M., Shimomura, Y., Tomiyama, T.: Supporting conceptual design based on the function-behavior-state modeler. *Artif. Intell. Eng. Des. Anal. Manuf.* **10**, 275–288 (1996)
10. Sasajima, M., Kitamura, Y.: FBRL: a function and behavior representation language. In: *Proceedings of the 14th International Joint Conferences on Artificial Intelligence (IJCAI)*, pp. 1830–1836 (1995)
11. Mizoguchi, R., Kitamura, Y.: Foundation of knowledge systematization: role of ontological engineering. In: Roy, R. (ed.) *Industrial Knowledge Management*, pp. 17–36. Springer, London (2001). https://doi.org/10.1007/978-1-4471-0351-6_2

12. Koren, Y., et al.: Reconfigurable manufacturing systems. *CIRP Ann. - Manuf. Technol.* **48**, 527–540 (1999)
13. Koren, Y.: Reconfigurable manufacturing and beyond. In: *CIRP 3rd International Conference on Reconfigurable Manufacturing* (2005)
14. Sanderson, D., et al.: Advanced manufacturing: an industrial application for collective adaptive systems. In: *2015 IEEE International Conference on Self-Adaptive and Self-Organizing Systems Workshops*, pp. 61–67. IEEE (2015)
15. Gero, J.S., Kannengiesser, U.: Function-behaviour-structure: a model for social situated agents. In: *Workshop on Cognitive Modeling of Agents and Multi-Agent Interactions, International Joint Conference on Artificial Intelligence*. pp. 101–107 (2003)
16. De Silva, L., Felli, P., Chaplin, J.C., Logan, B., Sanderson, D., Ratchev, S.: Synthesising industry-standard manufacturing process controllers. In: *Proceedings of the 16th Conference on Autonomous Agents and MultiAgent Systems*, pp. 1811–1813. International Foundation for Autonomous Agents and Multiagent Systems (2017)
17. Business to Manufacturing Markup Language Operations Schedule Version 6.0. <https://services.mesa.org/ResourceLibrary>
18. ANSI/ISA-95, Enterprise-Control System Integration, Parts 1–5. <https://www.isa.org/standards-publications/>
19. Data Distribution Service. <http://www.omg.org/spec/DDS/Current>



Production and Maintenance Scheduling Supported by Genetic Algorithms

Duarte Alemão^(✉), Mafalda Parreira-Rocha, and José Barata

UNINOVA, CTS, Faculdade de Ciências e Tecnologias,
NOVA University of Lisbon, Caparica, Portugal
{d.alemao, mafalda.rocha, jab}@uninova.pt

Abstract. The market demand has changed in recent years due to increased interest in more customized and diversified products by the consumers, leading to a change in production lines, which are becoming more flexible and dynamic. At the same time, the amount of data available in the factories is growing more and more, thereby the number of errors in the production schedule may occur often. Several approaches have been used over time to plan and schedule the shop-floor production. However, some only consider static environments, where the tasks are allocated to the machines, not considering that machines may not be available and sometimes maintenance interventions are needed. The introduction of maintenance increases the scheduling complexity and makes it harder to allocate the tasks efficiently. So, new solutions have been proposed, giving manufacturing systems the ability to quickly adapt to some disturbances that may occur. Thus, Artificial Intelligence approaches have been adopted to do the task allocation for the shop-floor. Those approaches can find suitable solutions faster than traditional approaches. This article proposes an architecture, based on Genetic Algorithm, capable of generating schedules including both production and maintenance tasks.

Keywords: Dynamic job-shop scheduling · Maintenance task allocation
Genetic algorithms · Manufacturing systems

1 Introduction

Nowadays market demands for more diversified and customized products are forcing factories to change from mass production standard systems to more dynamic and agile shop-floor systems. This change grants factories the ability to reconfigure and quickly adapt to market requirements. However, factories have several types of machines, each one with their own specific technical features, which can execute different tasks, located in different places of the factory, instead of a straightforward production line system. This fact makes the task allocation process more complex since the products do not follow all the same path anymore. Furthermore, it is most of the times a prerequisite from companies that machines should be kept working as much time as possible to maximize the production and consequently the income. Nevertheless, sometimes those machines need to be subject to maintenance operations, to keep them producing high-quality products. To create a more reliable schedule, those maintenance operations

should be defined along with the production operations. To cope with the presented difficulties this article proposes a solution based on Genetic Algorithm (GA), which aims to solve the task allocation problem in a job-shop, known as Job-Shop Scheduling Problem (JSSP). It includes both production and maintenance tasks in the same schedule with the objective of minimizing the total execution time in the shop-floor. Thus, a more reliable schedule of the factory is available, which should decrease the delays and the unexpected number of fails in the shop-floor. The architecture was designed to generate schedules based on the existing tasks and stations available on the shop-floor.

The proposed paper is organized as followed. Section 1 introduces an overview of the document. Subsequently in Sect. 2 the concept of scheduling and the importance of maintenance task allocation in Agile Manufacturing Systems is depicted, followed by the solution description in Sect. 3. Section 4 presents the systems execution environment, with a brief explanation of how it works. Finally, Sect. 5 presents the solution analysis and the further developments.

2 Related Work

The manufacturing industry is subject to market requirements, which are constantly changing. This change is imposed by consumers' demand for more customizable and unique products and their variants. So, the manufacturing processes needed to change as well. To produce this wide variety of products demanded by many consumers, the factories need to adapt quickly to market requirements [1]. Thus, to provide a fast and efficient response to the market demand, manufacturing systems need to be agile, which is the ability to survive and prosper in competitive markets and environments of change [2]. In that way, it is important to have an efficient planning of the shop-floor. Namely, it is necessary to allocate products to machines in the shop-floor, as well as maintenance interventions. They are needed to keep machines working without causing defects on products, which are reflected in cost for the company. By scheduling maintenance operations, some unpredictable failures may be avoided, such as machine breakdowns.

Reflecting this, in Agile Manufacturing Systems (AMS) a large variety of machines with specific requisites need to stay functional as many time as possible to maximize the production. However, sometimes, they need to be the subjected to maintenance operations to deliver high-quality products. There are different maintenance types, which can be mainly divided into Corrective Maintenance (CM), Time-Based Maintenance (TBM) and Predictive Maintenance (PdM). CM is applied after a failure occurs, such as a machine breakdown, and tries to recover the resource to its functional state [3, 4]. TBM is applied to prevent, in advance, potential failures and it is taken while the system is still working, at predefined time intervals [3, 4]. Finally, PdM can be applied to prevent future failures when there is a deteriorating physical parameter, such as pressure or voltage, that can be measured instead of doing it in predefined intervals [5]. It infers the current state of a machine and predicts the future progression to estimate the time before a failure occur [6]. Based on that information it is possible to define an appropriate schedule for a production system, including maintenance tasks.

Scheduling is the process of time optimization, where the time of a set of tasks (jobs) performed on a product is assigned to the available time of a group of stations [7, 8]. It defines the sequence by each job is executed on a machine during a predefined time horizon, trying to avoid overlaps and to optimize some objectives [7]. The JSSP is a Non-deterministic Polynomial-time Hard (NP-Hard), which means they are quite difficult to solve using traditional optimization techniques [9]. Although mathematical optimization methods can achieve the optimal solution for small problems, for large-scale problems those optimization techniques are very limited [10]. Besides that, manufacturing systems are very dynamic, meaning new products frequently arriving, inconstant job durations and machines that are not always available, which represented the need for more dynamic approaches. Thus, many researchers have concentrated their efforts on heuristic approaches, such as Tabu Search, Simulated Annealing, Ant Colony Optimization, Particle Swarm Optimization, Neural Network and Genetic Algorithm (GA). The interest in GA has grown in the past years due to its high flexibility to adapt to different problems, to find near-optimal solutions and because it is easy to handle.

3 Dynamic Scheduling Solution

In this section, an overview of the scheduling tool architecture is presented and described. The proposed scheduling architecture is capable of generating schedules including both production and maintenance tasks, which are allocated to different production stations.

3.1 System Overview

The scheduling tool architecture was designed to generate a schedule to the shop-floor including production and maintenance tasks in a given time horizon. Those tasks are allocated to the available stations in empty time spaces, in order to get the minimum total execution time (makespan) within the established time horizon. The scheduling tool interacts with another tools as well as the shop-floor in order to acquire the necessary data to generate the schedules. Thus, the scheduling tool can access the information about the available stations and the tasks to allocate. The scheduling architecture is represented in Fig. 1.

The scheduling collects the information about the available stations in the shop-floor and the tasks to be allocated. Then, using a GA, it is possible to allocate those operations to each station, i.e. to set the start and end times of each task, in the empty spaces, avoiding the overlapping between tasks in the same station or tasks of the same product. After that, is possible to determine the execution time of each station and get the station with the higher makespan value, which represents the minimum makespan found in that process. The collection of schedules, containing a schedule for each station, is then stored.

The shop-floor provides the topology of the factory, i.e. the present stations and human operators to perform the maintenance tasks. The production tasks are provided by the management unit. It provides the information about each task and the time horizon window in which the schedule should be performed. The maintenance section

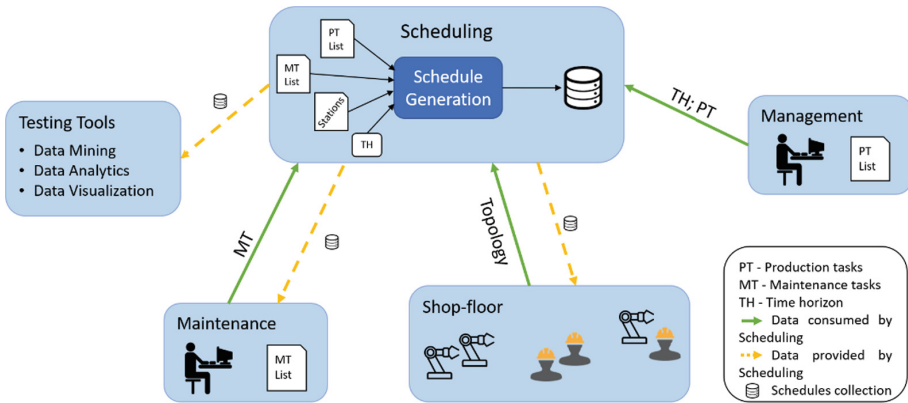


Fig. 1. System interactions overview

is responsible for providing the maintenance tasks, based on the operator's knowledge or by analysis methods, such as data mining. After generating the necessary schedules, those are sent to the shop-floor, so the operators know the schedule of each station, to the maintenance unit and to other tools for analysis and testing purposes.

To generate a schedule, it is necessary to allocate the tasks efficiently to obtain a feasible and valid schedule, i.e. respecting some rules such as avoiding that a station is operating more than one task at the same time or preventing a product from being present in different machines at the same time. A GA architecture is proposed in this paper to solve this JSSP since it is a combinatorial problem.

3.2 Scheduling Algorithm

The scheduling tool was designed using GA. It is a stochastic searching adaptive approach to solve optimization problems based on natural selection mechanisms, first proposed by Holland [11]. GA allows to evolve a population of chromosomes (solutions) through a predefined number of generations and gets the best one that represents the best schedule found by the algorithm [10]. First, a random population is initialized based on the first chromosome created. Then, the fitness value of each individual is calculated. If a stop condition is reached, such as the predefined number of generations to evolve or a threshold fitness value, the process is finished, otherwise, it continues to the next generation. After that, the elite population, i.e. the best chromosomes present in the previous generation, is selected to be present in the current generation. Then, the selection process is done, and the selected individuals are matched with each other. Next, the mutation is applied in some individuals to provide some diversity in the population. Finally, the fitness value of each one is again calculated and the process is repeated till the termination criterion is reached [10, 12].

GA is known to be good solving optimization problems since it does not need to evaluate all the search space to extract a good solution. However, it not always can find an optimal solution but finds a near-optimal solution the most of the times [13].

The most important step in a GA is to define what is a chromosome. The representation of a chromosome influences the performance of the algorithm. In this problem, the chromosome represents the sequence of jobs assigned to each station, containing the times between which each task will be performed. It is a schedule solution for the entire shop-floor, where each gene represents a task to perform. Each task is composed of an ID, a duration, an associated product ID and an associated station ID. Assuming that Machine j , M_j only performs one type of tasks on a Product P_i . Each gene results from the merge of a product associated with a station, represented as P_iM_j , as demonstrated in the example of Fig. 2. The first operation of product 1 will be performed in machine 2, then the first operation of product 2 comes to be performed on machine 3, etc.

P_1M_2	P_2M_3	P_1M_1	P_3M_1	...	P_2M_2
----------	----------	----------	----------	-----	----------

Fig. 2. Chromosome encoding

After obtaining the best solution, the chromosome is divided into several schedules, one for each station present in the chromosome.

Then, it is necessary to define the maximum number of generations that the algorithm should evolve and the size of the population, i.e. the number of individuals present in each generation. The number of generations is the simplest way for terminating the evolution process. Low values may not be enough for the algorithm to evolve into good solutions, on the other hand high values may consume processing time unnecessarily because a good solution can be found too soon. At the same time, the population size should be large enough to have diversity among the individuals, but not too large that processing power and time are being consumed pointlessly. A small population could be very difficult to evolve into a good solution since the mating between individuals may not lead to a good offspring when the search space is too large. So, both parameters should be chosen cautiously to give the algorithm enough flexibility to evolve and do not consume time unnecessarily. These parameters depend on the size and complexity of each problem.

Another termination criterion is the steady fitness value. The steady fitness allows stopping the process if the fitness value remains the same for a given number of generations. This value needs to be smaller than the maximum number of generations. It helps when the evolution process is stagnant and does not evolve for a while.

Then, a small portion of the population, the survivor population, is selected to be present in the next generation, without being subject to crossover or mutation parameters. This is known as elitism and allows to keep the best individuals through the generations.

After that, the selection method for both the survivor and the offspring populations need to be chosen. In this case, was used the Roulette Wheel selector with size three, i.e. composed of three individuals. Firstly, is calculated the selection probability of each of the three individuals, which is obtained by dividing the fitness value of one

individual by the total sum of the fitness values of the three individuals: $(i) = \frac{f_i}{\sum_i f_i}$.

Then, the individual with higher fitness value has more chances to be chosen, so the new generation can be improved. This process is represented in Fig. 3.

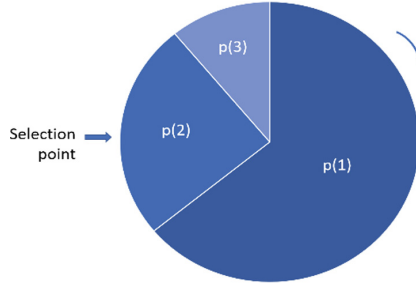


Fig. 3. Roulette wheel selection.

Next it is necessary to choose the crossover and mutation methods and their probabilities, which is the main factor to create new improved generations, since the characteristics of the parents are preserved to the children and the children can be improved. In this task allocation problem was chose a partially-matched crossover, which merges half of a parent chromosome with half of another parent and prevents duplicate genes in the child chromosome. The mutation is used to prevent the population to get stuck. The method selected was the Swap Mutation, which exchanges the positions of two genes with each other and does not duplicate genes. Both crossover and mutation probability values should be adapted to each situation since different values get better results in different situations.

Finally, it is necessary to define the fitness function. It evaluates and sets the fitness value of each chromosome. This value allows the evolution engine to select the offspring and survivor populations, as well as to know the best solution. In this task allocation problem, some rules were considered to define the fitness function:

- Only one operation of each job may be processed at a time;
- No pre-emption is allowed, which means that is not possible to interrupt a task and resume it later;
- Each job must be processed to completion;
- Jobs may be started at any time, no release times exist;
- Jobs may be finished at any time, no due dates exist (within the time window defined);
- No machine may process more than one operation at a time;
- Machine setup times are not considered;
- Machines may be idle within the schedule period;
- Machines are available at any time since they are considered available;
- An operation can only be performed once;
- Operations precedence within a product should be respected;
- Maintenance tasks must be executed during the maintenance shift.

The best fitness value is calculated by finding the minimum makespan among all generations, where the total makespan is given by the station with the maximum execution time in each generation. To obtain the fitness value of each individual, it is necessary to go through all the genes of each chromosome. The start and end times are set to the first job present in the chromosome, then to the second one and so on. At the same time, the makespan of each station is updated each time the times are assigned to a task.

The Eq. (1) describes the fitness function. The fitness value f is given by the minimum of the maximum completion time (makespan) of each generation times a weight which is increased if some task is not allocated in the right order.

$$f = \text{Min}[C_{max} * \text{weight}] \quad (1)$$

The total makespan of the schedule, C_{max} , is represented in Eq. (2). It is represented by the maximum total time to process all the operations, including idle time between operations, i.e. the end time of the last operation being executed.

$$C_{max} = \text{Max}[fs_j], j = 1, \dots, n \quad (2)$$

The total execution time of each station j , fs_j , is set by the later final time of the operations allocated to that station, f_{ih} , calculated in (3) since the operation h is allocated to station j .

$$fs_j = \begin{cases} f_{ih}, fs_j < f_{ih}; h \in j \\ fs_j, \text{ otherwise} \end{cases}, i = 1, \dots, n; h = 1, \dots, m; j = 1, \dots, k \quad (3)$$

The finishing time of each operation is calculated in (4), where the start time of operation h of product i , s_{ih} , is replaced by the start time of maintenance task h , sm_h , and the process time of operation h of product i , p_{ih} , is replaced by the process time of maintenance task h , pm_h , when the task involved is a maintenance task.

$$f_{ih} = s_{ih} + p_{ih}, i = 1, \dots, n; h = 1, \dots, m \quad (4)$$

The start time of each operation depends if it is a production operation or a maintenance operation. In a production operation, constraint (5), it is calculated based on the previous operation of the corresponding product if any, otherwise starts at time zero. Though, if there is already another operation allocated in the same station, to that specific time slot, this one is altered to a new time, starting at the end of that task, fjh .

$$s_{ih} = \begin{cases} s_{ih-1} + p_{ih-1}, \text{ no overlapping} > 1 \\ 0, \text{ no overlapping}; h = 1 \\ f_{jh-1}, \text{ overlapping} \end{cases}, i = 1, \dots, n; h = 1, \dots, m \quad (5)$$

On the other hand, if it is a maintenance operation, the start time of the operation is calculated based on the user intent. It could be desirable to have the maintenance tasks allocated as soon as possible, as late as possible or a third option where there are no

pretensions about maintenance tasks allocation. However, the maintenance tasks should be executed only during the maintenance shift.

The maintenance task's start-time to "as soon as possible" scenario is calculated in (6). The production tasks are allocated only after the maintenance tasks. The Maintenance Shift Start time is represented by MSS, the Maintenance Shift End time is represented by MSE, DT represents the day the task is performed and 1440 min are the total minutes of one day. An operation start time is assigned and if a conflict occurs due to an overlay of operation that time is changed to the next slot within the maintenance shift time. If that maintenance shift is already full, it is allocated to the beginning of the maintenance shift of the day after and so on.

$$sm_h = \begin{cases} MSS + 1440 * DT, & \text{there is overlapping; } f_{ih} > MSE \\ s_{ih-1} + p_{ih-1}, & \text{there is overlapping; } f_{ih} \leq MSE \\ MSS, & \text{there is no overlapping between tasks} \end{cases} \quad (6)$$

To calculate the start time of a maintenance task "as late as possible", the constraint (7) is used. In this case the maintenance tasks are allocated after the production tasks. First, the task is allocated to the last shift maintenance slot of the time window. If there is overlapping with another task, it is allocated to the next slot in that shift. In the case that shift is already full, it is allocated to the previous day and so on. The time window, TW, represents the number of days reserved to the schedule.

$$sm_h = \begin{cases} MSS + 1440 * (DT - 2), & \text{there is overlapping; } f_{ih} > MSE \\ s_{ih-1} + p_{ih-1}, & \text{there is overlapping; } f_{ih} \leq MSE \\ MSS + 1440 * (TW - 1), & \text{there is no overlapping between tasks} \end{cases} \quad (7)$$

Finally, when there are no pretensions about the maintenance allocation, the maintenance and production tasks are randomly chosen, and the maintenance tasks are allocated as in the "as soon as possible case" (Eq. (6)).

To check the operations order, each product contains the information about all operations belonging to that product. If an operation is executed after another one with higher priority, then a parameter representing the weight of the errors occurred is incremented (multiplied by 10), leading to a very large fitness value when the solution is invalid. If the total makespan is, for example, 254, but there is one error, so the fitness value will be 2540. This way is possible to know the number of errors present in each generation.

Finally, it is obtained a solution containing a schedule for each station in the shop-floor, with the respective start and end times of each operation.

4 Execution Environment

Every existent station is obtained from the shop-floor and each task to allocate is obtained from the maintenance (if it is maintenance task) or the management (if it is production task). Each time a new schedule is requested, the previous data are stored in the scheduling tool, except the maintenance tasks which are stored when inserted in the

system by a maintenance human operator. Each station stored in the scheduling tool contains a unique ID, the total execution time of that station (updated each time a new task is assigned there) and a collection of skills which it can execute, each skill contains a collection of possible configurations containing the duration of that skill with that configuration. However, for simplicity, it is assumed that each skill only contains one configuration. In turn, each task to allocate is stored in the scheduling tool containing a unique ID, an associated skill ID, an associated product ID, an operation number which is used to order the operations in an ascending way per product, an associated station ID, a completion field to check if the task was already performed and the start and end times of the task which are inserted during the algorithm execution. When it comes a new task from a new product, it is also created the correspondent product, containing the ID of the product, a collection with all the tasks associated with that product and a collection with the precedent products, which need to be allocated before this one. This way, the information of each product can be accessed. The available maintenance teams are considered infinite. However, they only operate between 6 a.m. and 2 p.m. of each day, which means that maintenance tasks need to be allocated in that gap.

Then a new schedule generation can be triggered by a human operator, through a graphical user interface, or by the system itself at predefined times. When it happens, it generates a schedule which allocates the maintenance tasks as soon as possible, another that allocates the maintenance tasks as late as possible and another one which allocates them without preference. The scheduling algorithm starts by set the times for each task, then it checks if the operations order is correct, if it is not, reallocates the current task, and finally checks if there is no other task allocated to that station at the same time. At the end, the collection of schedules is sent to the other tools, to test the efficiency of the schedules. This process is represented in Fig. 4.

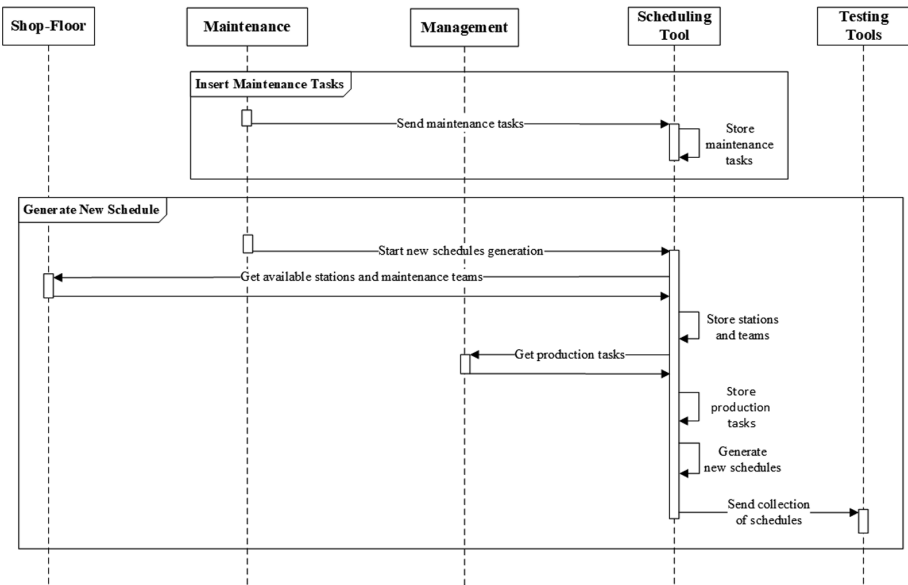


Fig. 4. Execution environment sequential diagram

5 Conclusions and Further Work

5.1 Conclusions

This paper presents a generic architecture designed to solve a JSSP including both production and maintenance tasks. Considering the maintenance operations to be performed on the production stations this architecture allows to have a more reliable schedule for the shop-floor. The presented solution is a GA based architecture, where the main goal is to perform the task allocation based on the information of the tasks and stations provided.

This way, this scheduling tool will try to allocate the tasks to the stations in order to minimize the total execution time of all the machines and respecting the order of the tasks of each product. Furthermore, the maintenance operations need to be allocated during the maintenance shifts times. Nevertheless, each operation needs to have the information about the station where it will be performed, since the developed architecture only sets the times of each one and does not choose on which machines they will be performed.

This tool was designed to avoid the overlapping of products on the same station at the same time, as well as to have the same product allocated to different machines at the same time, while the operations' sequence is preserved. After obtaining the schedule with the minimum makespan, this one will be divided into smaller schedules, one per station, and that collection can be sent to other tools, for higher level tests and analyses.

5.2 Further Work

In the future, the presented architecture will be improved in order to deal with the precedence between products, once some products may require that other ones are finished so they can start to be operated as well as date constraints, such as start and due dates of each product.

This tool will be implemented and tested in a real demonstrator using different problem sizes, i.e. with different numbers of tasks, products and stations used.

References

1. Azab, A., Naderi, B.: Modelling the problem of production scheduling for reconfigurable manufacturing systems. *Procedia CIRP* **33**, 76–80 (2015)
2. Chalfoun, I., Kouiss, K., Huyet, A.L., Bouton, N., Ray, P.: Proposal for a generic model dedicated to reconfigurable and agile manufacturing systems (RAMS). *Procedia CIRP* **7**, 485–490 (2013)
3. Aissani, N., Beldjilali, B., Trentesaux, D.: Dynamic scheduling of maintenance tasks in the petroleum industry: a reinforcement approach. *Eng. Appl. Artif. Intell.* **22**(7), 1089–1103 (2009)
4. Ruiz, R., Carlos García-Díaz, J., Maroto, C.: Considering scheduling and preventive maintenance in the flowshop sequencing problem. *Comput. Oper. Res.* **34**(11), 3314–3330 (2007)

5. Raza, A., Ulansky, V.: Modelling of predictive maintenance for a periodically inspected system. *Procedia CIRP* **59**, 95–101 (2017). TESConf 2016
6. Ladj, A., Varnier, C., Tayeb, F.B.S.: IPro-GA: an integrated prognostic based GA for scheduling jobs and predictive maintenance in a single multifunctional machine. *IFAC-PapersOnLine* **49**(12), 1821–1826 (2016)
7. Do Chung, B., Kim, B.S.: A hybrid genetic algorithm with two-stage dispatching heuristic for a machine scheduling problem with step-deteriorating jobs and rate-modifying activities. *Comput. Ind. Eng.* **98**, 113–124 (2016)
8. Asadzadeh, L.: A local search genetic algorithm for the job shop scheduling problem with intelligent agents. *Comput. Ind. Eng.* **85**, 376–383 (2015)
9. Sharma, P., Jain, A.: Performance analysis of dispatching rules in a stochastic dynamic job shop manufacturing system with sequence-dependent setup times: simulation approach. *CIRP J. Manuf. Sci. Technol.* **10**, 110–119 (2015)
10. Balin, S.: Non-identical parallel machine scheduling using genetic algorithm. *Expert Syst. Appl.* **38**(6), 6814–6821 (2011)
11. Holland, J.: *Adaptation in Natural and Artificial Systems*. University of Michigan Press, Ann Arbor (1975)
12. Kundakcı, N., Kulak, O.: Hybrid genetic algorithms for minimizing makespan in dynamic job shop scheduling problem (2016)
13. Li, J., Huang, Y., Niu, X.: A branch population genetic algorithm for dual-resource constrained job shop scheduling problem. *Comput. Ind. Eng.* **103**, 330 (2016)

Human Robot Cooperation and Machine Vision



A Learning Method for Automated Disassembly

Julius Wolff^(✉), Torge Kolditz, and Annika Raatz

Institute of Assembly Technology, Leibniz Universität Hannover,
Hannover, Germany

wolff@match.uni-hannover.de

Abstract. While joining tolerances, and therefore forces, are known in the assembly process, the determination of disassembly forces is not possible. This is caused by changes in the product properties during the product operation, which has multiple reasons such as thermal or mechanical stress on the product. Regarding the planning of disassembly tasks, disassembly times and tools cannot be planned properly. They have to be determined in the process or stay undefined, which can result in damaging of the product.

This article shows an approach to describe the necessary disassembly forces without having to investigate the complex physical influences caused by the usage of the product. To do so, a Learning Method is developed, which is sustained by a Lookup-Table for the estimation of disassembly forces based on basic input data such as hours of operation and operating characteristics. Missing values will be interpolated by using multiple linear regression. The concept will be illustrated in the example of a turbine blade connection.

Keywords: Disassembly · Automation · Planning · Turbine blades

1 Introduction

The disassembly properties of a product depend on the assembly connections, which can be divided into detachable and non-detachable connections. With regard to a product-friendly disassembly, detachable connections are preferred and fixed connections, such as welded connections, are avoided. However, detachable connections can solidify to a high degree so that they seem to be fixed. In contrast to an assembly process, where joining forces are known due to defined product properties, disassembly forces are therefore unknown.

To make the disassembly and thereby the whole regeneration cycle, plannable, cost efficient and component-saving, it is necessary to be able to estimate the necessary disassembly forces. Knowledge of the disassembly forces is fundamental for the planning of disassembly tools and times. This is particularly worthwhile for products with valuable components like the engine of an airplane.

In a product's life cycle the disassembly is arranged directly after the product operation. The defined joining tolerances are lost and the assembly joints of highly stressed products solidify to an unknown degree. With regard to the example of turbine blades, reasons for the solidification of their connection to the turbine disc are the high

temperatures and operation forces, and the intrusion of foreign particles like sand and corrosion. During the disassembly process, this lack of knowledge about the degree of solidification can cause a damage to the connecting partners, originating in the undefined reaction forces acting inside the connections. The exact calculation of the disassembly force is not possible, because a simulation would require exact knowledge about all the operation conditions (composition of air, intrusion of foreign particles) at any point in the operating phase of the engine.

An approach that seems more promising is the assignment of the disassembly forces to the operation history of the product. To do so, a Learning Method for determining the necessary disassembly force based on the input of different parameters by the user is developed. The method is developed with the support of a learning Lookup-Table. As an example of a disassembly connection, the connection of a blade and a disk of a high-pressure turbine of an aircraft engine is considered.

2 Related Work

The disassembly of turbine blades is usually characterized by manual labor. This is due to the unknown state of the assembly connection. In order to describe the undefined forces with a physical model of all the several influences on the solidification state, a big effort would be required, which remains unsuccessful in the worst case [1]. This process of solidification can have various causes. In a turbine, hot gas corrosion and adhesion are major wear mechanisms. Hot gas corrosion is caused by components of the fuel and the air (e.g. sea salt) flowing through the engine and produces solidifications in the contact surfaces of a connection. Surface corrosion can increase the loosening torque of a screw, for example, up to 45% [2]. Adhesion in contrast is caused by molecular interactions on the boundary surfaces of the assembly connection. Deformations of roughness peaks and the separation of material fragments can increase the adhesion forces [3]. Besides the solidification caused by separated particles of the connection itself, foreign particles like sand can cause additional blockades in the connection.

The various causes and their interaction for solidification complicate the calculation of the necessary disassembly forces beforehand. This lack of forces requires an increased flexibility in the process and the turbine blades are therefore knocked out of the disc manually, using simple tools such as a hammer. High manual forces are difficult to control, and thus damage can occur [4]. Especially in the regeneration of products with a high value, it is necessary to use methods that save the components from damage. One disk of a high-pressure turbine has around 70 blades, so that an automated disassembly of these blades can be economically viable [4]. To choose the right dimension of tools, the disassembly forces have to be estimated.

A simplified solidification model was developed, to describe the solidification and the resulting disassembly forces of a connection. Figure 1 shows the solidification model. It becomes clear that the disassembly force $F(z)$ and the weight load mg of the turbine blade have to exceed the solidifying force $R_z(z)$. Only with a slight exceeding, can component-saving disassembly be achieved. The disassembly force therefore follows to:

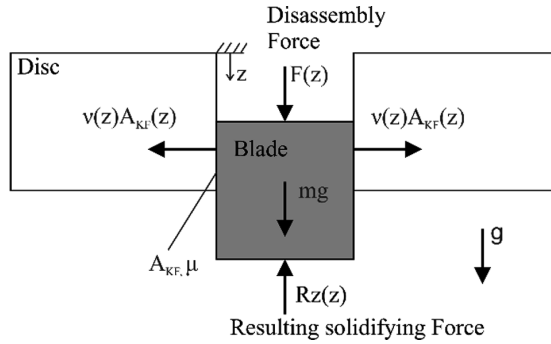


Fig. 1. Simplified solidification model

$$F(z) > R_z(z) - m \cdot g \tag{1}$$

Since the weight load is in general much lower than the solidifying force, the centre of attention is the solidifying force $R_z(z)$. The solidifying force is determined by the contact surfaces A_{KF} of the joining partners, a solidification pressure v of the components to each other and the coefficient of static friction μ . Following the simplified model, the solidifying force can be described as:

$$R_z(z) = \mu \cdot v(z) \cdot A_{KF}(z) \tag{2}$$

Nevertheless, research showed that the solidifying force is not only dependent upon the absolute amount of the contact surface, but also upon the geometry of the connection. Figure 2 shows two types of connections that are common in the aviation industry. Each connection geometry has its specific solidifying characteristics, so that a method for the quantification of R_z would be helpful for the predictive determination of disassembly forces.

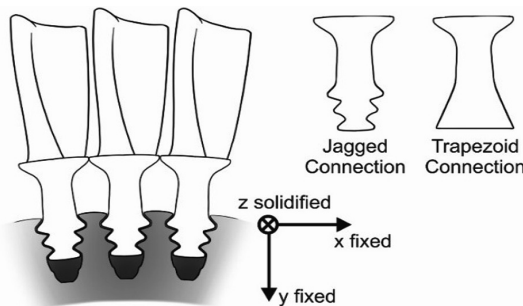


Fig. 2. Connection geometries of turbine blades

3 Learning Method for Disassembly Processes

The major requirement for a Learning Method is a known history of the product. This narrows the number of products where the Learning Method can be of use. Most of the consumer products that are fed into the regeneration cycle have an unknown usage history. Nevertheless, there are products or components of high value and/or high safety-relevance, which need a recording of the product's history - for example the recording of the hours of operation, which determine the maintenance intervals. For the engine of an airplane, a lot of information are available about the product's history: The hours of operation are recorded anyway and since an airplane is navigating using GPS, data about the characteristics of operation (flight over sea or desert) are also known. In the following a Learning Method is described, which implements a product's usage history into the disassembly planning.

Figure 3 shows the schematic layout of the Learning Method. In a first step, the relevant characteristics regarding the product history such as hours of operation or workload are collected. In the disassembly planning, already acquired data and the characteristics of the product are used to estimate the parameters of the disassembly process. During the disassembly process, data that are useful for future reference are collected and stored into the database.

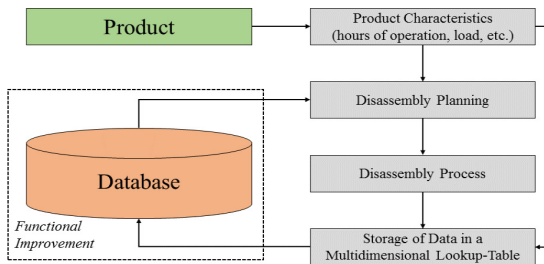


Fig. 3. Schematic layout of the learning method

The database has the structure of a multidimensional Lookup-Table, which grows bigger and more accurate with each disassembly process. In the following, the input of product characteristics, the structure of the Lookup-Table and the multiple linear regression used in the disassembly planning are explained in detail.

3.1 Product Characteristics

The first step is the input of the necessary data. In the case being considered here (turbine blades), the necessary data are the hours of operation of the turbine, the characteristics of the flight routes (e.g. over desert or sea) and the geometry of the blade. The hours of operation are of great interest, because of an enormous impact on the degree of solidification.

Frequent flights over desert and sea can increase hot gas corrosion and solidification in general, as described in Sect. 2. While the hours of operation are put in

unprocessed, the characteristics of the flight have to be converted into a number. The number has to represent the impact on the solidification done by the different flight routines. It is taken into account that short flights are particularly demanding due to the lower flight altitude and a higher number of take-offs. The best case is only long-distance flights over land, which will then be represented by the characteristic factor “1”. The worst case would be the short-distance flight over desert and sea, which would be represented by the factor “5”. Depending on the actual history, which will always be somewhere between those extreme cases, a rational number between one and five will be calculated.

The geometry of the blade also has an influence on the disassembly force. In contrast to the characteristics of flight, there are no intermediate values that can be calculated, because there are no fluent transitions between different geometries. This has an impact on the structure of the Lookup-Table, which will be explained in the next section.

By determining the disassembly forces of various combinations of input data, the Lookup-Table grows bigger and more detailed. Given the event that the user puts in a combination of input data that has never been disassembled, an approximated disassembly force has to be interpolated by multiple linear regression. The regression is supported by all disassembly forces that have been recorded at that time. After the actual disassembly took place, the recorded disassembly force is stored in the Lookup-Table for future reference and for improving the regression.

3.2 Lookup-Table

The structure of the exemplary Lookup-Table is very simple. Since there are three input variables, a three-dimensional matrix is needed to store the discrete values for the disassembly force depending on the input data. A closer look at the input variables shows that the geometry of the blade only has a limited number of discrete values, while the hours and characteristics of operation, theoretically, can have an infinite number of values. Dividing the three-dimensional matrix into layers, each represents one geometry. Without fluent transitions between different geometries, there is no need to interpolate values between those layers. This reduces the multiple linear regression by one dimension, which leaves a two-dimensional linear regression. The disadvantage of this method is that every new geometry has to be taught from scratch. The advantage is the simplicity of the calculation, which is possible without a big effort during the disassembly. For every geometry, there is an independent two-dimensional matrix, within which the regression is calculated.

3.3 Multiple Linear Regression

The multiple linear regression is the key to the success of the Lookup-Table. Using regression, it is not necessary to calculate or simulate the disassembly force based in physical models, but instead the disassembly force can be approximated using interpolation from already disassembled data. In the following, a short introduction of multiple linear regression is given, followed by an example, to show how the regression works.

Multiple linear regression can deliver an output which is dependent on multiple input variables [5]. In the case of turbine blade disassembly, there are three inputs (hours of operation, characteristics of operation, geometry) of which only the hours and the characteristics of operation are considered for the multiple linear regression, because for the geometry no intermediate values exist that could be interpolated. The equation for the regression thereby follows to:

$$Y_i = \beta_1 X_{i,1} + \beta_2 X_{i,2} + \beta_3 X_{i,3} + e, \quad i = 1, \dots, n \tag{3}$$

In this equation, Y_i is the output of the observation i , while $X_{i,1}$, $X_{i,2}$ and $X_{i,3}$ are the input data. The input $X_{i,1}$ is usually set to 1 to introduce a constant into the regression model. Furthermore, n is the number of observations and β_1 , β_2 and β_3 are the parameters of the regression. The output Y shows a natural diversification, so that the calculated regression will not intersect with all output values [5]. Therefore, a residuum e is added to the equation.

3.4 Example of Use

Table 1 shows a Lookup-Table for a fictional geometry. In this case, 50 turbine blades with different operation histories have already been disassembled.

Table 1. Disassembly Forces [N] of turbine blades with different operation histories

Geometry A		Hours of operation [1000 h]									
		1	2	3	4	5	6	7	8	9	10
Characteristics of operation	1	100	220	317	430	525	610	700	821	903	1043
	2	230	380	421	490	620	712	860	980	1110	1200
	3	250	432	576	632	778	890	910	1000	1150	1200
	4	370	570	600	790	800	870	1119	1150	1200	1300
	5	570	600	703	845	930	1120	1180	1200	1350	1470

Figure 4 shows the disassembly forces of Table 1 as a function of the input data. It also illustrates the multiple linear regression of the disassembly forces. In this example the values are evenly distributed, which, of course, will not be the case in reality. Still, the example illustrates how the Lookup-Table works after 50 blades with different operation history have been disassembled.

The multiple linear regression shown in Fig. 4 has the parameters:

$$\beta_1 = -91.5733; \quad \beta_2 = 0.1028; \quad \beta_3 = 103.6400.$$

Using these parameters, every combination of operation hours and characteristic of operation can be determined. For example the disassembly of a turbine blade with 6,400 operation hours and a characteristic factor of 2.7 would have an estimated disassembly force of 846.175 N calculated using the interpolation shown in Eq. 4.

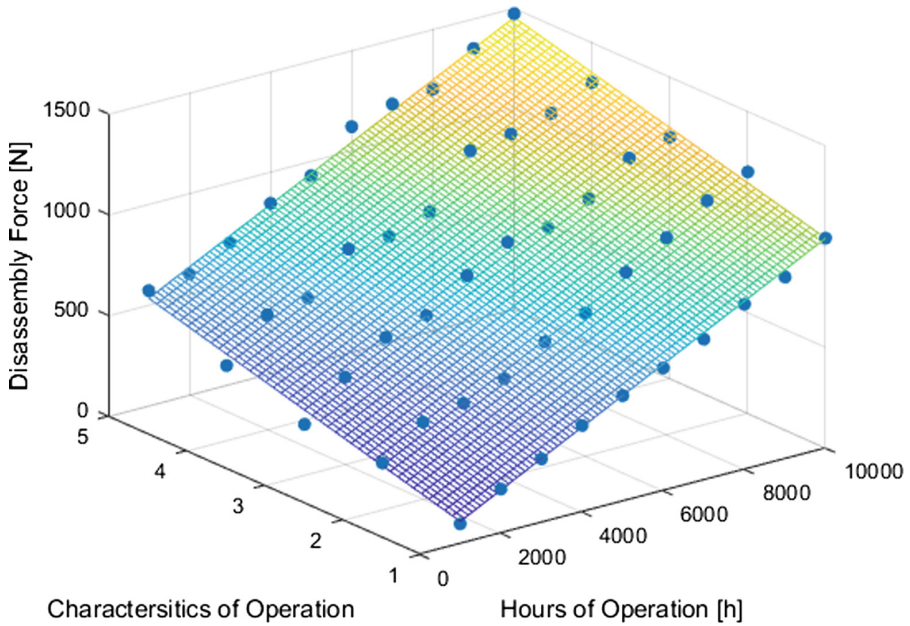


Fig. 4. Multiple linear regression of the disassembly forces of a turbine blade

$$Y = -91.5733 + 0.1028 \cdot 6400 + 103.6400 \cdot 2.7 = 846175 \quad (4)$$

Figure 5 shows the corresponding dot (red) in the regression known from Fig. 4. The value interpolated using the regression is an estimation of the actual disassembly force and is used to choose the right tools and as an initial value for the control system. During the disassembly, the actual disassembly force is measured and afterwards stored in the Lookup-Table. The matrix has grown by one entry and the regression is calculated again, to make it more reliable for future estimations.

3.5 Mean Value

Variations in the process are taken into account by calculating the mean value from two identical products with an identical history. In this case a disassembly force for a turbine blade with the history and geometry is already stored in the Lookup-Table, and thus a mean value is generated. The disassembly forces of turbine blades even from the same engine vary to a certain degree, so that a mean value is the best way to counteract these variations. However, the generated value is not an arithmetic mean, but is created using Eq. 5:

$$h_{i,j,k,new} = \frac{h_{i,j,k,old} \cdot h_{i,j,k,number} + F_{disassembly}}{h_{i,j,k,number} + 1} \quad (5)$$

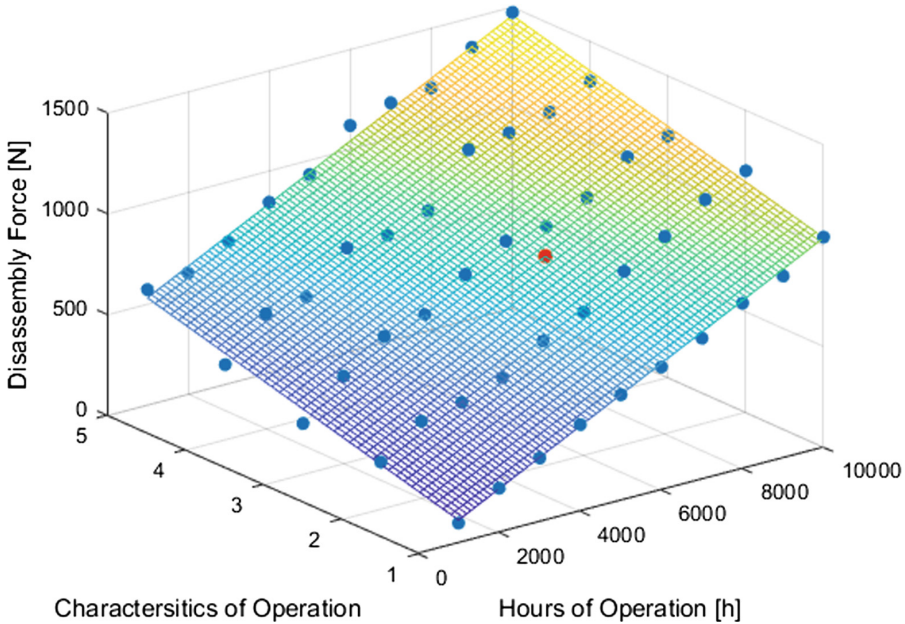


Fig. 5. Calculated disassembly force for 6.400 h of operation and a characteristic factor of 2.7 (Color figure online)

In this equation, $h_{i,j,k,new}$ represents the new value of the Lookup-Table, while $h_{i,j,k,old}$ represents the old value of the Lookup-Table in dependence to the three input variables. $h_{i,j,k,number}$ is a scalar entry in a counter matrix that contains how often a combination of the three input variables has been selected from the Lookup-Table. $F_{disassembly}$ is the measured disassembly force which is needed to carry out the disassembly task. After the mean value is generated, the corresponding counter $h_{i,j,k,number}$ is increased by one. This way the forces measured at each disassembly are all brought into the mean value equally and outliers do not have a critical impact on the mean value stored in the Lookup-Table. Thus, the existing entries are improved and, on the other hand, are continuously expanded, so that the learning process would be usable in a real repeatable disassembly task.

4 Conclusion and Outlook

At this time, all the input data and the corresponding disassembly forces are fictional for showing the Learning Method for disassembly tasks. Nevertheless, it was shown that the multiple linear regression is suitable for the requirements of the disassembly process. The storage of disassembly forces of products with a known history benefits the planning of the regeneration process. Using a force sensor in the disassembly tool and a software environment for storing the forces, the implementation of the Learning Method would be very simple.

In future work, the aim is to feed the process with data from real disassembly processes, to see if the concept of a Learning Method also works in a real environment. After filling the matrixes with a set of values from past disassembly processes, the multiple linear regression has to deliver disassembly forces for future disassembly processes, to examine the reliability of the process.

When the Learning Method has proven its reliability it will be implemented in a test stand, where solidified connections are disassembled in an automated process, and the disassembly forces can be measured and regulated.

Acknowledgments. The authors kindly thank the German Research Foundation (DFG) for the financial support to accomplish the research project A5 “Adaptable and Component-Protecting Disassembly in the Regeneration Path” within the Collaborative Research Center (CRC) 871 - Regeneration of Complex Capital Goods.

References

1. Selinger, G.: Sustainability in Manufacturing – Recovery of Resources in Product and Material Cycles, pp. 217–311. Springer, Heidelberg (2007). <https://doi.org/10.1007/978-3-540-49871-1>
2. Kahmeyer, M.: Flexible Demontage mit dem Industrieroboter am Beispiel von Fernsprech-Endgeräten, pp. 50–60. Springer, Stuttgart (1995). <https://doi.org/10.1007/978-3-642-47876-5>. Faculty of Engineering Design and Production Engineering
3. Ahgary, A.: Eine Analyse der Verschleißmechanismen in der Anwendung der Hüftgelenk-endoprothetik unter realistischen Randbedingungen. diplom.de, Berlin (2002)
4. Lufthansa Technik Hamburg: Visiting the disassembly department in March 2014
5. Toutenberg, H., Schomaker, M., Wißmann, M.: Arbeitsbuch zur deskriptiven und induktiven Statistik, pp. 227–239. Springer, Berlin (2006). <https://doi.org/10.1007/3-540-32142-X>
6. Wolff, J., Yan, M., Schultz, M., Raatz, A.: Reduction of diassembly forces for detaching components with solidified assembly connections. In: 6th CIRP Conference on Assembly Technologies and Systems Institute of Assembly Technology, Leibniz Universität, Hannover (2016)



Gesture-Based Robot Programming Using Microsoft Kinect

Sebastian Blankemeyer^(✉), Joshua Göke, Tobias Grimm,
Benedikt Meier, and Annika Raatz

Institute of Assembly Technology, Leibniz Universität Hannover,
An der Universität 2, 30823 Garbsen, Germany
{blankemeyer, raatz}@match.uni-hannover.de

Abstract. Companies have to face constantly changing framework conditions. Product lifecycles are reduced and the number of variants increase as a result of increasing product individualization. To ensure that production systems such as robots can achieve this flexibility, more and more programming procedures are being developed that do not require a high level of qualification. This thesis deals with an intuitive approach that can be used for programming adhesive joints. With the help of the simple pointing to surfaces, a path corresponding to the intersection line of the two planes is calculated. The required algorithm for fingertip recognition is implemented with the help of Voronoi diagrams. The recognition of the planes is based on a region growing algorithm. The accuracy of the whole process is limited by the current technical state of the art and does not yet meet the necessary requirements.

Keywords: Robot programming · Intuitive human machine interface
Gesture recognition

1 Introduction

Nowadays a high degree of automated processes exist, especially in productions with high unit numbers. For small and medium-sized companies however, fully automated production processes are not cost-efficient due to the lower number of units and the highly specialized processes that are tailored to the customer requirements. Human robot collaboration (HRC) is an approach trying to increase productivity especially in small to medium-sized production quantities. Here the advantages of a robot, such as its precision and repeatability, are combined with the problem-solving and adaptability of humans. On the one hand it is important to ensure the safety of the human worker, who must work with the robot in its immediate environment and, on the other hand, to find approaches that enable people to interact quickly and intuitively with the robot, thus to guarantee the optimal workflow. In the research area of HRC different types of programming methods are developed. One approach is learning from demonstration, where the user programs the robot by showing it successful examples. This can happen through guiding the robot through its path (also called kinesthetic teaching) or by capturing the movements of the user that the robot has to imitate [1].

In addition, some work has already been done developing gesture based programming methods. To implement the programming methods, many of the projects use the Kinect v2 as camera system. The Kinect v2 has been analyzed, exploited and continuously optimized, since its first release [2, 3]. Additionally, an accompanying Software Development Kit (SDK) exists that comes with a lot of practical features like an implemented body tracking function, different types of images and depth measurement [4].

In [5], an approach has been presented that allows the user to teach in points to a welding robot over gestures. For saving start or end points the position of the right hand is saved when the user's left arm is raised. This approach allows even inexperienced users to communicate with a robot. For industrial usage, however, the result might be too inaccurate due to the usage of the system-integrated hand joint tracking of the Kinect, as the position detection of the hand was fluctuating [5]. One way to improve accuracy of the process could be implementing a more precise finger detection. In Canal et al. [6] a programming method for assistive robotics is described in which a user points to objects that is detected by the robot. Then the robot will move to the object pointed to. In order to determine the resulting pointer direction the software calculates the angles between the separate arm bones and the body.

In this paper we present the description of a new approach to an intuitive programming and interaction method for industrial robots, especially for adhesive application. The approach is based on gesture control using a Kinect v2. By pointing on planes, the operator can show the objects that need to be glued together. After that the robot path is determined by calculating the cutting edge. The needed and implemented fingertip recognition algorithm is described as well as the required plane detection and the corresponding precision of the approach. On the basis of the conclusions, the future work is elaborated and described.

2 Concept of Programming

The goal of this approach is to develop and implement an intuitive operating concept for industrial robots in human-robot collaboration. For this purpose, a gesture control system is developed which enables interaction with the robot only with the help of hands and does not require any other input devices. To do this, the operator points to two adjacent objects one after another (Fig. 1). By specifying the areas, the program then calculates the cutting line so that it can be transferred to the robot. This can be used in particular for the production of glued joints especially when the position is moved from one object to the next. However, the process can also be used to produce welded joints or carry out press processes. In order to ensure that the robot can also be moved intuitively and without the aid of a hand-held user panel, an additional mode for moving the robot with the aid of a hand movement is implemented. This mode includes both positioning and orientation of the end effector.

A Kinect v2 is used to implement the gesture control. These time-of-flight cameras can generate 3D data of the environment and are often used in research and development. Using the supplied API, people can be easily recognized and transferred to a skeleton model. The Kinect is fixed to the workstation so that the operator is always in view.

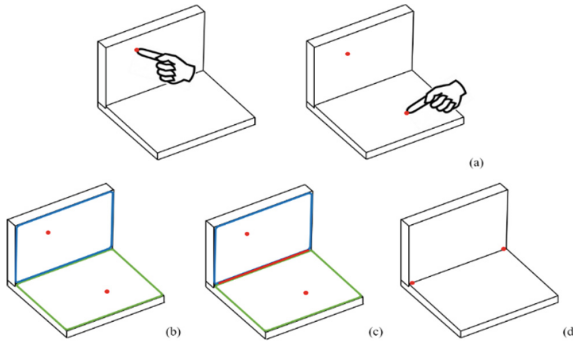


Fig. 1. Principle of corner point detection, (a) selection of planes, (b) plane detection, (c) receiving cutting line, (d) corner points

In the “teach in points” mode, the layers are defined by simply pointing to the surfaces (Fig. 2). These planes are saved and then the common intersection line is determined. Finally, this line is translated into a movement command for the robot.

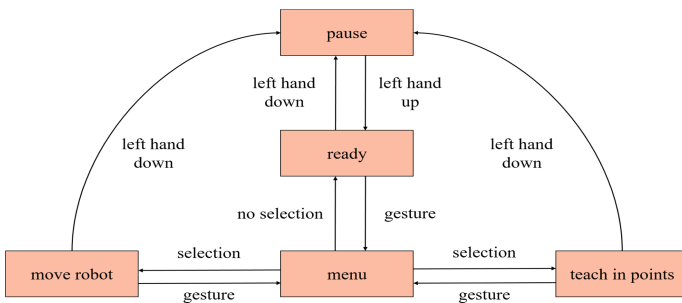


Fig. 2. Concept of interaction

To switch between modes, an intuitive interface is provided in the form of a menu. The inputs can also be made here without any further operator panels.

To ensure safety for humans at all times, an additional safety function is added. Thus, entries can only be made if the user’s hands are both above the navel. This makes it possible to distinguish between intentional and unintentional entries. In addition, the program is paused and the movement commands are not forwarded to the robot.

The challenges in creating the programming procedure are, on the one hand, the recognition of the fingertip to show the layers. This must be precise and reliable in order to select the correct plane. On the other hand, a surface detection is required so that the surroundings can be detected. Finally, the cutting edge must be reliably detected and calculated. The corresponding explanations for the fingertip recognition and the surface recognition will follow in the next chapters.

3 Recognition of Fingertips

The recognition of fingers and fingertips belongs to the research area of computer vision. Traditional algorithms are looking for skin-colored areas within the images. This is a challenging task due to changing lighting conditions and different skin colors [6]. Since the introduction of consumer depth camera like the Kinect a lot of research has been done to use depth images and the identified skeleton of the Kinect for recognition algorithms [7].

The Kinect v2 can track up to six persons and calculates a skeleton with 26 joint positions in 3D coordinates for every person. The accuracy of the recognized hand position is unfortunately not very precise. However, we are using it as a first estimate for our algorithm to set the region of interest and to create a field of view (FOV) of the depth image.

The size of a hand in an image is dependent on the distance to the camera. Therefore, we are using the recognized hand position of the Kinect as the center of the image and calculate the image size dynamically to get the best FOV. Afterwards we are using a foreground segmentation which uses the depth information of the hand position to remove unwanted parts of the image. Following this, we implemented a finger detection algorithm which is based on the hand recognition algorithm of Yeo [8]. We have adapted the algorithm in order to obtain a higher reliability and accuracy, as this is necessary for our approach.

Many feature-based algorithms are using the palm of the hand to determine the size of the hand in the image. Yeo calculates the largest empty circle (LEC) within the hand contour to approximate the palm of the hand. This is a computation-intensive task, so Yeo is sampling down the image and checks every N-point instead of all points in the hand contour. For these points the shortest distance to the contour is calculated to get the radius of the LEC.

The problem of finding the LEC is analyzed in Gesing [9] and a solution is presented using a Voronoi-Diagram. Gesing shows that the center of the LEC can be either on a Voronoi node or on an intersection between a Voronoi edge and the convex hull of the points. For our application we are approximating the palm of the hand by the LEC, so the center must be inside the contour on a Voronoi node. Thus, we are calculating the convex hull of the contour and create a Voronoi-Diagram. Afterwards we examine every Voronoi node and calculate the shortest distance to the contour to get the radius of the LEC.

The feature-based recognition of fingertips utilizes several criteria to filter possible fingertips. Yeo uses a circle with 3.5 times the radius of the LEC to remove unwanted points in the arm area (outer red circle in Fig. 3 left). In our use case it turned out that we had too many false detections for a reliable execution of the algorithm. We solved this by using additional information from the Kinect to filter possible fingertips. The identified joints of the hands include the hand wrist (blue point in Fig. 3) as well as the recognized center of the hand by the Kinect (pink point in Fig. 3). Our algorithm creates a line through both points and calculates the angle to the potential fingertips. We are limiting the angle to 110° because it is anatomically hard to create a greater angle. Figure 3 (right) shows the line through the points as well as the resulting angle limit (dark area). By using this method, we are independent of the hand orientation and we can filter more potential fingertips.

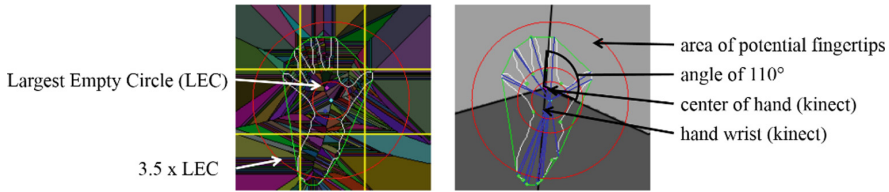


Fig. 3. Voronoi-Diagramm of the hand contour (left) and filtering points in the arm area (right) (Color figure online)

Sometimes there are multiple detections on the same finger, so Yeo is checking the surrounding area of each detection and deletes points nearby. Our approach uses k-curvature to find the fingertip as well, but we are creating a region of interest (ROI) around every possible fingertip. This is done by adding the surrounding points on the contour in forward and backward direction to a list. After creating individual lists for every possible fingertip, we are checking the lists for overlaps and combine them if necessary. This approach eliminates multiple detections for one fingertip and we can reduce the calculation of the k-curvature because every point is checked only once.

Afterwards we calculate the k-curvature to find the exact position of the fingertip. The last step of the finger recognition algorithm is the identification of a gesture. The possible gestures can be seen in Fig. 4. For our application we are distinguishing between a fist (zero fingers), a pointing finger (one finger), a pistol (two fingers) and a rock gesture (three fingers). The open hand belongs to four to six detected fingers to react to one false detection or nearby fingers. For safety reasons, the gesture must be recognized in several consecutive images until it is published.

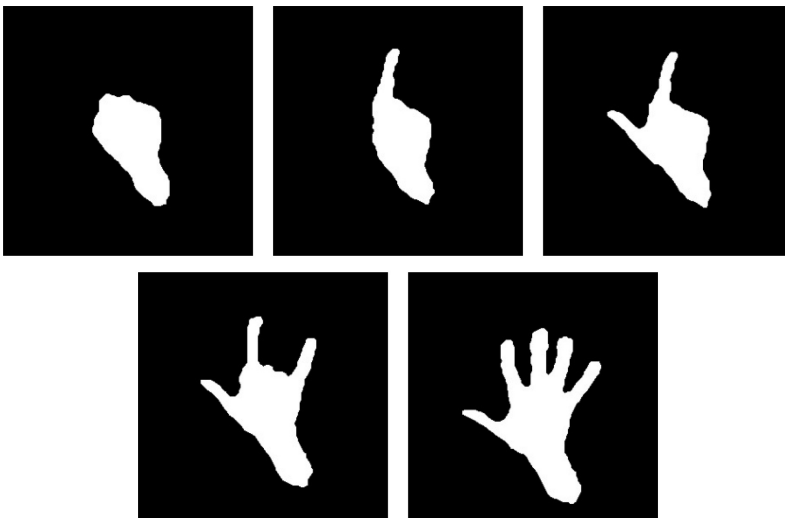


Fig. 4. Recognizable gestures: fist (top-left), pointing finger (top-mid), pistol (top-right), rock (bottom-left), full hand (bottom right)

In our program, we need all gestures except “pistol”. The most important gestures to interact with the program are the “pointing finger” and “fist” to mark or save the planes. With the help of the described finger detection we are able to reliably interact with the program. Furthermore, we detect the fingertip to recognize the correct surface.

4 Recognition of Planes

The next part of this work deals with the question of how the starting and end points of linear movements can be defined. In this section we present an algorithm which identifies and locates the edge, so the robot can move along it, as it is usually used in welding or gluing processes. To identify the edge, a recognition algorithm of two adjacent planes is presented, which are selected through the finger recognition already presented.

4.1 Related Work

Past research projects have been concerned with the optimal recognition of planes from images and three-dimensional point clouds for some time now. In principle, the methods for the identification of planes in 3D can be categorized into three classes according to Holz et al. [10]: Methods representing the RANSAC algorithm that iteratively try to represent a plane in space as best as possible by a random choice of points. In order to describe a plane the number of points needed, three points in total, is taken randomly. Furthermore the number of points that are within a certain tolerance band around the newly created plane are considered. The plane regression, which describes the real plane the best after a predetermined number of iterations is stored. In [11] a RANSAC algorithm is used for identifying the plane of a table in order to distinguish objects laying on the table of the same. Advantages of this approach are the robustness and accuracy even in data sets with a large proportion of outliers. However, the random selection of samples makes them slower than procedures that can handle ordered records. A further disadvantage is the tendency of the algorithms to simplify complex structures. For example, two parallel planes with only a small distance between them can be recognized as one [12]. Furthermore, there are methods of 3D-Hough-transformation. The Hough transformation is the de facto standard for line and circle recognition in images. There are different extensions existing for three-dimensional space. For an overview, reference is made to [13] and [14].

The third category of methods for the identification of planes in 3D point data is Region-Growing, in which the image structure is used for orderly search for geometries within the image. Starting from a point, the neighborhood is examined for previously defined properties. In [10] the authors present their method for plane recognition. In doing so, they derive a grid of 3D points from the image structure and use the neighborhood to create a local surface normal and estimate curvatures. In order to get noise reduction, the points are filtered through a bilateral filter and segmented based on the region growth.

4.2 Plane and Edge Detection

After testing the procedures, our approach is based on the region growing algorithm as well. We decided to take this method, because in our program only two separate planes need to be detected and thus the computing effort is practicable. To recognize the surfaces, we compare the surface normal vector with the ones of the neighborhood. The algorithm associates the pixels to one surface as long as the normal vectors are in a defined range. This will be done until all neighbors of the surface are examined and declared as outside.

At first in order to be able to compare surface vectors a normal frame is produced every time the user starts to communicate with the robot. The frame contains a surface vector for every pixel in the image. To receive a better normal frame, five depth frames are saved and the average of them is computed. According to Lachat et al. [15] a high number of averaged frames does not correlate with increased accuracy, which is why a small number of frames is sufficient. They tested the accuracy of the depth image with different numbers of frames from 20 to 200. Results for fewer frames may be less smooth, but above 50 frames no major changes could be observed. Trying to keep the computing time low, we decided to average only five frames. In addition to this the frame is edited with a bilateral filter to smooth the 3D points even further. The starting point of the region growing algorithm is defined as the point where the fingertip is detected in. In order to determine a first provisional plane, the average normal vector is then formed from all normal vectors belonging to a 10×10 quadrat of points around the starting point. Starting from this square, the neighbors are examined for the orientation of their normal vectors and their distance from the previously defined plane. For each point newly added to the plane, the surface vector is recalculated as the mean value of all normal vectors whose points have been added to the plane so far.

If a point cannot be assigned to the plane due to the fact that the normal vector is differently orientated, it will be saved as an “edge point”. Its surrounding will not be examined any further. The plane detection is finished as soon as no further neighborhood points can be added to the plane, so that the plane is surrounded by edge points completely. The surface detection is executed for both planes that are needed. In Fig. 5 an example is shown, where two planes of an object have been identified.

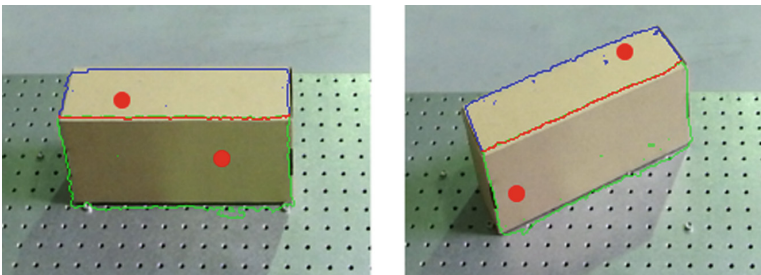


Fig. 5. Detected edge points of the layers on a carton. The red dots represent the starting points of the region-growing algorithm. (Color figure online)

In order to get the intersection line that the two planes have in common, every surrounding point of the first plane is examined whether it is also part of the surrounding of the other plane. If a surrounding point of the first plane is also a surrounding point of the second plane, or at least in the near of it, the point will be marked as edge point. After all points have been examined, the result is only approximately a line, which is caused by not accurate measurements (see red “line” in Fig. 5). A linear regression is applied to get a real line for a straight robot movement.

After determining the edging line by the use of the linear regression, the start and endpoint are transferred to the robot. Then, the robot can execute the task of applying the glue. In order to determine the precision of the process and thus of the product quality, we conduct some tests that are described in the next chapter.

5 Precision of Surface Recognition

Since in production environments varying light conditions can be assumed, we use 3D information for our plane detection instead of color differences in an image that can be distorted heavily by light reflection. Nevertheless, in order to investigate the accuracy, experiments were first carried out on a matte object as well as later on a highly reflective object. It has been assumed that the positioning accuracy of the robot is two decimal potencies better than the accuracy of the depth information of the Kinect, as the Kinect’s accuracy was extensively examined by [4] and [15]. With this assumption, the measurement of the robot was set to be accurate. The mean value, standard deviation and repeatability out of 20 attempts for each corner point were examined to measure the accuracy of the corner points. In every attempt the surfaces were selected, the intersection line calculated and then the outermost corner points computed. After that the robot moved to these two points and the distance between the edge points of the real object and the robot tool was measured. The results are listed in Table 1.

Table 1. Accuracy edge point detection

Test object	Mean value in [mm]	Standard deviation [mm]	Repeatability [mm]
Cardboard	5.14	1.24	8.85
Aluminum	6.99	4.44	20.3
Aluminum treated	7.17	1.7	12.68

One of the points that have been noticed is that the calculated corner points are placed inwards along the edge compared to their real counterpart. The reason for this is the use of the surface normal also at the surrounding of the planes. For the calculation, vectors of points are needed which do not belong to the object and thus lead to inaccurate normal vectors in the area. This results in rounded edges and also in the high mean value stated in Table 1.

Looking at the second examined object, an angle of aluminium, it has been found that the reflective properties of the aluminium significantly impairs the recognition of

the planes. Unfortunately, the 3D information are influenced by the surface of the object, since the Kinect v2 operates with infrared radiation to maintain the depth information. Thereupon, the object was treated with a developer, as found, for example, in material testing applications to minimize the reflection characteristic. Figure 6 shows the difference.

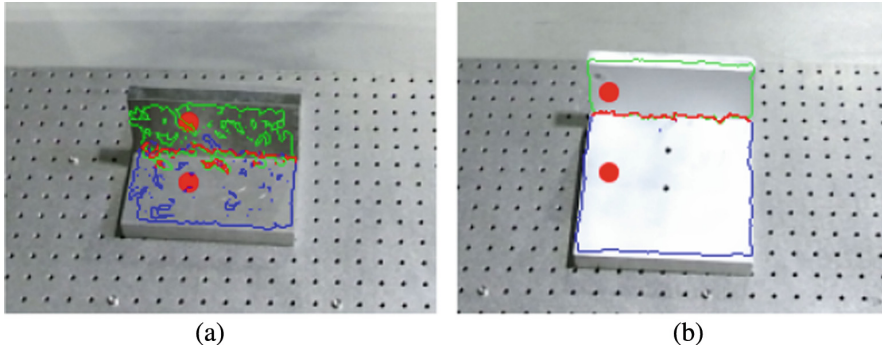


Fig. 6. Layer detection on metal. (a) untreated, highly restricted detection; (b) treated, better but not optimal

Our approach allows users to easily teach in points for the robot that would be otherwise difficult to reach. It enables movements along edges of workpieces that can be used for example for welding or gluing processes. In tests we demonstrated that our work can be used for processes that do not have high precision requirements. For matte objects such as cardboards or treated metals, the trajectory planning works reliably, however, especially for welding applications the distortion of Kinect’s depth information through reflective surfaces can be seen as a challenge, as it leads to false surface detections and thus to unusable paths.

6 Conclusion and Outlook

This paper provides an approach to simplified programming of industrial robots. The main focus of the applications is on adhesive application and welding processes. The programming process is designed in such a way that it is very intuitive and does not require any specialist knowledge. With the help of a menu, it is possible to switch between the two modes “Move robot” and “Teaching points”.

The implemented algorithm for fingertip recognition is necessary, as this is not provided by the API of Kinect. Recognition is based on the use of the human skeleton and the determination of the region of interest. The fingertips are determined with the help of Voronoi diagrams and appropriate filters.

The subsequent detection of planes is based on a region growing algorithm. Since the edge of the planes is not recognized by the algorithm as a straight line, a linear regression is applied through the point cloud. In this way, the start and end points of the

robot movement are determined in addition to the path. The results show that the available accuracy is not yet sufficient to use in production environments. Particularly in the case of reflecting surfaces, very high deviations are still achieved in some cases, so that these materials cannot be processed.

In future research, the use of other camera systems will be tested in order to be more independent of the material properties and thus increase system accuracy. Furthermore, the detection of more types of edges (circles, ovals etc.) will be investigated in order to expand the application areas.

References

1. Akgun, B., et al.: Trajectories for kinesthetic teaching: a human-robot interaction perspective. In: Proceedings of the Seventh Annual ACM/IEEE International Conference on Human-Robot Interaction, vol. 12, pp. 391–398 (2012)
2. Lun, R., Zhao, W.: A survey of applications and human motion recognition with microsoft kinect. *Int. J. Pattern Recogn. Artif. Intell.* **29**(5), 1555008 (2015)
3. Yang, L., et al.: Evaluating and improving the depth accuracy of kinect for windows v2. *IEEE Sens. J.* **15**(8), 4275–4285 (2015)
4. Windows Dev Center. <https://developer.microsoft.com/de-de/windows/kinect/hardware>. Accessed 08 Nov 2017
5. Landa-Huartado, L., et al.: Kinect-based trajectory teaching for industrial robots. In: Pan-American Congress of Applied Mechanics, vol. 14 (2016)
6. Canal, G.: A real-time human-robot interaction system based on gestures for assistive scenarios. *Comput. Vis. Image Underst.* **149**, 65–77 (2016)
7. Taylor, J., et al.: Efficient and precise interactive hand tracking through joint, continuous optimization of pose and correspondences. *ACM Trans. Graph. (TOG)* **35**(4), 143 (2016)
8. Yeo, H., et al.: Hand tracking and gesture recognition system for human-computer interaction using low-cost hardware. *Multimed. Tools Appl.* **74**(8), 2687–2715 (2015)
9. Gesing, S.: Approximation von Punktmengen durch Kreise (2005)
10. Holz, D., Behnke, S.: Fast range image segmentation and smoothing using approximate surface reconstruction and region growing. *Intell. Auton. Syst.* **12**, 61–73 (2012)
11. Stueckler, J., et al.: Real-time 3D perception and efficient grasp planning for everyday manipulation tasks. In: European Conference on Mobile Robots, vol. 5 (2011)
12. Zhang, L., et al.: Fast plane segmentation with line primitives for RGB-D sensor. *Int. J. Adv. Robot. Syst.* **6**, 1–8 (2016)
13. Vosselmann, G., et al.: Recognising structure in laser scanner point clouds. *Inf. Sci.* **46**(8), 1–6 (2004)
14. Borrmann, D., et al.: The 3D Hough transform for plane detection in point clouds: a review and a new accumulator design. *3D. Research* **2**, 1–13 (2011)
15. Lachat, E., et al.: First experiences with kinect V2 sensor for close range 3D modelling. In: International Workshop 3D-ARCH, vol. 6, pp. 93–100 (2015)



The Comfort Zone Concept in a Human-Robot Cooperative Task

Alireza Changizi^(✉) and Minna Lanz

Faculty of Engineering Sciences, Tampere University of Technology,
P.O. Box 589, 33101 Tampere, Finland
alireza.changizi@student.tut.fi

<http://www.tut.fi/en/about-tut/faculties/engineering-sciences>

Abstract. The global rise in interest towards robotics and artificial intelligence is increasing the technology acceptance among companies. This further encourages manufacturing companies to invest more in robotics on their factory floor. A robot manipulator can be sufficiently mobile and dexterous to operate alongside a human as would any other colleague. However, a human-centric viewpoint is needed in the design of the work cell to provide optimal working conditions for humans and thereby enhance employee performance. We identified a set of factors required for human comfort during cooperation with robots. These factors were divided into two main groups: mental and physical. Both mental and physical factors were based on scientific work reviews, robotics standards, and recognized human factors via a case study. These factors together are the basis for a comfort zone concept in human-robot collaboration. This concept forms design principles for developing the physical work environment of the future.

Keywords: Comfort zone concept · Human robot cooperation
Interaction · Collaboration · Cognition

1 Introduction

Currently, robots and needed safety equipment and clearance distances are taking up considerable space on factory floors. Production demands on factory floors are subject to continuous development. The diversity of product inquiries and the unpredictability of the marketplace are well recognized. These inherent changes require flexibility in the manufacturing processes, networks, factory layouts, and management systems. Moreover, local markets with low production levels must become competitive in the global marketplace and alongside mass production industries. As such, regional manufacturers must have highly customizable and personalized product lines in countries characterized by high production costs, low commitment rates, and high-quality requirements [1].

Collaboration between humans and industrial robots is now a critical consideration due to the aging population, which, during the last decade, was six

times greater than the overall population growth in Europe. In addition, there is a demand from manufacturing companies to postpone the age of retirement [9]. Older workers typically have precious work experience that can be utilized for longer periods if these workers are provided with physical assistance on the production line as their physical abilities decline. Moreover, replacing this age group with younger generation workers requires the development of skills in these workers, which likewise takes time and money. Currently, there is shortage of experienced workers in all of Europe, and Finland has one of the severest shortages of skilled workers [10] in comparison with other European countries.

A robotic partner on the production line can physically assist a worker and be trained with the skill set required on the production line. While a human can perform more complex operations that require higher cognition, robots can do repetitive jobs, heavy material handling, and tasks requiring high physical flexibility. Furthermore, the European Union's support for the consideration of collaboration scenarios involving human-technology interaction is highlighted in the INDUSTRIE 4.0 vision, which provides a roadmap for the so-called 4th industrial revolution [2].

The main aim of this current research is to develop a comfort zone concept (CZC) that can be used as a design guideline for designing better workplaces in the future. This paper presents a human-robot CZC that comprises a set of factors to optimize the production line environment. CZC prioritizes human comfort when working with an industrial robot.

2 Related Works

Here, we explore human behavior regarding interactions in the work environment. The main difference between humans and other creatures is our ability to engage in teamwork with shared intentions and objectives [26].

To achieve a desired goal, teammates must have strong commitment and determination to share learned behaviors and related cognitive abilities. During work interactions, two humans continuously observe each other to optimize the comfort of their work process. Human psychology and ergonomics contribute to these observations. Therefore, a robotic teammate and the surrounding workspace should mimic this cooperative behavior to optimize human comfort. Table 1 shows a review path of existing work related to the psychology, cognitive aspects, and human brain function with respect to cognition in human-robot Interaction (HRI) and human-robot collaboration (HRC).

An effective use of robots that considers human personality types and daily life preferences will produce a more trusting and satisfactory relationship between humans and robots [27]. Production line workers not only physically interact with the system, but their behavior is also a factor as they engage with the system during teamwork. As shown in Table 1, the main trends indicate that many studies have focused on HRI and HRC issues related to specific human cognitive needs, ergonomics, and the adoption and implementation of technology. These focuses are essential but not sufficient when considering each approach

Table 1. The summary of most relevant contributions associated to this research.

Main trends	Existing works
Psychology	From Human Factors to Human Actors: The Role of Psychology and Human-Computer Interaction Studies in System Design [11] The psychology of emotion [12] What Is Satisfying About Satisfying Events? Testing 10 Candidate Psychological Needs [13] Goal constructs in psychology: Structure, process, and content [20]
Cognitive Aspects	Design for aging [6] Meeting of minds: the medial frontal cortex and social cognition [21] Human Factors Experiences in Context - Comparing Four Industrial Cases Using a Soft Systems Framework [22]
Cognitive Robotics/Automation	Finding Trends in Human-Automation Interaction Research in Order to Formulate a Cognitive Automation Strategy for Final Assembly [15] Knowledge-based social networking app for collaborative problem-solving in manufacturing [17]
HRI/HRC	Two Faces of Human-Robot Interaction: Field and Service Robots [14] On a human-robot collaboration in an assembly cell [16] An implemented theory of mind to improve human-robot shared plans execution [18] Human-Robot Interaction-Review and challenges on Task planning and Programming [19]

individually. Therefore, there is a gap in research regarding the concept of creating a zone that covers the principal human aspects required to fully support workers in manufacturing settings or an assembly line.

In the following section, we propose a general implementation roadmap for creating the CZC. In the next section, we identify the mental and physical factors related to the design model of the Comfort Zone, and the task types in which humans and robots engage. In the last section, we suggest future prospects for the development and application of the CZC.

3 Comfort Zone Concept

Communication between interactive systems that is based on human preference requires a user model. In this study, we propose a guideline for facilitating progress from the current state-of-the-art field of industrial robotics with respect to interaction and collaboration, as well as associated human factors (in ergonomics and cognition). Our goal was to choose factors to realize an industrial robotic work cell model, for which human operator comfort is its primary design key.

3.1 Research Methodology

The main aim of the research is to create definition of CZC and design guidelines based on the CZC. The methodology for the research consists of 4 steps (Fig. 1).

Step 1: Extract robotic work states and human features that make people feel most supported. For this step, we reviewed related standards (in robotics and human factors) and scientific works to identify and select the most appropriate physical and mental features. Step 2: Create a concept for an interactive or collaborative zone between a robot and human, in which the robot continues to work and the human feels supported. This zone contains the features identified in step 1.

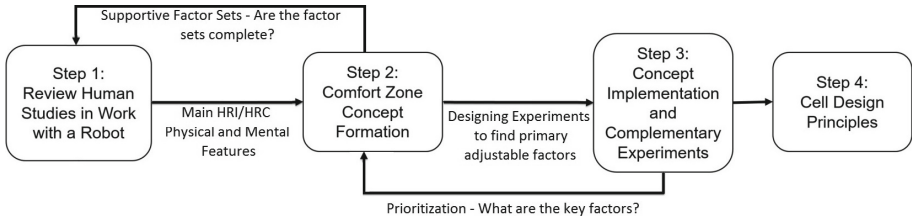


Fig. 1. Main steps in comfort zone concept.

Step 3: Sensor data are integrated with the collaboration methods to establish the actual assembly steps. The data from sensors are fused with the CZC to control robot behavior in supporting the human CZC. The experimental study of human behavior is performed in this step to adjust each factor. Step 4: Create a complete workcell design with sensors in place and the human engaged in an actual manufacturing task.

The workcell includes the personalized work station adjusted according to user preferences with respect to lighting, table height, size/reach of operator, and user seating preference while working or user distance preference (personal comfort zone). In this paper, we focus on steps 1 and 2.

There are two aspects to cooperation: mental and physical (Fig. 2). When starting a task, a human worker will automatically consider how to do the work and, at the same time, have a positive or negative feeling about the job. The physical aspects involve human factors and ergonomics. Human physical factors in an environment adjacent to a robot can be categorized into three main sectors: human, environment, and task. The second aspect involves important human mental functions such as attention, memory, language comprehension, and executive control, which is also known as human cognition [3, 6, 21].

3.2 Factors Relating to Mental Comfort

The mental aspects of human work include human brain functions or the so-called cognitive aspects. Cognitive aspects are generally grouped into attention, memory, language comprehension, and executive functions [6] (Fig. 2). Attention involves the ability to focus on a particular process (while disregarding useless information generated by the environment) and the capacity of humans

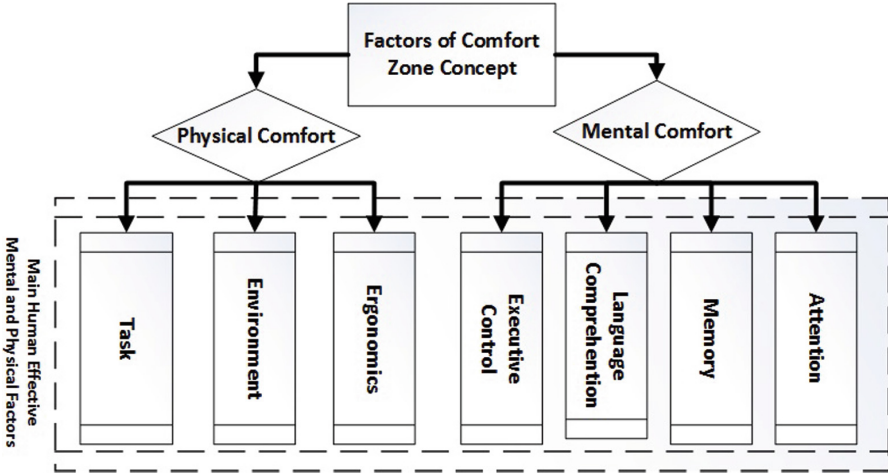


Fig. 2. Overview of CZC based on mental and physical comforts factors.

to multi-task. Memory refers to the ability of a human to mentally encode data, to store that data in the brain, and to recall the data when required. Language comprehension has a direct connection with memory and refers to the ability of the human to use perception for understanding a written or vocal message and to represent that meaning to the brain. The executive control function comprises cognitive skills correlated with the preservation and updating of cognitive and behavioral objects, the outlining and sequencing of operations, problem-solving, and the withholding of automatic replies. Studies show executive control to directly affect the aging person's life and, therefore, must be carefully considered [4, 5]. Figure 3 shows the brain's four cognitive functions.

Maintaining human motivation in the workspace enables the maintenance of memory and attention and helps the individual to exhibit good performance and sustain a high-quality work level during extended working hours [28]. Motivation can be considered to be an implemented preference with respect to the task goal during the work process, whereas personal satisfaction is related to performance-related rewards [28]. Hence, a worker can be dissatisfied regarding his/her working style, task execution, or awards, but could still be deeply motivated to accomplish the task at hand, which confers ambition, good performance, and the inclination to keep working for a longer period of time.

Based on the work of [13], main motivational factors were adjusted with respect to the four main factors of autonomy, competence, relatedness, and self-esteem, the first three of which are also proposed by the self-determination theory [3]. Motivational aspects were also tested in experiments for this paper and confirm the importance of the psychological factors considered during an assembly case study with a robot (Fig. 4). Tests included interaction and collaboration tasks for human beside a collaborative robot (Universal Robot model UR5). In the experiments, 42 test subjects participated in Lego assembly phases

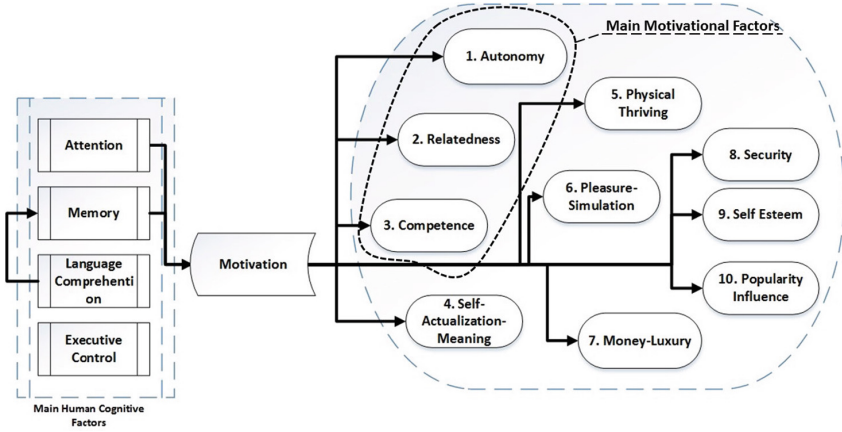


Fig. 3. The human mental functions are always engaged with the job at hand. The motivation to work beside the robot is critical during joint operation. By sustaining motivation, the human can retain the necessary level of attention and memory while performing a task.

that required high accuracy and a robot helped by delivering the main body and parts in the correct order to the participant. The participants then gave feedback about how they felt about their interaction or collaboration with the robot. The results showed a range of participant cognition-level engagement in the work, which demonstrated the importance of considering all cognitive factors and specifically autonomy, competence, and relatedness.

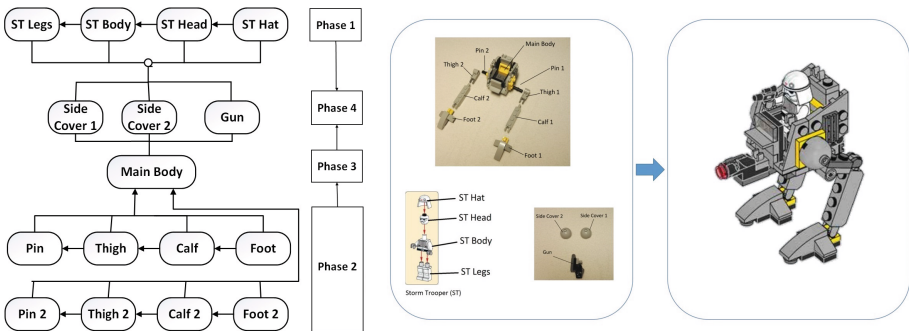


Fig. 4. Assembly state decomposition model [23] of the task performed using HRI and HRC.

Language comprehension refers to the human ability to observe texts and signs and then mentally translate them to generate meaningful phrases and an appropriate reaction. Comprehension is an essential skill set for a person employed beside a robot. However, comprehension will rely profoundly on

memory. By maintaining appropriate workcell instructions, signs, and human-machine interfaces (HMI), humans can remember to use them as necessary. Therefore, supporting memory will also help humans to comprehend textual information.

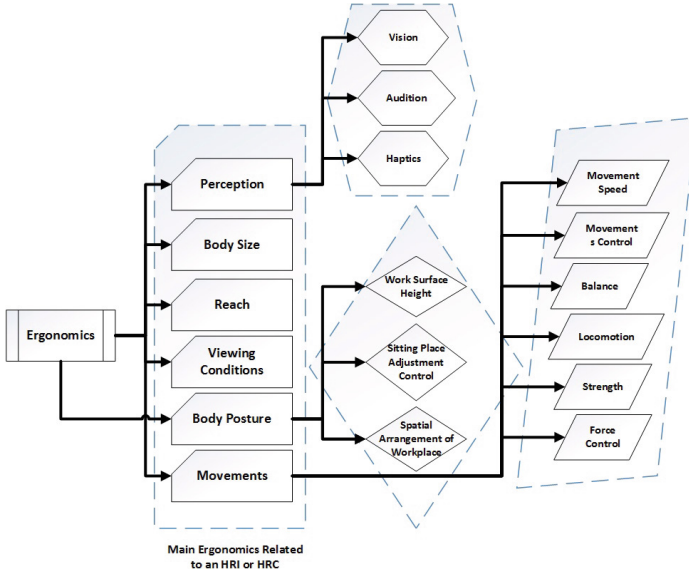


Fig. 5. List of human ergonomic factors that are valuable in a human-robot workcell. Elements with no sub-branches are adjustable; otherwise, only the sub-branches are adjustable.

3.3 Factors Relating to Physical Comfort

Factors relating to physical comfort can be divided into three categories - ergonomics, environmental features, and the task type to be performed beside the robot (Fig. 2).

Ergonomics. Ergonomics relate to the human physical features engaged during a manufacturing task next to a robot. We identified these factors by reviewing and selecting robotics standards as well as aspects identified in human factor studies [7, 8, 24]. Robots that adjust to a person’s ergonomic condition or that can consider a person’s limitations will help to provide more acceptable working conditions for the human during work hours. The main factors examined with respect to the human physical state include sensory perception (vision, hearing, and haptics), bodily dimensions, reachability, viewing statuses, body posture, and movements.

Body posture can be maintained by adjusting the work height and sitting area as well as the spatial arrangement of the workcell. Human movement [6] factors include speed, movement control, balance, locomotion, strength, and force control.

Environment. The environment includes human comfort factors related to the workspace, such as climate, noise, lighting, coloring, contact temperature, air quality, vibration, acceleration force, moisture level, and cleanliness of the workspace [24].

Climate factors [25] comprise room temperature, humidity, air flow, and thermal radiation, all of which can usually be adjusted by a central automation system. However, human climate comfort is an essential aspect when there is frequent interaction with a robotic partner.

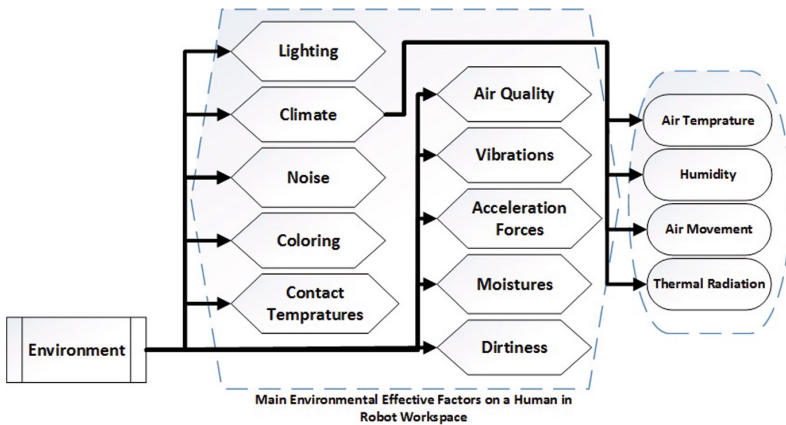


Fig. 6. List of valuable environmental factors in a human-robot workcell. Elements with no sub-branches are adjustable; otherwise, only the sub-branches are adjustable.

Task Type. Tasks performed when working next to a robot can be categorized into two types - interaction and collaboration. Interaction occurs when a robot simply passes parts to the human or takes elements away. The interaction task shown in Fig. 4 is performed by the robot moving the assembly parts and the main body into the human work area and then taking the main body away from the work area once the work is completed by the human.

Collaboration refers to instances in which the robot and human touch or operate on the same product at the same time. The human and robot have common goals at each step in their collaboration. For example, in Fig. 4, phases 3 and 4 are performed while the robot holds and rotates the main body to facilitate the reach of the human when installing legs and auxiliary parts in the assembly.

4 Conclusion

The domain of this research includes the study of human performance and adaptation to industrial robots and available technologies. This work is significant for the consideration of the factors to include in design models. This study provides a guideline for creating the Comfort Zone Concept. During the investigations, identification of the most relevant factors relating to design a better cooperation between human and machine was performed. CZC refers to a set of factors that relate to a design that addresses both human mental and physical comfort in a workspace. Moreover, the autonomy, relatedness, and competence were proved during experiments to be the drivers for human motivation in HRI and HRC.

In future work, each element will be modified to optimize its value for human productivity and comfort. We note that increasing all these factors will not necessarily result in human comfort, but their adjustability is the primary goal. These adjustments should be based on individual factors and the effects of other factors. Ultimately, we expect workers to enter a human-friendly space modeled on their personal CZC.

References

1. Lanz, M., Tuokko, R.: Concepts, methods and tools for individualized production, 4th edn. In: Handbook of Human Factors and Ergonomics, Production Engineering (2017)
2. Kagermann, H., Wahlster, W., Helbig, J.: Recommendations for implementing the strategic initiative INDUSTRIE 4.0: Final report of the Industrie 4.0 Working Group. German Federation Ministry of Education and Research (2013)
3. Ryan, R., Deci, E.: Self-determination theory and the facilitation of intrinsic motivation, social development, and well-being. *Am. Psychol.* **55**(1), 68–78 (2000)
4. Resnick, S.M., Pham, D.L., Kraut, M.A., Zonderman, A.B., Davatzikos, C.: Longitudinal magnetic resonance imaging studies of older adults: a shrinking brain. *J. Neurosci.* **23**, 3295–3301 (2003)
5. Royall, D.R., Palmer, R., Chiodo, L.K., Polk, M.J.: Declining executive control in normal aging predicts change in functional status: the freedom house study. *J. Am. Geriatr. Soc.* **52**(3), 346–352 (2004)
6. Boot, W.R., et al.: Design for aging, 4th edn. In: Handbook of Human Factors and Ergonomics, pp. 1442–1471 (2012)
7. ANSI B11.TR: Standard for Ergonomic Guidelines for the Design, Installation And Use of Machine Tools, p. 1 (2016)
8. ISO/TS 15066: Standard for Robots and robotic devices - Collaborative robots (2016)
9. Eurostat Statistics: People in the EU: who are we and how do we live? Publications Office of the European Union, Luxembourg (2015)
10. Reyman, D., et al.: Labour Market Shortages in the European Union. Economic and Scientific Policy, European Parliament, Brussels, Policy Department A (2015)
11. Bannon, L.J., Greenbaum, J., Kyng, M.: From human factors to human actors: the role of psychology and human-computer interaction studies in system design. *J. Des. Work.: Coop. Des. Comput. Syst.* 25–44 (1991). Brussels
12. Strongman, K.T.: The Psychology of Emotion, 5th edn. Wiley, Hoboken (2003)

13. Sheldon, K.M., Elliot, A.J., Kim, Y., Kasser, T.: What is satisfying about satisfying events? Testing 10 candidate psychological needs. *J. Pers. Soc. Psychol.* **80**(2), 325–339 (2001)
14. Ventura, R.: Two faces of human-robot interaction: field and service robots. *J. Mech. Mach. Sci.* **16**, 57–74 (2014)
15. Fast-Berglund, A., Mattsson, S., Bligard, L.: Finding trends in human-automation interaction research in order to formulate a cognitive automation strategy for final assembly. *Int. J. Adv. Robot. Autom.* **1**, 1–7 (2016)
16. Tsarouchi, P., Matthaïakis, A.S., Makris, S., Chryssolouris, G.: On a human-robot collaboration in an assembly cell. *Int. J. Comput. Integr. Manuf.* **30**(6), 580–589 (2017)
17. Mourtzis, D., Doukas, M., Milas, N.: A knowledge-based social networking app for collaborative problem-solving in manufacturing. *Manuf. Lett.* **10**, 1–5 (2016)
18. Devin, S., Alami, R.: An implemented theory of mind to improve human-robot shared plans execution. In: *ACM/IEEE International Conference on Human-Robot Interaction*, pp. 319–326 (2016)
19. Tsarouchi, P., Makris, S., Chryssolouris, G.: Human-robot interaction-review and challenges on task planning and programming. *Int. J. Comput. Integr. Manuf.* **29**(8), 916–931 (2016)
20. Austin, J.T., Vancouver, J.B.: Goal constructs in psychology: structure, process, and content. *Psychol. Bull.* **120**(3), 338–375 (1996)
21. Amodio, D.M., Frith, C.D.: Meeting of minds: the medial frontal cortex and social cognition. *Nat. Rev. Neurosci.* **7**(4), 268–277 (2006)
22. Berlin, C.: Human factors experiences in context-comparing four industrial cases using a soft systems framework. *Ergon. Open J.* **4**, 131–144 (2011)
23. Lanz, M.: Logical and Semantic Foundations of Knowledge Representation for Assembly and Manufacturing Processes, Ph.D. thesis, Tampere University of Technology (2010)
24. Bullinger, H.-J.: *Ergonomie–Produkt–und Arbeit–platzgestaltung*. Teubner, Stuttgart (1994)
25. Spath, D., Braun, M., Meinken, K.: Human factors in manufacturing. In: *Handbook of Human Factors and Ergonomics*, vol. 4, pp. 1643–1666 (2012)
26. Tomasello, M., Carpenter, M., Call, J., Behne, T., Moll, H.Y.: Understanding and sharing intentions: the origins of cultural cognition. *Behav. Brain Sci.* **28**, 675–735 (2005)
27. Kahn, P.H., et al.: Will people keep the secret of a humanoid robot? In: *Proceedings of the Tenth Annual ACM/IEEE International Conference on Human-Robot Interaction - HRI*, pp. 173–180 (2015)
28. Luczak, H.: Task design and motivation, 4th edn. In: *Handbook of Human Factors and Ergonomics*, pp. 397–440(2012)



A Low-Cost Automated Fastener Painting Method Based on Machine Vision

Ran Zhao¹(✉), Adrien Drouot², Joseph Griffin³, Richard Crossley³,
and Svetan Ratchev³

¹ College of Information and Electrical Engineering,
China Agricultural University, Beijing, China
ran.zhao@cau.edu.cn

² Institut FEMTO-ST, CNRS, UMR 6174, UFC – ENSMM - UTBM,
25 000 Besançon, France
adrien.drouot@femto-st.fr

³ Institute for Advanced Manufacturing, University of Nottingham,
Nottingham NG7 2TU, UK
{joseph.griffin, richard.crossley,
svetan.ratchev}@nottingham.ac.uk

Abstract. Fastener painting of aerospace structures, in particular legacy products, relies heavily on the skill or rather craftsmanship of the human operator. This process is time-consuming while automated operations with industrial robots can be a more efficient solution. Spray painting robots have been widely used in industry, however, they are not suitable for painting fasteners individually because it will cause a significant waste of materials. Thus, it is essential to develop proper tools and automated methods to replace manual work in order to reduce the cost and improve product quality. This research topic has been receiving more and more attention from both academia and industry.

In this article, we present a low-cost and flexible solution for automated fastener painting using a painting dabber and machine vision. A specific nozzle for the dabber is designed to apply paint on fasteners. The system locates the fasteners on aerospace structures with a Cognex camera, then painting is done by the robot with off-line programming. Experimental results show the effectiveness and practicality of automated painting system developed in this paper.

Keywords: Low-cost · Automated fastener painting · Machine vision

1 Introduction

Painting is widely used in industry, especially in automotive and aerospace manufacturing. It is an indispensable procedure for engineering machinery products in the process of surface manufacturing, which has various effects such as protection, beautification, water avoidance, antifouling, hidden and so on [1].

As intelligent equipment, painting robots can improve the efficiency and quality of painting operations, meanwhile reducing the labor costs [2]. However, painting robots are usually used in traditional spray painting that applies a coating (paint, ink, varnish, etc.) through the air onto a surface. They are often programmed to follow a specific

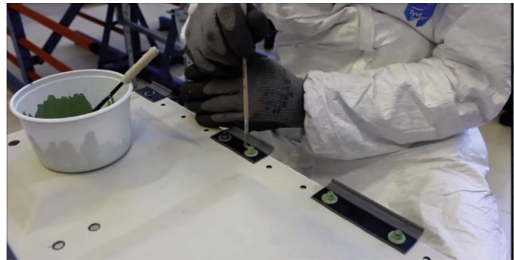
path and to spray material precisely and consistently, as shown in Fig. 1a. The main drawback of a spraying robot is that it is only suitable for surface painting. For the case of fastener painting where paint only needs to be applied on several discrete regions on a surface, it is not competent anymore.

Meanwhile, traditional painting robots are usually programmed using a teach pendant which, although it is an intuitive programming approach and doesn't require high programming skills, does suffer from the reliance on the human programmer to make changes to the robot path. This manual teaching process often takes a long time, and during this stage, the robot cannot be used in the production. Moreover, workers are exposed to toxic and hazardous environments. Therefore, this type of automation is not cost effective for aircraft manufacturing where the geometry of the parts and the required operations vary considerably.

In this paper, a low-cost automated fastener painting system is presented. The traditional fastener painting process is usually carried by operators using brushes to paint every fastener on the product, as shown in Fig. 1b. This is a highly repetitive task and the manual process is time-consuming and labourious. Moreover, the product quality is based on the operator's skills, experience, and knowledge of the production facilities. The operators must work in a hazardous environment. All such disadvantages will restrict the efficiency of the manual painting process. The proposed system emulates the human operation but in a fully automated manner. A painting dabber is used to apply paint instead of brushes which are unsuitable for an industrial robot to use. A machine vision system is implemented on the industrial robot to determine the position of the fasteners on the structure.



(a)



(b)

Fig. 1. (a): A FANUC industrial spray painting robot is applying the coating onto a curved surface. Source: <http://www.fanuc.eu>. (b): The manual process of fastener painting where the human operator paints each fastener on a wing structure using a brush.

2 Related Work

One of the challenges in fastener painting is to locate each fastener quickly and accurately. In this perspective, good sensing ability is essential to provide robots with an increased level of autonomy. Vision systems are highly suited for providing the robot's environment information as well as for the recognition of objects and their

features, providing information about their position and pose, allowing it to more reliably act in an unconstrained cell. Furthermore, to ensure any automated process is carried out effectively after the manual operation, vision can be used for in-line visual quality inspection to confirm that the assembly's sub-components are mounted within design specification.

Machine vision has been used widely in manufacturing and production, in a number of applications [3]. Indeed, the state of the art presents various solutions that use different techniques (both 2D and 3D) such as monocular vision [4], CCD cameras [5] or laser range-imaging [6]. Many types of vision systems and range sensors are available today, but the design and integration of them needs to take consideration of many issues such as: accuracy, speed, reliability, and cost, as well as environmental operating constraints such as: lighting, temperature, and humidity.

Besides good sensing abilities, it is necessary to develop systems that can reduce the time and difficulty associated with tool path programming. In this respect, offline programming software (OLP) [7] has been developed in recent years, both as commercially available products (such as KUKA.Sim for KUKA [8], RobotStudio for ABB [9] and MotoSim for Motoman [10]) as well as in academic research field (for example ROBOMO [11] and Robott [12]). Such software has the ability to model and to present graphically the robot and other equipment, generate programs and then simulate the robot behavior for a given task. However, most software still relies on the teach pendant for robot motion generation, such as tag creation and trajectory planning. Therefore, this paper proposed an automated OLP approach with the help of external sensors. It is low-cost, efficient and sufficient for the use in the manufacturing operations of small and medium-sized enterprises (SMEs).

The remaining content of this paper is organized as follow: Sect. 3 describes the machine vision-based fastener painting system, including the system overview and detailed techniques. Experimental results carried on an ABB industrial robot are presented in Sect. 4. Finally, this work is concluded in Sect. 5.

3 The Automated Fastener Painting System

3.1 System Overview

The automation of the fastener painting has been thought as a partially automated process where the human operator presents the parts to be operated by the robot, after having performed other manual operations on it previously. Each part is provided by an RFID tag that is scanned before presenting the part to the robot, and that allows uploading from a database the corresponding part information. After the manual operation, the part will be transferred to the painting robot by a conveyor. As the part will be placed randomly on the conveyor by the operator, painting robot must rely on external sensors to detect the exact position and orientation of the part in front of it. Meanwhile, specific painting end-effector will need to be designed as well for different fastener models in a real-world application.

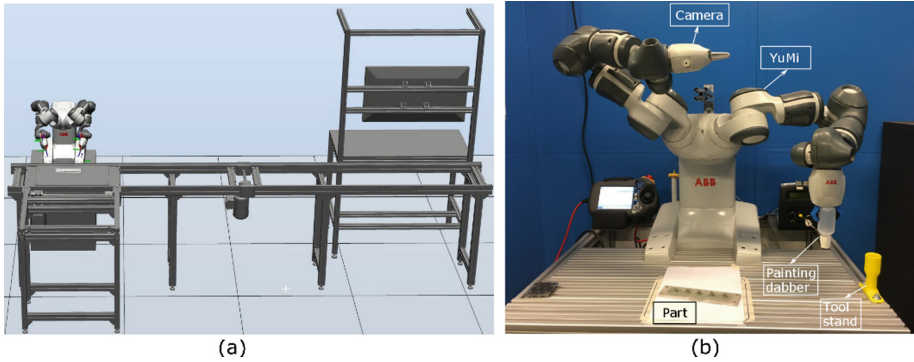


Fig. 2. (a): The designed fastener painting cell with a conveyor and a manual workbench. (b): The experimental setup of the painting cell.

Figure 2 shows the designed fastener painting workbench and the physical setup used for the experiments of the developed system. The robot used in this paper for implementation is the ABB IRB-14000 (also known as YuMi). It is a dual-arm manipulator platform which is designed for small parts assembly. It has only a 0.5 kg payload but this is adequate for small fastener painting. Compared with the large-sized industrial robot, YuMi is cheaper and the manufacturer specified accuracy of 0.02 mm is more than sufficient for painting applications. Also, YuMi is equipped with a built-in safety system, such as padded arms and light-weight design. Therefore, YuMi is quite suitable for working alongside human operators without the requirement for fully enclosed guarding. Meanwhile, YuMi has a built-in machine vision camera module in its right hand. The vision module contains a Cognex AE3 In-Sight 2D camera and provides powerful and reliable vision and identification tools. Table 1 details the camera specification.

Table 1. Specification of the integrated machine vision camera system.

Description	Data
Resolution	1.3 Megapixel
Lens	6.2 mm f/5
Illumination	Integrated LED with programmable intensity
Software engine	Powered by Cognex In-Sight

3.2 Painting Process

To emulate the human's skill in the fastener painting process, a painting dabber is used to apply paint on the fasteners, as shown in Fig. 3. The painting dabber is composed of a bottle which contains the paint and a nozzle which is used to apply paint. During the usage, a piece of foam is placed inside the nozzle to control the flow of the paint. The foam will soak up the paint and store it. When the dabber contacts the fastener, the paint will be squeezed out and then applied evenly on the fastener.

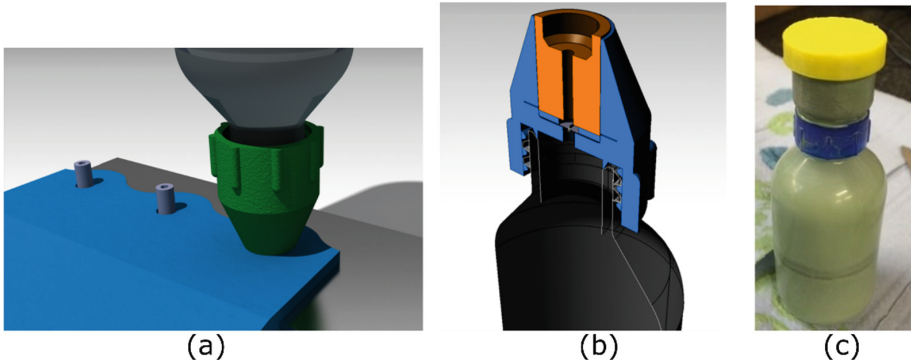


Fig. 3. (a): The working principle of the painting dabber. (b): The internal structure of the nozzle attached to the painting dabber. (c): A real painting dabber used in the cell.

Nozzles of different sizes can be substituted with respect to different fasteners. Painting dabber is easy to obtain, therefore it is suitable for the proposed low-cost scenario.

According to the working principle of the painting dabber, the robotic fastener painting process is designed as follows:

Step 1: Locate each fastener with the machine vision system.

Step 2: The robot grabs the dabber and moves to the position that is 20 mm above the located fastener.

Step 3: The robot goes down and keeps the fastener is entirely covered by in the nozzle.

Step 4: Rotate the dabber clockwise by 180° and then rotate 180° counter-clockwise.

Step 5: The robot goes up and moves on to painting the next fastener.

3.3 Vision-Guided Programming

The system configuration of vision-guided programming is shown in Fig. 4a. A hybrid position/vision control platform is developed to control the robot motion. The position control is used to maintain the tool orientation. Vision sensing is used to locate the fasteners on the part. The part image is captured by a single camera. Then the image is processed using the PatMax [13] algorithm for the 2D (x and y) coordinates. Figure 4b shows an example of the image processing results. The depth coordinate (z) cannot be obtained from the camera. However, it is able to be detected by the contact between the painting dabber and the fastener, according to the variation of the robot's motor torque.

3.4 System Calibration

One of the most important steps of using vision system is the camera-robot calibration. The calibration consists of two basic steps. First the camera calibration which converts the image pixels to mm, and second the camera to robot calibration which relates the camera coordinates to a robot frame. Camera calibration is the process of estimating the parameters of a pinhole camera model approximating the camera that produced a given

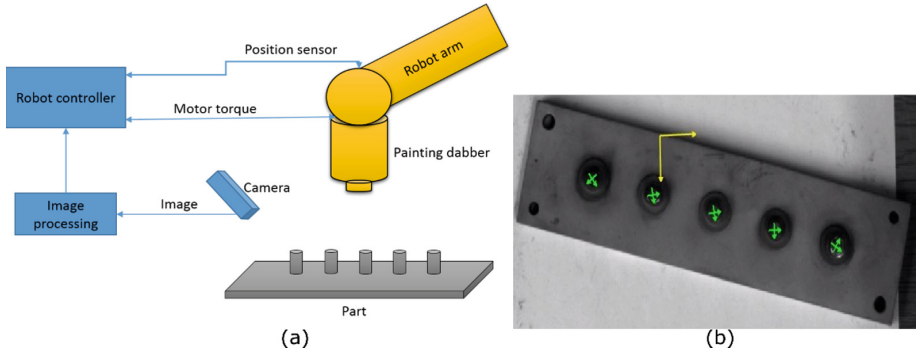


Fig. 4. (a): The system configuration of the vision-guided programming for controlling the robot moves to each fastener that is on a piece of part. (b): The image processing result. The green coordinates indicate the center position (x and y) of each fastener in the camera frame (the yellow coordinate). (Color figure online)

photograph. For 2D cameras, a checkerboard with fiducial is usually used for calibration. The calibration process will find the origin in the camera frame \mathcal{F}_c which is used to determine the position of the fastener in \mathcal{F}_c . We denote this position as P_F^C . Then this position needs to be transformed to the robot frame \mathcal{F}_R . Finally, we will get the fastener's position in the robot coordinate P_F^R .

3.5 Singularity Avoidance

During the movement from the initial robot position to the painting position (the position where the fastener is), the robot may pass through the singularity pose. It is because the fastener is a symmetrical object, the orientation from the vision system may vary from each result although the fastener's position never changes. As shown in Fig. 5, two camera results give the same position of the object but completely different orientation. As the motion path is planned by the robot's own controller, it can provide the shortest solution but it cannot avoid the singularity. For example, in Fig. 5b, the robot's wrist joint (joint 6) has to rotate a large angle during the movement. Singularity may occur in this case. Thus, to avoid the singularity, we can simply fix the orientation value that comes from the vision result as zero. Consequently, the robot's wrist joint will not rotate during *Step 2*. If the initial position of joint 6 is programmed properly (for example, $j_6 = 5^\circ$), the singularity will be avoided in the whole painting process. The joint value is set approximately to zero so that the joint boundary of the 6th joint will not be exceeded during the rotation in *Step 4* in Paragraph 3.2. Another advantage of fixed orientation is that the execution time is largely reduced. For multi fasteners, the robot doesn't need to rotate to the exact results coming from the camera as the orientation result of each fastener can be completely different (It can be clearly seen from Fig. 4b).

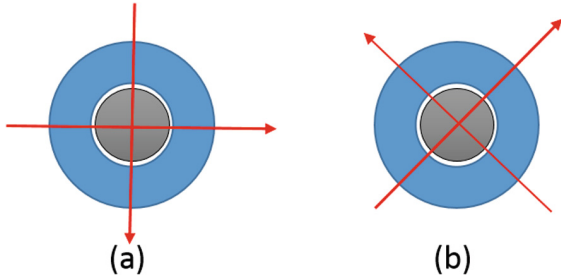


Fig. 5. Different orientation results from the same object.

4 Experimental Results

To evaluate the proposed painting system, a test part with five fasteners was used in the experiment. Software running on the robot is written by the ABB RAPID programming language. Experiments were conducted with the set-up as shown in Fig. 2b. Experimental results are illustrated in Fig. 6. From the results, we can see that the fasteners can be successfully painted with the proposed system.

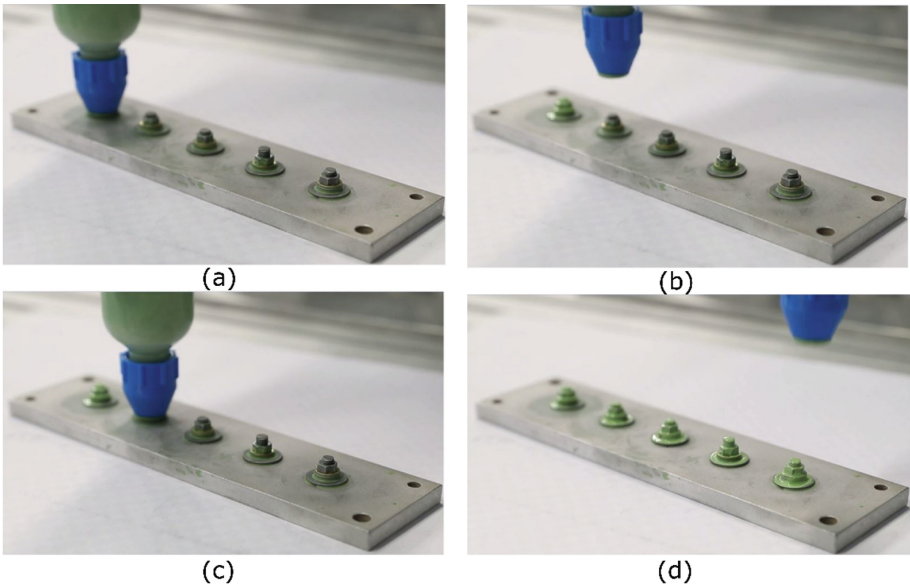


Fig. 6. (a): The robot is painting the first located fastener. (b): The robot moves to the next fastener. (c): The robot is painting the second fastener. (d): The final result after all of the fasteners have been painted.

It was observed that the vision accuracy could be affected by the ambient light. 5 camera acquisitions of the part were made at the shortest possible time span one after the other at four different times during the day (10am, 1pm, 2pm, 5pm) in order to test the camera with different levels of light and different light directions. The average errors between the camera results and the real positions are measured for all cases. Meanwhile, we also calculated the rate that the system can successfully recognize all fasteners. Table 2 shows the accuracy and the success rate of each condition. The minimum error is 1 mm in the morning and in the late afternoon while the maximum error is 4.5 mm at 5pm. The light conditions in the workshops were partially controllable because of a skylight in the ceiling. To achieve greater accuracy, it has been decided to leave the available neon lights always turned on.

Table 2. Results of the calculations of camera accuracy under each light conditions (The experiments were done under the day light condition of mid-November in Nottingham, UK. Results may vary at different time and different places).

Time	Error	Success rate
Morning light (10am)	1 mm	99%
Lunch light (1pm)	1.8 mm	98%
Early afternoon light (2pm)	2.2 mm	98%
Dusk light (5pm)	4.5 mm	90%

5 Conclusion and Future Work

In this paper, an automated fastener painting system was presented. It is based on a simple machine vision system and a painting dabber to emulate the skilled human operation. An ABB YuMi robot with built-in vision sensor is deployed, which reduces the total system cost. The proposed system is currently able to locate and paint fasteners on flat surfaces. This platform could enable SMEs to cost efficiently automate fastener painting or similar processes such as small part sorting and sealing. The preliminary experimental results presented in this paper validate the effectiveness of the proposed approach.

In future work, we will consider the integration of more sensors, such as the force/torque sensor. Such sensors are able to provide the essential contact feedback information, which can be used to compensate for the error from the camera. For 3D curved surfaces a low-cost 3D sensor (such as the Kinect RGB-D sensor) could be added. To fully evaluate the proposed system, more experiments with standard aerospace structures are required with additional quality control measures to enable process certification.





References

1. Xuewei C., et al.: Rapid generation of spraying instructions for painting robot basing on automatic programming technology. In: Proceeding of IEEE International Conference Mechatronics and Automation, pp. 669–674. IEEE, New York (2014)
2. Hepling, C.: Automated industrial robot path planning for spray painting process: a review. In: Proceedings of 4th IEEE Conference on Automation Science and Engineering, pp. 522–527. IEEE, New York (2008)
3. Elias, N.M., et al.: A survey on industrial vision systems, applications and tools. *Image Vis. Comput.* **21**(2), 171–188 (2016)
4. Liangyu, L.: A machine vision system for inspecting bearing-diameter. In: Proceedings of the Fifth World Congress on Intelligent Control and Automation, pp. 3904–3906, IEEE, New York (2004)
5. Wrong, A.K., Rong, L., Liang, X.: Robotic vision: 3D object recognition and pose determination. In: Proceedings of International Conference on Intelligent Robots and Systems, pp. 1202–1209. IEEE, New York (1998)
6. Antonio Ramon, J., Ceres, R., Pons, J.L.: A vision system based on a laser range-finder applied to robotic fruit harvesting. *Mach. Vis. Appl.* **11**(6), 321–329 (2000)
7. Zengxi, P., et al.: Recent progress on programming methods for industrial robots. *Robot. Comput.-Integr. Manuf.* **28**(2), 87–94 (2012)
8. KUKA Homepage. <http://www.kuka.com>. Accessed on 2017 Dec 10
9. ABB Homepage. <http://new.abb.com/products/robotics/fr/robotstudio>. Accessed on 2017 Dec 09
10. Motoman Homepage. <https://www.motoman.com/>. Accessed on 2018 Jan 01
11. Chang-Sei, K., et al.: PC-based off-line programming using VRML for welding robots in shipbuilding. In: Proceedings of IEEE Conference on Robotics, Automation and Mechatronics, pp. 949–954. IEEE, New York (2004)
12. Bottazzi, V.S., Fonseca, J.C.: Off-line robot programming framework. In: Proceedings of the Joint International Conference of Autonomic and Autonomous Systems and International Conference on Networking and Services, pp. 71–76. IEEE, New York (2005)
13. <http://www.cognex.com/pattern-matching-technology.aspx?pageid=11368&langtype=1033>. Accessed on 2017 Dec 26

Assembly Methods and Models



A Probabilistic Approach for Trade-off Analysis of Composite Wing Structures at the Conceptual Phase of Design

Konstantinos Bacharoudis^(✉) , Thomas Turner , Atanas Popov ,
and Svetan Ratchev 

University of Nottingham, Nottingham NG7 2RD, UK
Konstantinos.Bacharoudis@nottingham.ac.uk

Abstract. One of the major elements when performing a design for manufacturing and assembly methodology is the cost modelling method. A probabilistic cost approach is introduced herein for the series production of a composite wing structure. The proposed methodology should be able to capture changes in the design, the materials and the fabrication processes. Critically, the assembly strategy of the product should also be included to enable realistic multi-disciplinary trade-off studies among several potential build philosophies of the wing structure at the early phase of the design. Furthermore, uncertainty related to the various input parameters, i.e. production, process and cost parameters due to incomplete knowledge, can be considered. Thus, the main effort of the present work is to set up the framework of this methodology, to develop the appropriate cost approach in order to capture manufacturing and assembly costs and further to establish a sensitivity analysis module in order to clarify the dominant cost-drivers of the product. To deal with the uncertainty, Monte Carlo simulation is implemented while Spearman's correlation coefficients are evaluated and used to perform the sensitivity study. The efficacy of the suggested methodology is demonstrated by comparing a traditional wing design against new more integrated manufacturing techniques, e.g. the co-curing process, for a simplified wing configuration.

Keywords: Cost modelling · DFMA · Composite wing · Process plan
Monte Carlo simulation

1 Introduction

Concurrent engineering is increasingly the preferred approach to product development as a way of shortening the development time of the product. Its main characteristics can be summarised as working within multi-disciplinary teams and implementing in parallel from the very early stages of the product development. Design for manufacturing and assembly methods (DFMA) are essential features of the concurrent engineering approach and have developed and evolved over the past years. There are several available commercial DFMA methods [1] of qualitative and quantitative types, e.g. the Hitachi Assembly Evaluation Method [2], or the Boothroyd-Dewhurst DFMA approach [3], respectively. All these techniques help to develop a structured

environment in which to evaluate designs in terms of manufacturability and assemblability, to explore feasible manufacturing/assembly solutions, to identify fabrication/assembly constraints of the draft designs, to estimate the cost implications when selecting a specific route, and to report to the design team areas for further improvements to the design. There are many challenges associated with these tasks, particularly when techniques are put in place for the development of aerospace components made of composite materials. A distinctive characteristic of processes for composite materials is that they are mainly additive processes while the material properties of the structure are determined as the part is manufactured. Furthermore, manufacturing and assembly processes for composite materials are relatively new compared to the processes used for the metallic materials and the processes lack in maturity, commonality and standardisation among different manufacturers. On the other hand, composite materials offer an overwhelming number of manufacturing routes to fabricate a given product making classification difficult. Considering at the same time strict aerospace requirements such as the demand for rapid one-way assembly, introduction of low cost flexible tooling and automation, quality assurance and control and tight tolerances of the aircraft components, the establishing of a robust and intelligent DFMA method is particularly challenging.

The main effort of the present work, as a first step toward the implementation of a DFMA methodology is to set up the framework of the cost methodology, that is, to identify and develop the appropriate cost approach. The aim is to capture manufacturing and assembly costs as well as to identify the cost-driver parameters at a phase in the design process when relatively little information is available. It should be stated that several cost modelling approaches exist for the cost estimation of aircraft component [4]. However, most of them lack a module that can deal with the uncertainty introduced in the input variables mainly due to the incomplete knowledge in the early stage of the design.

Thus, a process-based cost estimation method (PBCM) [5] is adopted and implemented. Recurring and non-recurring costs are estimated by placing an emphasis on the reasonable allocation of non-recurring cost over time as well as among the several operational steps of the candidate processes. Time equations are developed for every process step based on simple analytical equations correlating some basic process parameters with specific design variables. Process plans are developed for fabrication and assembly processes related to the composite components. Finally, to deal with the uncertainties of the input variables, a Monte Carlo simulation is implemented giving additionally the opportunity to perform a sensitivity analysis by evaluating the Spearman's rank correlation coefficients to identify the most important parameters or the so-called cost drivers. Having identifying cost drivers, more effort in their modelling can be devoted in order to improve the accuracy of the cost estimation. An illustrative, simplified example is performed to demonstrate the efficacy of the suggested methodology comparing a traditional wing design against new fabrication techniques that composite material offers, i.e. towards more integrated designs with fewer parts.

2 Cost Modelling Method

Several cost estimation methods have been developed for the estimation of manufacturing and assembly costs for aircraft structures, among them one can identify analogous, parametric, activity and technical based methods [4]. Every method has advantages and disadvantages and should be carefully selected to fit the purpose. In the present work, a bottom-up approach is selected, i.e. a process-based cost method (or technical cost modelling approach) which is suitable for making trade-off analysis at the early stage of the design process, capturing differences in various designs and build philosophy strategies of a wing structure [5]. The method is based on the estimation of the recurring and non-recurring cost for every operational step of a manufacturing/assembly process. Material, labour (direct) and energy costs are considered as recurring costs in the present cost model. Non-recurring costs are the capital recovery of the machines/equipment/tooling/fixtures necessary for the production, maintenance costs of those machines and tools as well as the floor-space costs to accommodate the production.

The major steps to estimate the manufacturing and assembly costs are the identification of the operations related to the preferred processes, the estimation of the cycle time of each process in relation to the design, industrial and process parameters, the determination of the appropriate number of resources, e.g. number of tools, based on parameters such as the cycle time of every operation and finally the calculation of the costs using appropriate cost parameters.

2.1 Process Based Cost Model

In PBCM, the total manufacturing cost per component (or the total assembly cost per product) can be derived into the sum of the recurring and non-recurring costs by

$$C_{\text{Total}} = C_{\text{Material}} + C_{\text{Labour}} + C_{\text{Energy}} + C_{\text{Equipment}} + C_{\text{Tooling}} + C_{\text{Building}} \quad (1)$$

To calculate each of these elements of per piece cost, the annual cost of each element is divided by the target annual production, PV . The process of interest, especially fabrication/assembly processes for carbon fibre reinforced plastic (CFRP) materials, can accommodate several operations/stages in order to be performed and be completed. Thus, the annual costs for each element are the sum of that element's costs calculated for each stage of the manufacturing/assembly process.

For the recurring costs, the unit method [6] is implemented. For the non-recurring costs, i.e. cost to buy and maintain machines/equipment, tools/fixtures, or cost to accommodate the production i.e. floor-space cost, the time value of money is considered, and the annual worth value is computed by summing the capital recovery (CR) and the annual operating and maintenance costs (AOC) of the asset given by:

$$AC_{\text{asset}}^j = CR_{\text{asset}}^j + AOC_{\text{asset}}^j \quad (2)$$

where asset = machines, tooling and building. The capital recovery is composed by the sum of the products of the initial investment, P with the capital recovery factor (A/P , i , n) and the salvage value, S_n after n years with the sinking fund factor (A/F , i , n).

Usually, the annual operating and maintenance costs of the asset are expressed as a percentage of the capital recovery ($\alpha_j.CR$), where α_j is in [%].

It should be highlighted that the resources needed to achieve the annual production volume is of high importance. Thus, the number of parallel lines NPL_j (or the number of machines) necessary to achieve the effective annual production volume $PV_{\text{effective}}^j$ is calculated by the ratio of the required time per year to produce $PV_{\text{effective}}^j$ parts divided by the annual uptime of the plant, its formulation is given by:

$$NPL_j = \begin{cases} \frac{\tau_j}{UT_j} & \text{non - dedicated} \\ \left\lceil \frac{\tau_j}{UT_j} \right\rceil & \text{dedicated} \end{cases} \quad (3)$$

If the machine/equipment is dedicated to the fabrication of a part of interest then the value of Eq. (3) is rounded up to the next integer value. If the machine/equipment is not dedicated to a part of interest then a real value is calculated by Eq. (3). If the machine is shared among several operational steps or among the production of several parts, e.g. an autoclave to cure composite parts, then, in Eq. (3), τ_j becomes the sum, $\sum \tau$, from all the operations with which the machine was involved. Concerning the tooling/fixture, the number of tools necessary to run the production for a specified program life time T_{PL} is given by:

$$NT = \max \left(\left\lceil \frac{PV_{\text{effective}}^j T_{PL}}{T_{TL}} \right\rceil, \lceil BS_j \cdot NPL_j \rceil \right) \quad (4)$$

The first part in the max-function indicates the number of the tools that are necessary to produce the production volume for the lifetime of the project. The second term indicates the necessary number of tools to achieve the annual target production volume. The maximum between these two quantities is the necessary number of tools for the lifetime of the project. Where $PV_{\text{effective}}^j$ is the effective production volume for the stage of the process that the tool actually wears and T_{TL} is the useful tooling/fixture life in [hits]. Tools are always considered to be dedicated to the part production.

2.2 Monte Carlo Simulation and the Rank Correlation Coefficient

A Monte Carlo (MC) simulation method is selected to deal with the uncertainty related to the input parameters. Design, industrial, process and cost parameters are considered as random variables in an attempt to express the degree of confidence for their value at the early stage of the design. MC is quite straightforward in its application. It is based on the random sampling of the vector of the input variables. Sample values for every random variable are formed and repetitive simulations performed through the developed process based on the cost model. A sample of values of the desired output parameter, e.g. the total cost, is obtained and statistically analysed further. A major step in implementing the MC method is the random number generators. MC analysis is implemented using VBA into Excel spreadsheets and thus the respective generators are used while several distributions for the input variables are given.

Further, sensitivity analysis is performed estimating the Spearman's rank correlation coefficient, see e.g. [7]. The Spearman's rank correlation coefficient is a non-parametric measure of a monotonic relationship between pair data. Its formulation is given by

$$r_s = \frac{\text{cov}(rg_X, rg_Y)}{\sigma_{rg_X} \sigma_{rg_Y}} \quad (5)$$

Where rg_X , rg_Y stand for the ranks of two samples X_i and Y_i , $\text{cov}(rg_X, rg_Y)$ is the covariance matrix of the rank variables, and σ_{rg_X} , σ_{rg_Y} are the standard deviations of the rank variables. Thus, the closer r_s to ± 1 the stronger the monotonic relationship between the two variables. Herein, X_i corresponds to the industrial, process and cost input variables, while Y_i is the total cost (manufacturing and assembly cost).

3 Case Study

Advanced composite materials are relatively new materials, introducing specific advantages in the design of aircraft components and thus resulting in better performance and lighter structures. An area of particular current interest is in more highly integrated solutions, e.g. by using co-curing technique where the cycle time for the assembly can be reduced or eliminated. There may also be structural benefits (e.g. through a reduction in fastener count). Although these advantages clearly point towards the use of a DFMA approach, it is not obvious that the integrated design with the fewer parts will actually lead to a more economical solution overall. Therefore, there is a need for a trade-off study to be made investigating manufacturing and assembly costs, based at the same time on quantitative results. The probabilistic approach described in Sect. 2 is implemented to investigate a traditional design approach against the new capabilities of integration that a composite material offers.

3.1 Concepts

The two sample configurations of this analysis are depicted in Fig. 1. The case study concerns a simplified wing structure of approximately 4 m length with 1 m chord line. For simplicity, which will be very often the case in the conceptual design phase, only basic parts are considered in the analysis and presented in Fig. 1.

The baseline concept comprises of two spar beams in "C" shape, one J-nose upper cover, a lower panel and a trailing edge cover.

The joining method of the parts is assumed to be mechanical fasteners, while all the laminates are considered monolithic. There are six interface areas (two on the suction side, i.e. upper spar flanges with the J-nose; and four in the pressure side of the wing, i.e. lower spar flanges with the J-nose, lower panel and trailing edge cover).

For the integrated concept, there are two spar beams in "L" shape, a J-nose upper cover with co-cured T-returns, a lower panel and the trailing edge cover. The joining method is assumed as structural adhesive bonding of the "L" spars to the T-returns with mechanical fasteners for the lower flanges of the spars to the mating parts.

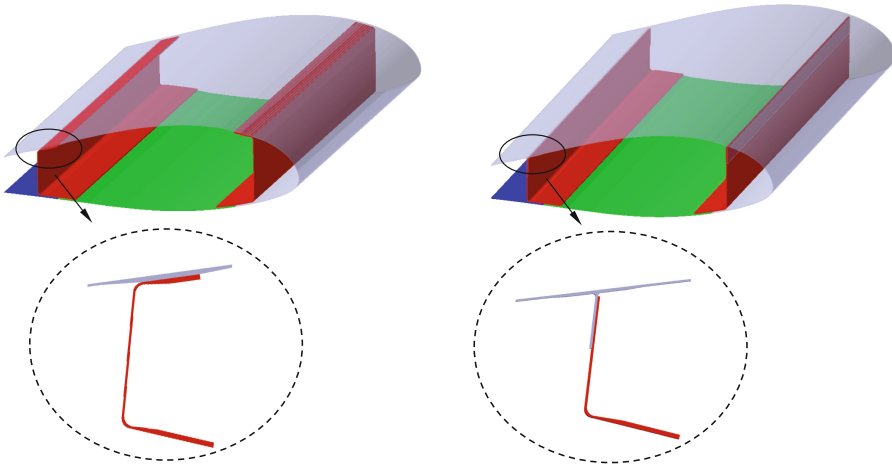


Fig. 1. Baseline (left) and Integrated (right) concept geometry

For both configurations, the most widely used process in the manufacturing of aerospace components is considered, that is, hand lay-up of carbon/epoxy preregs on a mould, bagging and then using autoclave for curing. Additional plies for specific areas are considered for drilled mating surfaces.

It should be mentioned that co-curing is a technique where more complex, integrated components made of composite materials can be manufactured. Therefore, a more advanced tooling strategy is needed. The philosophy presented in [8] is adopted for the J-nose with the T-returns. In summary, it is assumed that five lay-up tools, one for the J-nose skin and four ‘half’ tools for the T-returns, and further four curing tools (caul plates) are employed. For both configuration, a manual assembly, typical for aerospace structures, is adopted.

3.2 Scope of the Model

The scope of the developed model is to estimate both manufacturing and assembly costs for the two concepts and further to compare and identify any benefits of using one concept over the other in terms of cost.

3.3 Manufacturing and Assembly Process Plan

Having determined the scope of the cost model, the first step of the methodology is to identify the necessary process steps for the fabrication of every part as well as the processes for the final assembly. Process flow diagrams are developed. They are depicted in Fig. 2 for both configurations. In this diagram, for every process step, recurring and non-recurring costs are indicated, while the type of the production system to be installed is also defined, e.g. cure system/metrology system, etc. It should be highlighted that the difference in the manufacturing process plan for the J-nose (baseline concept) and the co-cured J-nose is depicted by the additional red boxes in

Fig. 2. The granularity of the process plan is quite important and can be condensed as the design progresses mature and information becomes available.

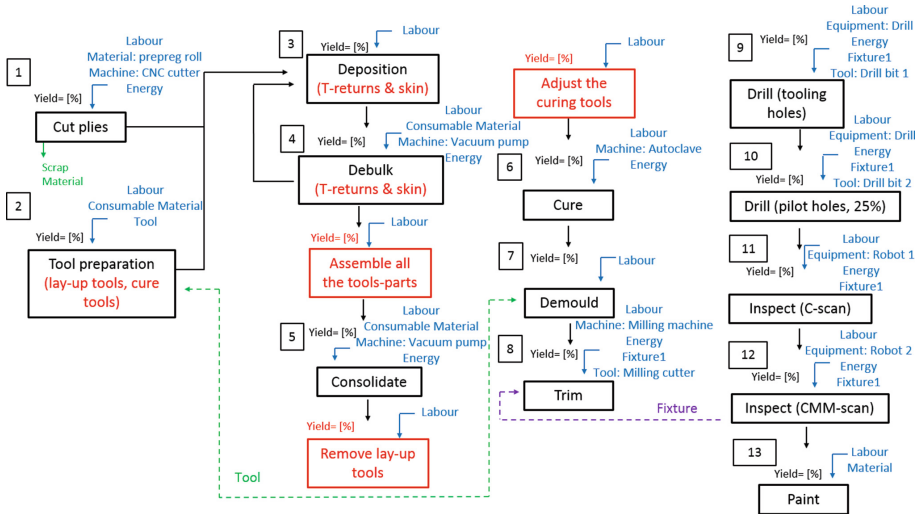


Fig. 2. Fabrication process flow for both concepts (black characters: all parts except J-nose & T-returns, black & red characters: J-nose & T-returns)

Regarding the assembly process plan, similar diagrams are developed, including process steps such as shimming, drilling, deburring and sealing. The assembly diagrams accumulate almost 100 operations for the baseline configuration, while 67 operations are needed for the integrated concept.

The cycle time for every process step is estimated based on specific design and process parameters, e.g. part area or the lay-up rate.

Further production parameters are set up, such as the programme lifetime, the working days per year, the number of shifts per day, the paid hours per shift, the paid breaks, and the target annual production volume.

In total 66 input variables, namely industrial, process and cost parameters, are considered to be random, assuming a normal distribution with coefficient of variation ranging from 10% to 30%, depending on the confidence of the modeller in their actual values.

4 Results and Discussion

Results of the probabilistic analysis are presented in Fig. 3. MC was set up to perform 5,000 iterations. The mean values of the total cost of each concept (baseline or integrated) is presented with respect to the target annual production volume, the two continuous lines. Additionally, plus-minus one standard deviation of the total cost is

presented in the graphs with the error bars. For clarity and to be able to visually compare the curves in Fig. 3, the annual production volume in the graph starts from 10. As expected, in this case the cost for one product per year is extremely high - almost £0.4 M. Typically, aircraft production volumes go into the hundreds and thus 100 products per year is assumed as a target volume in this work.

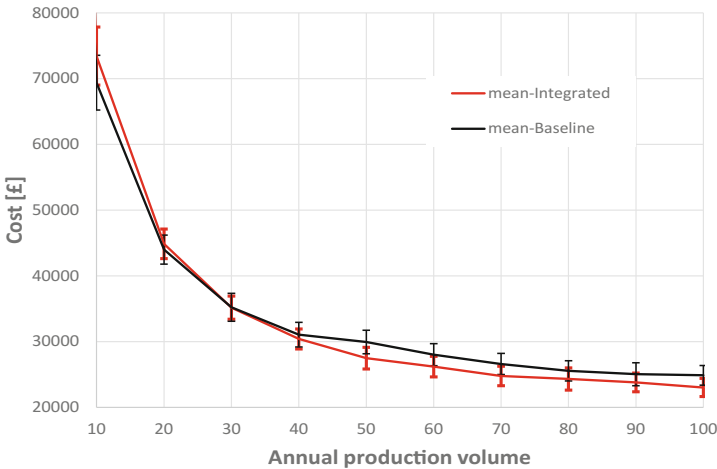


Fig. 3. Total cost (manufacturing and assembly costs) per product for the two concepts with respect to the target annual production volume

From Fig. 3, it is clear that the most beneficial concept in terms of cost is not an easy answer and is highly dependent on the target annual production volume. More specifically, observing the mean value curves for low production volume of less than 20 products, the baseline concept offers a more attractive solution. This is due to the overwhelming manufacturing costs in the low production volumes, due to the installation of all production systems. Considering that the fabrication of the J-nose & T-returns is more complex and thus more expensive, the baseline concept turns out cheaper for low volume production.

This trend changes when production volume is 20 to 40 products per year. Both concepts result in quite similar costs. For production volumes greater than 40 products per year, the integration concept seems to be the best approach because assembly cost is the major driver.

The total cost exhibits a rather small variation with a coefficient of variation of approximately 7%, although most of the input parameters are assigned a coefficient of variation equal to 20%-30%.

Finally, the identification of the cost drivers is performed by estimating the rank correlation coefficients as described in Sect. 2. Part of the matrix is presented in Fig. 4. Input variables are listed in the first column and they are correlated with the manufacturing cost of the main components as well as the assembly cost of overall product and the total cost.

RVs	Manufacturing cost (J nose)	Manufacturing cost (FW spar)	Manufacturing cost (Aft spar)	Manufacturing cost (Lower cover)	Manufacturing cost (Lower cover flap)	Assembly cost	Total cost
Interest rate	0.09	0.13	0.13	0.12	0.14	0.07	0.11
Labour rate - Direct	0.78	0.71	0.67	0.73	0.66	0.91	0.89
Floorspace rate	-0.01	0.01	0.01	0.01	0.01	0.04	0.02
Electricity cost	0.01	0.00	0.01	0.00	0.01	0.01	0.01
CNC cutter rate	0.02	0.00	0.00	0.01	0.00	0.00	0.01
Clean tool surface rate	0.00	-0.01	-0.01	-0.01	-0.01	0.00	-0.01
Release agent application rate	0.01	-0.01	-0.01	0.00	-0.01	0.00	0.00
Shim application rate	0.00	0.00	0.00	0.00	-0.01	0.01	0.00
Hand lay-up prepreg rate	0.11	0.06	0.20	0.12	0.19	0.00	0.08

Fig. 4. Spearman’s rank correlation coefficient for a subset of the random input variables for a target annual production volume equal to 100 (integrated concept)

Note that when the rank correlation coefficient value for an input variable results in a value close to unit, it means that the input variable is quite critical, highlighted with red colour in Fig. 4. Rank correlation coefficients greater than 0.2 are assumed as critical cost drivers in this exercise. The identified critical cost drivers of the integrated concept along with their rank correlation coefficient are presented in Table 1. It is obvious from Table 1 that although 66 input parameters were initially assumed, only 10 of them significantly contribute to the manufacturing/assembly costs. From Table 1 (and Fig. 4), the influence of direct labour rate is considerable and should therefore be modelled as accurately as possible. This was expected due to the high emphasis on manual activities considered both for fabrication and assembly processes. Moreover, the total cost of the integrated design concept is mainly driven just by two input parameters, namely by the labour rate and the cost of the curing system (the autoclave).

Table 1. Critical cost drivers along with their rank correlation coefficient

Critical RVs	J-nose Man. Cost	FW spar Man Cost	Aft spar Man Cost	Lower cover Man Cost	TE cover Man Cost	Assy cost	Total
Labour rate	0.78	0.71	0.68	0.73	0.68	0.91	0.89
HLU prepreg rate	-	-	0.20	-	-	-	-
CNC cutter	-	0.25	0.27	0.23	0.27	-	-
Autoclave	-	0.36	0.4	0.29	0.40	-	0.21
CNC milling mach.	-	0.2	0.24	-	0.24	-	-
CNC drill	-	0.25	-	-	0.26	-	-
Crane	-	-	-	-	-	0.28	-
Metrology system	-	-	-	-	-	0.20	-
AS4-12 k/8552 UD	0.26	-	-	-	-	-	-
Assembly fixture	-	-	-	-	-	0.21	-

Having this information, critical input parameters can be modelled more accurately. Therefore, iterative loops of refinements can be performed as the design of the product progress, resulting in more reliable cost estimations. By assuming that a more intensive investigation for cost data is conducted, and by reducing the coefficient of variation of the input variables of Table 1 to their half, the statistics for every main component cost

for manufacturing/assembly and overall product cost are estimated once more. Implementing this iterative loop, it was found that the associated uncertainty for the total cost is reduced almost proportionally with refinement on the critical input parameters.

5 Conclusions

The development of a cost tool is perhaps the most crucial element of a DFMA methodology. A process-based cost methodology has been developed to translate changes in the design, manufacturing process plan and the build philosophy of a product into cost. Furthermore, in order to deal with the uncertainty in the input parameters, which can be quite common in the conceptual phase of the design when detailed info is often missing, a Monte Carlo analysis has been implemented. Spearman's rank correlation coefficient has been evaluated to identify cost drivers and critical input parameters.

The approach has been implemented to estimate manufacturing and assembly costs of a simplified composite wing structure and to compare two different approaches, namely a baseline concept of a traditional design consisting of several parts versus integrated solutions based on co-curing techniques for composite materials. The selection of a specific concept, baseline or integrated one, is dependent on the annual production volume. The most important finding, however, of this analysis is the identification of the critical cost drivers. Having identified the critical input parameters, iterative loops of refinement can be performed as the design of the product progresses to estimate more reliable costs. The associated uncertainty is reduced almost proportionally with the refinement of the critical input parameters. It has been found that the variability on the total cost drops by half, if the variability in the critical parameters is reduced to their half.

Acknowledgements. This project has received funding from the Clean Sky 2 Joint Undertaking (JU) under grant agreement No 671436. The JU receives support from the European Union's Horizon 2020 research and innovation programme and the Clean Sky 2 JU members other than the Union.




References

1. Eskilander, S.: Design for Automatic Assembly - A method for product design: DFA2. Ph.D. thesis, KTH Royal Institute of Technology (2001)
2. Miyakawa, S., Ohashi, T., Iwata, M.: The hitachi new assemblability method (AEM). In: Transactions of the North American Manufacturing Research Institution of SME, USA, pp. 352–359 (1990)
3. Boothroyd, G., Dewhurst, P., Knight, W.: Product Design for Manufacture and Assembly, 3rd edn. CRC Press, Boca Raton (2011)
4. Hueber, C., Horejsi, K., Schledjewski, R.: Review of cost estimation: methods and models for aerospace composite manufacturing. *Adv. Manuf.: Polym. Compos. Sci.* **2**(1), 1–13 (2016). <https://doi.org/10.1080/20550340.2016.1154642>

5. Johnson, M., Kirchain, E.: Quantifying the effects of product family decisions on material selection: a process-based costing approach. *Int. J. Prod. Econ.* **120**, 653–668 (2009). <https://doi.org/10.1016/j.ijpe.2009.04.014>
6. Blank, L., Tarquin, A.: *Engineering Economy*. McGraw-Hill, New York City (2012)
7. Sheskin, D.: *Handbook of Parametric and Non-parametric Statistical Procedures*, 3rd edn. Chapman & Hall/CRC, Boca Raton (2004)
8. Gaddiker, K., Gowda, M., Sundaram, R., Subba Rao, M.: Innovative tooling concepts for cocured composite structures in aircraft applications. *Int. J. Adv. Eng. Sci.* **6**(3–4), 142–147 (2014). <https://doi.org/10.1001/s12572-015-0119-0>



Precision Assembly of Optical Backplanes

Serena Ruggeri^(✉) , Gianmauro Fontana , and Irene Fassi 

Institute of Intelligent Industrial Technologies and Systems
for Advanced Manufacturing, National Research Council of Italy,
Via A. Corti 12, 20133 Milan, Italy
serena.ruggeri@stiima.cnr.it

Abstract. Full optical backplanes can be seen as a promising technology for high bandwidth ICT (Information and Communication Technology) apparatuses and high performance computing systems. According to a recent frame-based solution, the backplane mounts a number of independent optical interconnect circuits mainly consisting of a set of optical fiber ribbons of different lengths arranged to fulfill a specific planar ribbon routing. A non-negligible problem is related to the development of suitable techniques for the efficient and cost-effective assembly of such sub-circuits. New systems are required that combine ultimate hardware and software capabilities and derive from a synergic implementation of digital and advanced manufacturing technologies. The successful assembly of the optical interconnection circuits lies in the development of cyber-physical production systems within the framework of Industry 4.0. In this context, this work will present and discuss how different innovative technologies and consolidated technologies applied in a novel context were exploited to demonstrate the feasibility of the automated backplane assembly. The achieved results are discussed in terms of design of the work-cell layout and related equipment, simulation tests, tool path planning, and final task execution.

Keywords: Optical backplane · Robotic assembly · Cyber-physical work-cell

1 Introduction

The manufacturing industry is going through the fourth industrial revolution where the physical world is coupled with the cyber world mainly exploited for design, simulation, monitoring, computing, and networking purposes. These cyber-physical systems contribute to the efficiency, sustainability, and security of production systems. The key technologies enabling such a revolution include both hardware and software resources, from advanced robotic systems to additive manufacturing, up to cloud computing and system simulation.

Recent considerable improvements in robotics are offering advanced robotic solutions with reduced labor costs and increased efficiency. Advanced robotics is introducing a new generation of machines capable of executing dexterous and delicate tasks, such as recognizing, computing and acting on information, and even collaborating and learning from humans [1].

A fundamental goal of this emerging new industrial paradigm is to develop autonomous production methods, plants and factories powered by robots that can

execute different tasks smartly, with the focus on safety, flexibility, versatility, and collaboration. Without the need to isolate its working area, its integration into human workspaces becomes more economical and productive, and opens up many possible applications in industries, with robots and humans working hand in hand on inter-linking tasks and using smart sensors and human-machine interfaces [2]. The cognitive aspects in an advanced robotic system are important for its context awareness. Smart sensors, as on-board vision systems or optical sensors, allow the robots to measure the object distance and attain 3D coordinates with high precision, e.g. by sophisticated image recognition methods. Moreover, the robot control strategy plays a fundamental role in the achievement of smart, robust and versatile behavior of a robotic system. For example, the adoption of hybrid force-motion control, as well as indirect force control, allows for the execution of interactive tasks where it is more important to precisely control and limit the exchanged force/torque by the robot, rather than to control the robot position or its path. Robots using force, tactile, distance, and visual feedback can operate in unstructured environments, cooperating safely with the human to perform different tasks.

The paper discusses the development of a robotized work-cell for the automatic assembly of an optical backplane for high-bandwidth ICT apparatus, to be integrated in a production line implementing the concepts of digital manufacturing. After a brief overview of the apparatus, the technologies enabling the Industry 4.0 concepts are reviewed and their (successful) application to the use case is critically addressed.

2 Backplane Design and Assembly Challenges

2.1 Optical Backplane for ICT Apparatus

High-effectiveness optical connections are requested in high-bandwidth ICT apparatus (data centers, servers, routers, switching stations, etc.) and high-performance computing systems [3] to overcome the limits of traditionally used electrical PCBs, in terms of power dissipation and data transmission capacity. These devices are based on optical backplanes where a plurality of cards are connected to each other with optical interconnection circuits, allowing signal transmission between cards on the backplane.

In recent years several solutions have been proposed for optical backplane interconnection circuits [4, 5].

The novel backplane design considered in this paper and better described in [6–8] features a “full-mesh” topology: each card can transmit data to any other card or be connected to itself, i.e. loop-back connection. This specific design allows for the division of the backplane optical circuit into n independent optical interconnection sub-circuits, each with different ribbon routing and encapsulated into a different rigid frame.

The main components of each sub-circuit (Fig. 1) are: a frame support, a frame cover, eight 12 core multimode (MM) ribbons each with two terminations (MPO connectors and MT ferules), 16 ribbon termination housings.

The interconnection solution is based on controlled deformations of the optical fiber ribbons, using an optimized layout and customized components as fibers support and protection (frame). These frames have been designed with mechanical features

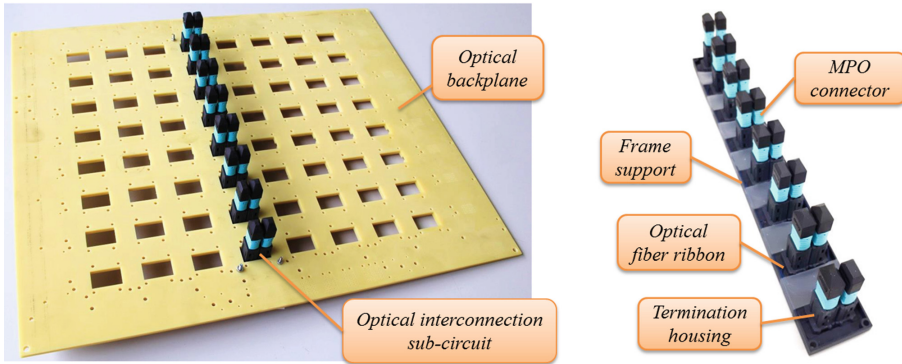


Fig. 1. Backplane optical interconnection sub-circuit.

(i.e.: pins, boundary walls) to constrain the ribbons in an optimized position which minimizes optical power losses. The entire routing is thus planarly developed on the backplane surface, exploiting a customized parametric algorithm [7].

A non-negligible effort is required in order to develop a fully automated solution for the efficient and cost-effective assembly of full optical backplanes combining the flexibility of a robotic cell with customized assembly tools. Indeed, the novelty of such products called for new methods and systems to enable their development. It required transversal competencies and a synergic integration of different engineering disciplines, boosted by digital and advanced manufacturing. The technologies behind the successful assembly of the optical interconnection circuits could be then identified within the framework of Industry 4.0, towards the development of a cyber-physical production system.

2.2 Assembly Strategy and Main Steps

The backplane assembly features many challenges, which can be summarized as follows

1. The flexibility of the optical fiber ribbons implies their unpredictable and undefined behavior.
2. Ribbon length varies: different connector couples, at different distance, have to be connected and the ribbons have to be managed.
3. N different (predefined optimized) routings have to be implemented.
4. Objects with different geometrical and mechanical properties (ribbons, connectors, mechanical customized components, frames) have to be handled and assembled.
5. Positioning requires high accuracy and repeatability.

Fully automatized assembly technologies, based on vision systems, robotics, and industrial automation devices can be used for the circuit assembly.

Firstly, the main phases of the assembly process were identified and detailed:

1. Delivery of the commercial ribbon in the workspace with the ferrules and the connectors at both ends.
2. Mounting of the termination housings on both ribbon ends.
3. Pick of the pre-headed ribbon with termination housings from the specific storage buffer.
4. Insertion of the termination housings in the proper receptacles on the assembly tool, according to the topology of the interconnection sub-circuit.
5. Repetition of steps 2–4 for each ribbon of the sub-circuit in process.
6. Sliding of the assembly tool to align the receptacles in a straight line.
7. Pick of the frame from a storage buffer.
8. Positioning of the frame over the aligned termination housings.
9. Snap of the frame on the line to transfer the ribbons.
10. Pick of the circuit (frame with transferred ribbons) and warehousing.
11. Repetition of steps 2–10 for all the circuits of the backplane.

It has to be noted that, analyzing the process, steps 5 and 6 could be not consequent, but specific ribbons could be placed and inserted after the alignment of the receptacles on the assembly tool. This would reduce the need of longer ribbons to handle the distances between the receptacles on the assembly tool.

3 Automatic Assembly: Enabling Technologies

A high-performance work-cell resulted from the exploitation of Industry 4.0 principles. Indeed, the requirements of the work-station were flexibility, reconfigurability and safety. This includes the work-cell layout, its specialized stations to execute specific operations, all the devices and modules for handling and assembling the different components, as well as the components themselves, both those constituting the interconnect sub-circuit (re-design for assembly) and the auxiliary equipment and elements necessary for a correct assembly. In the following, the enabling technologies of Industry 4.0 exploited to develop an automated backplane assembly method and work-cell will be discussed.

3.1 Robotized Assembly Solution

The work-cell was equipped with a robot with smart sensors and advanced control strategies. The work-station was designed according to a circular layout where an anthropomorphic robot is at the center and the assembly sub-stations are arranged around it. In this way, the robot can reach all the sub-stations in order to support all the phases of the assembly process. Therefore, the robot tasks are many: manipulate the sub-components and the sub-circuit of the backplane, load and unload the components from the different sub-stations, and check all the assembly phases to guarantee the high assembly standard demanded. The sub-stations were designed for the specific sub-assembly tasks, as can be seen in Fig. 2. In particular, the robot has to assemble the circuit placing the ribbons on the tool according to the TX/RX optical ribbon path.

Then, the termination housings have to be aligned on the assembly tool by pneumatic actuation and finally the robot has to snap the frame on the line.

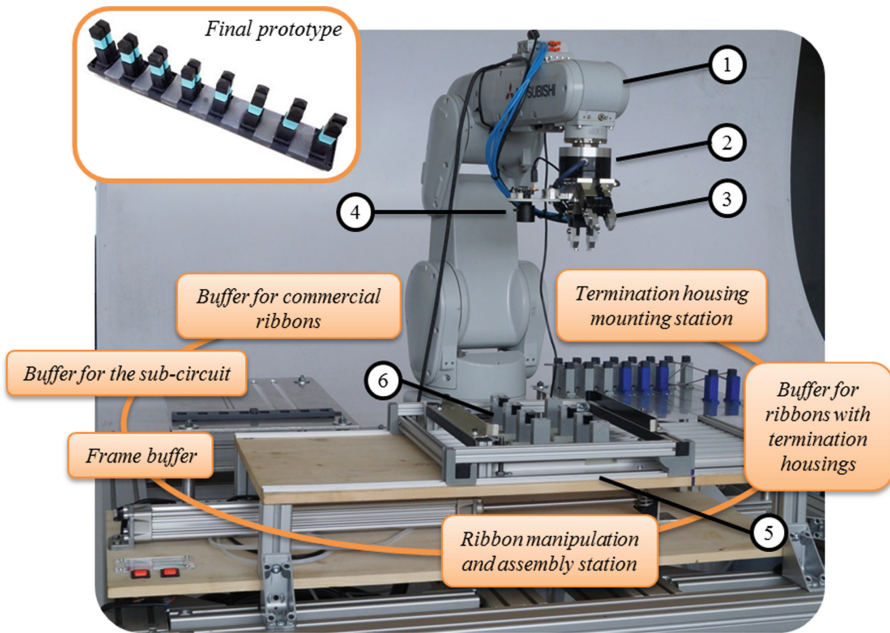


Fig. 2. The assembly work-cell. (1) Mitsubishi Melfa RV-4FL robot: position repeatability of $\pm 20 \mu\text{m}$; operating volume (hollow sphere) with outer radius of 648.7 mm); maximum load capacity of 4 kg; end-effector maximum x-y-z composite speed of 9048 mm/s; cycle time of 0.36 s for a back-and-forth movement over a vertical distance of 25 mm and a horizontal distance of 300 mm when the load is 1 kg. (2) 6 DOF Mitsubishi 1F-FS001-W200 force sensor: rated load of 200 N for F_x , F_y , F_z and of 4 Nm for M_x , M_y , M_z ; maximum static load of 1000 N for F_x , F_y , F_z and of 6 Nm for M_x , M_y , M_z ; breaking load of 10000 N for F_x , F_y , F_z and of 300 Nm for M_x , M_y , M_z ; resolution of approx. 0.03 N for F_x , F_y , F_z and of approx. 0.0006 Nm for M_x , M_y , M_z ; linearity of 3% FS; hysteresis of 5% FS. (3) End-effector: two Schunk MPG40-plus grippers: stroke of 6 mm; repeatability of 0.02 mm; mass of 0.36 kg; maximum manipulation mass of 0.7 kg; maximum closing force less than 50 N (maximum value to avoid the damage of the components) with a command pressure of about 2 bar. (4) 2D vision system: 5 MPixel sensor; focal length of 10 mm; field of view of $155 \times 116 \text{ mm}^2$; spatial resolution of 55 μm ; working distance of 220 mm. (5) Customized assembly tool. (6) Receptacle on the assembly tool.

The work-cell was equipped with a highly precise compact 6 DOF anthropomorphic robot (see Fig. 2 for technical data). A 6 DOF force sensor, directly connected to the bottom part of the TCP flange allows for the implementation of force control, besides the standard motion control. Indeed, the robot has to perform tasks where the final goal is to reach defined positions following specific paths and adopting a velocity/position (motion) control strategy, but it also has to perform snap operations

between the frame and the line of termination housings where it is necessary to control the force, adopting a hybrid force-motion control strategy. When this strategy is used, the robot is positioned over the first contact point of the frame, the z-axis is force controlled limiting the force to 60 N (maximum pushing force), while the x and y-axes are motion controlled. The robot is then moved downwards to the contact point and, once the contact is established, the robot pushes until the maximum pushing force is achieved. In case the maximum force is not achieved, a threshold height is set to avoid the task getting stuck. The robot then moves upwards and the previous operations are repeated for all the contact points defined on the frame surface to guarantee the complete snap with the terminations housings. These features make the system suitable for complex assembly tasks, such as the backplane assembly.

The robot end-effector was designed coupling two commercial pneumatic grippers by an angular interface. The two grippers were equipped with designed fingers able to manipulate the different components (i.e. the ribbon acting on the termination housing and the frame) and handle the optical ribbon path according to the specific sub-circuit topology. Each termination housing of the same ribbon was picked and inserted by each gripper, while the frame was picked, positioned, and pushed on the line of the aligned termination housings by only one of the grippers.

The robot is equipped with a 2D vision system consisting of a mobile camera mounted on the gripper interface. It is used to identify the components (i.e. the termination housings and the receptacles) by different search and match algorithms (i.e. pattern matching, geometric matching, particle analysis), measure their planar pose, and then identify the pick and release poses to be reached by the tool tip during the sub-circuit assembly in order to perform a look and move control strategy. Moreover, the vision system was used to check the effectiveness of the assembly phases in all the sub-stations. A diffuse illumination of the scene was used to assure a robust recognition and reliable measurement of the parts.

The vision system and the robot were calibrated to allow the automatic identification of the parts in the robot reference system for the grasp and the release. Indeed, a calibration algorithm was implemented to calibrate the work-cell, compensating for perspective, distortion, spatial referencing and end-effector errors.

In order to control the work-cell and the different devices (i.e. robot, end-effector, vision system, and tools) for the execution of the sub-circuit assembly tasks, a dedicated control system was designed and implemented.

This control system, implemented in NI LabVIEW[®], provides simple tools for the scheduling of the operations to be performed in the work-cell and for the supervision of the automatic task during its execution; manages and supervises the execution of the defined task, sending commands to the various devices involved and making decisions based on their responses; supervises the system and manages the alarms. The control system integrates an HMI both for the automatic task and manual control of the different devices. Finally, the control system also allows for communication with external systems via TCP/IP protocol, e.g. for the remote control and data exchange in the case of integration of the work-cell in a production plant.

3.2 Digital Work-Cell Design

The design spanned different levels, from the overall system perspective to the detailed features of the single component, taking into account the mutual effects of a design choice on those considered consolidated solutions and on the subsequent ones. In this way, the possibilities of the virtual prototyping were exploited to rapidly investigate multiple system changes and facilitate layout and task planning.

In addition to the work-cell main components (robot, work-stations and assembly tools), virtual prototypes were created for the buffer of ribbons with termination housings, the ribbon manipulation and assembly station, the frame buffer, and the buffer for the complete interconnection sub-circuit, as well as the manipulation tool on the robot end-effector. A set of receptacles were designed to support and make available for picking all the ribbons required for the production of the specific interconnection sub-circuit and the related ribbon routings.

The assembly work-cell was developed immediately after the first backplane components conception; several iterations were carried out in order to achieve a fully automated solution, re-designing the components of the interconnect sub-circuit and integrating additional elements on the assembly tool. This required a continuous verification of the feasible integration of the various parts of the system but allowed us to solve critical aspects that arose during the development stages.

The design modifications required a downstream verification of both the maximum allowable gripping force on the termination housing to avoid its damaging and the maximum allowable push force to snap the frame onto the aligned termination housings. Therefore, a FEM analysis was carried out using SolidWorks[®] and compared with the first FEM analysis performed during the original design. The results were comparable showing that the termination housing mechanical resistance was not negatively affected by the modifications, thus validating the new design. Thanks to a synergic second-stage development of the components and development of the automation devices, the frame also passed through a re-design to avoid the need for a gripper for the frame different from those used to manipulate the termination housings, therefore for a gripper change and changing system. The double-gripper solution was conceived and modeled using Solidworks. The grippers were equipped with custom fingers with multiple original features. The fingers should meet a wide set of specifications, that is those deriving from the components to manipulate (e.g. size, shape, surface for gripping, applicable forces), from the gripper (e.g. connection, size, mass), and from the assembly operations (e.g. avoiding interference with ribbons and other components).

Besides the components, an intervention on the original assembly tool was required. Indeed, to achieve a correct positioning in the layer of the assembly tool, the flexible part between the termination housings had to be controlled. For this reasons, additional retaining brackets on the assembly tool to constrain the ribbons within the desired space were added and auxiliary elements were created both on the receptacles and on the retaining brackets to support the ribbons then keep them at the proper height.

3.3 Additive Technologies for Components' Manufacturing

A prototype of the work-cell was developed and installed at the Laboratory of Micro Robotics at ITIA, Milan. The different components of the interconnection sub-circuit and of the devices for the assembly were developed considering the most convenient manufacturing technologies. Additive manufacturing represented a promising solution in different cases, thanks to the possibility of obtaining highly customized products with different shapes and sizes, since they do not suffer from many of the geometrical limits constraining subtractive and formative processes, in small quantities at a relatively low cost per unit and in a short time. Moreover, the combination with digital technologies enabled and widened the fabrication possibilities.

In the work-cell, different components were developed by means of additive manufacturing technologies. The different releases of the termination housings, the frame, and the receptacles and their fixturing elements on the slides were produced by stereolithography. They were made of the Accura XTreme Plastic resin which simulates the properties of ABS. Part of the side fixturing for the on-board camera was manufactured by Fuse Deposition Modelling (FDM) process in ABS.

3.4 Virtual Simulation and Off-line Programming

Numerous simulation tests were carried out using Melfa Works, an add-on for Solid-Works released by Mitsubishi. It converts the paths for the process in output data that can then be used for the creation of the robot program by the Mitsubishi software RT-ToolBox2. With Melfa Works, it is possible to select grippers, sensors and other components from libraries and integrate them directly in the environment [9]. The main phases of the simulation process included: the creation of the workspace, the calibration in the virtual environment, and the creation of the workflow. In more detail, the simulation environment allowed us to:

- load the model of the robot and define its settings;
- connect the gripper model;
- load and change the layout of all the devices (a functional simplified model of the devices was often used) in the work-cell assembly model, as well as the processing parts;
- teach the robot all the working positions (and intermediate configurations) to reach, as well as those for the calibration;
- check possible interference among robot and devices;
- create the sequence of the necessary operations to define the path.

4 Work-Cell and Interconnect Circuit Prototypes

The work-cell was tested in the assembly of one of the eight interconnect sub-circuits, i.e. the +2 routing, that was considered challenging from both the functionality of the circuit and the automatic assembly points of view, featuring two closed loops, a high number of bendings and four ribbon lengths.

The behavior of the flexible ribbon between the connectors was not easily predictable and impossible to simulate with the software available. However, the control of that part was necessary, to avoid stressing the ribbon, curving it below the allowed bending radius or creating undesirable interferences in the working area. For this reason, a few modifications were applied to the task operations after their first run and to the devices and components to improve the ribbon manipulation and assembly.

Figure 2 shows the final work-cell and the final prototype of the interconnect circuit that resulted from the successful implementation of the automatic assembly process. Indeed, the enabling technologies presented in the paper were implemented for both the design and manufacturing of the different devices and tools, and the planning and execution of the different steps of the assembly process.

5 Conclusions

The implementation of advanced manufacturing and digital technologies is currently considered a key factor for the development of intelligent and interconnected systems, according to the Industry 4.0 paradigm.

In this framework, this paper discussed the exploitation of a set of enabling technologies for the conception and set up of a novel robotized work-cell for the automatic assembly of optical interconnect sub-circuits that constitute an innovative optical backplane. Indeed, optical backplanes appear as a promising solution for the development of high capacity ICT apparatuses that could impact the whole ICT sector.

To this end, a synergic integration of robotics, vision and force sensing, additive manufacturing, digital design and simulation, and off-line programming proved to enable the automatic assembly task.

An improvement in the choice of the robot path planning would derive from the use of a simulation environment able to take into account the behavior of the flexible and free part of the ribbon between the two termination housings.

Moreover, the engineering of the end-effector should consider the possibility to manipulate ribbons shorter than the current minimum length. Indeed, in case of non-simultaneous gripping, the current manipulation tool preliminary prototype cannot manipulate ribbons with free length less than 85 mm. However, in the case of the +1 routing, it would be necessary to use shorter ribbons so that they could be accommodated in the frame. An alternative would be the reduction of the angular offset between the two grippers, then verifying again that they do not collide with the ribbon plane on the assembly tool. A second solution would consider an alternative mounting of the grippers where, for example, one gripper would be mounted horizontally, while its fingers would be mounted in order to project the picking point as required.

Future developments of this work include the extension of the study to the automatic mounting of the termination housings on the connectors. The ribbons could be arranged in the ribbon buffer in a different way, avoiding the need for operator interventions. In a general case the ribbon could be randomly arranged on a plane, and the vision system mounted on the robot end-effector would recognize the termination housing and identify their pose to be sent to the robot controller to enable them to be picked.

Moreover, the online virtual monitoring of the task execution could allow for a remote verification of unpredictable situations and a rapid intervention. Finally, the provision of an interconnection network for the smart integration of the work-cell in the manufacturing plant at different process levels would further pave the way for its successful industrial exploitation.

Acknowledgments. The activity was funded by the PON project “BACKOP” - Optical Backplane for high-capacity ICT apparatus – PON 01-01209 (2011–2015), EU FERS, IMiSE, MIUR. The authors would like to thank M. Leco, D. Casartelli, M. Riccardi, and S. Osio for their contributions to the activities presented in this paper. The authors also thank Mr. J.C. Dalberto and Mr. R. Bozzi for their contributions to the development of the prototypes and the setup of the system.

References

1. Kearney, A.T.: Technology and innovation for the future of production: accelerating value creation. White paper, World Economic Forum (2017)
2. Bahrin, M.A.K., Othman, M.F., Azli, N.H.N., Talib, M.F.: Industry 4.0: a review on industrial automation and robotic. *Jurnal Teknologi* **78**(6–13), 137–143 (2016)
3. Benner, A.F., Pepeljugoski, P.K., Recio, R.J.: A roadmap to 100G Ethernet at the enterprise data center. *IEEE Commun. Mag.* **45**(11), 10–17 (2007)
4. Beals IV, J., Bamiedakis, N., Wonfor, A., et al.: A terabit capacity passive polymer optical backplane based on a novel meshed waveguide architecture. *Appl. Phys. A* **95**(4), 983–988 (2009)
5. Sepehr, K.: High density fiber optic backplane, method of making the same, and fiber optic network assembly comprising a fiber optic backplane. PCT Patent No. WO2002063365 (A1). Priority Date 06 Feb 2001
6. Ruggeri, S., Basile, V., Fontana G., Fassi I.: Design and development of a fully automated assembly solution for optical backplane interconnection circuits. In: 9th International Conference on Micro- and Nanosystems, 20th Design for Manufacturing and the Life Cycle Conference, ASME International Design Engineering Technical Conferences and Computers and Information in Engineering Conference 2015, vol. 4 (2015)
7. Basile, V., Guadagno, G., Ferrario, M., Fassi, I.: An optimized routing algorithm for the automated assembly of standard multimode ribbon fibers in a full-mesh optical backplane. *Opt. Fiber Technol.* **41**, 56–63 (2018)
8. Ferrario, M., et al.: Full-mesh optical backplane with modular fiber ribbon-based sub-circuits. In: *Optical Fiber Communications Conference and Exhibition (OFC)* (2016)
9. Mitsubishi Electric, Melfa Works Product Webpage. https://eu3a.mitsubishielectric.com/fa/en/products/rbt/robot/melfa_works. Accessed 15 Nov 2017



Prefabrication and Automated Micro Assembly of Piezoceramic Fiber Array Transducers in Microstructured Surfaces of Sheet Metals

Marek Schmidt^(✉) and Volker Wittsock

Professorship for Machine Tools and Forming Technology,
Chemnitz University of Technology,
Reichenhainer Str. 70, 09126 Chemnitz, Germany
marek.schmidt@mb.tu-chemnitz.de

Abstract. In order to realize resource-efficient products and manufacturing processes, lightweight construction solutions have become enormously significant in many areas. Generally, material savings are always done at the expense of rigidity. However, additional weight can be saved through functional integration. One possibility is given by the functional material piezoceramic. This material can be used as sensor or actuator. A new approach for the structural integration of piezoceramic in sheet metals is with the technique joining by forming. Therefore, PZT fibers are assembled in a local microstructure of a sheet metal, which is followed by the joining operation. The article is a contribution to transfer this approach into a high-volume production process, which is necessary for the industrial area to take root. Manufacturing processes for PZT fiber arrays with minimal manufacturing tolerances are presented. The process of stacking PZT plates with distance elements and subsequent dicing into slices is shown as a suitable variant. Furthermore, an automated assembly system is tested with regard to the measuring technology. A machine vision and a chromatic confocal sensor are compared in the assembly system. The results show that the machine vision system is better suited for pose measurement of the PZT fiber arrays and the chromatic confocal sensor achieves better results for the microstructured sheet metals.

Keywords: PZT fiber · Tolerance management · Micro assembly
Chromatic confocal sensor · Machine vision

1 Introduction

Nowadays sensors and actuators based on piezoceramic material are indispensable parts of our daily life. Some known applications include lighters, printers and diesel injection engines. However, special fields of application as piezoelectric patch transducers were only opened up by the possibility of embedding the brittle and fragile piezoceramic in polymer. So-called Macro Fiber Composites (MFC) and Active Fiber Composites (AFC) are much more flexible and commercially available [1]. This type of patch transducer usually only allows subsequent mount by means of adhesive on the

surface of the finished component or product. The connection with an adhesive layer and the polymeric intermediate layers (see Fig. 1(a) and (b)) negatively affects the mechanical coupling and thus also the electromechanical behavior [2, 3].

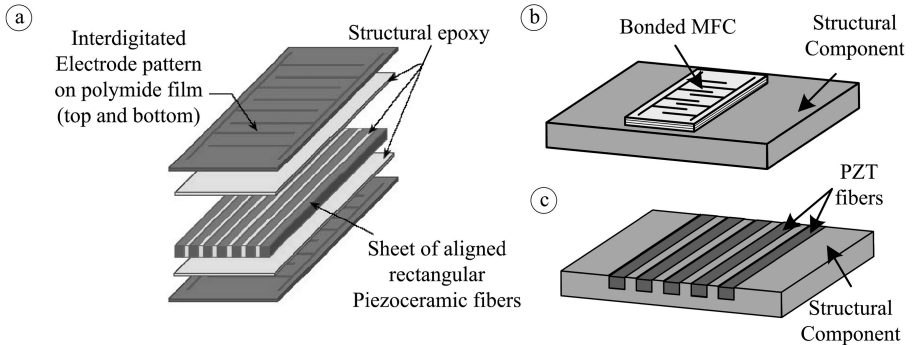


Fig. 1. (a) Design of Macro Fiber Composites (MFC) [1]; (b) Application of MFC with adhesive on the surface of a structural component; (c) New approach with structural integration of PZT fibers into a structural component

One approach to eliminate the polymer interlayers is considered by embedding the PZT ceramic in metal structures as shown in Fig. 1(c). Comparable with the embedding of the piezoceramic in a polymer, also the embedding (forming operation) in a sheet metal should support the brittle material and protect it against fractures, but achieves a better acoustic coupling. The feasibility of the direct integration via joining by forming of piezoceramics has already been demonstrated in [4]. Possible application areas are Structural Health Monitoring (SHM) [5], active noise reduction [6] and energy harvesting [7].

The structural integration into the sheet metal can also take place in an early stage of the production of metallic components. This leads to the fabrication of active semi-finished products, so-called piezo-metal modules, with which further mechanical machining as well as forming operation steps are possible [8]. This opens up new opportunities regarding the application locations of transducers on structural components.

High-volume production processes have to be realized to transfer the new technology in an industrial environment. For this purpose, the paper presents possibilities for high-volume production of ready-to-integrate lead zirconate titanate (PZT) fiber arrays transducers. Furthermore, the realization of an automated micro-assembly of the PZT fiber arrays into local microstructures of sheet metals is part of the paper. The joining operation itself is not a subject of the current investigation.

2 PZT Fiber Arrays for Direct Functional Integration in Microstructured Sheet Metals

2.1 Design Concept of Piezo-Metal Modules

Figure 2 shows the schematic structure of the piezo-metal modules. The active elements are PZT fibers with a rectangular cross-section and the nominal dimensions of $10 \times 0.26 \times 0.24 \text{ mm}^3$. These fibers are integrated in defined distances into a local microstructure of a sheet metal. The microstructure consists of several micro channels with the dimensions of $10 \times 0.3 \times 0.3 \text{ mm}^3$ and with webs (width 0.2 mm) between them. The microstructure can be produced, among other things, by micro milling or micro impact extrusion. An assembly gap of 0.04 mm results from the nominal dimensions for the width of both joining partners (0.3 mm and 0.26 mm) for one fiber.

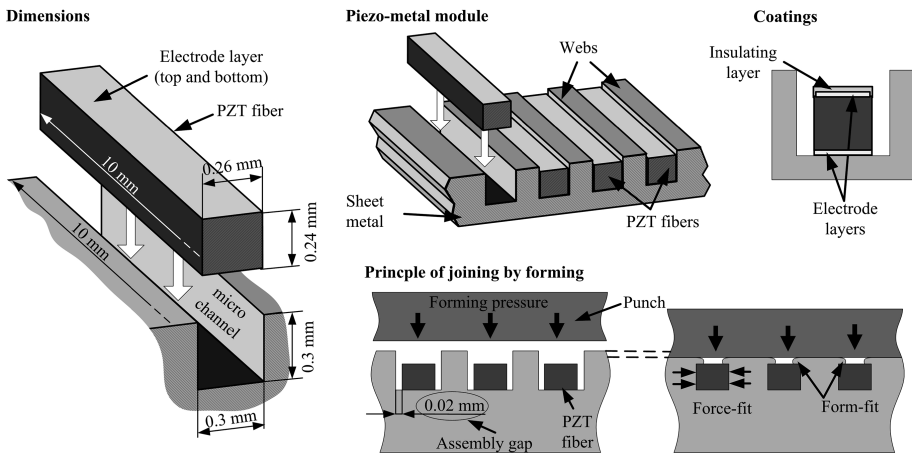


Fig. 2. Schematic design of the piezo-metal module and the principle of structural integration with joining by forming

Thus, a gap of 0.02 mm ensures for each side surface of a fiber to the channel wall, which is also illustrated by the Fig. 2. The actual piezo-metal module is the result of the deformation of the webs. A stamp moves on the surfaces of the webs and then deforms until the assembly gap is closed, so that the fibers are clamped force-fit and form-fit in the metal structure. A demonstration of the procedure is shown in Fig. 2. The PZT fibers are provided on the top and bottom with an electrode layer. The lower side has electrical contact with the sheet metal. On the upper side the signal can be measured. To avoid a short circuit, the upper side is additionally provided with an insulating layer. The presented design is for the use of the piezoelectric transverse effect. Other piezoelectric effects are possible with another arrangement of the electrode layers and the insulating layers.

2.2 Principle for High-Volume Production of PZT Fiber Arrays

The handling of single PZT fibers with geometrical dimensions in the microscopic area represents an enormous challenge. Therefore, the manufacturing concept envisages the production of arrays with several PZT fibers, as Fig. 3(a) exemplifies. PZT fiber arrays consist of ten PZT fibers, which are mechanically connected in series. This increases the dimensions of the handling part to the macroscopic level and simplifies the assembly. Furthermore, the advantage of the PZT fiber arrays is that not every single fiber has to be aligned, assembled and electrically contacted. The mechanical connection simultaneously represents the electrical coupling. These facts lead to a significant time saving in the production of the active modules. The concept is based on stacking of PZT plates with a defined distance, connecting the ends and followed by cutting into slices. The principle is demonstrated in Fig. 3(b). In the next step the fibers get coated with an electrode layer and insulating layer.

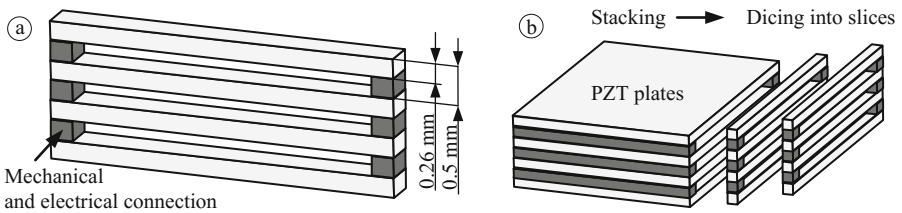


Fig. 3. (a) PZT fiber array; (b) Stacking and dicing of PZT plates to generate PZT fiber arrays

As mentioned above, the nominal assembly gap between the PZT fibers and the channel walls amount 0.02 mm. However, tolerances will occur, which are caused by variation of the PZT plates' thickness and by the method of stacking. Connecting the PZT fibers into an array, the treatment of the tolerance analysis is much more complex than for a single fiber-channel pairing. In the following, an arithmetical and a statistical tolerance analysis will be performed.

Arithmetic tolerance calculation is based on the approach of complete interchangeability. Two requirements have to be fulfilled for each PZT fiber in an array with this approach. They arise from the possible extreme cases of the fiber positions in the microstructure. One requirement relates the maximum distance from an outer edge of a fiber to the outer edge of every other fiber which is illustrated in Fig. 4(a). This distance must be smaller than the distance of the corresponding channel walls. The first requirement can be expressed by the Eq. (1):

$$a_{mn} < (m - n)p_{sheet} + w_{channel} \tag{1}$$

where p_{sheet} is the pitch, which comprises the nominal channel width w_{cav} and the nominal web width w_{web} .

The second requirement relates to the opposite sides of PZT fibers as shown in Fig. 4(b). This distance must be greater than the distance of the corresponding channel walls and can be expressed by Eq. (2):

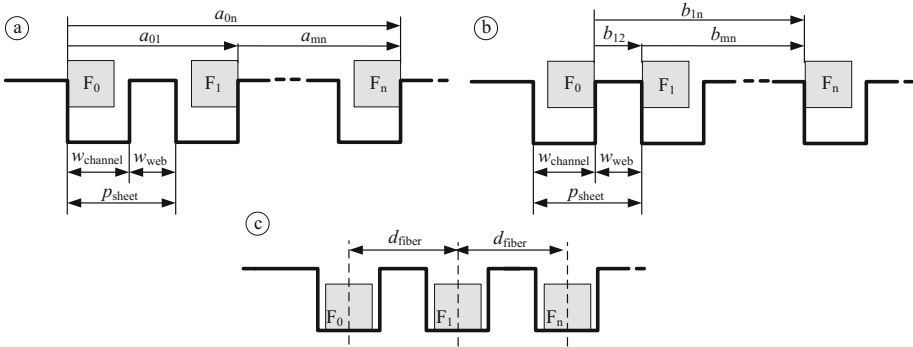


Fig. 4. (a) Extreme case 1 – the PZT fibers are far from each other; (b) Extreme case 2 – the PZT fibers are close to each other (c) Considered value for the statistical tolerance calculation

$$b_{mn} > (m - n - 1)p_{sheet} + w_{web}. \tag{2}$$

The statistical tolerance calculation provides a prognosis of the distribution of an investigation feature and has its advantages in the consideration of large quantities and causal research. For the present case, only the pitch d_{fiber} from one fiber to the adjacent fiber are considered, as Fig. 4(c) shows. The point of investigation is the statistical behavior for compliance of the distance d_{fiber} .

3 Automated Micro Assembly

3.1 Design of Micro-Assembly System

High volume capability demands automation, which in turn requires a high level of measurement technology. Micro assembly tasks often reach in this case the limits of physical resolution. For this purpose, two different measuring methods are compared for the measuring task at hand. As usual for measuring tasks a machine vision system is used for the pose measurement of the two joining partners. The second measuring instrument is a chromatic confocal sensor. This sensor can be easily integrated into the system, measures contactless and has a high resolution. In addition, further information about fiber height and channel height can be obtained. However, the latter plays no role in the current investigations.

Both methods are compared with regard to their measuring accuracy in the experimental part. The micro-assembly system consists of 4-axes, as shown in Fig. 5(a) and (b). The x-axis is attached to a portal frame. Furthermore, the z-axis is located at the x-axis, on which turn a vacuum gripper is located. The base plate supports the y-axis. On this axis are the mounting device for the sheet metal (as demonstrators are used 50×50 mm pieces of sheet metal with a local microstructure) as well as the storing space for several PZT fiber arrays. The mounting device or rather the sheet metal is also rotatable about the c-axis. The planned sequence of assembly is illustrated in a short version in Fig. 6.

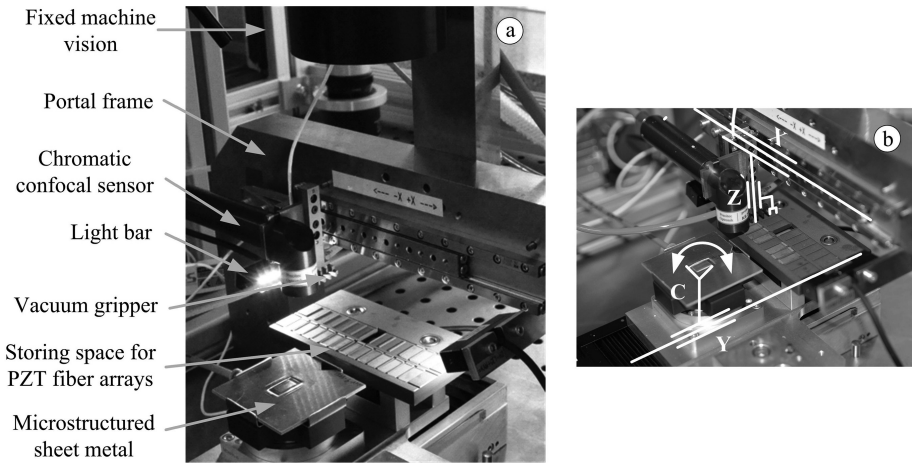


Fig. 5. (a) Basic structure of the micro assembly system; (b) Assignment of the axes

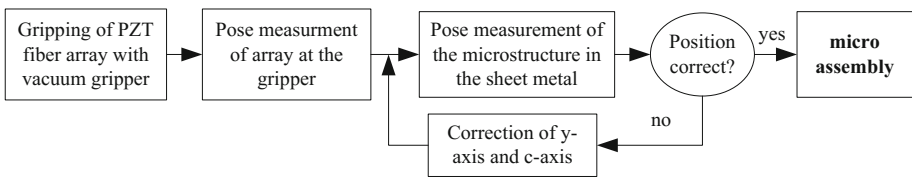


Fig. 6. Sequence of micro assembly

3.2 Machine Vision System

The machine vision system has a fixed camera position. Therefore, the parts which have to be measured are positioned with the axes under the camera. The aim is to detect the edges of the PZT fiber array and the edges of the webs in the micro-structure. When measuring the array, transmitted light (coaxial light) is used. As a result, the fibers appear as dark areas in the image as shown in Fig. 7(a). The transition from light to dark, and vice versa, is used for edge detection.

The microstructure is illuminated with a light bar from the side. This causes the webs to cast a shadow over the channels. The surfaces of the webs appear in the image as bright areas and the channels as dark areas (Fig. 7(b)). Again, the transition from light to dark and dark to light is used for edge detection.

3.3 Chromatic Confocal Sensors

The chromatic confocal point sensor (CHRcodile SE from company Precitec) is attached to the z-axis. Consequently, the sensor is guided over the component, whereby a line scan is performed. The line scans are executed in the upper, middle and lower area. Then the measured values are averaged. The result is a depth measurement of the structure (Fig. 7(c)), which is used for the exact determination of the edges.

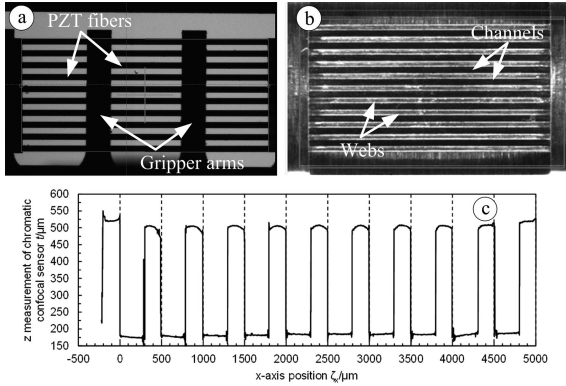


Fig. 7. (a) Machine vision image for a PZT fiber array with transmitted coaxial light; (b) Machine vision image for microstructure with side lighting; (c) Measuring result for the chromatic confocal sensor

4 Experimental

4.1 Manufacturing of PZT Fiber Arrays

Different methods for stacking and connecting the PZT plates were tested, because of the tight tolerance requirements. The first method was the stacking device 1, which consists of two blocks with grooves in which distance plates (thickness 0.23 mm) were assembled. According to Fig. 8(a), ten PZT plates were stacked between the distance plates. Subsequently, the PZT plates were connected at the ends. One series of test samples were connected with an adhesive layer (JB Weld) and another series with a solder (Sn62Pb36Ag2). The distance plates can be released from the grooves after hardening of adhesive or solder and the stack can be removed.

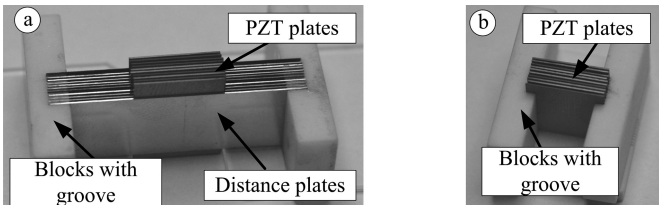


Fig. 8. (a) Stacking device 1 with distance plates; (b) Stacking device 2

The second version to manufacture a PZT plates-stack was with stacking device 2. It also consists of two blocks with grooves. But now the PZT plates were placed in the grooves, as demonstrated in Fig. 8(b). The plates were connected again in one series with adhesive and in another series with solder. Finally, all stacked blocks were separated in arrays by a diamond wire saw. For functional PZT fiber arrays, the fibers

should have to be coated with an electrode layer and insulation layer. However, the sensor capability of the modules is not relevant for the tolerance treatment and the micro assembly process. Therefore, the coatings were omitted.

Five PZT plate-stacks were fabricated for every test series and from each stack six manufactured PZT fiber arrays were measured. Each fiber edge position in an array was determined with a microscope (Nikon MM400) and $200 \times$ magnification. For the arithmetic tolerance calculation, there were thus more than 1300 edge distances to be checked per requirement. In the first part of Table 1 the number of edges is given in percent which satisfy the requirements.

Table 1. Arithmetic and statistical tolerance results for the stacking devices

		Arithmetic Tol.		Statistical Tol.	
		Equation 1 fulfilled	Equation 2 fulfilled	Mean value	Standard deviation
Stacking device 1	Adhesive	72.2%	99.7%	491.3 μm	10.3 μm
	Solder	98.1%	100%	497.5 μm	14.0 μm
Stacking device 2	Adhesive	75.9%	100%	488.0 μm	19.1 μm
	Solder	85.1%	100%	494.0 μm	12.5 μm

For statistical analysis, the measurement data was used to calculate the middle of every fiber. Subsequently, the mean value and the standard deviation of the distance from one fiber to the next were determined as shown in Fig. 4(c). The results are presented in the second part of Table 1.

Looking exclusively at the results of the arithmetic tolerance calculation, the series stacking device 1 and solder appears with the best results. The requirement 1 according to Eq. (1) satisfies 98.1% and requirement 2 according to Eq. (2) 100% of the manufactured arrays.

The other variants provide significantly worse results, especially related to the fulfillment of the requirement 1. Including the statistical tolerance calculation the series stacking device 1 with adhesive provides the lowest scattering of the results. However, the mean value of this series deviates by $-8.7 \mu\text{m}$ from the nominal value of $500 \mu\text{m}$. All mean values are below the nominal value. Here it can be assumed that shrinkage occurs during curing of the adhesive and also after soldering. A systematic increase of the distance of the distance plates in the stacking device can be counteracted this effect.

The PZT plates showed no visible deflection during the preparation of the stacks and the distance plates should also prevent possible deflections of the plate. Therefore, form deviations on single fibers in an array were considered to be negligible and were not investigated in this work.

4.2 Pose Measurement with Micro Assembly System

With the two measuring systems, the width w_{fiber} of the PZT fibers and the pitch p_{fiber} were measured for the arrays. In total, more than 200 measurement data are available

for each measured value. The results are summarized in box plots in Fig. 9. For a better comparison, the measured data of the microscope measurement are listed too.

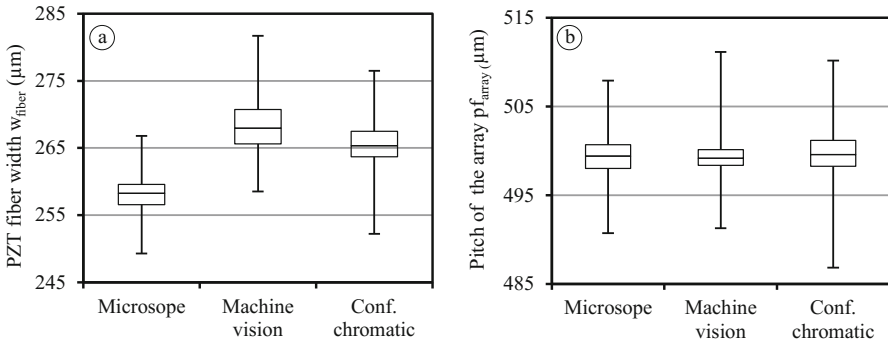


Fig. 9. (a) Box plot for PZT fiber width; (b) Box plot for the pitch in the PZT fiber arrays

Based on the box plots, it can be seen that the scattering of the measured values are similar for both measuring methods. The machine vision is slightly better. The scattering also corresponds approximately to the microscopic measurement, therefore both measuring systems are considered suitable. However, the machine vision system is recommended for use. This is justified by the significant faster image measurement compared to time for the three-line scans of chromatic confocal sensor.

Further on the channel width w_{channel} and the pitch p_{sheet} were detected for the sheet metals. Again the results are shown in box plots in Fig. 10. Here, the results differ significantly. The scattering for machine vision is much higher than for the chromatic confocal sensor. The worse result is due to poor edge detection. As it can be seen in Fig. 7 (b), the bars are not recognizable as clear bright areas. Thus, the measurement inaccuracy is greatly increased. Despite the longer measuring time, the chromatic confocal sensor is the suitable sensor for measuring the microstructure of the sheet metals.

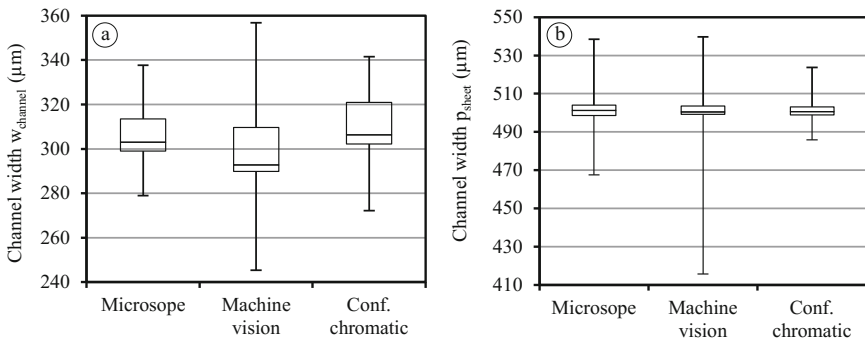


Fig. 10. (a) Box plot for channel width; (b) Box plot for the pitch in the microstructured sheet metal

5 Summary

Different concepts to manufacture PZT fiber arrays with minimal manufacturing tolerances were compared. The manufacturing by stacking PZT plates with distance plates and connecting the plates with an adhesive achieved the best results. This method showed the lowest scatter of the measured values. Deviations from the absolute nominal values were still too high due to the shrinkage of the adhesive during curing. By a slight increase of the pitch for distance plates over the nominal values, this effect should be compensated. Further work deals also with the slightly increase of distance plate thickness. This is intended to further reduce the manufacturing tolerances, but the assembly of the PZT plates in the device still has to be ensured.

The second part of the paper comprised the micro assembly of the PZT fiber arrays in the microstructured sheet metals. Two measuring systems were examined with regard to their suitability for the pose measurement of the joining partners. It has been shown that the machine vision is better for the measurement of the PZT fiber arrays due to the faster measurement. In the case of microstructures the chromatic confocal sensor is clearly ahead because of a significantly lower scattering of the measured values.

Acknowledgement. This research is supported by the Deutsche Forschungsgemeinschaft (DFG) in context of the Collaborative Research Centre/Transregio 39 PT-PIESA, subproject A03.

References

1. Williams, R.B., Park, G., Inman, D.J., Wilkie, W.K.: An overview of composite actuators with piezoceramic fibers. *Proc. SPIE* **4751**, 421–427 (2002)
2. Madhav, A.V.G., Soh, C.K.: An electromechanical impedance model of a piezoceramic transducer-structure in the presence of thick adhesive bonding. *Smart Mater. Struct.* **16**, 673–686 (2007)
3. Bhalla, S., Soh, C.K.: Electromechanical impedance modeling for adhesively bonded piezo-transducers. *J. Intell. Mater. Syst. Struct.* **15**(12), 955–972 (2004)
4. Schubert, A., et al.: Smart metal sheets by direct functional integration of piezoceramic fibers in microformed structures. *Microsyst. Technol.* **20**, 1131–1140 (2014)
5. Konka, H.P., Wahab, M.A., Lias, K.: Piezoelectric fiber composite transducers for health monitoring in composite structures. *Sens. Actuators A: Phys.* **194**, 84–94 (2013)
6. Gabbert, U., Duvigneau, F., Shan, J.: Active and passive measures to reduce the noise pollution of combustion engines. In: *Proceeding of the IEEE, International Conference on Information and Automation* (2014)
7. Upadrashta, D., Yang, Y.: Experimental investigation of performance reliability of macro fiber composite for piezoelectric energy harvesting applications. *Sens. Actuators A: Phys.* **244**, 223–232 (2016)
8. Müller, M., et al.: Structural integration of PZT fibers in deep drawn sheet metal for material-integrated sensing and actuation. *Procedia Technol.* **15**, 658–667 (2014)



Towards a Cloud-Based Analytics Framework for Assembly Systems

German Terrazas^(✉), Lavindra de Silva, and Svetan Ratchev

Faculty of Engineering, University of Nottingham, Nottingham, UK
german.terrazas@nottingham.ac.uk

Abstract. Advanced digitalization together with the rise of cloud technologies is a key enabler for a fundamental paradigm shift known as Industry 4.0 which proposes the integration of the new generation of ICT solutions for the monitoring, adaptation, simulation and optimization of factories. With the democratization of sensors, assembly systems can now be sensorized and the data generated by these devices can be exploited, for instance, to monitor their utilization, operations and maintenance. However, analyzing the vast amount of generated data is resource demanding both in terms of computing power and network bandwidth, especially when dealing with real-time changes to product, process and resource domains. This paper presents a novel cloud-based analytics framework for the management and analysis of assembly systems. It brings together standard open source technologies and the exploitation of cloud computing which as a whole can be adapted to and deployed on different cloud providers, thereby reducing infrastructure costs, minimizing deployment difficulty and providing on-demand access to virtually infinite computing power, storage and network resources.

Keywords: Precision assembly systems · Cloud computing · Data analytics

1 Introduction

The integration of the new generation of ICT solutions for the monitoring, adaptation, simulation and optimization of factories have enabled cyber-physical production systems (CPPS) to break from the traditional assembly systems automation pyramid comprising the *field level*, *control level*, *process control level*, *plant management level* and *enterprise resource planning level*. This traditional structure now comprises just the control and field levels (i.e., PLCs are kept close to technical processes to deliver the highest performance), with a complete decentralization of the higher levels. With this new organization, some of the features fully automated CPPS are expected to have are autonomy, self-organization, remote diagnosis, predictability, interoperability, real-time control, global tracking and tracing, and efficiency to name a few [1]. This has not affected the way production takes place in an assembly system, which is based on a series of tasks systematically developed and executed throughout the so-called *product domain*, *process domain* and *resource domain*. Although current sophisticated approaches can reflect product changes in the assembly sequence and, in turn, push this assembling change through the realization process [2], little has been said on how

automated assembly systems could learn from the increasing amount of manufacturing data to predict, adapt and control changes at any domain level in real time and efficiently, especially when analyzing the vast amount of generated data is resource demanding both in terms of computing power and network bandwidth. While there is related work in computer-aided process planning, most of them generate outdated and unfeasible process plans due to the lack of integration with the shop floor to capture resource availability or other dynamic changes [3, 4]. Other approaches propose bespoke cloud-based solutions in terms of resource monitoring and optimized adaptive process planning but operate across the process domain and resource domain only and fail to address big data scalability issues [5, 6]. In what follows: Sect. 2 presents an implemented cloud-based data analytics framework built in terms of open source technologies for the collection and management of shop floor data; Sect. 3 presents two automated assembly test beds; and Sect. 4 discusses how they could be integrated within a complete CPPS, and the challenges and opportunities in real-time assembly monitoring at all levels.

2 A Data Analytics Framework for the Cloud

The architecture for our cloud-based data analytics framework can be conceptually seen as a set of layers that, as a whole, depict different types of domain entities arranged across different levels of abstraction together with their relationships and associated behaviors (see Fig. 1). A layer is a logical division that groups software components by functionality without taking into account their physical location. We define four different levels of abstraction comprising the *Knowledge* layer, the *Analytics* layer, the *Application* layer and the *Presentation* layer. These layers can be seen as sequentially arranged, one upon another, where components in a given layer can only communicate with those in the layer above or the layer below. The fundamental concept behind this idea [7] is the isolation of layers, i.e., software components within a layer are independent from those located in other layers and have no knowledge of their internal structure. While the most challenging part of designing an architecture of this kind is to define the layers and their functionalities, using a layered scheme brings domain independence, loose-coupling and reusability benefits. Additionally, the logical separation offered by the four levels of abstraction contributes to the flexibility and scalability of the proposed framework.

The Knowledge Layer. This comprises the storage and retrieval of persistent assembly data which forms the basis for data analytics. Technically speaking, this layer comprises document databases, which are one of the main categories of NoSQL databases. Document databases store all the information relating to a given object in a single instance in the database, which makes a document database attractive for cloud-based applications [8, 9], where speed of deployment is important. While implementations differ, this technology assumes that documents encapsulate data in some standard format, such as Java-Script Object Notation (JSON). Document databases allow different types of document structures in a single store and allow the fields within them to be optional, hence providing flexibility when organizing and storing the application

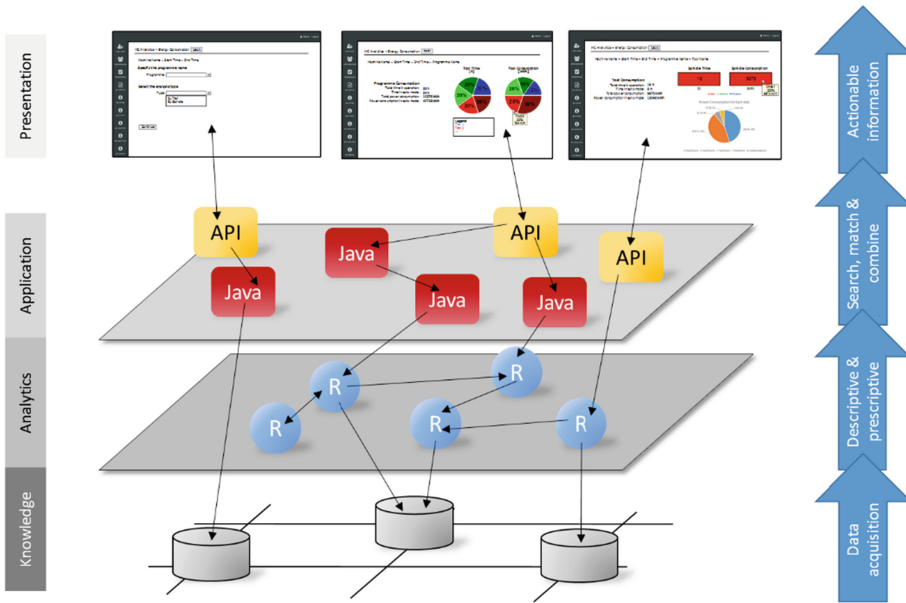


Fig. 1. The conceptual architecture of our analytics framework comprising domain entities across different levels of abstraction. The *Knowledge* layer captures relevant data sources of manufacturing data. This is accessed by descriptive and prescriptive business logic which is searched, matched, combined, configured and effectively provided to consumers for decision making.

data used in the analytics framework as well as a reduction in the storage space and associated costs. In addition, the simplicity of JSON makes it easy to transpose object structures from almost any programming language, making it possible to flexibly manage data both online and offline, similarly to the platform described in [10].

The Analytics Layer. This layer provides a dedicated environment where business logic related to data analysis and data mining takes place. The main goal is to deploy software components that are suitable for remote invocation, and in such a way that they encapsulate layer-specific logic, by controlling transactions and coordinating responses in the implementation of the layer's operations. In order to implement analytic components, we have chosen the R programming language, and Rserve [11] as the technology to support a neat linkage with the *Application* layer, so that the latter may use the services offered by the former. The R technology is chosen because of its well-known support for complex descriptive analytics, through the provision of mechanisms for multicore task distribution, readily usable tests, and many libraries, including specific technologies such as Spark¹, TensorFlow [12], and ProActive [13]. R has also become an important development tool for numerical analysis and machine learning.

¹ <https://spark.apache.org/docs/latest/sparkr.html>.

The Application layer. This layer provides a dedicated environment implementing logic related to service orchestration. The software components residing in this layer implement the *Command* pattern [14] which will allow the *Presentation* layer, and in fact any other client, to make requests to unspecified business components. Thus, the key participants in this pattern include an abstract *Command class* which declares an interface for executing behavior and *Command subclasses* each of which uses a well-defined REST API² for external communication, and implements the specific behavior needed for invoking the actual request on an *Online Service* at the *Analytics* layer. We have chosen Java in order to implement these components, and Jersey as the technology to support a neat link with the *Presentation* layer.

The Presentation Layer. This layer displays actionable information to end users. It comprises components needed to display visual content as well as to capture and manage external interactions. Data exchange with the *Application* layer occurs through its well-defined REST API using the JSON data format. Depending on specific use cases associated to data visualization, components in this layer will need to implement suitable methods for processing and presenting results to end users.

3 Deployment on the Cloud

Elastic computing is considered one of the central elements of the cloud paradigm. The term elastic has its origins in physics, where the elasticity of a material is the ability to return to its original state after deformation. In cloud computing, elastic computing is the ability to adapt to workload changes by scaling up and scaling down computing resources automatically, in such a way that at a given point in time the available computing resources match current demand [15–17]. Thus, elastic computing yields significant cost savings compared to the traditional cloud infrastructure since organizations simply rent computing power on demand as the workload changes. The Amazon Elastic Compute Cloud (Amazon EC2) provides scalable computing power in the Amazon Web Services (AWS) cloud platform. One of the advantages to using the former is the elimination of the need to invest in hardware and systems administration up front, allowing applications to be developed, tested and deployed faster. Amazon EC2 can be used to launch as many or as few virtual servers as needed, configure security and networking, and manage storage. In particular, AWS enables users to create tailored *Amazon Machine Images* (AMIs) to quickly and easily start instances customized with everything that is needed to run applications. An *instance* is associated to a *type of instance* that, essentially, defines the hardware configuration of the host computer. In this way, Amazon EC2 provides each instance with a consistent and predictable amount of CPU and memory capacity. Thus, in order to deploy the analytics framework in the cloud, a specific AMI equipped with Apache Tomcat³, R components and Rserve has been created as depicted in Fig. 2.

² <https://restfulapi.net/>.

³ <http://tomcat.apache.org>.

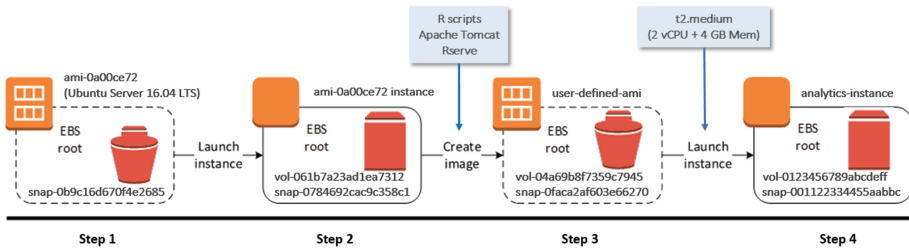


Fig. 2. The instantiation of an AMI which, after being equipped with Apache Tomcat, R components and the Rserve library (steps 1 and 2), becomes a user defined image launched and embodied in a t2.medium instance type (steps 3 and 4).

4 Deployment on Assembly Lines

We envision the instantiation of our analytics framework on at least two assembly lines located at the University of Nottingham. The first of these is the Precision Assembly Demonstrator (PAD) [18], which assembles detent hinges for the interiors of certain vehicle models. The PAD comprises six modular stations: two KUKA six-axis robotic arms with corresponding workspaces, a shared tool changing rack, a testing station, and a shuttle transport system, which links the stations to each other and a loading/unloading station (see Fig. 3). The parts to be assembled into a product are mounted on a pallet and placed on the conveyer, which moves the pallet to each of the stations. When the pallet reaches a robotic arm, it removes the individual parts and performs various assembly operations on them before returning the resulting partial-product back to the pallet. Data that could be collected from these stations includes the specification (e.g. as a sequence of parameterized assembly operations) of the product being assembled, the current layout of the assembly line, the specific operations performed (e.g. picking and gripping), the tools used to perform them (e.g. a gripper and suction tool), the parts on which the operations were performed (e.g. a spring and a ball-bearing), and the parameters used (e.g. pressure and depth of cut). The testing station can additionally store 2D images of the product being assembled, which are taken to check whether the product is being correctly assembled. This station can also store the force applied when testing hinges, and which ones pass/fail the tests. All data collected can be associated with specific hinges, as they have serial numbers.

The second assembly line is the SMC Pneumatics HAS-200 platform, which has been used to mimic the production of customized pharmaceuticals [19]. The SMC has 8 modular stations connected in a ring-shaped topology by default, which is manually adapted as necessary (see Fig. 4, bottom left). Stations operate as follows. The first loads empty containers (‘pills’) onto the conveyor belt as customized requests for pills are received by the assembly line. The next three stations are blue, red and yellow particulate (‘ingredient’) dispensers, respectively, which pick a container, add the required quantity of particulate by weight, and return the container to the belt. The next two stations are testing stations, which measure the absolute quantity of particulate in the container. These stations connect to one that puts a lid on a container, prints a custom label, and sticks it on the lid. Finally, a palletization station removes completed

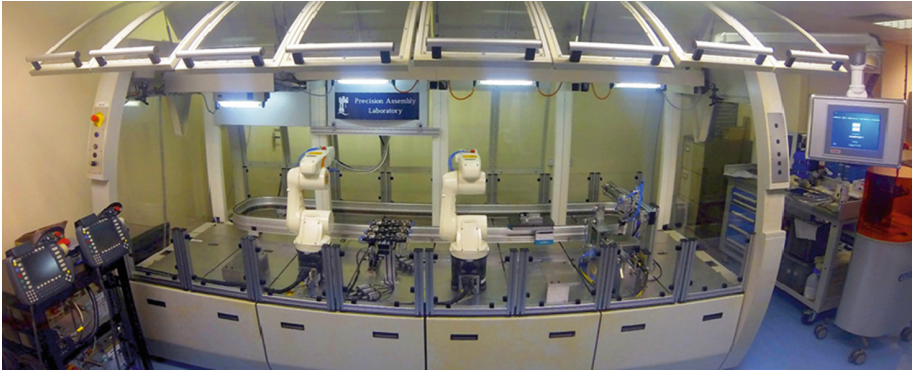


Fig. 3. The PAD assembly system [18] comprising two KUKA six-axis robotic arms with corresponding workspaces, a shared tool changing rack, a testing station, and a shuttle transport system, which links the stations to each other and a loading/unloading station.

containers for packaging. Data that could be collected from these stations include the layout and operations as before, the weight of each type of particulate added to each container, and the total volume of particulate in each container. All data can be uniquely associated with containers as each of them has a barcode.

5 Real-Time Monitoring of Assembly Lines

Both the PAD and the SMC assembly lines are used in an environment where their layouts or *topologies*, products, and processes can ‘evolve’ [19]. This can be reflected by the variety, velocity and volume of collected data which could potentially vary over the course of assembly. For instance, if a new ‘pill’ is requested that uses a previously unused ‘ingredient’; a station module is removed for maintenance, resulting in container-weight data being no longer collected; a new process is added that takes thermal images during a force test; a process is upgraded to now take 3D (instead of 2D) images; or the assembly line’s throughput is ramped up. We recognize that these scenarios may represent a real challenge, and envision the big data characterization and subsequent capture, collection, processing, organization and storage for both online and offline data management in the *Knowledge* layer being addressed by the cloud-based platform schematically presented in Fig. 4.

At the resource level, one interesting question to explore would be how transformations in the SMC’s topology relate to factors such as the month of the year, the kind of product being assembled, and the availability of assembly stations. For instance, we could verify whether, during peak season, the stations connected in a ‘Y’ shaped topology tend to be more effective than when they are connected in a ring-shaped topology (which may cause longer queues of containers on the single conveyor belt). At the product level, we could analyze which raw material vendors (if any) tend to be associated with a significantly higher percentage of force-test failures on the PAD, which might be suggestive of lower quality raw materials. At the process level, we

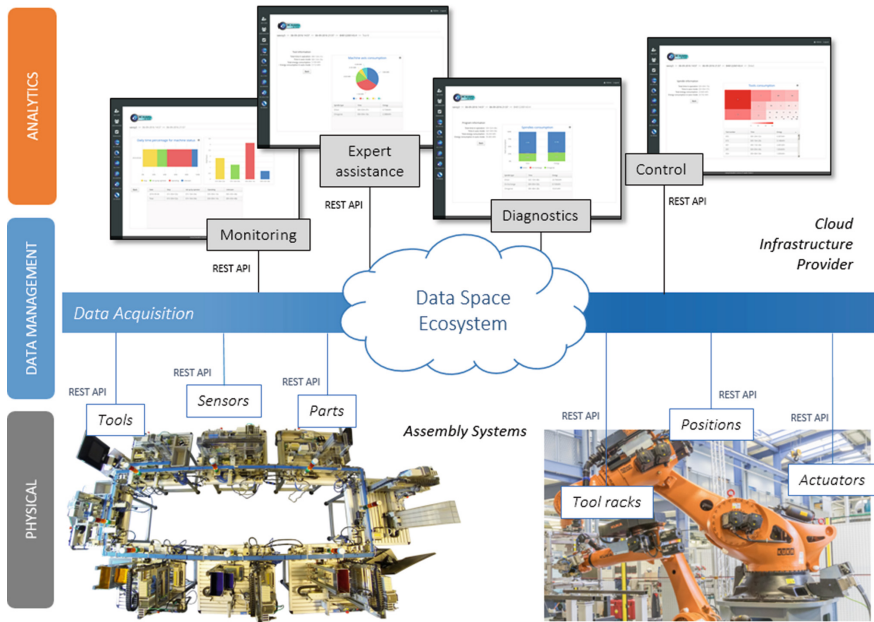


Fig. 4. Assembly lines connected to a data space ecosystem that comprises the data management and analytics framework. Shop floor generated data is collected, processed, stored and made available for monitoring, diagnosis and other types of analytics.

could enhance product quality with offline image processing of the stored hinge images in order to recognize and classify hinge defects such as surface cracks, dents and spots. The end user could be presented with analytical insights as depicted in Fig. 4, regarding whether and how such defects correlate to variations in assembly processes and parameters, e.g. in gripper-tool models or the pressure applied during assembly operations.

6 Conclusions

In this work, we have described an implemented architecture for a cloud-based analytics framework comprising different levels of abstraction and based on open source technologies. We have also introduced two different assembly lines, i.e., their layouts, products, and processes, each of which is able to evolve. In this context, we have shed light on challenges and opportunities associated with the product, process, and resource domains, particularly when analyzing large amounts of data is resource demanding in terms of storage and processing power. The authors would like to thank the support of the *EPSRC Cloud Manufacturing – Towards Resilient and Scalable High Value Manufacturing* project under grant agreement EP/K014161/1.

References

1. Monostori, L.: Cyber-physical production systems: roots, expectations and R&D challenges. *Proc. CIRP* **17**, 9–13 (2014)
2. Ahmad, M., et al.: A framework for automatically realizing assembly sequence changes in a virtual manufacturing environment. *Proc. CIRP* **50**, 129–134 (2016)
3. Mourtzis, D., Doukas, M., Vlachou, A., Xanthopoulos, N.: Machine availability monitoring for adaptive holistic scheduling: a conceptual framework for mass customization. *Proc. CIRP* **25**, 406–413 (2014)
4. Tapoglou, N., Mehnen, J., Vlachou, K., Doukas, M., Milas, N., Mourtzis, D.: Cloud-based platform for optimal machining parameter selection based on function blocks and real-time monitoring. *J. Manuf. Sci. Eng.* **137**(4), 040909 (2015)
5. Zhong, R., Xu, C., Chen, C., Huang, G.: Big data analytics for physical internet-based intelligent manufacturing shop floors. *Int. J. Prod. Res.* **55**(9), 2610–2621 (2017)
6. Mourtzis, D., Vlachou, E., Xanthopoulos, N., Givchchi, M., Wang, L.: Cloud-based adaptive process planning considering availability and capabilities of machine tools. *J. Manuf. Syst.* **39**, 1–8 (2016)
7. Richards, M.: *Software Architecture Patterns*. O’Reilly Media Inc., Sebastopol (2015)
8. Hashem, I., Yaqoob, I., Anuar, N., Mokhtar, S., Gani, A.U., Khan, S.: The rise of big data on cloud computing: review and open research issues. *Inf. Syst.* **47**, 98–115 (2017)
9. Pokorny, J.: NoSQL databases: a step to database scalability in web environment. *J. Web Inf. Syst.* **9**(1), 69–82 (2017)
10. Ferry, N., Terrazas, G., Kalweit, P., Solberg, A., Ratchev, S., Weinelt, D.: Towards a big data platform for managing machine generated data in the cloud. In: *IEEE Industrial Informatics*, pp. 263–270 (2017)
11. Urbanek, S.: Rserve – a fast way to provide r functionality to applications. In: Hornik, K., Leisch, F., Zeileis, A. (eds.) *The 3rd International Workshop on Distributed Statistical Computing* (2003)
12. TensorFlow: a system for large-scale machine learning. In: *Proceedings of the 12th USENIX Conference on Operating Systems Design and Implementation*, pp. 265–283. USENIX Association (2016)
13. ProActive. <https://doc.activeeon.com/latest/admin/ProActiveAdminGuide.html>. Accessed 01 Oct 2017
14. Gamma, E., Helm, R., Johnson, R., Vlissides, J.: *Design Patterns: Elements of Reusable Object-Oriented Software*. Addison-Wesley Longman Publishing Co. Inc., Boston (1995)
15. Herbst, N.R., Kounev, S., Reussner, R.: Elasticity in cloud computing: what it is, and what it is not. In: *Proceedings of the 10th International Conference on Autonomic Computing*, pp. 23–27. USENIX (2013)
16. Galante, G., de Bona, L.C.E.: A survey on cloud computing elasticity. In: *Proceedings of the 2012 IEEE/ACM Fifth International Conference on Utility and Cloud Computing*, pp. 263–270. IEEE Computer Society (2012)
17. Coutinho, E.F., de Carvalho Sousa, F.R., Rego, P.A.L., Gomes, D.G., de Souza, J.N.: Elasticity in cloud computing: a survey. *Ann. Telecommun.* **70**(7–8), 289–309 (2015)
18. Antzoulatos, N., Castro, E., de Silva, L., Rocha, A.D., Ratchev, S., Barata, J.: A multi-agent framework for capability-based reconfiguration of industrial assembly systems. *Int. J. Prod. Res.* **55**(10), 2950–2960 (2017)
19. Chaplin, J.C., et al.: Evolvable assembly systems: a distributed architecture for intelligent manufacturing. *IFAC-PapersOnLine* **48**(3), 2065–2070 (2015)

Digital Technologies and Industry 4.0 Applications



Information-Rich Manufacturing Metrology

Richard Leach¹(✉), Patrick Bointon¹, Xiaobing Feng¹,
Simon Lawes¹, Samanta Piano¹, Nicola Senin^{1,2},
Danny Sims-Waterhouse¹, Petros Stavroulakis¹, Rong Su¹,
Wahyudin Syam¹, and Matthew Thomas¹

¹ Manufacturing Metrology Team, University of Nottingham,
Nottingham NG7 2RD, UK

richard.leach@nottingham.ac.uk

² Department of Engineering, University of Perugia, 06125 Perugia, Italy

Abstract. Information-rich metrology (IRM) is a new term that refers to an approach, where the conventional paradigm of measurement is transcended, thanks to the introduction and active role of multiple novel sources of information. The overarching goal of IRM is to encompass and homogenise all those measurement scenarios where information available from heterogeneous sources, for example, from the object being measured, the manufacturing process that was used to fabricate it, the workings of the measurement instrument itself, as well as from any previous measurements carried with any other instrument, is gathered and somewhat incorporated with an active role into the measurement pipeline in order to ultimately achieve a higher-quality measurement result (better metrological performance, shorter measurement times, smaller consumption of resources). Examples of IRM in action in precision and additive manufacturing will be presented, including the measurement of form and texture.

Keywords: Manufacturing metrology · Form measurement
Texture measurement

1 Manufacturing Metrology

To support the manufacture of next-generation high-value products, increased reliance will be placed on metrology. This article will discuss an approach to metrology that, in our opinion, has the potential to significantly enhance the metrology capability in advanced manufacturing. While traditionally metrology has been applied to the inspection of the final part, after the manufacturing process is completed, nowadays the trend is to bring metrology in to the production line (Everton et al. 2016). This may just mean performing part inspection right after each step of the manufacturing process (for example, between a roughing and a finishing operation in a machine tool), or we can push integration even further by carrying out the measurement tasks during the execution of each individual manufacturing operation, where the nature of the operation allows it (for example, within an additive manufacturing process, measuring the properties of a layer while it is being fabricated). Also, when considering integration between metrology and manufacturing, considerations about the measurement data are

important. One integration scenario may see a measurement triggering an alarm if something goes wrong during a manufacturing operation (i.e. detection of an out-of-tolerance condition); more complex integration scenarios may see some form of implementation of feedback mechanisms, for example, the triggering of a corrective action, or the real-time modification of some manufacturing process control parameter to bring the process back to an in-tolerance state.

Such integrated metrology needs to be compatible with the manufacturing cycle time (we do not want metrology to prohibitively slow down the process), and measurement systems need to be spatially located to be compatible with the type of integration: i.e. on the production machine, or close enough if measurement is to be performed between manufacturing stations.

Developments in integrated measurement and control have allowed significant enhancement of advanced manufacturing techniques and marked improvements in surface texture and material properties, along with a reduction in process variation and defects. Integrated measurement and control technologies can also offer cost reductions and process efficiency improvements, but the scale of up-front investment required can often seem daunting, and the benefits may not be easily quantified. Cost considerations aside, there are a number of potential barriers to integrated metrology that can prevent its wide-scale adoption in industry. These include, but are not limited to the following. Note that we will concentrate mainly on dimensional and surface metrology using optical technology in this paper, but many of the arguments can be generalised to any metrology discipline.

- i. *Measure over larger dynamic ranges*: all measuring instruments have a finite dynamic range, defined here as the ratio of their range to their resolution in terms of either lateral and/or height capabilities. Often the trade-off is to have either a large range or a high resolution, but rarely both (Leach et al. 2013). For example, in optical surface metrology, there are two distinct classes of instrument which are commercially available: 1. those that measure over large areas (metres squared) with low spatial resolution – a few hundreds of micrometres (for example, fringe projection, photogrammetry and moiré interferometry) (Harding 2013; Van der Jeught and Dirckx 2016 and Zuo et al. 2016) and 2. those that measure over small areas (up to a few millimetres squared) with spatial resolutions of the order of a micrometre (for example, coherence scanning interferometry, confocal microscopy and focus variation microscopy) (Leach 2011). Essentially, the former class is camera-limited (sensor resolution and depth of field issues), while the latter is objective-limited (diffraction limited through finite numerical aperture) and can be prohibitively slow due to the need for scanning in both lateral and often axial directions. In order to meet the demands of advanced manufacturing, there have been several attempts to try and combine the two classes (see for example, Kaysar et al. 2004; Weckenmann et al. 2009), but more progress is required before such hybrids can be used in earnest. This dynamic range issue is especially problematic for industries that manufacture small features over large areas in a highly parallel fashion, for example, for roll-to-roll applications such as printed electronics.
- ii. *Measure higher slope angles*: all optical instruments are fundamentally limited by finite slope measurement capabilities, mainly due to their numerical apertures and,

in many cases this limitation is related to the dynamic range limitation above (see Leach et al. 2014 for an outline review of these limitations). This fundamental limitation will be treated in some depth in Sect. 3.2, as it is one of the key limitations that hinder progress in optical metrology.

- iii. *Measure difficult materials*: all surface measuring instruments have limits on the types of surface that they can measure. Also, where mathematical models of the imaging or scattering process are necessary, some instruments make assumptions about the surface being measured that may not be met in practice, for example, that the surface is a highly-reflecting metallic surface. Polymer and ceramic surfaces can cause significant issues due to translucency and rough surfaces can cause multiple-reflection and slope effects (see ii). Surfaces with mixed materials and/or produced using multiple processes are especially challenging (Mathia et al. 2011), and surfaces produced by additive manufacturing have significant material challenges for optical instruments (Grimm et al. 2015; Launhardt et al. 2016 and Townsend et al. 2016).
- iv. *Measure at high speed*: for integrated metrology, and especially for in-line/in-situ metrology, there must be significant increases in the speed of measurement (Allwood et al. 2015). The high-speed metrology task is increasingly limited by the fundamentals of optical interrogation of the surface, such as: the compromise between spatial resolution and field of view; the loss of effective spatial resolution due to motion blur; or the dynamic range of optical properties across the inspected region. Such limits imply that faster “brute-force” measurement of the whole surface cannot be a solution. Whilst there have been valiant attempts to speed up conventional measurement techniques (see for example, Jiang et al. 2010; Zhang 2012 and Hahn et al. 2016), often speed increases of several orders of magnitude are required for integrated metrology to become realistic. Scatterometry (Madsen and Hansen 2016) and scattering methods (Leach et al. 2013) have been applied in-process, especially in the integrated circuit and optics manufacturing industries respectively, but both methods are highly specific in the types of surface they can measure (although both methods are arguably information-rich in nature). In order to overcome the metrology speed challenges, it is essential to exploit a priori knowledge about the production task, the nature and functional significance of relevant defects, and any potential repair steps to dramatically simplify the measurement task. Development of existing measurement techniques to simplify integration, hybridisation and increased environmental tolerance will also help. A range of research strands needs to be followed including: optical system modelling and defect extraction, global control of substrate and defect location, intelligent sampling and data throughput, and fast feature inspection.

The conventional approach to address the issues above is simply to improve our existing measurement technologies. But, as has been pointed out in iv above, there are a number of reasons why this is not the whole solution. In many cases, we have come up against barriers that prevent us from significant further improvements in instrument performance. Such barriers are due to limitations in current technology and due to the fundamental laws of physics (or a combination). Examples of limitations due to physics include: the shot noise limit, either due to the discrete nature of electrical charge in

electronics or to the particle nature of light in optical detectors; the diffraction limit in optics, due to the wave nature of radiation, there is diffraction caused by the limiting edges of the optical system's aperture (this means a point will always be imaged with finite blur); the slope angle limitation in an imaging system due to its finite numerical aperture (see Sect. 3.2); and the limit on sampling due to Shannon's theorem (all these limitations are summarised in Boreman 2001). Examples of technology limitations are the finite processor speed or memory limits of computing systems. When we attempt to produce integrated measurement solutions, such technology limits are a frequent issue and often the only way around this is to use pre-processing methods, for example adaptive or intelligent data reduction and sampling techniques, effectively trying to reduce the data overhead (Wang et al. 2012; Yu et al. 2012).

2 Information-Rich Metrology

Information-rich metrology (IRM) is a term that we introduce to refer to the use of any type of additionally-available information to improve a measurement process. Information may come from knowledge of the manufacturing process, knowledge of the object to be measured, and/or knowledge of the physical interactions/principles underlying the measurement technology itself. Additional information may be pre-existing (i.e. "a priori"), or obtained through other measurement processes, even concurrently to the measurement we are aiming to improve. An overview of the primary sources of information typically exploitable when IRM is applied to a manufacturing environment is provided in Fig. 1.

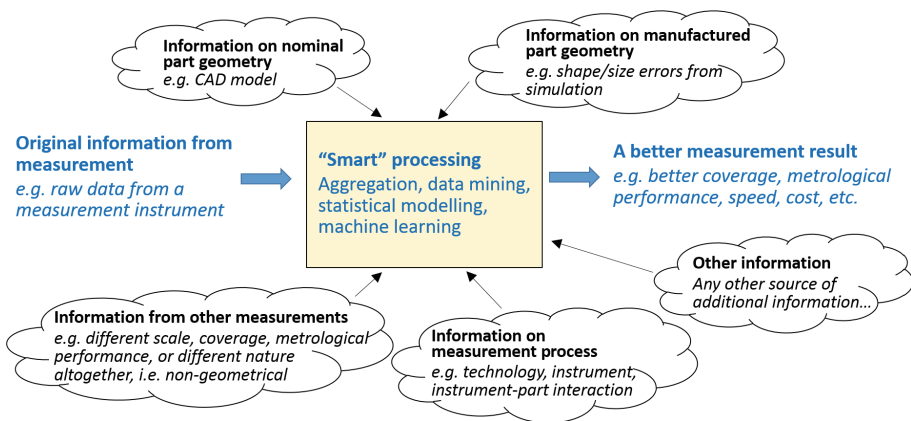


Fig. 1. The information-rich metrology paradigm: typical sources of information that can be exploited to improve the measurement process.

The idea of using available information related to the product, or process, or product-measurement-instrument interaction, makes intuitive sense because metrology in manufacturing takes place in controlled and predictable conditions, with a sensible

amount of information which is known in advance. Often when we manufacture something, and especially when we use digital manufacturing methods, we have a large amount of information about the object being manufactured, for example, the CAD data gives us the nominal form and we have usually characterised the surface texture to a high degree of confidence. Analogously, we do have – or we can acquire – a significant amount of information about the manufacturing process, in terms of its capability, the features and defects it generates, the materials it is designed to operate with, and the types of geometries and surfaces it typically produces. Most of the above information becomes available at product development and at manufacturing process planning, and we are asserting that such information may also bring benefit to metrology.

One of the most promising paradigms for IRM is based on using additional information about the manufacturing process and the object that is fabricated, to develop improved mathematical models that describe the interactions between the measured object and the measurement probe (see Fig. 1). In practice, mathematical models that describe physical principles and phenomena underlying many measurement technologies are already available, although one has to be careful that oversimplifications are not abused. In optical measurement, for example, many models have been developed over the decades, to support the theory of focus-variation measurement, coherence-scanning interferometry, confocal microscopy, fringe projection, photogrammetry, etc. It is safe to say that the totality of current commercial optical measurement systems are already making use of complex mathematical models to interpret raw data acquired through their probes. However, because such models aim to be general, which means that they must be applicable with little prior knowledge of the measurement scenarios, they can make very few assumptions about the nature of the surface which will be measured, the material properties they will encounter, and other factors. Thus, such models are limited in the information they can provide. A typical example is the interpretation of signals originated by light captured by the detector after multiple reflections and scattering. Trying to reconstruct what determined the patterns captured by the detector typically implies the solving of complex (often non-linear) inverse problems, which are typically unsolvable or ambiguous without resorting to additional sources of information. The advantage of working in the scenarios typically encountered in manufacturing metrology is that we often have such additional information, for example, because we have an approximate idea of the part geometry, and/or because we have a clear idea of what type of signature features a specific manufacturing process leaves on a surface.

The predictability of operating conditions, and the wealth of information available in a typical manufacturing metrology scenario explain why our research in IRM is focusing on one of its most promising paradigms, that is, to develop advanced models of probe-surface interaction in order to improve measurement quality, whilst using externally available information (from the product, process, or other) to develop such models.

One last comment must be reserved on the need for IRM to revisit the way information is aggregated and processed. As a matter of fact, the addition of a potentially high number of heterogeneous information streams raises a whole series of challenges regarding how such information should be homogenised, aggregated and

finally exploited towards achieving a better measurement result overall. Challenges are in how to handle large amounts of data in increasingly shorter times (possibly verging towards big data issues), in how to data mine the relevant relationships between variables, and finally in how to obtain mathematical and statistical models that ultimately support what we call the “smart” measurement paradigm, which is meant to supersede the conventional metrology pipeline of “blind” processing (i.e. where knowledge is extracted exclusively from the raw data provided by the measurement instrument, with no help from any other sources of information). As in many other applications involving big data, we believe that artificial intelligence (AI) technology in general, and machine learning in particular, can provide significant support to the development of the smart measurement solutions of the future.

Several examples will be given in the following, together with additional examples that show that a priori information also has additional uses, other than for improving measurement models, but before proceeding, it is important to discuss why IRM is important to manufacturing metrology, and to integrated metrology in particular.

As stated earlier, central to IRM is the aim to improve measurement quality. Quality is here intended as a generic term encompassing multiple facets. Improving quality may mean: reducing measurement times, improving measurement performance indicators (accuracy, precision, etc.), expanding the range of covered scales (spatial resolution and range - in terms of spatial frequencies we will often refer to expanding the bandwidth of a measurement), and improving coverage, intended as the capability to reach surfaces which may be harder to reach, for example measuring beyond the maximum permissible slope for a given measurement technology (see below). Improving measurement quality may also mean that we can obtain the same results that we obtained before, but at a fraction of the cost, or of the time, or with smaller, cheaper, more rugged and more affordable instruments; these are all essential aspects to better integrate metrology into the production line.

IRM is nothing new; the use of additional sources of information to enhance a measurement system’s performance, and thus the quality of its measurement output, has been carried out for hundreds of years. Perhaps the first and most well-known example of IRM is that of optical super-resolution in microscopy and astronomy (Leach and Sherlock 2013). A number of further examples of IRM are given in Sects. 3.1, 3.2 and 3.3.

3 Examples of IRM Research at Nottingham

3.1 An All-Optical Dimensional Measuring System

We present here the design of an original, flexible and open-architecture, all-optical dimensional measuring system (AODMS) for measuring the geometry and surface topography of micro-scale components and components with microscale features (Fig. 2). The system is designed to operate in a cube of 100 mm sides, with micrometre or sub-micrometre measurement uncertainties. The key aspects of AODMS are flexibility and open-architecture. The system is designed to accommodate a wide array of heterogeneous optical sensors, ranging from 3D measurement to 2D imaging, from

prototype to commercial sensors, and is being designed to be particularly suitable to support the investigation of multi-sensor data fusion solutions (Wang et al. 2015) – another example of IRM, where different resolution data are combined; one effectively acting as the a priori data for the other. The open nature of the architecture allows full flexibility in the design and configuration of the instrument control and communication software, as well as of the data analysis and processing software, thus presenting itself as an ideal platform to investigate IRM through the support to the development of solutions to enable knowledge-driven measurement, for example, through the interaction with CAD/CAM systems, product data-management systems and any other IT-based knowledge-management solutions.

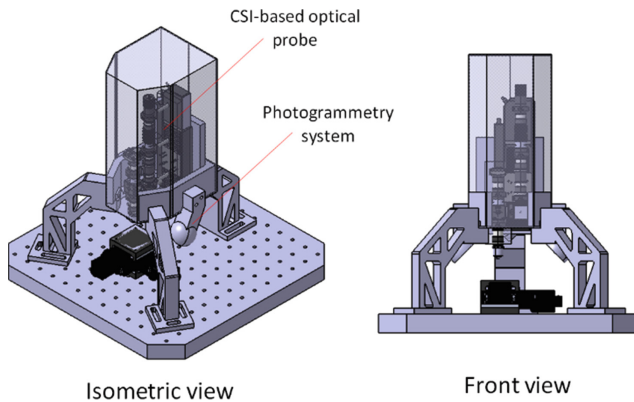


Fig. 2. Schema of the all-optical dimensional measurement system.

The AODMS prototype includes a moving stage, a support and interface to a photogrammetric system dedicated to form measurement (Sims-Waterhouse et al. 2017), and a support and interface to a hybrid prototype sensor that integrates coherence scanning interferometry (CSI) and focus variation microscopy (FVM) for surface topography measurement. The metrology frame of the AODMS is fabricated using additive manufactured lattice structures for vibration isolation within a pre-defined bandgap (Syam et al. 2017). AM fabrication technologies and lattice structures are being investigated for the AODMS also because of their potential to support modularity and increased architecture reconfigurability to accommodate different inspection scenarios. The AODMS is currently being developed to support the experimental activities of a number of IRM-related research projects: (1) fusion of photogrammetry, CSI and FVM data; (2) CAD information and speckle enhancement technologies to improve photogrammetry; (3) self-calibration solutions for CSI and FVM (Ekberg et al. 2017); (4) motion stage calibration using photogrammetry (Sims-Waterhouse et al. 2017); (5) calibration and adjustment of the CSI measurement using the ‘foil’ model of the surface (Su et al. 2017); and (6) bandwidth enhancement of CSI for high slope surface measurement based on rigorous modelling of the signal response (Coupland and Lobero 2017, see next section).

3.2 High Slope Measurement

Complex surfaces often have features which have high slope angles, either through design, for example prismatic arrays for safety signage, or due to the nature of the manufacturing method, for example in additive manufacturing (Townsend et al. 2016). The most complex surfaces may have very large ranges in terms of spatial frequencies (and hence surface slope angles), for example, a highly aspheric surface with a micro-scale Fresnel grating (Fang et al. 2013). Deterministically-textured surfaces with complex geometries are abundant in mechanical engineering fields for such applications from fluid control, adhesion, tribology and bio-compatibility, and such surfaces present significant metrology challenges (see Bruzzone et al. 2008; Malshe et al. 2013 and Thomas 2013). Instruments that use contrast to detect the surface (for example, FVM), require a certain degree of roughness on the surface (or other contrast mechanism), therefore, can detect out-of-aperture slope angles (Leach 2013; Hiersemenzel et al. 2012). However, such instruments cannot measure smooth surfaces and the reconstruction process is complex and prone to error (Nikolaev et al. 2016). With fringe projection systems, powder sprays are used to give the surface a matt coating to exploit the use of scattered light and hence capture information from slopes outside the aperture range, but can contribute several micrometres to the measurement uncertainty (Palousek et al. 2015).

The above methods to overcome the fundamental slope limitation either require the surface to have a specific nature (for example, to be rough on specific scales) or require a coating to be applied. However, another potential approach to extend the slope angle limitations of optical instruments is to use rigorous modelling of the optical interaction with the surface to solve the non-linear inverse problem of multiple reflection. For example, in CSI, the effects of multiple scatter would be considered a source of error (Gao et al. 2008; Lehmann and Xie 2015) and, therefore, neglected. However, multiple scattering can be considered as a mechanism that redirects into the instrument light that would otherwise fall outside the limits of the numerical aperture. Consequently, the effects of multiple scattering have the potential to reveal 3D features described by spatial frequencies that are outside of the usual bandwidth of the instrument (i.e. that would be described by simple linear imaging theory). For general 3D objects, a priori information is needed to distinguish the effects of single and multiple scattering. For the case of surfaces, however, knowledge that the scattering is due to the interface of two homogenous media can be sufficient. This method has been demonstrated as an iterative optimisation routine using finite element analysis to calculate the optical fields scattered from a silicon step (Coupland and Lobero 2009) and is illustrated in Fig. 3. Figure 3 (left) shows computed CSI fringes that clearly reveal the upper and lower horizontal surfaces of the step. From this data (the a priori), a more accurate scattering model can be implied, as shown in Fig. 3 (centre). The changes to this model necessary to explain the data in Fig. 3 (left) were then computed resulting in the higher order interferogram shown in Fig. 3 (right). The vertical wall of the step is now apparent and further iterations of the method can be applied. Such a method for measuring outside the numerical aperture limit can be used to measure a range of structures, for example, high aspect ratio holes and pillars found in MEMS devices or X-ray optics.



Fig. 3. Left: measured CSI interferogram. Centre: finite element model from CSI interferogram. Right: second-order CSI interferogram, clearly showing the vertical sidewall Coupland and Lobero 2009).

The results shown in Fig. 3 are a good illustrative example of IRM as they show many of the essential ingredients shown in Fig. 1 in an obvious manner. However, the research effort required to realise such a technique should not be underestimated. There are significant challenges in performing the measurements (mainly in optimising the contrast of the second-order and potentially higher-order fringes), for the modelling of the second-order effects (a finite element model was used in this example and we are currently working on a more time-efficient boundary element method) and in the interpretation of the (information-rich) data. There may be opportunities to use this approach with other optical systems and for rough surfaces (perhaps using low aperture measurements as the a priori data), but the rigorous models need to be developed and optimised to operate in reasonable times.

3.3 Measurement Enhancement Using Artificial Intelligence

AI promises to be one of the most disruptive technologies of the next century, but researchers are up against critics who claim that it is nothing but another hype cycle of the same old recycled technology. The main reason for the new ‘hype’ in the commercial market today is mainly the availability of ubiquitous multi-core GPU computing, which enables the low-cost training of simple AI networks at home or in small businesses. Another reason is the proliferation of low-cost and relatively powerful computing platforms (such as the Raspberry Pi which retails for well under £100) which can take advantage of trained models to perform autonomous tasks. With the advent of the Internet of Things, AI algorithms on low-cost platforms will become even more pervasive and ubiquitous in society in the near future, and manufacturing industry is trying to position itself in order to be at the forefront of AI technology.

In terms of IRM, AI can be used to take advantage of the a priori data, the measured object (even past measurements) and, in combination with a functional measurement model, accelerate the measurement procedure and make it more efficient. An example of IRM which leverages AI to perform the measurements can be found in the micro-electronics industry, where scatterometry data is used to accurately predict track resistance and, therefore, pre-empt failures in integrated circuits (Rana et al. 2015). The advantage in doing this is that silicon wafers can be discarded early in the manufacturing cycle to avoid expensive processing and testing further down the manufacturing

line, thus avoiding the time required to produce and test the wafer at the end of the process.

AI can also assist within an actual measurement system by converting the various parts of the measurement system (for example, cameras, stages, light sources) into smart ‘agents’ and thus viewing the machine as a ‘perceptive agency’, with agents working collaboratively to optimise the measurement result in terms of accuracy and coverage on a specific object (Amigoni et al. 2003). At Nottingham, we are currently developing a system to measure the 3D form of complex components (our main target industry is additive manufacturing). A fringe projection system is effectively converted into a ‘perceptive agency’ that is able to predict the source and camera positions (using inverse rendering) with respect to the measured object in real time, i.e. a frameless, self-calibrating measurement system (Stavroulakis et al. 2017a).

In fringe projection, where either the camera or projector setup can change significantly between measurements or the object needs to be tracked, self-calibration has to be carried out frequently to keep the measurements accurate. It is common to use methods developed initially for photogrammetry for the calibration of the camera(s) in the system in terms of extrinsic and intrinsic parameters. To calibrate the projector(s), an extra correspondence between a pre-calibrated camera and an image created by the projector is performed. These recalibration steps are usually time consuming and involve the measurement of calibrated patterns on planes, before the actual object can continue to be measured after a motion of a camera or projector has been introduced in the setup and hence do not facilitate fast and efficient 3D measurement of objects. By employing and combining a priori information via inverse rendering, on-board sensors (Stavroulakis et al. 2017b), deep learning and leveraging a graphics processor unit, we have developed a fine camera pose estimation method which is based on optimising the rendering of a model of a scene and the object to match the view from the camera (see Fig. 4). We have found that the success of this calibration pipeline can be greatly improved by using adequate a priori information from the aforementioned sources. The ultimate plan is to have a simple-to-use projector and camera set-up that can be

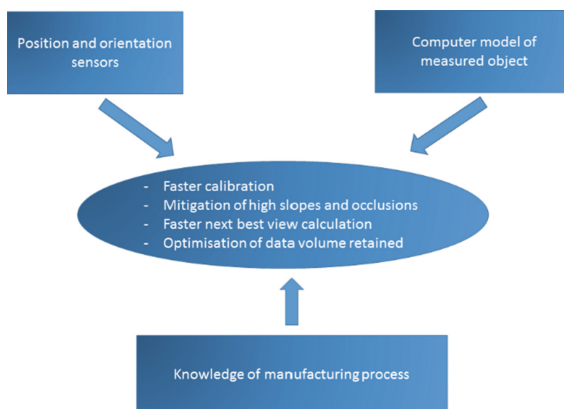


Fig. 4. A priori data used for the fringe projection system under development at Nottingham.

re-configured for different 3D object shapes and can allow for effects such as shadowing, occlusions and different textures. The complexity of the system is transferred to the AI-based software and the hardware can be cost-effective and fit-for-purpose.

4 Discussion

We are led to believe that we are currently experiencing a new industrial revolution; one that will be data-driven, agile and autonomous. One of the key ingredients in this revolution will be the need for fast, integrated metrology. However, many of the current metrology tools have hit fundamental and/or technical barriers that result in them being seen as a process overhead rather than potentially leading to innovative and commercial successes. Information-rich metrology is essentially a marriage of metrology with information technology and makes use of all the available information sources to enhance a given measurement scenario. We believe that IRM will allow many of the metrology barriers to be leap-frogged in the future and ease in integrated metrology as an essential part of any modern manufacturing process – not as an overhead, but as something that will enhance quality, enhance efficiency and ultimately, reduce costs. By making use of all the available information resources in our measurement and manufacturing processes, we can significantly enhance the way we make things.

Acknowledgements. We would like to thank EPSRC Grant No. EP/M008983/1 for supporting this work. Thanks also to all members of the Manufacturing Metrology Team at University of Nottingham who have contributed significantly in the development of IRM.

References

- Allwood, J., et al.: Manufacturing at double the speed. *Mat. Process. Technol.* **229**, 729–757 (2015)
- Amigoni, F., Brandolini, A., D’Antona, G., Ottoboni, R., Somalvico, M.: Artificial intelligence in science of measurements: from measurement instruments to perceptive agencies. *IEEE Trans. Instrum. Meas.* **52**, 716–723 (2003)
- Boreman, G.D.: *Modulation Transfer Function in Optical and Electro-Optical Systems*. SPIE Press, Bellingham (2001)
- Bruzzzone, A.A.G., Costa, H.L., Lonardo, P.M., Lucca, D.A.: Advances in engineered surfaces for functional performance. *Ann. CIRP* **57**, 750–769 (2008)
- Coupland, J.M., Lobera, J.: Measurement of steep surfaces using white light interferometry. *Strain* **4**, 69–78 (2010)
- Ekbart, P., Su, R., Leach, R.K.: High-precision lateral distortion measurement and correction in coherence scanning interferometry using an arbitrary surface. *Opt. Express* **25**, 18703–18712 (2017)
- Everton, S.K., Hirsch, M., Stavroulakis, P., Leach, R.K., Clare, A.T.: Review of in-situ monitoring and in-situ metrology for metal additive manufacturing. *Mater. Des.* **95**, 431–445 (2016)
- Fang, F.Z., Zhang, X.D., Weckenmann, A., Zhang, G.X., Evans, C.: Manufacturing and measurement of freeform optics. *Ann. CIRP* **62**, 823–846 (2013)

- Gao, F., Leach, R.K., Petzing, J., Coupland, J.M.: Surface measurement errors using commercial scanning white light interferometers. *Meas. Sci. Technol.* **19**, 015303 (2008)
- Grimm, T., Wiora, G., Witt, G.: Characterization of typical surface effects in additive manufacturing with confocal microscopy. *Surf. Topogr. Metrol. Prop.* **3**, 014001 (2015)
- Hahn, R., Krauter, J., Körner, K., Gronle, M., Osten, W.: Single-shot low coherence pointwise measuring interferometer with potential for in-line inspection. *Meas. Sci. Technol.* **28**, 025009 (2016)
- Harding, K.: *Handbook of Optical Dimensional Metrology*. Taylor & Francis, London (2013)
- Hiersemenzel, F., Petzing, J., Leach, R.K., Helml, F.S., Singh, J.: Areal texture and angle measurements of tilted surfaces using focus variation methods. In: *Proceedings of 3rd International Conference on Surface Metrology, Annecy, France*, pp. 85–89 (2012)
- Jiang, X., Wang, K., Gao, F., Muhamedsalih, H.: Fast surface measurement using wavelength scanning interferometry with compensation of environmental noise. *Appl. Opt.* **15**, 2903–2909 (2010)
- Kayser, D., Bothe, T., Osten, W.: Scaled topometry in a multisensor approach. *Opt. Eng.* **43**, 2469–2477 (2004)
- Launhardt, M., et al.: Detecting surface roughness on SLS parts with various measuring techniques. *Polym. Testing* **53**, 217–226 (2016)
- Leach, R.K.: *Optical Measurement of Surface Topography*. Springer, Berlin (2011). <https://doi.org/10.1007/978-3-642-12012-1>
- Leach, R.K., Jones, C.J., Sherlock, B., Kryszinski, A.: Metrology challenges for highly parallel micro-manufacture. In: *Proceedings of 4M, San Sebastian, Spain*, pp. 25–28 (2013)
- Leach, R.K., et al.: Open questions in surface topography measurement: a roadmap. *Surf. Topogr. Metrol. Prop.* **3**, 013001 (2014)
- Leach, R.K., Sherlock, B.: Applications of super-resolution imaging in the field of surface topography measurement. *Surf. Topogr. Metrol. Prop.* **2**, 123001 (2014)
- Lehmann, P., Xie, W.: Signal formation in depth-scanning 3D interference microscopy at high numerical apertures. In: *Proceedings of SPIE*, vol. 9660, pp. 966015–966015-12 (2015)
- Madsen, M.H., Hansen, P.-E.: Scatterometry – fast and robust measurements of nano-textured surfaces. *Surf. Topogr. Metrol. Prop.* **4**, 023003 (2016)
- Malshe, A., Rajurkar, K., Samant, A., Hansen, H.N., Bapat, S., Jiang, X.: Bio-inspired functional surfaces for advanced applications. *Ann. CIRP* **62**, 607–628 (2013)
- Mathia, T.G., Pawlus, P., Wiczorowski, M.: Recent trends in surface metrology. *Wear* **271**, 494–508 (2011)
- Nikolaev, N., Petzing, J., Coupland, J.M.: Focus variation microscope: linear theory and surface tilt sensitivity. *Appl. Opt.* **55**, 3555–3565 (2016)
- Palousek, D., Omasta, M., Koutny, D., Bednar, J., Koutecky, T., Dokoupil, F.: Effect of matte coating on 3D optical measurement accuracy. *Opt. Materials* **40**, 1–9 (2015)
- Rana, N., Zhang, Y., Wall, D., Dirahoui, B.: Predictive data analytics and machine learning enabling metrology and process control for advanced node IC fabrication. In: *IEEE Advanced Semiconductor Manufacturing Conference*, pp. 313–319 (2015)
- Sims-Waterhouse, D., Piano, S., Leach, R.K.: Verification of micro-scale photogrammetry for smooth three-dimensional object measurement. *Meas. Sci. Technol.* **28**, 055010 (2017)
- Stavroulakis, P., et al.: Combined use of a priori data for fast system self-calibration of a non-rigid multi-camera fringe projection system. In: *Proceedings of SPIE*, vol. 1033, p. 1033006-1-12 (2017a)
- Stavroulakis, P., Sims-Waterhouse, D., Piano, S., Leach, R.K.: A flexible decoupled camera and projector fringe projection system using inertial sensors. *Opt. Eng.* **56**, 104106 (2017)
- Stock, T., Seliger, G.: Opportunities of sustainable manufacturing in Industry 4.0. *Proc. CIRP* **40**, 536–541 (2016)

- Su, R., Wang, Y., Coupland, J.M., Leach, R.K.: On tilt and curvature dependent errors and the calibration of coherence scanning interferometers. *Opt. Express* **25**, 3297–3310 (2017b)
- Syam, W.P., Jianwei, W., Zhao, B., Maskery, I., Elmadih, W., Leach, R.K.: Design and analysis of strut-based lattice structures for vibration isolation. *Precis. Eng.* (2018)
- Thomas, T.R.: Roughness and function. *Surf. Topogr. Metrol. Prop.* **2**, 014001 (2013)
- Townsend, A., Senin, N., Blunt, L.A., Taylor, J., Leach, R.K.: Surface texture measurement and characterisation for additive manufacturing. *Precis. Eng.* **46**, 34–47 (2016)
- Van der Jeught, S., Dirckx, J.J.J.: Real-time structured light profilometry: a review. *Opt. Lasers Eng.* **87**, 18–31 (2016)
- Wang, J., Jiang, X., Blunt, L.A., Leach, R.K., Scott, P.J.: Intelligent sampling for the measurement of structured surfaces. *Meas. Sci. Technol.* **23**, 085006 (2012)
- Wang, J., Leach, R.K., Jiang, X.: Review of the data fusion techniques in surface metrology. *Surf. Topogr. Metrol. Prop.* **3**, 023001 (2015)
- Weckenmann, A., et al.: Multisensor data fusion in dimensional metrology. *Ann. CIRP* **58**, 701–721 (2009)
- Yu, M., Zhang, Y., Li, Y., Zhang, D.: Adaptive sampling method for the inspection planning on CMM for free-form surfaces. *Int. J. Manuf. Technol.* **67**, 1967–1975 (2012)
- Zhang, Z.H.: Review of single-shot 3D shape measurement by phase calculation-based fringe projection techniques. *Opt. Lasers Eng.* **50**, 1097–1106 (2012)
- Zuo, C., Huang, L., Zhang, M., Chen, Q., Asundi, A.: Temporal phase unwrapping algorithms for fringe projection profilometry: a comparative review. *Opt. Lasers Eng.* **85**, 84–103 (2016)



Aerospace Assembly Gap Measurement Using Low Cost Smart Tools with Machine Vision

Richard Crossley^(✉)  and Svetan Ratchev 

Centre for Aerospace Manufacturing, University of Nottingham, Advanced Manufacturing Building, Jubilee Park, Nottingham NG7 2GX, UK
richard.crossley@nottingham.ac.uk

Abstract. This paper details the conversion of mature machine vision technology from a fixed position automation line based device to a handheld technology and addresses the problems associated with maintaining a consistent camera distance and light source by using 3D printed hand tools. Specifically, the problem of gap measurement within aircraft wing assembly is used as an example application, however, the wider opportunities and functionalities associated with industry 4.0 are demonstrated and briefly discussed.

Keywords: Industry 4.0 · Smart tools · Smart factory · Machine vision
IOT · Aerospace assembly · Automation

1 Introduction

1.1 Industry 4.0 and Smart Tools

Industry 4.0, often termed the “smart factory” is defined as the next industrial revolution utilizing the latest groups of cyber-physical systems such as cloud computing, internet of things and cognitive computing [1]. It is based on a trend of increasing automation and data exchange where the physical manufacturing process is monitored analyzed and optimized with minimal engineering input.

In order for the optimization process to take place, the system must have accurate quantitative, digitized data from the process. This is often difficult to achieve in an aerospace manufacturing production environment where many tasks are performed manually using traditional hand tools or human inspection. This currently relies heavily on operators recording the value manually to a database system. This is time consuming, subjective, error prone, and provides no direct infallible record of the product.

The scientific field for machine vision inspection and associated algorithms is mature and well developed [2]. Various functions and methods for detecting features such as geometry and faces are well developed specialist subjects, for instance several papers focus specifically on edge detection functions used in this development [3–5]. Commercially available technology is also widespread and is accompanied by software support with extensive functions for the detection of a multitude of features [6]. However, such systems are typically expensive £4k – 15k, require the use of a microcomputer with significant processing power, and are intended to be permanently

positioned on a production line where conditions such as lighting and camera position remain consistent.

Hand tools with data driven functions are recently becoming more available and widely accepted. They can automatically record data about the process, such as the torque of fasteners, connect wirelessly and save process data to a central database. These tools are commonly termed “smart hand tools” as they perform some type of process data management in addition to completing the engineering task [7]. They may also be aware of the process and product context, via RFID, Bar or QR codes on components, and have the ability to adjust settings accordingly to suit the assembly component or the task at the point of use [8] (Fig. 1).

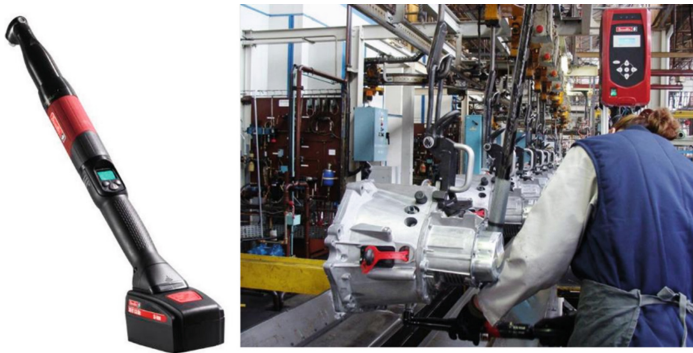


Fig. 1. An example of a “smart tool” for tightening of fasteners to controlled torque values with process data logging capability [7].

The ability to significantly reduce the cost and mobility of machine vision technology without compromising reliability would dramatically widen its application. The aim of this development determines the ability and reliability of the technology when used with the latest low-cost portable microprocessors such as MyRIO and to show that lighting conditions and camera positions can be controlled via the use of bespoke rapid prototype hand held tools to maintain the reliability of the technology. The paper also highlights how the productivity of the manual worker, when using such a handheld device, can be increased with greater integration into the factory 4.0 data network.

1.2 Hand Held Machine Vision Application; Gap Measurement in Aerospace

In aerospace assembly, the torque values of fasteners and the gaps are critical for product quality and safety and are required to be controlled and recorded. Fastener torque values can be controlled and logged via commercially available smart tools [7]. However, gap measurement is more difficult in practice. A number of devices and methods exist (Fig. 2) but each has associated high costs and limitations (Table 1). Therefore, measurements are typically taken by hand using feeler gauges and recorded manually. The process is slow and subject to human error requiring manual data input

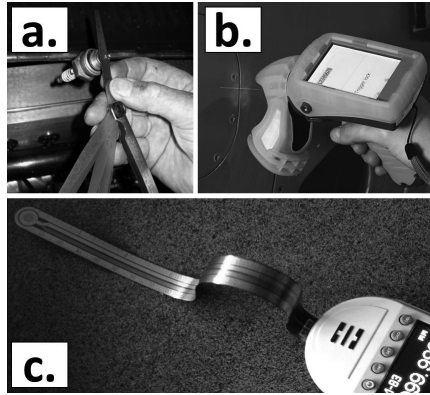


Fig. 2. Commercially available assembly gap measurement devices include: traditional feeler gauges (a), laser line gap profile scanning systems (b) and capacitive film sensor devices (c)

for industry 4.0 compliance and additional electronic proof or quality checks may be required. Additionally, none of the devices is able to capture gap closure during tightening and co-ordinate torque data with hand tools to measure the loads required to close gaps. Such data is valuable to determine assembly build stresses and fastener assembly load specifications.

Table 1. Commercially available gap measurement device types

Ref.	Type	Advantages	Disadvantages
Figure 2a	Feeler gauges	Low cost Simple	Very slow Subject to human error No electronic data Can cause surface scratches
Figure 2b	Laser gap measurement	Fast Electronic logging	High cost Can be unreliable Complicated Requires edge radius calibration
Figure 2c	Capacitor film	Fast Simple Electronic logging	Expensive (£3k approx.) Becomes trapped when gap is closed Cannot measure gaps below a certain limit

1.3 Rapid Manufacturing, Machine Vision and IOT Devices

Rapid manufacturing and 3D printing systems are now prolific with hobbyists and design engineers. The process is particularly suited for producing low volume customized components such as prosthetics [8]. It has also been used to produce hand tools

for various purposes [9]. However, the most commonly available PLA material can be brittle, soft and break easily. Therefore, it is ideally suited as a prototyping tool in the rapid development of industry 4.0 hand tools provided no significant load is experienced in use. It can also be used as a temporary prototype to perfect the design before a more rugged production model is completed. Therefore, it was selected as the most suitable method for the rapid development of smart hand tools for machine vision inspection.

Machine vision, computer vision or image-processing has been in development since the 1980s and has a number of applications within the automation industry. Typically, it is used as a quality control or sorting method where typical applications include checking label positions on consumer packaging [10]. Its use is also now common place in large robot automation cells used for finding hole centers, edges and other well defined part features. However, apart from rare specialist exceptions such as droplet measurement [11, 12], it is not currently in widespread use in hand tools. It offers great potential for handheld monitoring of processes provided the cost and size of the technology can be reduced along with simplifying the programming and deployment method.

IOT (Internet Of Things) devices are defined as a self-contained smart device or computer comprising of a micro-processor and controller with the capability to connect the internet, gather and transmit data, read physical sensors and operate switches.

A number of low cost development IOT microcomputers are now commercially available to both the hobbyist and industrialist alike, such as Arduino, Raspberry PI and Siemens IOT 2040. However, very few have machine vision capability. Raspberry PI appears to function using Open CV [13], however, it is not a native function. These low cost devices have the potential to significantly transform data acquisition and control in the production environment once they become reliable and widely available. National Instruments MyRIO supports machine vision capability, however, its cost is still relatively high in comparison to most other IOT devices and each additional device requires a software license at an additional expense, increasing the cost of deployment further. Nevertheless, it was found to be the most convenient tool with the greatest amount of customer support for the development and concept proving of self-contained programmable vision applications.

2 Research Methodology

2.1 Experimental Set-Up

The hand tool was designed to work as a self-contained casing for a commercially available low cost USB microscope. It was also required to project a high incidence light source over the measured edge to highlight the intended gap to be measured whilst eliminating as much light as possible from other sources, thus improving measurement reliability. The prototype casing also allowed the adjustment and experimentation with the camera angle. The casing was also required to be as small as possible for access within the aerospace structure. The final prototype included a clamp for the microscope wire as it was found that movement of the wire resulted in some movement of the

optical sensor inside the microscope. Figure 3 shows the latest prototype design which also included a variable resistor to adjust the intensity of the high incidence LED light source and customizable buttons with indicators for initiating a measurement and storing images. The initial device is reasonably small but has excellent potential for further miniaturization for increased measurement access.

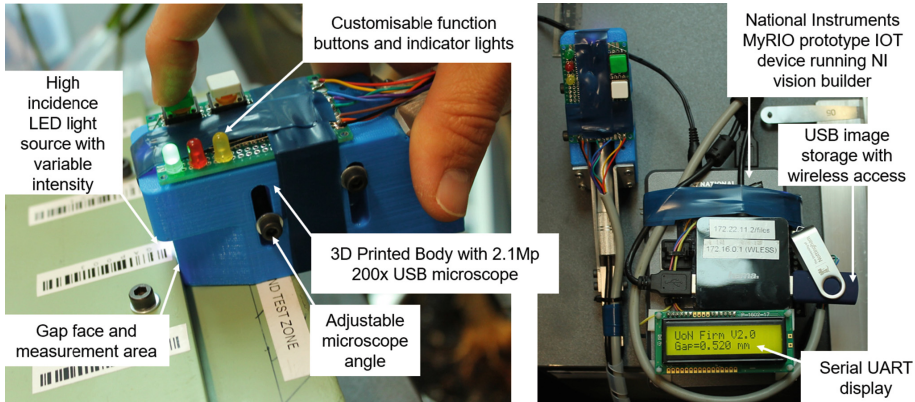


Fig. 3. Smart hand tool development prototype for optical aerospace assembly gap measurement

The National Instruments MyRIO device was chosen as the main IOT processor due its ability to be programmed via LabVIEW with predefined vision functions with relative ease. The platform also provides wireless capability and serial/digital IOs. Although the system does not support a VDU screen onboard, the image output can be monitored using any internet browser via a wireless PC, tablet or smartphone and the saved image captures can be saved directly to the attached USB for either wireless or USB connected transfer. It also supports interfaces such as UART serial LCD displays for output of symbols, text and numbers. A Maplin 16×2 Serial UART was utilized in this case to display the gap dimension, chosen for its availability and low cost.

A generic USB 2–5 Mp camera with 10–300x magnification and 30FPS sampling rate was selected for imaging device due to its very low cost and widespread availability. The high incidence light source, buttons and indicators are powered and controlled via digital and analog I/O sockets provided on the MyRIO. The microscope camera was connected to the NI MyRIO device via USB hub along with a standard USB drive for image storage.

2.2 Control Algorithms and Decision-Making Environment

An example of the overall integration of the handheld device in a factory 4.0 aerospace assembly environment is shown in Fig. 4. The component being measured and the position of the gap measurement may be obtained via laser tracker and/or QR code on the component. The Gap data can then be sent via ODBC connection to the manufacturing

bus, this value can then be cross checked for quality assurance. Once passed the data can then be archived against the part number. On failure, the relevant decision processes for rework or concession can be made facilitating an evolvable assembly systems architecture [15] similar to that demonstrated for aerospace assembly [16].

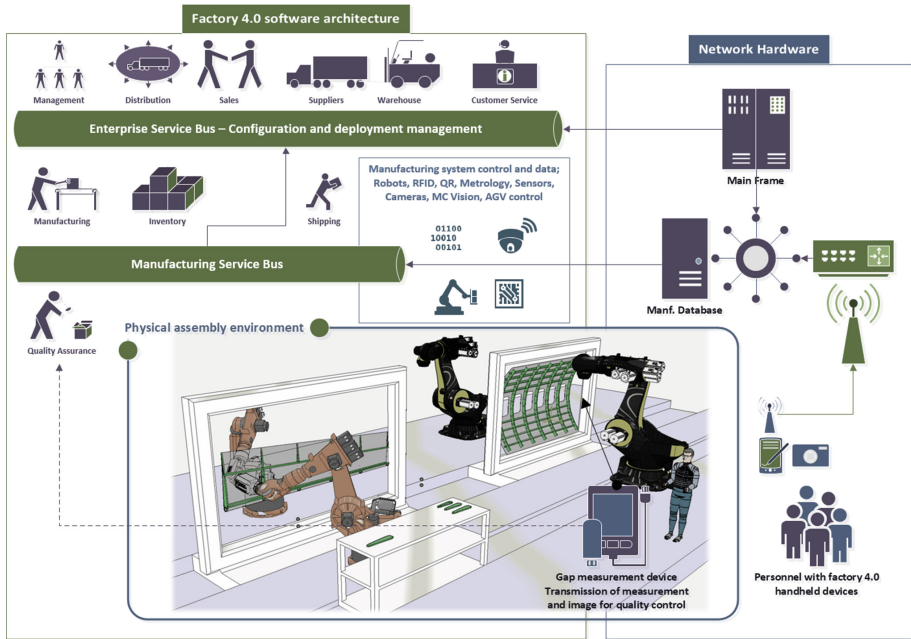


Fig. 4. Integration of the handheld machine vision device into the EAS factory 4.0 system architecture

The overall approach for decision making is demonstrated in Fig. 5. A number of processes run locally on the MyRIO device such as image acquisition, image processing, edge detection algorithms and calculations to convert pixel values to actual gap via a calibration table. Decisions on image quality and edge measurement quality of points and edge line fit are made locally with the operator notified to remeasure if an edge has not been detected with adequate certainty. Once an adequate measurement has been made the image and gap value can be passed to the manufacturing execution system (MES) via wireless connection. In order to work with the MES the location of the measurement on the assembly must be known, this could be entered manually, via a QR or bar code on the assembly or by RFID or laser tracker co-ordinates. Once the measurement location is known the MES can look up the gap requirements from the product database and ensure that the gap measured is within tolerance. If so, then the operator can be notified of a successful measurement and carry on to the next measurement point. If not, additional instructions may be issued.

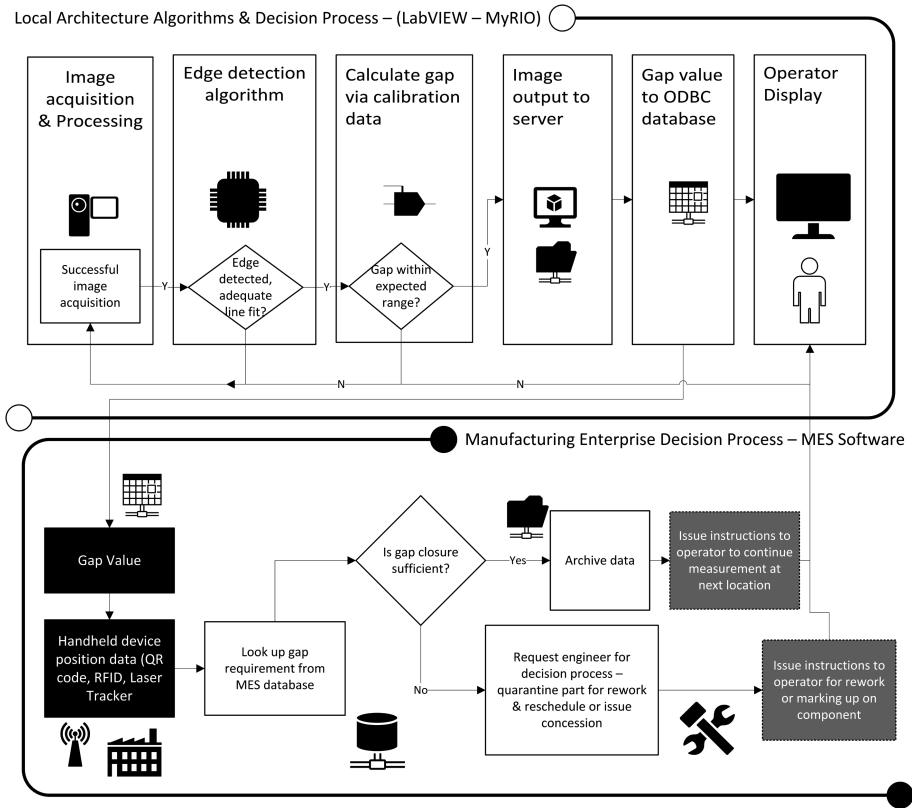


Fig. 5. Integrated control architecture

The MyRIO was programmed visually using LabVIEW functions combined with the Vision builder workbench. The program works by grabbing an image from the USB camera converting to high contrast black and white. Then a linear edge contrast recognition function was used searching from top to bottom for the top edge and bottom to top for the bottom edge to output a linear average. The pixel distance between the two averaged edges is then calculated. Values obtained from a linear fit of calibration results allows the conversion of pixel distance to the actual gap in mm. This value is obtained via a calibration procedure discussed in the results chapter.

Once the gap result is obtained it is communicated to the operator via a number of solid lit LEDs if the gap is in range. If the gap is out of range or an edge has not been detected LEDs are set to flash using digital I/O functions. The actual GAP value is also displayed on the LCD display via a UART3 LabVIEW function. Images are also saved to a selected file location and the value can also be published for reading from any Wi-Fi enabled device with an internet browser.

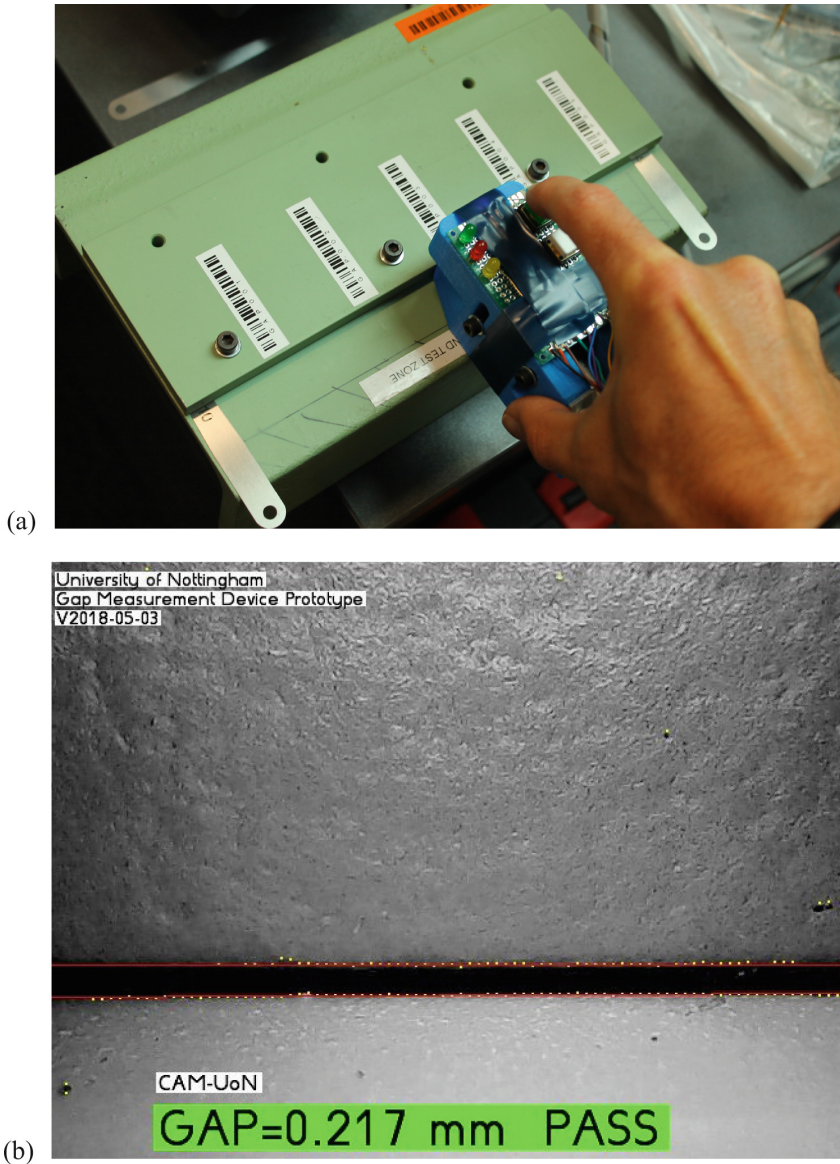


Fig. 6. Aerospace gap measurement test set up to replicate wing rib foot to cover measurement, showing handheld device and typical output image of the gap under the top plate with automatically generated text overlay of results.

3 System Implementation and Discussion of Results

3.1 Calibration and Variability

A typical aerospace gap measurement process was recreated using mild steel flat and channel section coated with typical green zinc chromate aerospace primer (Fig. 6). The gap was adjusted and measured using feeler gauges to various gap sizes between zero and 0.7 mm with five optical measurements taken at each gap using the newly developed device. Table 2 shows the results of the calibration procedure with an excellent linear fit to the results (Fig. 7) yielding the required conversion constants for converting pixel gap to mm within the LabVIEW code. An average range of 20 microns was found in the measurements with an average standard deviation of 7 microns, well within the gap measurement requirements for typical aerospace assemblies. However, a zero gap measurement did not necessarily result in a zero pixel measurement. This was due to the presence of a radius on the edge of flat bar at the top edge of the gap. A small radius on a gap edge is typical in most assembly situations. Therefore, a calibration may be necessary on each new gap measurement procedure for new parts and assemblies. Parts will also require consistent edge radius dimensions to give reliable measurements.

Table 2. Optical gap measurement calibration results

Gap	Pixel measurement					Avg	σ	Max	Min	Range (pix)	Range (mm)	σ (mm)	
0.7	49.04	49.24	48.61	48.54	49.33	48.95	0.3225	49.33	48.54	0.79	0.0154	0.0063	
0.5	38.05	38.13	37.95	38.45	38.71	38.26	0.2813	38.71	37.95	0.76	0.0148	0.0055	
0.3	28.22	28.39	28.75	27.43	28.04	28.17	0.4362	28.75	27.43	1.32	0.0258	0.0085	
0.1	19.61	19.68	19.5	18.77	18.04	19.12	0.6303	19.68	18.04	1.64	0.0320	0.0123	
0.05	15.12	15.34	15.41	15.6	15.38	15.37	0.1536	15.6	15.12	0.48	0.0094	0.0030	
0	11.65	12.24	12.13	12.94	12.76	12.34	0.4618	12.94	11.65	1.29	0.0252	0.0090	
Pixel ratio	51.23										AVG (mm):-	0.020	0.0074
Zero gap pixel	12.94										AVG (μ m):-	20.4	7.4

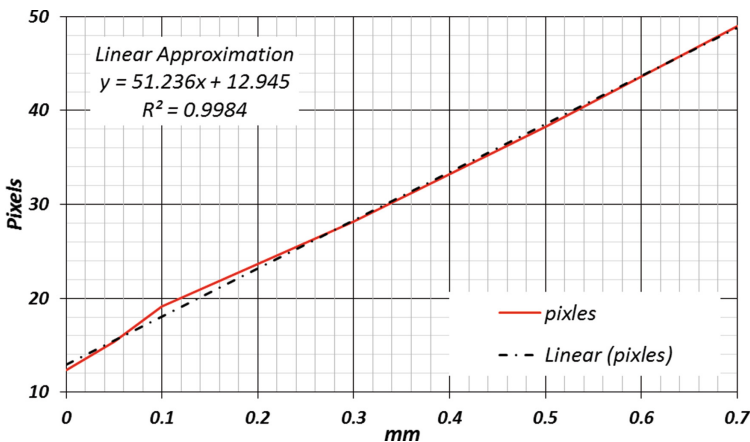


Fig. 7. Linear approximation of calibration results to give results in mm

4 Conclusions

The results show that the development of machine vision technology in a hand tool is now possible using low-cost portable microprocessors and readily available machine vision software functionality. The reliability of the technology can also be maintained by the careful design of bespoke rapid prototype tools which maintain camera position relative to the measurement workpiece, shield external light sources and provide their own consistent self-contained light source. This development widens the potential application of the technology to a large range of hand held inspection processes and could greatly improve the connectivity and productivity of labor within the assembly industry.

The device developed here specifically for microscopic optical gap measurement of wing skin to rib foot has shown great promise with a maximum 20 μm error and standard deviation of 7 μm under lab conditions. The cost of equipment is estimated at £600 plus the cost of software licensing which could be further reduced by development on an open source platform. However, the method requires refinement in the following areas before reliable workshop deployment is feasible:

- Graphical interface for the operator
- Robust procedure to account for edge radius in measurements
- Rugged housing and long life battery
- Automated procedure for networking and saving data.

References

1. Hessman, T.M.: The Dawn of the Smart Factory. <http://www.industryweek.com/technology/dawn-smart-factory>. Accessed 14 Feb 2013
2. Steger, C., et al.: Machine Vision Algorithms and Applications. Wiley, Hoboken (2017)
3. National Instruments: Image Processing with NI Vision Development Module (2016). <http://www.ni.com/white-paper/3470/en/>
4. Wang, N., Gao, X., Tao, D., Yang, H., Li, X.: Facial feature point detection: a comprehensive survey. Neurocomputing (2017)
5. Mahmoud, T., Ibrahim, M.: Efficient edge detection technique based on hidden Markov model using canny operator. Int. J. Comput. Inf. Technol. **06**(01) (2017). ISSN:2279-0764
6. <http://www.cognex.com>
7. Earls, A.: Smart Tools will Drive Efficiency in the Factory of the Future. <https://www.smartindustry.com/blog/smart-industry-connect/smart-tools-will-drive-efficiency-in-the-factory-of-the-future/>. Accessed 17 Mar 2015
8. Boria, S.: NI Website. Developing Smart Tools for the Airbus Factory of the Future. <https://www.desouttertools.com/>. Accessed 25 Oct 2017
9. Birrell, I.: The Guardian. 3D-printed prosthetic limbs: the next revolution in medicine. 19/2/2017
10. <https://www.thingiverse.com/explore/popular/3d-printing/hand-tools/page:4>
11. Atkinson, K.B.: Close Range Photogrammetry and Machine Vision. Whittles publishing, Caithness (1996)
12. <https://btglabs.com/surface-analyst/>

13. https://www.gardco.com/pages/surface_tension/pgx.cfm
14. <https://www.pyimagesearch.com/>
15. Chaplin, J.C., et al.: Evolvable assembly systems: a distributed architecture for intelligent manufacturing. *IFAC-PapersOnLine* **48**, 2065–2070 (2015)
16. Drouot, A., Irving, L., Sanderson, D., Smith, A., Ratchev, S.: A transformable manufacturing concept for low-volume aerospace assembly. *IFAC-PapersOnLine* **50**, 5712–5717 (2017). The reported research has been funded by the EPSRC grant EP/K018205/1



Towards Industry 4.0: The Future Automated Aircraft Assembly Demonstrator

Adrien Drouot¹(✉), Ran Zhao², Lucas Irving³, and Svetan Ratchev³

¹ Institut FEMTO-ST, CNRS UMR 6174, UFC – ENSMM – UTBM,
25000 Besançon, France

adrien.drouot@femto-st.fr

² College of Information and Electrical Engineering,
China Agricultural University, Beijing, China

ran.zhao@cau.edu.cn

³ Institute for Advanced Manufacturing, University of Nottingham,
Nottingham NG7 2TU, UK

{lucas.irving, svetan.ratchev}@nottingham.ac.uk

Abstract. As part of the Future Automated Aircraft Assembly Demonstrator developed by the University of Nottingham, this paper presents a new flexible production environment for the complete manufacturing of high-accuracy high-complexity low-volume aerospace products. The aim is to design a product-independent manufacturing and assembly system that can react to fluctuating product specifications and demands through self-reconfiguration. This environment features a flexible, holistic, and context-aware solution that includes automated positioning, drilling and fastening processes, and is suitable for different aircraft structures with scope to address other manufacturing domains in the future (e.g. automotive, naval and energy). The assembly cell features industrial robots for the handling of aircraft components, while intelligent metrology and control systems monitor the cell to ensure that the assembly process is safe and the target tolerances are met. These three modules are integrated into a single standardized interface, requiring only one operator to control the cell. Performance analyses have shown that, using the reconfigurable production environment described hereafter, a positioning accuracy better than ± 0.1 mm can be achieved for large airframe components.

Keywords: Intelligent and flexible manufacturing systems
Positioning systems · High accuracy · Industrial robots

1 Introduction

Over the last decade, the merging of the virtual and physical worlds and the fusion of the technical and business processes have led the way to a new industrial age known as *Industry 4.0* [5]. This has been achieved through the deployment of Cyber-Physical Systems (CPS), creating a networked world in which intelligent objects communicate and interact with each other. Therefore, CPS-based production systems, being optimized according to a global network of reconfigurable and self-organizing production units, greatly exceed classic production systems in terms of flexibility, adaptability,

autonomy, efficiency, reliability, safety, and costs. Such flexible and reconfigurable production systems will inevitably be required in the assembly stage of both military and commercial aircraft by any manufacturer who intends to remain competitive in the future.

Traditional aerospace assembly solutions see the aircraft components manually located and constrained using large monolithic steel structures called assembly fixtures or jigs. These structures are expensive to manufacture and offer little or no adjustment at all to accommodate design changes or product variants, meaning the capital investment may not be recovered. Additionally, there is no real-time indication of the structure condition and it is not uncommon for an aerospace assembly fixture to fall out of tolerance, causing assembly errors which are passed downstream. Unfortunately, it is not until the product inspection, often many processes later, that these issues are detected and identified, causing product and assembly post-processing and increasing both the cost and lead-time of the product.

Highly automated, flexible systems hence offer an alternative solution for aircraft manufacturers to shorten the product lead-time, increase the product diversity and efficiency, all the while reducing the production costs. Some ideas were suggested to materialize these smart assembly systems, e.g. Flexible Manufacturing Systems [3, 21], Reconfigurable Manufacturing Systems [16] or Holonic Manufacturing Systems [14, 23]. A relevant comparison of the latter with the concepts of bionic and fractal manufacturing systems has been performed in [22]. However, only few of these approaches were dedicated to the manufacturing of aerospace products, and they generally provided no reconfigurability properties, just as the *Lean Automation* strategy [12], or were dedicated to one main task only. Indeed, the *Automated Flexible Assembly System* [9] was a concept designed to allow a single machine cell to fasten and assemble exclusively geometrically similar aircraft parts. As for the *EcoPositioner* developed by Dürr [15], it was a modular and reconfigurable system limited to the high precision positioning process of aircraft components during the assembly.

This paper presents the University of Nottingham Evolvable Assembly Systems model and its grounding in the Future Automated Aircraft Assembly Demonstrator (FA3D), a real-world aircraft structure assembly cell. The FA3D smartly combines the industrial robots' relatively low cost and high flexibility through programming and changeable end-effectors with a high precision metrology system to reach the narrow tolerances in terms of absolute accuracy and repeatability in use in the aerospace assembly processes. This specific layout hence compresses the capabilities of a traditional assembly line into a single reconfigurable multi-purposes cell resulting in massive cost, space, and throughput improvements (see Fig. 1).

Section 2 of the paper briefly introduces the concept of Evolvable Assembly Systems, to whom the FA3D belongs. Section 3 outlines the features of the FA3D in more detail and describes how it is able to adapt itself to multiple product families and variants. Section 4 focuses on the accurate positioning of the aircraft components and how to deal with their dimension uncertainties. Finally, conclusions and work remaining to be done are discussed in Sect. 5.

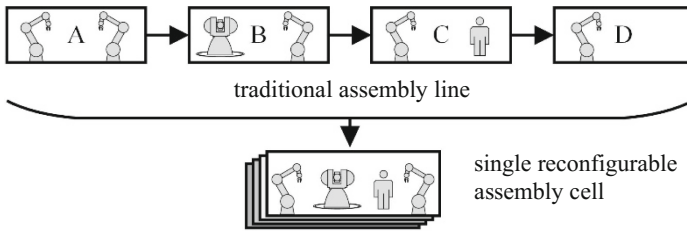


Fig. 1. Compression of an assembly line down to an assembly cell

2 Evolvable Assembly Systems

The concept of Evolvable Assembly Systems (EAS) is a novel approach to a transformable manufacturing environment enabling the production of high-complexity and high-variability products more effectively than it has previously been possible [4]. The transformability property of EAS lies in their ability to respond to any change in product, process, or market and to any disruption at all times. This is achieved through a foundation of a context-aware adaptation scheme managed by distributed agent-based control.

As shown in Fig. 2, the context-aware adaptation scheme of EAS is cyclic in nature. The phase *Operation* represents the normal execution of the processes within the manufacturing system. The configuration of the production line is settled and the resources complete their function, creating value for the business. At the same time, the phase *Monitor* is active and records information about the manufacturing system as it operates, e.g. current state and performance of the system, or operations performed on the components. Once the system has gathered enough data and identified a gap between the current and target performance or a possible improvement to be made, the *Internal adaptation* phase may be activated. A set of modifications to be done during the *Reconfiguration* phase will then be generated to mitigate or exploit the identified feature. Alternatively, the *Definition* of external pressures may be desired by the system operator, e.g. evolution of the product specifications, or changes to the capabilities of the available resources. As a response to the external stimuli, the *External adaptation* phase will produce a set of changes to be carried out during the *Reconfiguration* phase, e.g. a physical rearrangement of the resources, or an alteration to the parameters in the software. Depending on how the manufacturing system has been set up, the *Reconfiguration* phase may occur automatically or after the approval of the operator.

The core of the EAS architecture is the intelligent agent's environment. Intelligent agents are autonomous pieces of software that interact with their environment and proactively act upon defined goals [24]. They also have the interesting ability to communicate with each other and control a resource, e.g. an operator with a smart device, or manufacturing equipment ruled by a Programmable Logic Controller. Therefore, by using distributed agents as part of the management unit, intelligence and communication capabilities are distributed throughout the manufacturing system, resulting in a reliable and resilient framework. Further details on this particular, innovative architecture can be found in [4].

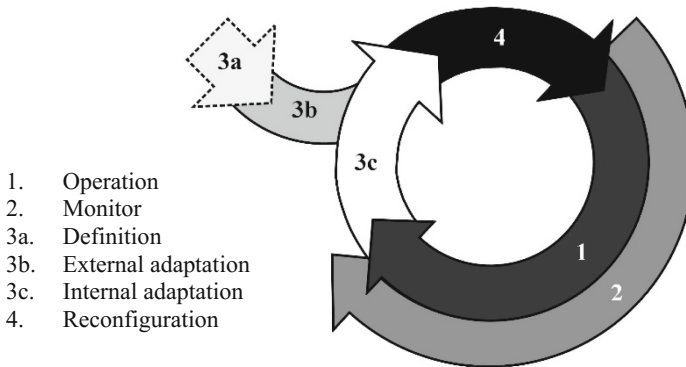


Fig. 2. The adaptation cycle of Evolvable Assembly Systems

3 EAS for Aerospace: The FA³D

The Future Automated Aircraft Assembly Demonstrator (FA3D) has been designed to allow a single cell production environment to automatically assemble a wide range of aerospace products. The objective being to replace the traditional large, dedicated, monolithic steel aerospace assembly fixtures that offer no feedback on the structure condition. To this end, it achieves the safe handling and the accurate positioning of the aircraft components and operating processes, such as drilling and fastening. Indeed, the reachable absolute accuracy and repeatability is respectively below ± 0.1 mm and ± 0.05 mm, which is suitable for the narrow tolerances imposed by aircraft manufacturers. In addition, the assembly cell is intended to be able to reconfigure from both the hardware and software perspectives, and evolve rapidly in time according to the market demand. Finally, the FA3D has an independent metrology system that inspects the structure at each step of the building process, stopping it should anything fall out of tolerance. This environment, using a smart combination of standard industrial robots, high precision metrology system and control system, offers an attractive alternative to the classical outdated under-utilized assembly lines. The reconfigurable assembly cell of the FA3D is shown in Fig. 3.

3.1 Industrial Robots and Operating End Effectors

The FA3D features three off the shelf industrial robots, each of which can be used as fixtures for the accurate positioning of aircraft components. The larger one is a KUKA KR1000 Titan, able to carry loads up to 1 000 kg, while the other two are the KUKA KR270 R2700 Ultra, controlled by a KR C4 unit. The function of the Titan is to convey the structures that cannot be held by the two smaller robots and transfer the assembly out of the cell when completed. It can also be used to support the workpiece between the two operating robots while they work on it, thereby functioning as an adaptive fixture. The additional functions of the KR270 robots are to perform the drilling and riveting processes of the aircraft components in order to complete the whole assembly. The operation to be carried out dictates to the robots the appropriate end effector to



Fig. 3. Reconfigurable assembly cell of the Future Automated Aircraft Assembly Demonstrator developed by the University of Nottingham

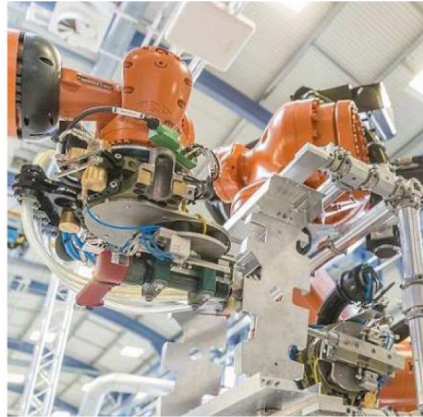
retrieve, where to find it, and specifies its target position. The use of these robots, being able to automatically swap end effectors to execute different applications, offers a level of flexibility that classical assembly methods cannot. Furthermore, it has to be noted that the two KR270 robots are fastened onto pre-drilled plates allowing them to be moved forward or backward to adapt the work envelope to the required configuration. Indeed, while the metrology and control systems remain approximately the same for any task to be done, the set up of the production environment strongly relies on the task and may need reconfiguration. Additionally, in order for the FA3D to handle a wide range of aerospace products, three sizes of bits, and therefore three sizes of rivets, are available within the assembly cell. Each end effector and each size of bits, having a different internal resistance, can be automatically identified by the robots, hence avoiding any process errors.

The drill end effector, presented in Fig. 4(a), has interchangeable countersunk drill bits depending on the size of the hole to be drilled. Those holes, ranging from 5 mm up to 8 mm, are made using a one shot process by sliding the spindle linearly towards the aircraft component. This mechanism ensures that the parallelism between the spindle axis of the drill and the normal axis of the component is preserved during the operation. Beforehand, the end effector, through its nosepiece, and its counterpart on the other KR270 robot will have come in contact with the workpiece to apply a suitable clamp load on it. Naturally, the clamp force, the spindle feeds and speeds, as well as the depth of the holes (up to 15 mm), are controlled during the process and depend on the required geometry and material properties. Swarf and dust collection and extraction is built in to the drill nosepiece end effector.

The rivet end effector, shown in Fig. 4(b), is directly connected to three rivets feeders corresponding to the three sizes of drill bit available on the drill end effector.



(a) Drill end effector



(b) Rivet end effector

Fig. 4. Drill and rivet end effectors of the FA3D

Once in position, the robot requests the delivery of a rivet from the appropriate feeder and blows it into the hole. In order to form the rivet and therefore fasten the components together, the two robots work in a synchronized way. While the first robot slides slightly over to align the air hammer with the head of the rivet, the second robot brings the rivet forming end effector against the back of the assembly. Controlled forming pressure is then applied by both end effectors using pneumatic cylinders and the first robot runs the air hammer for the required time, which is also controlled.

3.2 Metrology Systems

In order for the positioning, drilling, and fastening operations to be effective, the end effector must reach the process location accurately and repeatably. Yet, off the shelf industrial robots are affected by inherent errors [20] and cannot achieve the absolute accuracy nor repeatability required by aircraft manufacturers unaided. Internal sources of errors in robotic manipulators include the manufacturing tolerances of its linkages, the stiffness of its segments and joints, the presence of backlash in its gears, the inability of its controller to compute and achieve the correct joints value... External sources of errors are usually changes to the working environment such as temperature and humidity fluctuations [8, 17].

A first solution to mitigate these errors is to characterize theoretically and/or experimentally some of these flaws and compensate for them in the control algorithm. Hence, the effects of the manufacturing tolerances of the robot arms, the backlash, and the drivetrain nonlinearities on the end effector position were investigated in [1]. A methodology to identify and compensate for the joints stiffness of serial robots, directly responsible for the displacements of the end effector, was suggested in [6], and later in [18]. A systematic procedure for the elastodynamic modeling of robotic manipulators in order to neutralize the nonlinearities that affect them has been

developed in [19]. As for the effects of temperature variation, they were investigated in [7], which also proposed a method to cancel them out by inverse calibration.

A second solution, requiring no calibration nor calculation and coping with all the aforementioned errors at once, is to use a high precision metrology system to automatically correct the positioning of the robots in real-time. The metrology technology that is used in the assembly cell is the Adaptive Robot Control (ARC) solution, provided by Nikon. The main element of this measurement system is the K-CMM camera, an optical device made up of three CCD¹ cameras triangulating the position and the orientation of multiple LEDs at the same time (see Fig. 5). Hence, by attaching LEDs to the workpiece and to the end effectors, ARC provides an accurate relative position of the end effectors in the workpiece coordinate system. Furthermore, if a target position is specified, the difference between the measured and target positions, i.e. the position error, is determined and automatically corrected for by the robots if it exceeds a defined tolerance. This tolerance is chosen by the operator according to assembly tolerance specification and can be lowered down to values below ± 0.1 mm. This solution, relying on optical measurement, is therefore completely independent of the flawed kinematic chain of the robotic manipulators. Besides, the K-CMM camera can be moved around to overcome line of sight issues and still be able to accurately measure data providing that the LEDs are visible. This feature is of paramount importance for the reconfigurability and the adaptability of the production environment.



Fig. 5. K-CMM camera of the FA³D

A second, and independent, metrology system available within the FA3D is a laser radar MV331, also provided by Nikon (see Fig. 6). This equipment offers automated and accurate non-contact measurement capability for large-scale geometry applications. This technology is well suited for the FA3D operations as it can take accurate measurements from novel materials such as carbon fiber following inspection plans generated offline using CAD. While the K-CMM camera are used to measure and correct the positioning of the industrial robots, the function of the laser radar is to inspect the aircraft assembly while it is being built. It is then possible to detect, and fix, any manufacturing irregularities at each step of the process, hence greatly reducing the

¹ Charge Coupled Device.

number of defects in the final structure as well as the amount of rework required. As the MV331 does not require any target for its measurements, it can be moved around within the cell, locate itself, and still be able to provide reliable data about the assembly. A report outlining the measurements and the deviation from nominal can also be generated upon request. An excerpt of this report is shown in Fig. 7, where the CAD model of the assembly has been blurred for obvious confidentiality reasons.



Fig. 6. Nikon laser radar MV331 in the FA³D

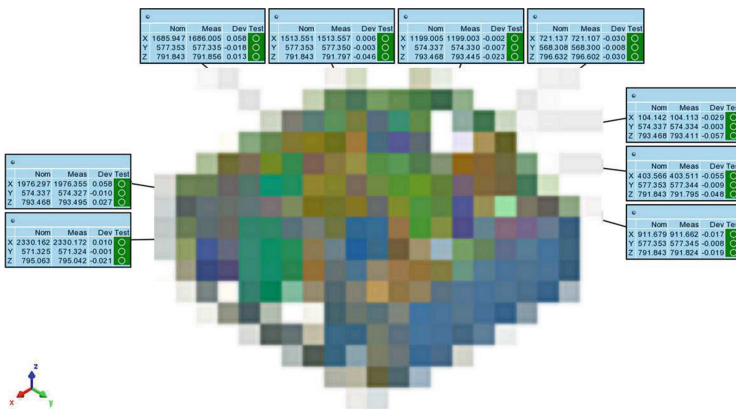


Fig. 7. A typical instance of the report generated by the laser radar in the FA³D

3.3 Safety

As the safety of the personnel on the workshop floor is imperative, the industrial robots and the metrology systems are located inside a guarded area monitored by four S3000 laser scanners from Sick. These compact systems, by scanning their surroundings, are the assembly cell primary interlock, whose function is to stop all machinery within the guarded area if anyone steps inside. If the beam is interrupted, the laser scanners communicate the information to the PLC, which will send the signal to the robot controllers to safely stop and inhibit any motive power to the robots. The PLC will also isolate the pneumatic power to the cell so that the end effectors do not fall off the manipulators to harm any personnel or damage any equipment. Some specific zones explicitly marked as safe can however be configured into the Sick system for operator access to encourage human machine collaboration. In addition to the safety scanners, the fence of the FA3D has two cable pull switches, each one having a steel wire rope connected to latching pull switches. Pulling on the rope in any direction and at any point along its length will trip the switch to cut off the machine power.

3.4 Communication

The communication between the laser scanners and the PLC is done over the PROFI-safe network, so is the communication among the PLC, the spindle slide servo drive and the spindle inverter drive. Indeed, the servo and inverter control units are each fitted with an Ethernet IP communication card, enabling the use of PROFI-safe. Each of these cards has two Ethernet ports and therefore can be connected in a ring topology using a standard Ethernet switch. In addition, as all the wiring for the PROFI-safe ring is inside the control panel, there is little chance of the cables getting damaged, therefore redundancy is not required. With that architecture, the management system, through the Ethernet communication, can control the spindle feeds and speeds, depending on the material to be drilled. Still using the Ethernet communication, the management system also controls each of the robots by sending specific commands, each with its own parameters structure, defining the operations to be carried out. Those commands, and all the associated data, is passed to the PLC which then forwards on the relevant commands to the robot controllers. Finally, the communication between the robots and the positioning metrology system is performed over Ethernet, the ARC metrology technology being called on by the robot program.

3.5 Radio-Frequency Identification

The FA³D is equipped with a Radio-Frequency Identification (RFID) system which performs two functions. Firstly, because the end effectors and components are tagged, the system has the ability to detect and 3D track them within the cell. This way, the system is able to send an alert to the operator if an end effector or a component required for the build is missing, or in the wrong location. Secondly, the RFID tag on each of the aerospace component contains relevant information pertaining to its condition, e.g. part number, issue number, operations to be performed, or inspection data. Once a sub-assembly is finished, it is also RFID tagged with the addition of process data, i.e.

constituent parts, non-conformities, and concessions. This then accompanies the sub-assembly throughout the whole assembly process, contributing to the entire product DNA. This also aids the inspection and verification procedures, as well as the airworthiness certification and maintenance course of actions. Furthermore, all the data stored within the RFID tags can be retrieved and shared among the resources of the manufacturing environment, contributing to the *Big Data* of the *Industry 4.0*.

4 Positioning Technology

The assembly process of an aircraft structure can be summarized to some extent as aligning the structural components with each other, checking they are correctly positioned, and fastening them together. The high-precision positioning of the components and end effectors, e.g. for drilling, riveting and sealant applying operations, hence represents the essential task during the whole assembly process. This section focuses on how the FA3D metrology systems guarantee a positioning accuracy better than ± 0.1 mm despite the errors inherent to the 6-axis industrial manipulators.

4.1 Preliminary Work

Before the positioning process begins, a coordinate system must be defined in the production environment, as well as on each end effector to be used. This is achieved by manually probing specific geometric features such as holes, lines, and planes, selecting the correct orientation of the coordinate system's axes, and choosing the location of its origin. Great care should be given to the probing step as it determines the exactitude, and therefore the effectiveness of the positioning process. Having in mind the fact that the probing stage has to be performed only once (before the first use of each end effector), spending extra time and effort to achieve a better accuracy is always worthwhile. Furthermore, in order to simplify the programming of the robots, the origin of the environment and end effectors' coordinate systems should match the one of the CAD files. Indeed, with such approach, all the information in the CAD files can function as location targets for the robotic manipulators and the metrology systems.

The next step is to attach multiple infrared LEDs to the production environment and to the end effectors, and relate them to the coordinate systems. During the positioning process, all the LEDs will be tracked and triangulated by the K-CMM camera, hence providing an accurate relative position and orientation of the end effectors in the environment coordinate system. The main issue to be addressed in this stage is to make sure that occlusion of one or more LEDs never occur when the robots are moving and interacting with the environment. As it will be explained in the next section, the ARC technology is only used at the very end of the positioning process when the end effectors are close to their final position. Hence, the option that was used was to bring the robots in the exact same state as the one in which they would be just before the call to the Nikon metrology solution, and visually investigate the most appropriate locations for the LEDs. Appropriate locations are such that the LEDs are 3D spread all around the manufacturing environment and the end effectors, hence maximizing the covered volume and therefore the positioning accuracy. Also, as distance decreases significantly

the accuracy of the measurement, the position of the K-CMM camera must be as close as possible to the working area. But to be able to detect all the infrared LEDs at the same time, the K-CMM camera has to be placed further away from the working area as the field of view increases with distance. Therefore, a difficult trade-off between distance of the K-CMM camera and accuracy of its measurement has to be found. A different option, more time consuming but more effective, would be to model the production environment with a CAD software and determine the optimal LED placement by algorithm.

4.2 Positioning Process

Considering the assembly of aircraft components delivered to CAD nominal specifications, the positioning process, as sketched in Fig. 8, can be structured as follows:

1. Pick up the component at specific jiggling holes located on it. In order to guarantee high holding, pull-in, and locking forces, the FA3D uses the zero-point clamping system from AMF.
2. Drive the industrial robots from the current position to a well-chosen close neighborhood of the target position defined by the CAD data (see {1} in Fig. 8). Indeed, in case of overshoot from the robotic manipulators, aiming at the exact target position may damage the component. The generation of the motion path is out of scope of this paper but some examples are described in [2] and [13].
3. Drive the industrial robots, now controlled by the ARC technology and the K-CMM camera, to the CAD target position and let the system operate until the desired tolerance is achieved (see {2} in Fig. 8). As the neighborhood of the target position is well chosen in the previous step, there is absolutely no risk of collision when the robots automatically adjust their position during the iterative process.
4. Inspect the assembly with the MV331 laser radar to make sure the location reached by the component suits the CAD data and all key characteristics have been achieved (see {3} in Fig. 8).

4.3 Addressed Issues

In practice, aerospace components are manufactured according to their own tolerance and rarely have zero deviation from nominal, meaning that the CAD target position may not be the best position for the components. Indeed, these inherent manufacturing uncertainties may be the cause for the component to collide with the assembly, or for theoretically matching holes to end up misaligned. In that case, a measuring step, performed by the MV331 laser radar, is added before the final move to improve the robustness of the demonstrator. Some points specifically located on the components as well as their corresponding points on the assembly are recorded, and the application of the algorithm developed by [10] and enhanced by [11] provides the best fitting rigid transformation, i.e. the new target position, that best aligns the two sets of points. In any case, an absolute accuracy and repeatability below ± 0.1 mm can be achieved by the industrial robots in the FA3D, as shown in Fig. 9. This figure displays the results of a repeatability test in which a robot, driven by the ARC technology, brings a

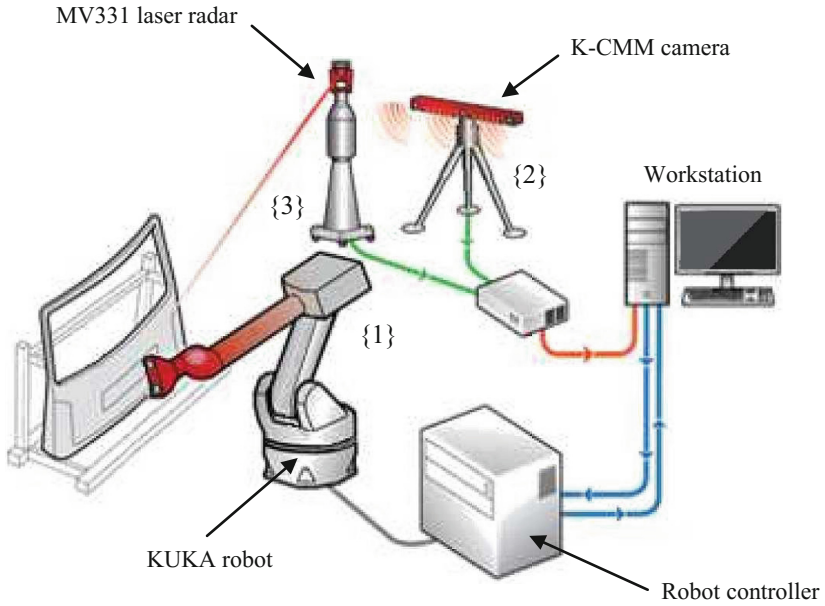


Fig. 8. Diagram of the FA3D positioning system

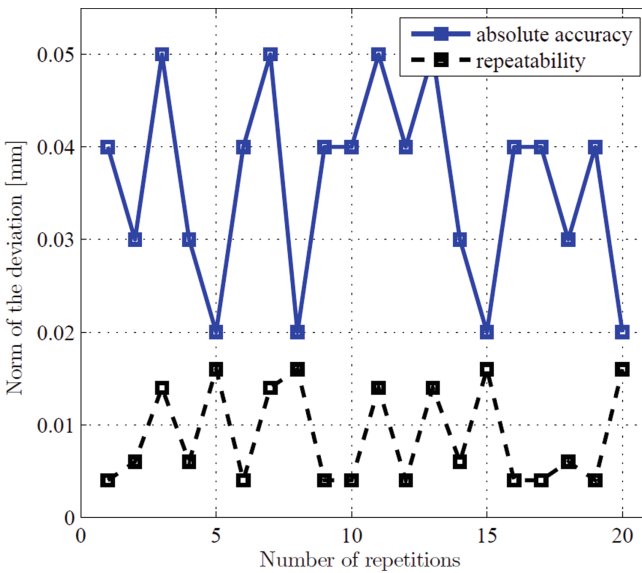


Fig. 9. Absolute accuracy and repeatability performance of the FA³D positioning system for a 2400 × 800 mm aircraft component

2400 × 800 mm aircraft component to a specific target position. It has to be noted that the initial position and orientation of the component are different at each time, proving that the positioning accuracy is independent from the direction of the move.

5 Conclusion

This paper briefly introduced the concept of Evolvable Assembly Systems (EAS), a novel approach to a manufacturing environment that is able to respond rapidly to changes in product, process, and market. A real world application of such a concept was presented through the Future Automated Aircraft Assembly Demonstrator, a single cell production environment able to automatically assemble a wide range of aerospace products. It has been shown that this system offers the adaptability and reconfigurability required to face the increasing pressure to manufacture more specialized and efficient products, often with shorter lifecycles, at a relatively reduced cost.

The research perspectives inherent to this system are multiple to improve its efficiency. For instance, it is well known in the aircraft industry that some of the most important functions associated with manufacturing, inspection and maintenance are conducted in confined spaces. Maintaining the same level of performance in such confined spaces represents a real challenge for the FA3D as the TCP would not be visible to the camera. Also, currently run independently, the laser radar could be integrated into the cell control system for automated confirmation of assembly completion and automated permission or ban to proceed with the next step. In addition, by communicating information to each other, the industrial robots could also work in collaboration for specific operations such as rotation of assemblies for fuselage inspection, hence enhancing the capability of the FA3D. Likewise, depending on past assemblies and their corresponding inspection reports, the system could generate by itself the operational planning in order to optimize the assembly process.

References

1. Ahmad, S.: Analysis of robot drive train errors, their static effects, and their compensations. *IEEE J. Robot. Autom.* **4**(2), 117–128 (1988)
2. Biagiotti, L., Melchiorri, C.: *Trajectory Planning for Automatic Machines and Robots*. Springer, Heidelberg (2008). <https://doi.org/10.1007/978-3-540-85629-0>
3. Browne, J., Dubois, D., Rathmill, K., Sethi, S.P., Stecke, K.E.: Classification of flexible manufacturing systems. *FMS Mag.* **2**, 114–117 (1984)
4. Chaplin, J.C., et al.: Evolvable assembly systems: a distributed architecture for intelligent manufacturing. *IFAC-PapersOnLine* **48**(3), 2065–2070 (2015). Proceedings of the 15th IFAC Symposium on Information Control in Manufacturing, Ottawa, Canada
5. Drath, R., Horch, A.: Industrie 4.0: hit or hype? *IEEE Ind. Electron. Mag.* **8**(2), 56–58 (2014)
6. Dumas, C., Caro, S., Chérif, M., Garnier, S., Furet, B.: A methodology for joint stiffness identification of serial robots. In: Proceedings of the IEEE-RSJ International Conference on Intelligent Robots and Systems, Taipei, Taiwan, pp. 464–469 (2010)

7. Gong, C., Yuan, J., Ni, J.: Nongeometric error identification and compensation for robotic system by inverse calibration. *Int. J. Mach. Tools Manuf.* **40**(14), 2119–2137 (2000)
8. Greenway, B.: Robot accuracy. *Ind. Robot: Int. J.* **27**(4), 257–265 (2000)
9. Inman, J., Carbrey, B., Calawa, R., Hartmann, J., Hempstead, B., Assadi, M.: A flexible development system for automated aircraft assembly. SAE Technical Paper 961878 (1996)
10. Kabsch, W.: A solution for the best rotation to relate two sets of vectors. *Acta Cryst.* **A32**, 922–923 (1976)
11. Kabsch, W.: A Discussion of the Solution for the Best Rotation to Relate Two Sets of Vectors. *Acta Cryst.* **A34**, 827–828 (1978)
12. Kihlman, H., Ossbahr, G., Engström, M., Anderson, J.: Low-cost automation for aircraft assembly. SAE Technical Paper 2004-01-2830 (2004)
13. Kröger, T.: *On-Line Trajectory Generation in Robotic Systems*. Springer, Heidelberg (2010). <https://doi.org/10.1007/978-3-642-05175-3>
14. Leitão, P., Restivo, F.: ADACOR: a holonic architecture for agile and adaptive manufacturing control. *Comput. Ind.* **57**(2), 121–130 (2006)
15. Meffert, G., Mbarek, T., Biyiklioglu, N.: High precision positioning system for aircraft structural. In: *Proceedings of the 15th International Conference on Experimental Mechanics*, Porto, Portugal (2012)
16. Mehrabi, M.G., Ulsoy, A.G., Koren, Y.: Reconfigurable manufacturing systems: key to future manufacturing. *J. Intell. Manuf.* **11**(4), 403–419 (2000)
17. Mooring, B.W., Roth, Z.S., Driels, M.R.: *Fundamentals of Manipulator Calibration*. Wiley, Hoboken (1991)
18. Olabi, A., Damak, M., Béarée, R., Gibaru, O., Leleu, S.: Improving the accuracy of industrial robots by offline compensation of joints errors. In: *Proceedings of the IEEE International Conference on Industrial Technology*, Kos, Greece (2012)
19. Rognant, M., Courteille, E., Maurine, P.: A systematic procedure for the elastodynamic modeling and identification of robot manipulators. *IEEE Trans. Robot.* **26**(6), 1085–1093 (2010)
20. Sciavicco, L., Siciliano, B.: *Modelling and Control of Robot Manipulators*. Springer, London (2000). <https://doi.org/10.1007/978-1-4471-0449-0>
21. Sethi, A.K., Sethi, S.P.: Flexibility in manufacturing: a survey. *Int. J. Flex. Manuf. Syst.* **2**(4), 289–328 (1990)
22. Tharumarajah, A.: Comparison of the bionic, fractal and holonic manufacturing system concepts. *Int. J. Comput. Integr. Manuf.* **9**(3), 217–226 (1996)
23. Van Brussel, H., Wyns, J., Valckenaers, P., Bongaerts, L., Peeters, P.: Reference architecture for holonic manufacturing systems: PROSA. *Comput. Ind.* **37**(3), 255–274 (1998)
24. Wooldridge, M., Jennings, N.R.: Agent theories, architectures, and languages: a survey. In: Wooldridge, M.J., Jennings, N.R. (eds.) *ATAL 1994*. LNCS (LNAI), vol. 890, pp. 1–39. Springer, Heidelberg (1995). https://doi.org/10.1007/3-540-58855-8_1



Does Industry 4.0 Pose a Challenge for the SME Machine Builder? A Case Study and Reflection of Readiness for a UK SME

Mark Jones^(✉), Leszek Zarzycki, and Gavin Murray

TQC Ltd, Nottingham, UK
mark.jones@tqc.co.uk

Abstract. TQC is a special purpose machinery builder. We became aware of the Industry 4.0 concepts and decided to investigate whether we were already pre-prepared for what has been termed the fourth industrial revolution, or whether there were new concepts and practices that our company should adopt.

This paper shows the process through which we evaluated the aspects related to the Industry 4.0 definitions. We dissected the various core concepts and then expanded the process to cover the nine pillars on which Industry 4.0 is built. We assessed ourselves against each significant element to see if we understood the concepts and requirements. We asked if these aspects were relevant to our business, we assessed whether our experience and actions to date covered the core of each element. We also looked at the challenges Industry 4.0 poses for the future of our business.

This paper is a review of the process and it presents our findings.

Keywords: Industry 4.0 · SME · Case study

1 Introduction

The continuing drive for improvements in industrial productivity combined with the technological advances in IT systems are driving manufacturing industries through what has been termed the fourth stage of the industrial revolution known as Industry 4.0. This paper reviews the technological advancement from a personal view of a UK SME, TQC Ltd, matching personal and company experience against the requirements of Industry 4.0 and asking “are we ready?”

It is acknowledged that since TQC Ltd supplies special purpose manufacturing and test machinery into large volume producers, our perspective on Industry 4.0 is influenced by the demands of our client base. It is our client base that drives TQC into addressing the challenges of Industry 4.0 as an early adopter within the SME sector.

TQC’s understanding of Industry 4.0 was first challenged by a request to give an SME perspective to a local workshop on the subject early in 2017. This meant that we had to research the definitions and the concepts behind Industry 4.0. We knew of the term but had no detailed understanding of the depth to which this terminology had been developed; this is perhaps a telling observation. As we researched the subject, it became apparent that although we were not familiar with the definitions, many

elements of Industry 4.0 had long since been adopted by our clients, and our machines had for many years incorporated some of the aspects that characterise Industry 4.0.

TQC therefore embarked upon an exercise to fully understand Industry 4.0. This started by:

- researching the definition of Industry 4.0, this led us to
- a review of the *nine pillars* of Industry 4.0, then
- assessing the challenges to implementation of Industry 4.0 and finally
- a review of the *6 Cs* related to big data

2 Assessment of the Definition of Industry 4.0

How has Industry 4.0 been defined? As a non-academic organisation the first port of call is Wikipedia, which asserts “Industry 4.0 is a name given to the current trend of increasing automation and data exchange in manufacturing technologies. It includes cyber-physical systems, the Internet of things, cloud computing and cognitive computing” As TQC has been a beneficiary of several funded research projects with Nottingham University and others in topics such as Evolvable Systems and Smart Factories, this definition of Industry 4.0 had a familiar resonance.

Industry 4.0 is portrayed as the beginning of the fourth industrial revolution (Fig. 1).

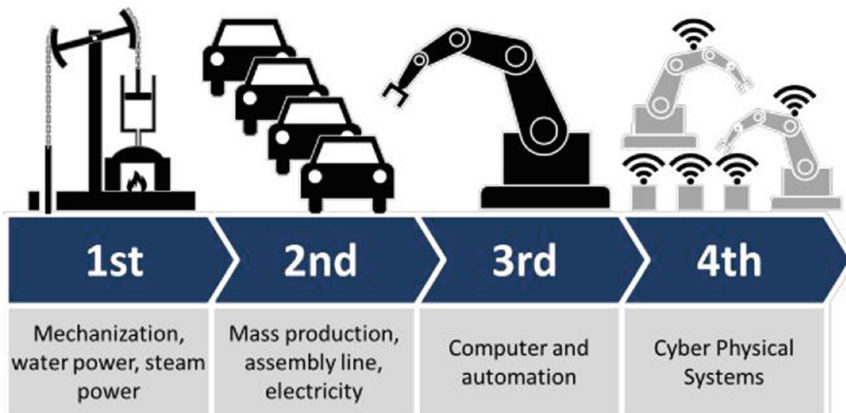


Fig. 1. The path to Industry 4.0 (Roser 2017)

Deeper investigation uncovered that there seems to be no agreed definition of the term Industrie 4.0 first coined in Germany. The origins of Industry 4.0, alternative definitions and a critique of the Wikipedia definition as “*What Industry 4.0 is not*” can be found in i-Scoop. (i-Scoop 2016) (<https://www.i-scoop.eu/industry-4-0/>). Nevertheless, the definitions concur that Industry 4.0 is the convergence of many of the technologies underpinning the smart factory.

There appear to be four basic design principles in Industry 4.0. (Hermann et al. 2016). These principles support the identification and implementation of Industry 4.0 scenarios. These can be listed as follows:

- Interoperability: machines, devices, sensors and people that connect and communicate with one another.
- Information transparency: the systems create a virtual copy of the physical world through sensor data in order to contextualize information.
- Technical assistance: both the ability of the systems to support humans in making decisions and solving problems *and* the ability to assist humans with tasks that are too difficult or unsafe for humans.
- Decentralized decisions: the ability of cyber-physical systems to make simple decisions on their own and become as autonomous as possible.

The above has been further divided into the Nine Pillars of Technological Advancement. (Rüßmann et al. 2015). TQC used this definition to further evaluate the differing aspects of Industry 4.0 in detail (Fig. 2).

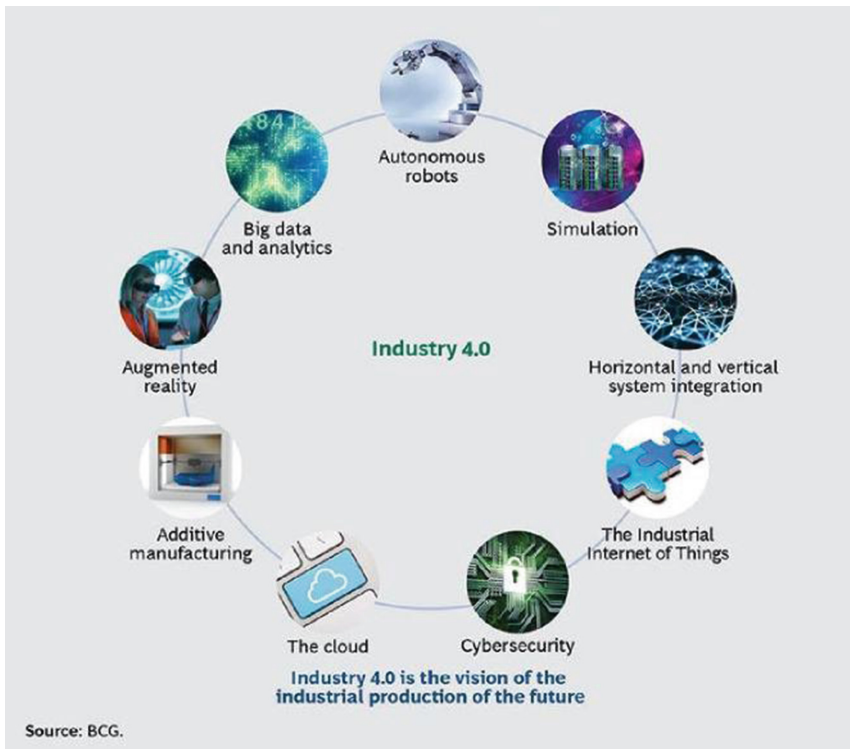


Fig. 2. The nine pillars of Industry 4.0 (Rüßmann et al. 2015)

3 Assessment of TQC Capability Against the Nine Pillars

3.1 Big Data and Analytics

The advancement in control systems in recent years has driven a number of key aspects for machine control and data acquisition. The relative low cost of large amounts of memory is allowing much more production information to be stored. This is further enhanced by the ever-increasing speed of processors reducing the control scan time and therefore allowing high transient rate signals to be stored and processed. So, the ability to create big data and then process it has driven the need for better analytical tools for data mining and to produce meaningful decision-making capabilities.

An example of a recent project engineered by TQC is a high-speed machine to perform a high-quality leak test on a medical device. The device is plastic, the technique for leak testing is helium mass spectrometry and the transient nature of the signal received by the instrument recorded the permeation of the plastic to helium. The challenge was to differentiate between permeation of helium and small level of leakage (Fig. 3).

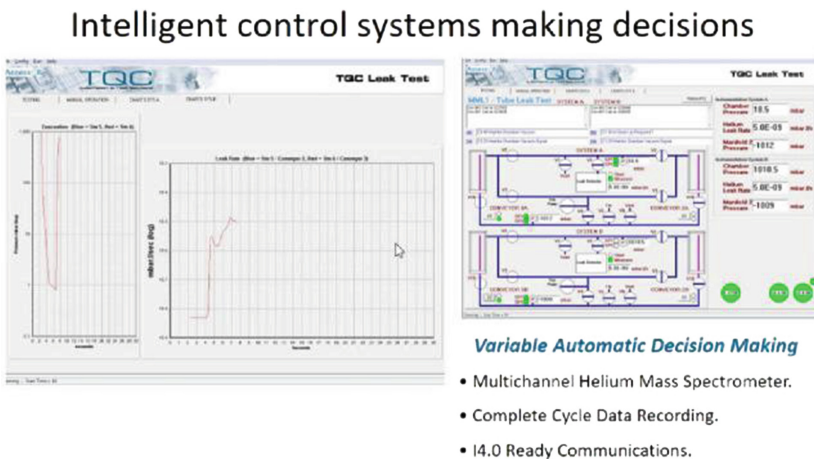


Fig. 3. Pages showing the high speed transient and the combination of machine status

In order to build in the decision making into their control system, TQC had to collect many sets of test data and from them identify the characteristics for permeation and leak. The data analysis tools used were spreadsheets, graphs and brains. Is this Big Data? Probably not. But it does involve the collection of a volume of data in real time leading to its rapid analysis at the machine level and the autonomous decision process described above.

Many in manufacturing may believe that they have always been collecting and analysing process and production data, and that Big Data is a marketing buzz word. (Littlefield 2015) However, this is a limited view in contrast with the concept that Big

Data requires advanced analytical methods to gain insights from structured and unstructured data sets garnered from a variety of sources, such as internal, customer, supplier and machine data (Littlefield 2015).

If the published benefits of Big Data are to be believed then, there are clearly opportunities for TQC to use data analytics to support maintenance and after-sales services, and to uncover insights into its own business. The former is dependent, however, on having the agreement of the client to process their data. Additionally, TQC would need in-house training on data analytics in order to understand its complexity and potential benefits to the company.

A further assessment of TQC with regard to big data is given in Sect. 5.

3.2 Autonomous Robots

There is no doubt that industry is adopting the use of more robotics in automated systems. The cost of sophisticated robots has decreased and the appearance of newly packaged low-cost motive elements known as “electric cylinders” that work like pneumatic cylinders but which are servo position programmable means that simple robotic elements are now commonplace. The integration of these technology modules is allowing more repeatable consistent control of processes, systems that do not tire and providing a lower cost compared to the employment of an operative. More complex



Fig. 4. Image of co-operating robot system for processing stockings

systems are also possible where robots can co-operate with other robots and safely cooperate with humans.

Approximately 10 years ago, TQC supplied a high-speed system whereby two cooperating robots shared a gluing station and a UV curing station for the production of stay up stockings. Both robots had to use common areas for the gluing and curing, with operators positioning the highly flexible and dimensionally inconsistent parts “the stockings” onto mandrels, where the operator ensured that the line where the glue was placed was aligned. Each robot knew where the other was and would not enter a space occupied by the other robot (Fig. 4).

3.3 Simulation

3D CAD has been used for many years for the production of drawings and assemblies, and TQC has for the past 8 years been using this for the production of our machine systems. Active mechanisms can be simulated within such packages and properties such as mass, tolerances and inertia, estimated before manufacture of parts. Simulation of motion control components like servo systems is now common place to aid system design and component selection.

TQC has also been involved in several EU Part Funded projects notably E-Race, EUPASS and PRIME all of which were focused on improving the production process through the use requirements capture, flexible and reconfigurable architecture and the development of new technology modules.

As a direct result of the EUPASS project, TQC was able to produce a robot manipulation system capable of manufacturing Wills Rings. Wills Rings are metal O-Rings for static face-sealing applications that give reliable performance over a large temperature range for gases and liquids. The system was capable of manufacturing a

Automation systems with connected data structures

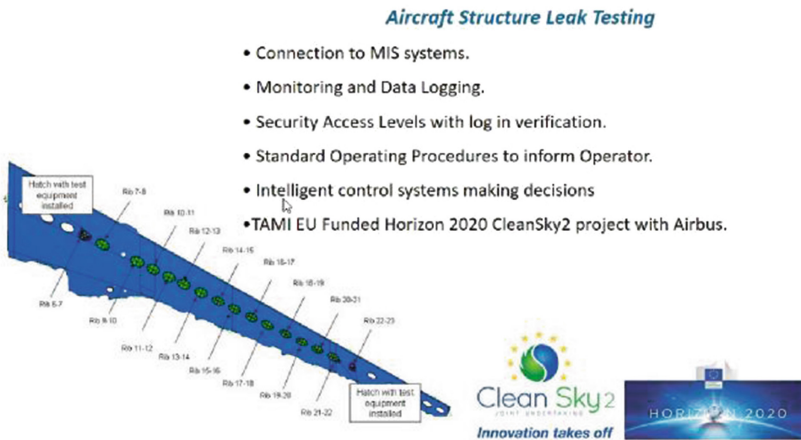


Fig. 5. Automation system with connected data structures

wide range of diameters and configuring itself to a different size at the push of a button, based on an operator recipe selection.

In addition, the images from the project below show an aerospace application engineered by TQC whereby the 3D CAD drawings were used to lead the operator through the standard operating procedure (SOP) (Fig. 5).

3.4 Horizontal and Vertical IT System Integration

Companies, departments, functions, and capabilities will become much more cohesive, as cross-company, universal data-integration networks evolve and enable truly automated value chains.

In recent years, the need to transfer data to the machine to configure the assembly process, and from the machine to convey checks and test parameters that define that the assembly process was correct, plus additional information about the exact measurements taken to address tolerance drift and tool wear has increased. Initially, TQC was just asked to time and date stamp correct and incorrect parts and assemblies. This was easily achieved by having a simple structure for the storage and backup of the data, usually.csv files. More recently, TQC has been asked to engineer machines that communicate directly with SQL type databases on our client's systems, storing both measurements and machine vision images.

It is recognized that these are only small steps in horizontal systems integration. Measures leading towards vertical integration are perhaps exemplified in Sect. 3.7 (The Cloud).

3.5 The Industrial Internet of Things

The internet has developed into a system where local and remote connectivity is common. There are now many technology modules for automated assembly that are internet ready. Most of the recent machine systems currently engineered by TQC have multichannel Ethernet hubs with the configuration, interrogation and communication of data being bi-directional.

As an example, TQC as an expert in Leak Testing has developed, with the aid of a UK Innovate Smart Grant, a new leak test instrument that is truly an Internet of Things device. The unit shown below has the ability to connect intermittently for dynamic configuration or be permanently connected for real time transfer of leak test parameters and results. Additionally, the unit has a simple communication protocol that can be used with fixture controllers that clamp, seal and then release an item that is being tested. This has been an interesting exercise and was completed before we knew what Industry 4.0 meant. The unit is Industry 4.0 ready (Fig. 6).

TQC developed technology modules ready for I4.0.



Micro Application Leak Tester

- Developed with an Innovate UK Smart Award.
- Monitoring and Data Logging.
- Ethernet Connectivity Built in.
- User Interface from PC, Tablet or smart phone.
- Built in Fixture Control.



Fig. 6. TQC leak tester module ready for Industry 4.0

3.6 Cybersecurity

Cyber security includes controlling physical access to the hardware, as well as protecting against harm that may come via network access, data and code injection.

Recent projects completed by TQC, specifically in the Aerospace, Medical device, Nuclear and Military sectors, have requested double PC firewalls and the provision of malware programs to protect the integrity of the control systems for automation from unwanted access and attack.

Indeed, one of our clients had a malware attack from the Wannacry virus. It stopped all production because of poor security by the underlying operating system.

Of course, the integration of machines into a company's data network requires careful planning of the infrastructure. Segregation of machine networks and IT networks is common place and advantageous in controlling access and security of machine systems.

3.7 The Cloud

To date, TQC has not been asked to use Cloud structures for production equipment. However, for some clients we are integrating high level PLC controllers that have embedded software for storage of data in SQL type databases. TQC knows that it is just a matter of time before this will become common place and extend to Cloud storage and associated functionality.

To prepare ourselves for Cloud based data structures and to improve our own Manufacturing Execution Systems (MES), TQC has embarked on transferring our 1980s DOS based internal management information systems onto Cloud based data structures. The project is part funded by an EU RDF Grant Funded Project within the Nottingham/Derby Local Enterprise Partnership as part of the regional Digital Growth Programme. The migration of our existing resource recording system to the Cloud has



Fig. 8. An example of 3D printed parts used as fixture nests in a TQC machine

3.9 Augmented Reality

This is the one of the nine pillars that we have yet to use in a commercial assembly environment. This is probably because TQC predominantly supplies test and assembly systems into volume producers. We see more of a use for this technology in low volume technically complex products both for assembly and for maintenance purposes. Nevertheless, augmented reality toolkits are readily available and TQC envisages the day when a client requests an AR application to complement machine maintenance and operation.

3.10 Summary of 9 Pillars Assessment

According to Freudenberg IT (2014) (in Sommer 2015). “The values concerning the important foundation pillars of Industry 4.0 like for example machine data collection, plant data collection, the connection of MES (=Manufacturing Execution System) to commercial systems as well as automatic production processes have all increased significantly”. TQC concurs with this statement, we are finding an increased number of requests to use more expensive and sophisticated control systems capable of processing the large amounts of data within the machine and to produce the data for MES systems.

4 The Challenges in Implementation of Industry 4.0

The challenges in implementation of Industry 4.0 are already well documented according to Lavanya B et al.:

1. “IT security issues, which are greatly aggravated by the inherent need to open up those previously closed production shops

2. Reliability and stability needed for critical machine-to-machine communication (M2M), including very short and stable latency times
3. Need to maintain the integrity of production processes
4. Need to avoid any IT snags, as those would cause expensive production outages
5. Need to protect industrial know how (contained also in the control files for the industrial automation gear)
6. Lack of adequate skill-sets to expedite the march towards fourth industrial revolution
7. Threat of redundancy of the corporate IT department
8. General reluctance to change by stakeholders
9. Loss of many jobs to automatic processes and IT-controlled processes, especially for lower educated parts of society” (Lavanya et al. 2017).

TQC has come across all these issues as we progress to produce machines currently being specified by our clients with various aspects of Industry 4.0 embedded into the systems.

The first two elements (1–2) listed above are developing as technology follows the requirements set by industrial standards and obliges an organization to follow continuous review and updating. The following three elements (3–5) mostly relate to cybersecurity which one should have under continuous review and reassessment. It requires that the automation system provider ensures that the relevant protection is installed, monitored, reviewed and updated these elements should be covered.

The lack of adequate skill sets and the reluctance to change are continuous challenges for the SME; it is important to nurture an environment that is open to new ideas, new technology and to change. The last element (9) is something to which one should be sympathetic and ensure that there is a corporate responsibility to continuous education, training and development.

5 An Assessment Related to Big Data

How big is big data? Clearly the data TQC is being asked to collect is more voluminous than in the past. The lowering cost of memory and increased transfer speed is making the collection of large amounts of data from quantitative sensor systems possible and so we collect more because we can! But does the quantity of data that machine system builders are likely to collect need to be addressed as big data? Some sources are indicating that big data is above 1 TB. In most of the machines and production lines we are asked to build it would take over 50 years for the system to collect that much data; so, are big data techniques really relevant to the machine or system builder?

TQC’s view is that knowledge of big data techniques including data mining, aggregation and analysis will become more important in the future and many of the techniques developed for handling very big data will be relevant for smaller data quantities. We must also have an appreciation of these techniques to be able to present machine data in portable formats, probably incorporating semantic information. Whereas in the past a simple table/matrix structure with column and row headers was acceptable, SQL type data structures may require each cell/field of data to also have a

tag associated with it to allow a more free-flowing data structure and one that can be data mined more easily. TQC is currently looking at projects where this type of data storage will be used by us for the first time.

5.1 The 6Cs of Data Analytics

According to Lee et al. (Lee et al. 2015) big data analytics consists of 6Cs in the integrated Industry 4.0 and cyber physical systems environment. TQC's assessment against each of these criteria is as follows:

1. **Connection (sensor and networks).** TQC's capability to engineer complex machine systems with a full set of connections to sensors through direct digital or analogue I/O or bus systems to either PC or PLC architectures at machine level is well developed having over 30 years' experience of instrumentation and data acquisition. The connection of PC or PLC systems through either Ethernet, WIFI or serial communications platforms has been performed as the technology has become available.
2. **Cloud (computing and data on demand).** TQC's exposure to Cloud based systems is a recent feature; it is certain that Cloud based technology will become an important aspect of our machine design in the future. To prepare ourselves for Cloud based systems, TQC has embarked on its own 'little' Big Data project by transferring our management information systems to the Cloud and to then attempt to extrapolate this data to improve the efficiency with which we are able to engineer special machines.
3. **Cyber (model & memory).** Increasingly, we are being asked to engineer extensive interconnected systems and provide a remote model of the system for production monitoring, servicing or maintenance. Complex models of aircraft wings have been recently adapted for use in guiding operators to do complex tasks. Sophisticated models of complete production lines have been duplicated to provide real-time data for use in monitoring and production planning. Web enabled camera systems have also been used on installed production systems for open monitoring of the status of production systems.
4. **Content/context (meaning and correlation).** It is clear that we must not provide Industry 4.0 systems just because we can, there needs to be a match between the commercial need and the provision of the tailored systems capable of exploiting the new technologies and understanding of what can be achieved to improve efficiency and profitability.
5. **Community (sharing & collaboration).** Open sharing has been arranged by negotiation to allow access to machine status and video streams into large multi-image screens showing working production. Some clients are more open than others, and some departments within companies are more open than others. Threats to the existing status quo are perceived and need careful negotiation.
6. **Customization (personalization and value).** Many of the systems that the special purpose manufacturer is asked to supply whereby an order for a specific realisation of a product, for example "Mr. Smith's right-hand drive sports car, red with parking sensors", is sent to the manufacturing/assembly machine for scheduling into the

sequence of assembly on the car line has been in existence for over 15 years. There has also been a need within the pharmaceutical and medical device industry under the direction of the US FDA for traceability of the circumstances of manufacture for individual and batch items.

According to Rübmann (2015) “Analytics based on large data sets have emerged only recently in the manufacturing world, where it optimizes production quality, saves energy, and improves equipment service. In an Industry 4.0 context, the collection and comprehensive evaluation of data from many different sources—production equipment and systems as well as enterprise- and customer-management systems—will become standard to support real-time decision making.” (Rübmann 2015) TQC believes that providing the full range of capabilities to all machine systems will not be necessary; having the capability to pick and mix to provide the optimum set of enhancements is the key to commercial success.

6 The Pressures on Manufacturing System Suppliers and Specifiers

As the technology in system components increases and as further possibilities for data streams develop, the system supplier will need to keep pace with the demands that these developments place on data management within machine, system, production line and its connection to the wider data environment.

This will require significant investment in IT resources: hardware, software and the software engineers who will be responsible for implementing systems that have Industry 4.0 requirements. TQC are already seeing many requests for increased data storage, the inclusion of video and screen information saved as images, and the requests for SQL type data structures. Despite the request for the additional data to be stored, when our clients are asked “what are you going to do with the data?” the response is often unclear.

There is a need for the specifiers of data structures within our client companies to also understand where their data requirements currently stand and plan forward for potential requirements in the future. The most cost-effective way to implement large data capture is to build the machine with this in place at the start. It is possible to retrofit the infrastructure but sometimes this requires a complete rebuild of the control system. Machines that we supply now will most probably be in production for many years to come, so when considering a new system or machine an in-depth assessment of these requirements needs to be performed before the fixed and firm price for the machine system is agreed.

You have all of this data; so, what do you do with it? The advancement of the use of big data algorithms and data mining in e-commerce, search engines and similar systems means that many tools are available if the system user knows what they want to achieve. The ultimate goals are more uptime, greater efficiency and lower labour costs to squeeze more out of what is available. It is important therefore to have a wider view of the process and the optimisation the client wants to achieve. This requires

people within our client organisations who have the correct skill set (a mixture of production know-how and IT skills) to be able to take advantage of Industry 4.0.

7 Conclusion

Our conclusion from the above assessment is that TQC is already dealing with many of the attributes covered by the Industry 4.0 definitions and the associated analyses published within recent papers on the subject that have expanded the Industry 4.0 concepts and drivers. This process was already in place before we knew of Industry 4.0.

Having undergone our company research into the topic and assessed the elements in detail we believe that we are now better prepared to address the challenges that may arise in the future.

References

- Brettel, M., Friederichsen, N., Keller, M., Rosenberg, M.: How virtualization, decentralization and network building change the manufacturing landscape: an Industry 4.0 Perspective. *Int. J. Mech. Aerosp. Ind. Mechatron. Manuf. Eng.* **8**(1), 37–44 (2014). <https://waset.org/publications/9997144/how-virtualization-decentralization-and-network-building-change-the-manufacturing-landscape-an-industry-4-0-perspective>
- Gorecky, D., Schmitt, M., Loskyll, M., Zühlke, D.: Human-machine-interaction in the Industry 4.0 era. In: *Conference Proceedings of 12th IEEE International Conference on Industrial Informatics (INDIN)*, pp. 289–294 (2014)
- Hermann, M., Pentek, T., Otto, B.: Design principles for Industrie 4.0 scenarios. In: *49th Hawaii International Conference on System Sciences (HICSS)*, pp. 3928–3937 (2016)
- i-SCOOP: Industry 4.0: the fourth industrial revolution – guide to Industrie 4.0 (2016). <https://www.i-scoop.eu/industry-4-0/>
- Kolberg, D., Zühlke, D.: Lean automation enabled by Industry 4.0 technologies. *IFAC-PapersOnLine* **48**(3), 1870–1875 (2015). www.sciencedirect.com/journal/ifac-papersonline/vol/48/issue/3
- Lavanya, B., Shylaja, B.S., Santhosh, M.S.: Industry 4.0 – the fourth industrial revolution. *Int. J. Sci. Eng. Technol. Res.* **6**(6), 2278–7798 (2017)
- Lee, J., Bagheri, B., Kao, H.: A cyber-physical systems architecture for Industry 4.0-based manufacturing systems. *Manuf. Lett.* **3**, 18–23 (2015)
- Littlefield, M.: What is big data analytics in manufacturing? LNS Research. <http://blog.lnsresearch.com/what-is-big-data-analytics-in-manufacturing>. Accessed 18 May 2015
- Roser, C.: Industry 4.0 – what works, what doesn't. All About Lean. <https://www.allaboutlean.com/industry-4-0-potentials/>. Accessed 3 Oct 2017
- Rußmann, M., et al.: Industry 4.0: the future of productivity and growth in manufacturing industries. https://www.bcgperspectives.com/content/articles/engineered_products_project_business_industry_40_future_productivity_growth_manufacturing_industries. Accessed 9 Apr 2015
- Schmitt, R., Dietrich, F., Dröder, K.: Big data methods for precision assembly. *Procedia CIRP* **44**(6), 91–96 (2016)

- Sommer, L.: Industrial revolution - Industry 4.0: are German manufacturing SMEs the first victims of this revolution? *J. Ind. Eng. Manag.* **8**, 1512–1532 (2015)
- Weyer, S., Schmitt, M., Ohmer, M., Gorecky, D.: Towards Industry 4.0 - standardization as the crucial challenge for highly modular, multi-vendor production systems. *IFAC-PapersOnLine* **48**(3), 579–584 (2015). <http://www.sciencedirect.com/journal/ifac-papersonline/vol/48/issue/3>
- Wittenberg, C.: Human-CPS interaction - requirements and human-machine interaction methods for the Industry 4.0. *IFAC-PapersOnLine* **49**(19), 420–425 (2016). <http://www.sciencedirect.com/journal/ifac-papersonline/vol/49/issue/19>

Gripping and Handling Solutions in Assembly



Sliding Mode Impedance Controlled Smart Fingered Microgripper for Automated Grasp and Release Tasks at the Microscale

Bilal Komati^(✉), Cédric Clévy, and Philippe Lutz

FEMTO-ST Institute, Univ. Bourgogne Franche-Comté, CNRS, 24 Rue Savary,
25000 Besançon, France

Bilal.komati@gmail.com, cclevy@femto-st.fr

Abstract. The grasp and release of objects have been widely studied in robotics. At the microscale, this problem becomes more difficult due to the microscale specificities which are notably manifested by the high dynamics of microsystems, their small inertia, their fragility, the predominance of surface forces and the high complexity of integrating adapted sensors.

In this paper, the problem of the grasp/release task is considered at the microscale. A new nonlinear controller design based on Sliding Mode Impedance Control (SMIC) is proposed to automate the grasp/release of the micropart. The proposed controller controls dexterously the dynamic interaction between the microgripper and the micropart and forces the system to follow the desired dynamic relation (impedance). To perform the grasp/release task, a new smart-fingered-microgripper is designed. The microgripper is composed of an active finger with integrated force sensor and a passive finger.

The grasp/release of a micropart of size $50 \mu\text{m} \times 350 \mu\text{m} \times 2 \text{mm}$ is tested in experiments using the control scheme and the developed microgripper. The microgripper design and the control scheme tested show their effectiveness for the grasp/release at the microscale.

Keywords: Sliding mode impedance control · Microassembly
Guiding task · Smart microgripper · Piezoelectric actuator · Force sensor

1 Introduction

The use of robotic microassembly has increased in recent years due to the development of complex microsystems and the need for microassembly to develop more complex 3D microsystems [1, 2]. Moreover, the microassembly enables the integration of heterogeneous components issued from incompatible microfabrication processes.

The scaling effect has a strong influence because it exhibits, at the microscale, many problems that are not faced at the macroscale. The microscale specificities could be briefly summarized by the high dynamics of microsystems, their small inertia, their fragility, the predominance of surface forces and the necessity and complexity to integrate sensors notably to measure contact forces that have predominant effects and high signal to noise ratio sensors [3]. These facts increase the complexity of the manipulation especially when the interactions forces are not measured; thus, the

importance of integrating force sensors into the microgripper to measure the interaction forces with high bandwidth.

The integration of force sensors into microgrippers has given rise to several works [4–11]. Most of the works present monolithic fabricated microgrippers composed of an active finger and a force sensing finger. However, in these grippers, the actuated finger is independent from the force sensing finger and in this case the contact could not be detected between the actuated finger and the micropart, leading to the loss of the micropart and consequently an unsuccessful grasp of the micropart. Moreover, in the releasing task, the control of surface forces cannot be mastered because the measure of force is not done on the same actuated finger. For this reason, it is interesting to integrate the force sensor inside the same active finger of the microgripper. In this paper, a microgripper composed of a piezoelectric based active finger with an integrated piezoresistive force sensor and a passive finger is presented. The use of the piezoelectric actuator and piezoresistive force sensor enables not only having very small resolution for the actuation and force sensing but also having very high bandwidth for both actuation and control.

Another issue which can be faced in microassembly is the need for high dynamics in the control of interaction between the microgripper and the micropart to perform a stable grasp/release of the micropart. Impedance control presented by Hogan [12] has shown its significance at the macroscale to control the interaction between the robot and the environment and has been proven to have a good advantage for microscale applications in [13, 14]. However, the main limitations of impedance control is the force tracking capability and the ability to follow the desired impedance despite robot dynamics and parameter uncertainties. Some works have proposed performing parameter estimation in order to perform force tracking [15] and others proposed combining sliding mode control [16] with impedance control to force the system to follow the desired impedance of the system [17, 18]. Thus, the main contribution of this paper is the use of Sliding Mode Impedance Control (SMIC) with online parameter estimation technique in order to guarantee both the force tracking and the desired impedance of the system.

The paper is organized as follows. Section 2 presents the microgripper design. Section 3 develops the model of the microgripper. Section 4 presents the impedance control with force tracking scheme. Section 5 presents the experimental setup used and the experimental investigations performed for the automated grasping task. Section 6 concludes the paper.

2 Microgripper Design

The microgripper is made of two fingers. One is called a *smart finger* composed of a piezoelectric actuator and piezoresistive force sensor. The second is a passive finger. The piezoelectric actuator presented in [4] is used. The piezoresistive force sensor has been presented in [19]. The fabrication of the complete gripper consists of assembling the force sensor on the tip of the piezoelectric actuator. Special care should be taken to perform the mechanical fixation of the actuator and the force sensor while separating the electrical signals. The dimensions, actuation and sensing ranges and resolutions will

be detailed in Sect. 6. A scheme of the microgripper is shown in Fig. 1. The rigid part shown in Fig. 1 is used to help the integration of the force sensor into the microgripper and to facilitate the realization of the whole microgripper. In the proposed microgripper, the smart finger deforms until entering in contact with the micropart first, and then the micropart, pushed by the first finger, enters in contact with the second finger. Two models need to be developed for the microgripper in the cases of free motion (non-contact) and constrained motion (contact).

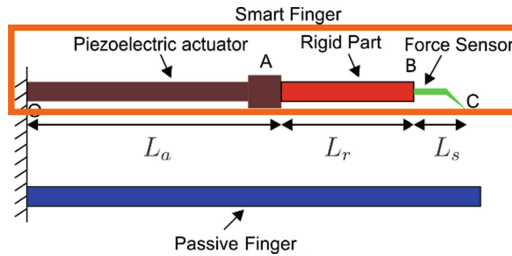


Fig. 1. Complete gripper scheme which is composed of two fingers: smart finger composed of a piezoelectric actuator with a piezoresistive force sensor; and passive finger.

3 Microgripper Model

In this section, the complete voltage/force/displacement model of the gripper is developed. The model is used to determine the control law and to estimate the position of the grippers end-effector.

3.1 Model of the Passive Finger and of the Microcomponent

The passive finger of the gripper is modeled as a mass-spring-damper system. The microcomponent to be manipulated is supposed to be rigid in the direction of the gripping and then it could be modeled as a mass. When a microcomponent is handled, the gripping force applied on the microcomponent by the gripper's smart finger, F_g , is given by the following:

$$F_g = m_p \ddot{y} + b_p (\dot{y} - \dot{y}_p) + k_p (y - y_p) \quad (1)$$

where b_p and k_p represents respectively the damping coefficient and the stiffness of the passive finger of the microgripper. m_p is the mass of the microcomponent and of the passive finger ($m_p = m_{p_1} + m_{p_2}$) where m_{p_1} and m_{p_2} are respectively the mass of the passive finger and of the micropart. y is the current position of the microcomponent and y_p is the position of the microcomponent just at contact (*i.e.* $f_g = 0$ if $y < y_p$).

3.2 Model of the Smart Finger

The smart finger of the microgripper is composed of a piezoelectric actuator (between points O and A in Fig. 1) where an end-effector is fixed on the actuator’s tip A. The end-effector is composed of a rigid silicon part (between points A and B in Fig. 1) and a piezoresistive force sensor (between points B and C in Fig. 1). The setup and details of the actuator and force sensor are presented in Sect. 5. The force sensor measures the force applied at the tip C. The sequence of the grasping task is shown in Fig. 2.

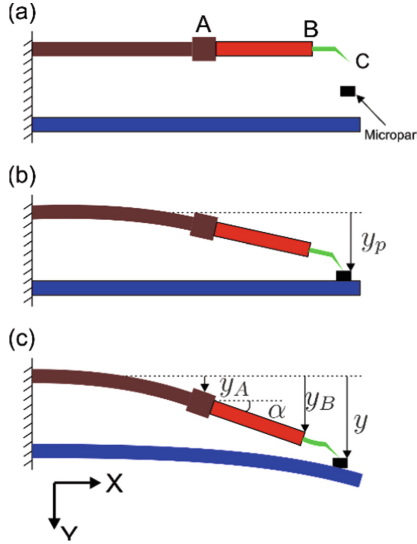


Fig. 2. Sequence of the microgripper during grasping: (a) without any applied voltage to the smart finger and no contact, (b) just at contact ($F = 0$) and (c) contact with $F \neq 0$.

The force sensor (between points B and C in Fig. 1) is modeled as a lever system with length L_s (between points B and D of Fig. 3) with mass-spring-damper system (between points D and C of Fig. 3). Then the complete scheme of the grasping task is shown in Fig. 3.

The complete model of the smart finger is developed in [20] but will be briefly summarized in this section. The model of the piezoelectric actuator is developed using existing models in literature [21–23] as follows:

$$\begin{cases} y_A(s) = \left[d_p U - s_p F_A - \frac{3}{2L_a} s_p M_A \right] D(s) - \Gamma(s, U) \\ \alpha_A(s) = \left[\frac{2}{L_a} d_p U - \frac{3}{2L_a} s_p F_A - \frac{3}{L_a^2} s_p M_A \right] D(s) - \frac{2}{L_a} \Gamma(s, U) \end{cases} \quad (2)$$

where s is the Laplace variable, y_A is the displacement of the actuator tip A and α_A is the angle at the actuator tip A, d_p is the piezoelectric constant, s_p is the elastic constant (it is the inverse of the stiffness), L_a is the length of the actuator, U is the applied voltage, $D(s)$ is a linear transfer function which models the dynamics of the actuator

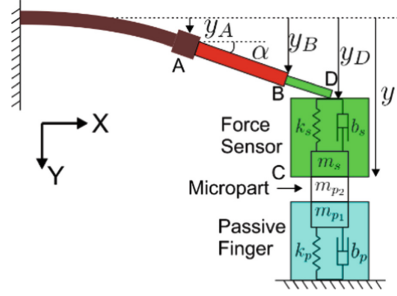


Fig. 3. Equivalent scheme of the complete gripper handling a microcomponent where the force sensor and the passive finger are modeled as mass-spring-damper systems.

with a static gain of 1 ($D(0) = 1$) and $\Gamma(U, s)$ is an operator to represent the rate-dependent hysteresis of the actuator if we neglect the creep of the actuator.

As developed in [20], the rate-dependent hysteresis of the piezoelectric actuator can be modeled as a static hysteresis followed by the dynamics of the piezoelectric actuator, $D(s)$, as follows:

$$\Gamma(u, s) = H_s(U) \cdot D(s) \quad (3)$$

where $H_s(U)$ is a static hysteresis which does not depend on the dynamics of the actuator. It can be modeled, according to [20, 23], by the Bouc-Wen method in the time domain as follows:

$$\dot{H}_s(U) = \lambda \dot{U} + \beta |\dot{U}| H_s(U) - \gamma \dot{U} |H_s(U)| \quad (4)$$

where λ is a parameter which determines the amplitude of the hysteresis and β and γ are parameters which determine the shape of the hysteresis.

According to literature, a piezoelectric actuator can be modeled as a mass-spring-damper system with an active part that is a second order transfer function and is sufficient to model the dynamics of the actuator [20]. The transfer function $D(s)$ can be written as follows:

$$D(s) = \frac{1}{as^2 + bs + 1} \quad (5)$$

In our work the force is not applied at the actuator tip A but at the force sensor C as shown in Fig. 2. A force applied on the force sensor tip C induces a reaction force and moment at the actuator tip A defined as follows:

$$\begin{cases} F_A = -F_s + m_s \ddot{y}_C = F_g + m_s \ddot{y}_C \\ M_A = -LF_s = LF_g \end{cases} \quad (6)$$

where F_g is the gripping force applied by the gripper's finger on the micropart ($F_g = -F_s$), $L = L_r + L_s$ is the length of the complete end-effector (rigid part + force

sensor), m_s is the mass of the force sensor and y_C is the displacement of the force sensor tip C.

Replacing (6) in (2), the following can be deduced:

$$\begin{cases} y_A(s) = \left[d_p U - H_s(U) - \left(1 + \frac{3L}{2L_a} \right) s_p F_g - m_s s_p s^2 y_C \right] D(s) \\ \alpha_A(s) = \left[\frac{2}{L_a} (d_p U - H_s(U)) - \left(\frac{3}{2L_a} + \frac{3L}{L_a^2} \right) s_p F_g - \frac{3}{2L_a} m_s s_p s^2 y_C \right] D(s) \end{cases} \quad (7)$$

The displacement at point D is given as follows:

$$y_D = y_A + L \sin \alpha_A \quad (8)$$

As the force sensor is modeled as a spring-mass-damper system, the force measured by the force sensor, F_s , is given as follows:

$$F_s = -F_g = m_s \ddot{y} + b_s (\dot{y} - \dot{y}_D) + k_s (y - y_D) \quad (9)$$

where m_s , b_s and k_s are respectively the mass, damping and stiffness of the force sensor; $y = y_C$ is the current location of the force sensor and of the micropart when the two are in contact and $\delta = y - y_D$ is the displacement of the force sensor due to the applied force on the force sensor ($F_s = -F_g$).

Using (7), (8) and (9), the model of the whole smart finger is given as follows:

$$Y = G_u(s) [d_p U - H_s - G_f(s) F_g] \quad (10)$$

where $Y = Y(s)$ is the Laplace transform of y , and $G_u(s)$ and $G_f(s)$ are given by the following:

$$\begin{cases} G_u(s) = \frac{\left(1 + \frac{3L}{L_a} \right) (b_s s + k_s)}{a m_s s^4 + c_1 s^3 + c_2 s^2 + (b_s + b k_s) s + k_s} \\ G_f(s) = \frac{a s^2 + b s + 1 + \left(1 + \frac{3L}{L_a} + \frac{3L^2}{L_a^2} \right) s_p (b_s s + k_s)}{\left(1 + \frac{3L}{L_a} \right) (b_s s + k_s)} \\ c_1 = b m_s + a b_s \left(1 + \frac{3L}{2L_a} \right) b_s m_s s_p \\ c_2 = a k_s + b b_s m_s + \left(1 + \frac{3L}{2L_a} \right) k_s m_s s_p \end{cases} \quad (11)$$

4 Impedance Control with Force Tracking for the Control of the Grasping Task

In this section, a force tracking impedance control scheme is presented to control not only the interaction between the gripper's and the micropart but also the grasping force of the micropart. First, the sliding mode impedance control scheme is presented, then the force tracking problem is discussed.

4.1 Sliding Mode Impedance Control Formulation

The impedance control formulation is given as follows:

$$M_d(\ddot{y} - \ddot{y}_r) + B_d(\dot{y} - \dot{y}_r) + K_d(y - y_r) = F_g - F_r \quad (12)$$

where M_d , B_d and K_d are respectively the desired mass, damper and stiffness to set the desired dynamics of the contact; y_r is the reference position to set for the position control. The sliding mode control (SMC), presented by [16], has shown its effectiveness for controlling nonlinear systems and for impedance control by forcing the system to slide along the sliding surface which is chosen using the impedance formulation [17] despite the robot dynamics.

The impedance error or what is also called the measure of impedance error is given in the following:

$$e_i = M_d(\ddot{y} - \ddot{y}_r) + B_d(\dot{y} - \dot{y}_r) + K_d(y - y_r) + e_f \quad (13)$$

where e_i is the impedance error and $e_f = F_r - F_g$ is the force error between the desired and the applied force. e_i and e_f have the unit of force.

A sliding surface is chosen in [17] using the impedance control formulation defined in (12). The sliding surface is given by:

$$\sigma = (\dot{y} - \dot{y}_r) + \frac{B_d}{M_d}(y - y_r) + \frac{K_d}{M_d} \int (y - y_r) dt + \frac{1}{M_d} \int (f_r - F_g) dt \quad (14)$$

when the system reaches the sliding surface and is in sliding mode, $\sigma = 0$ and $\dot{\sigma} = 0$. In this case, using (13), the following is deduced:

$$e_i = M_d \dot{\sigma} \quad (15)$$

The equivalent control u_{eq} is the solution of $\dot{\sigma} = 0$, then replacing (10) in the derivative of (14), the following could be deduced in the frequency domain:

$$U_{eq}(s) = \frac{Y_r - G_i F_r + (G_f + G_i) F_g}{d_p G_u} + \frac{H_s}{d_p} \quad (16)$$

where $G_i = G_i(s) = \frac{1}{M_d s^2 + B_d s + K_d}$ is the transfer function which represents the desired impedance formulation given in (12). The equivalent control takes effect in the sliding phase when the impedance trajectory reaches the sliding surface and is kept on it. If the system does not lie on the sliding surface, a discontinuous control is added to the equivalent control to determine the overall control action:

$$u = u_{eq} - K \text{sgn}(\sigma) \quad (17)$$

where K is a gain and sgn is the sign function. In many applications, the sign function causes oscillations, then the sign function could be replaced by the saturation function or others. Then the overall control action is given by the following:

$$u = u_{eq} - Ksat\left(\frac{\sigma}{\varepsilon}\right) \quad (18)$$

Where ε is a boundary which is a threshold chosen to reduce the oscillations and the saturation function is given as follows:

$$sat\left(\frac{\sigma}{\varepsilon}\right) = \begin{cases} sgn\left(\frac{\sigma}{\varepsilon}\right) & \text{if } |\sigma| > \varepsilon \\ \frac{\sigma}{\varepsilon} & \text{if } |\sigma| \leq \varepsilon \end{cases} \quad (19)$$

4.2 Force Tracking

The impedance control was proposed to control the interaction between the gripper and the component. However, one weak point of the impedance control is the lack of direct force control capability. The steady state force error in the impedance control scheme is given according to [15] by:

$$e_f^{ss} = k_{eq} \left[\frac{f_r}{k_p} + y_p - y_r \right] \quad (20)$$

where $k_{eq} = \frac{K_d k_p}{K_d + k_p}$.

In order to cancel the steady state force error, the position reference, y_r , could be chosen as follows:

$$y_r = y_p + \frac{f_r}{k_p} \quad (21)$$

In practice, it is difficult to determine exactly the position and the stiffness of the micropart and the passive gripper. The location of the micropart and the passive gripper could be estimated using the information given by the force sensor when the measured force is different from zero. The stiffness of the environment could be estimated using the static part of (1) as follows:

$$\hat{k}_p = \frac{F_g}{y - \hat{y}_p} \quad (22)$$

where \hat{y}_p is the estimated location of the micropart. However, in this paper, the passive finger's stiffness is known and so there is no need to estimate the stiffness, but the y_p is estimated online by \hat{y}_p .

Replacing (21) in (16), the final equivalent control action is given as follows:

$$U_{eq}(s) = \frac{\left(\frac{1}{k_p} - G_i\right)F_r + (G_f + G_i)F_g + \hat{Y}_p}{d_p G_u} + \frac{H_s}{d_p} \quad (23)$$

The final control action remains as in (18) with replacing U_{eq} by the one defined in (23). The complete impedance control scheme is given in Fig. 4 where the SMC is the sliding mode control.

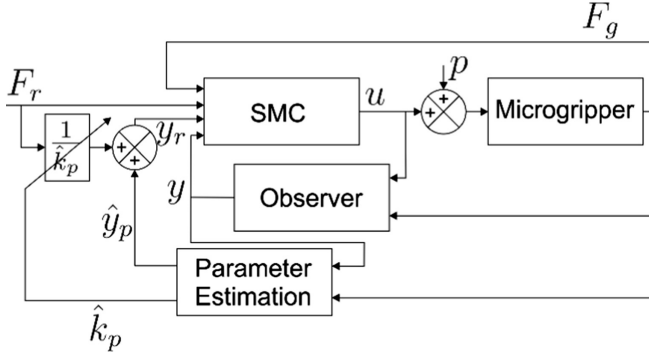


Fig. 4. Force tracking impedance control scheme.

5 Experimental Studies

5.1 Experimental Setup

The experimental setup is composed of a two fingers microgripper. The first finger, called in this paper smart finger, is a 2 DoF piezoelectric actuator presented in [4] where a piezoresistive force sensor is fixed at the actuator's tip. The actuator resolution is nanometric and it has a very fast response time. The force sensor design, fabrication process and performances are presented in [19]. The sensor's resolution is 100 nN and its sensing range is 2 mN and its natural frequency is 8 kHz. The second finger is passive, i.e. not actuated, and is made of Nickel.

A Keyence laser sensor measures the displacement of the actuator's tip, y_A . It is used to test the precision on the estimation of the position of the tip C, y . A micro-component with dimensions $2 \text{ mm} \times 350 \text{ } \mu\text{m} \times 50 \text{ } \mu\text{m}$ is used to test the developed grasping technique.

The microcomponent is initially manually placed onto a moving substrate which consists of a moving stage P-611.3 NanoCube from Physik Instrumente with $100 \text{ } \mu\text{m}$ range and 1 nm in resolution and a rotation stage SR-3610-S from SmarAct with $1.1 \mu^\circ$ in resolution. These two devices are used to position the microcomponent between the two fingers of the microgripper in order to handle it by the microgripper.

The whole system is controlled through dSpace1104 Board with a sampling frequency of 20 kHz. The complete setup used in this paper is presented in Fig. 5.

5.2 Experimental Results

The developed model of the complete microgripper has been validated and the method to experimentally identify the model parameters has been presented in previous works

[20]. Thus, in this section the control presented in Section IV is directly tested for the automation of the grasp/release of a micropart without validating the model of the microgripper.

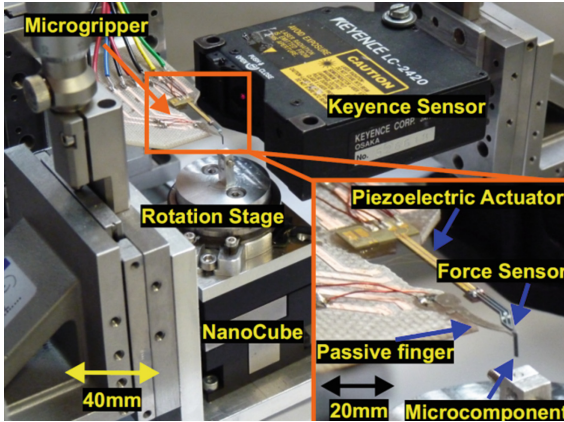


Fig. 5. The whole experimental setup including a microgripper holding a microcomponent, the nanopositioning and rotation stages and the laser sensor.

The strategy of manipulation is defined as follows:

- (1) the micropart is initially manually placed onto a substrate,
- (2) the micropart is positioned close to the passive finger by moving the substrate to a small distance from it,
- (3) the control action starts and the smart finger approaches the micropart, enters in contact with the micropart, pushes the micropart to the passive finger until the smart finger and the micropart enter in contact with the passive finger and then the controller sets the force to the desired force,
- (4) the microgripper is maintained for a long period in order to test the effectiveness of the control technique in the presence of some perturbations and in the presence of the creep of the piezoelectric actuator.

Figure 6 shows the experimental results for an automated grasp/release task of a micropart using the developed control and microgripper. The values used for the impedance are $M_d = 1$, $B_d = 200$ and $K_d = 10000$.

First, the position of the micropart is unknown between the fingers of the microgripper. In order to be able to handle the micropart, the initial estimate of y_p , \hat{y}_p^0 , is set to be big enough, $100 \mu\text{m}$, to be sure that the smart finger is able to touch the micropart. Then, the controller is turned ON at time $t = 50 \text{ ms}$ with no force reference, the TSFM fingers start to move to let the position tracks the position reference y_r which is equal to \hat{y}_p^0 because no force reference exists. Because \hat{y}_p^0 is bigger than the real value of y_p , the TSFM fingers enter in contact 1 with the micropart. When contact 1 appears, a new estimation of the environment location \hat{y}_p is calculated and the position

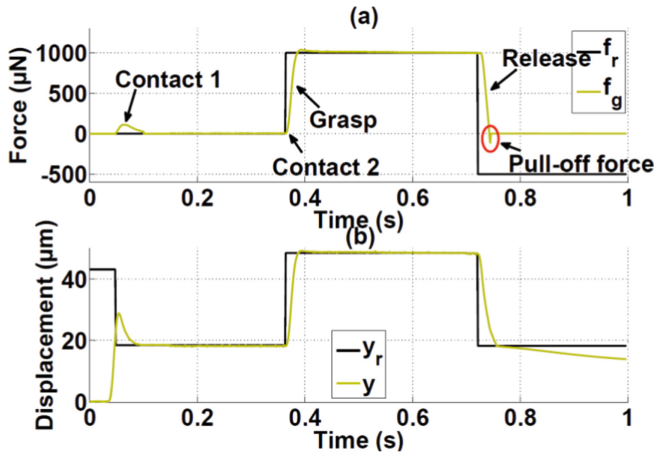


Fig. 6. The force and displacement responses of the system for the handling of the microcomponent: (a) Force response and (b) Displacement response.

reference y_r changes to the new estimated value \hat{y}_p ($y_r = \hat{y}_p$). Then at time $t = 0.37$ s, a force reference is set to the controller and contact 2 happens enabling the estimation of \hat{k}_p . The system reaches the steady state within a settling time of 20 ms and a small overshoot of 3.7% despite the online estimation of the stiffness of the micropart and the second finger. The steady state force error is null showing the significance of the parameter estimation technique and the SMIC. The automated grasping task is then achieved with success.

The release task is then tested. For that, a negative force reference is set to the system allowing the controller to break the contact between the TSFM and the micropart and succeeding the release task within a settling time of 19 ms. The advantage of this SMIC controller is that it can deal with pull-off force by simply applying a negative force reference to the system.

The experimental results show the significance of the approach. Comparing this approach to [15, 24], the dynamic performances are much better. Indeed, the overshoot is 10 times smaller and the response time is much smaller. Comparing the results to [18], the steady state force error is null in our work where it is bigger than 7% in the other work.

6 Conclusion

In this paper, a new microgripper design is proposed and tested for the automated manipulation of microcomponents. The microgripper is composed of two fingers: the first finger, called in this paper smart finger, is a piezoelectric actuator where a novel piezoresistive force sensor is fixed at the actuator's tip and the second finger is passive. A micropart of size $50 \mu\text{m} \times 350 \mu\text{m} \times 2 \text{mm}$ is grasped and released automatically

based on a sliding mode impedance control with force tracking scheme. The control used is based on a precise dynamic nonlinear model of the microgripper.

The control approach enables setting a desired dynamic behavior to the system and the controller forces the system to follow the desired impedance and to track the desired force. This is important at the microscale to manipulate microparts without losing them. Moreover, a method to deal with pull-off force has been also considered in this paper. The automation of grasp/release task of a micropart has been done with settling time of 20 ms and small overshoot (less than 3.7%). The experimental results are promising for the automation of the microassembly and micromanipulation while controlling the interaction between the microgripper and the manipulated microparts.

The proposed control approach can be extended to automate more complex microassembly and micromanipulation tasks.

Acknowledgment. These works have been funded by the Labex ACTION project (contract “ANR-11-LABEX-0001-01”), ANR COLAMIR (contract “ANR-16-CE10-0009”) and by the French RENATECH network through its FEMTO-ST technological facility.


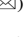





References

1. Dechev, N., Cleghorn, W., Mills, J.: Microassembly of 3-D microstructures using a compliant, passive microgripper. *J. Microelec. Syst.* **13**, 176–189 (2004)
2. Bargiel, S., Rabenorosoa, K., Clévy, C., Gorecki, C., Lutz, P.: Towards micro-assembly of hybrid meems components on a reconfigurable silicon free-space micro-optical bench. *J. Micromech. Microeng.* **20**, 045012 (2010)
3. Clévy, C., Rakotondrabe, M.: Microscale specificities. In: Clévy, C., Rakotondrabe, M., Chaillet, N. (eds.) *Signal Measurement and Estimation Techniques for Micro and Nanotechnology*. Springer, New York (2011). https://doi.org/10.1007/978-1-4419-9946-7_1
4. de Lit, P., Agnus, J., Clévy, C., Chaillet, N.: A four-degree-of freedom microprehsensile microrobot on chip. *Assembly Autom.* **24**(1), 33–42 (2004)
5. Beyeler, F., Neild, A., Oberti, S., Bell, Y.S.D.J., Dual, J., Nelson, B.: Monolithically fabricated microgripper with integrated force sensor for manipulating microobjects and biological cells aligned in an ultrasonic field. *J. Microelectromech. Syst.* **16**(1), 7–15 (2007)
6. Kim, K., Liu, X., Zhang, Y., Sun, Y.: Nanonewton force-controlled manipulation of biological cells using a monolithic meems microgripper with two-axis force feedback. *J. Micromech. Microeng.* **18**(5), 055013 (2008)
7. Piriyanont, B., Fowler, A., Moheimani, S.: Force-controlled meems rotary microgripper. *J. of Microelectromech. Syst.* **24**(4), 1164–1172 (2015)
8. Duc, T., Lau, G., Creemer, J., Sarro, P.: Electrothermal microgripper with large jaw displacement and integrated force sensors. *J. Microelectromech. Syst.* **17**(6), 1546–1555 (2008)
9. Rakotondrabe, M., Ivan, A.: Development and force/position control of a new hybrid thermo-piezoelectric microgripper dedicated to micromanipulation tasks. *IEEE Trans. Autom. Sci. Eng.* **8**(4), 824–834 (2011)
10. Wang, D., Yang, Q., Dong, H.: A monolithic compliant piezoelectric-driven microgripper: Design, modeling, and testing. *IEEE/ASME Trans. Mechatron.* **18**(1), 138–147 (2013)

11. Komati, B., Rabenorosoa, K., Clévy, C., Lutz, P.: Automated guiding task of a flexible micropart using a two-sensing-finger microgripper. *IEEE Trans. Autom., Sci. Eng.* **10**(3), 515–524 (2013)
12. Hogan, N.: Impedance control - an approach to manipulation i –theory, ii – implementation, iii – applications. *ASME Trans. J. Dyn. Syst. Measur. Control* **107**(1), 24 (1985)
13. Komati, B., Pac, M., Ranatunga, I., Clévy, C., Popa, D., Lutz, P.: Explicit force control v.s. impedance control for micromanipulation. In: *ASME International Design Engineering Technical Conferences and Computers and Information in Engineering Conference (IDETC)*, vol. 1, Portland (2013)
14. Xie, Y., Sun, D., Tse, H.Y.G., Liu, C., Cheng, S.H.: Force sensing and manipulation strategy in robot-assisted microinjection on zebrafish embryos. *IEEE/ASME Trans. Mechatron.* **16** (6), 1002–1010 (2011)
15. Seraji, H., Colbaugh, R.: Force tracking in impedance control. *Int. J. Rob. Res.* **16**(1), 97–117 (1997)
16. Utkin, V.: Variable structure systems with sliding modes. *IEEE Trans. Autom. Control* **22** (2), 212–222 (1977)
17. Lu, Z., Goldenberg, A.: Robust impedance control and force regulation: theory and experiments. *Int. J. Rob. Res.* **14**(3), 225–254 (1995)
18. Xu, Q.: Precision position/force interaction control of a piezoelectric multimorph micro-gripper for microassembly. *IEEE Trans. Autom. Sci. Eng.* **10**(3), 503–514 (2013)
19. Komati, B., Agnus, J., Clévy, C., Lutz, P.: Prototyping of a highly performant and integrated piezoresistive force sensor for microscale applications. *J. Micromech. Microeng.* **24**(3), 035018 (2014)
20. Komati, B., Clévy, C., Rakotondrabe, M., Lutz, P.: Dynamic force/position modeling of a one-dof smart piezoelectric micro-finger with sensorized end-effector. In: *IEEE/ASME International Conference on Advanced Intelligent Mechatronics, Besançon*, pp. 1474–1479 (2014)
21. Ballas, R.: *Piezoelectric Multilayer Beam Bending Actuators: Static and Dynamic Behavior and Aspects of Sensor Integration*. Springer, Heidelberg (2007). <https://doi.org/10.1007/978-3-540-32642-7>
22. Low, T., Guo, W.: Modeling of a three-layer piezoelectric bimorph beam with hysteresis. *J. Microelectromech. Syst.* **4**(4), 230237 (1995)
23. Rakotondrabe, M., Haddab, Y., Lutz, P.: Quadrilateral modelling and robust control of a nonlinear piezoelectric cantilever. *IEEE Trans. Control Syst. Technol.* **17**, 528–539 (2009)
24. Komati, B., Clévy, C., Lutz, P.: Force tracking impedance control with unknown environment at the microscale. In: *IEEE ICRA International Conference on Robotics and Automation, Hong Kong* (2014)



Fluid Dynamics Aided Design of an Innovative Micro-Gripper

Gianmauro Fontana¹  , Serena Ruggeri¹ , Antonio Ghidoni² ,
Alessandro Morelli², Giovanni Legnani² , Adriano Maria Lezzi² ,
and Irene Fassi¹ 

¹ Institute of Intelligent Industrial Technologies and Systems
for Advanced Manufacturing, National Research Council of Italy,
Via A. Corti 12, 20133 Milan, Italy

gianmauro.fontana@stiima.cnr.it

² Department of Mechanical and Industrial Engineering, University of Brescia,
Via Branze 38, 25123 Brescia, Italy

Abstract. The increasing miniaturization of more and more systems and products is supporting the necessity to develop and handle micro-objects and micro-assembling tools. However, in comparison to bigger scale systems, micro-scale tasks undergo greater challenges due to the effect of unwanted sticking forces whose relative value may be predominant at the micro-scale. Systems to overcome these limiting factors have to be specifically developed to enable an effective and successful manipulation. In the case of contact micro-grippers, specific additional devices or manipulating strategies are used to assure the success of the release phase. In this context, this paper presents an innovative vacuum micro-gripper with a low-cost and simple automatic releasing device which can effectively overcome the adhesive forces. The paper, after illustrating the working principle of the gripper, discusses the preliminary results of a first computational fluid dynamics model useful to represent the main gripper characteristics and able to support a design procedure.

Keywords: Vacuum micro-gripper · Fluid dynamic simulations
Micro-gripper design

1 Introduction

The necessity to manufacture a great variety of different micro-components with different characteristics (material, size, shape, etc.) is the result of the current trend towards the miniaturization of many objects and systems. These small components have to be manipulated and assembled undergoing a set of specifications related to their intrinsic properties including the maximum acceptable stress, the dimension of the area available for gripping, the presence of reference points, or the requirement for specific working conditions. Further constraints may be related to the assembly precision, the necessity to assure the stability of the coupling or to guarantee the possibility of disassembly, the presence of obstacles or the interference with other components. Generally speaking, these requirements appear similar to those for components and

systems with a bigger size, however some physical characteristics make the manipulation at the micro-scale more challenging mainly for the relative importance of the surface forces. In this environment, the adhesion forces between the gripper and the component to be manipulated may greatly influence the task execution. These forces include the van der Waals effect, the electrostatic one, capillary forces and others [1]. Such forces may be stronger than the weight of the component to be manipulated generating a sticking effect, preventing the detachment from the micro-gripper when the release is required and generally making the manipulation more difficult. To overcome these difficulties specific solutions and devices have to be designed to assure an effective manipulation and assembly.

Several different micro-grippers based on contact or contact-less principles have been presented in literature [2–4]. They take advantage of different technologies and strategies like: ultrasonic waves, acoustic, electrostatics, vacuum, capillarity, etc. Considering the contact grippers, a great role is played by vacuum actuators which are used in several industrial applications (for instance in MEMS, mechanical micro-objects, for rework and assembly of electronic boards, etc.). However, vacuum grippers are also used to manipulate biological samples (pick and place) for sample analysis or micro-injection of specific molecules. Vacuum micro-grippers generally have a simple structure, simple actuation, and working principle. They have a wide range of applicability also in the manipulation of fragile components. However, as with all the contact grippers, the adhesive forces may negatively affect their performance preventing their use in some applications.

Different release solutions based on active and passive principles have been described in literature to overcome this difficulty, but the realization of a general, precise, and reliable solution is still an open research field. Generally, active release strategies make use of a supplementary component to provide some actions forcing the detaching of the object from the gripper; other strategies are based on the reduction of the contact area. Other strategies are based on mechanical vibration [5], the generation of positive pressure impulses, the use of a supplementary tool or an edge touching the object to detach [6], snap-fasteners [7], gluing [8] or rolling [9] the object to the release workplace.

Having these issues in mind, this paper proposes an innovative vacuum micro-gripper with the capability to overcome the adhesive forces in a simple and effective way, without the use of additional actuators and preserving the simplicity and light design. This paper also presents a preliminary numerical model based on computational fluid dynamics analysis.

In the next sections, the working principle of this innovative micro-gripper is presented, also considering the evolution from a simpler and more traditional design to an advanced one. Then, the development of a preliminary computational fluid dynamic model is considered to rationally explain the main gripper characteristics and to sketch a rational design procedure.

2 The Working Principle of the Vacuum Micro-grippers

The micro-gripper proposed in this paper is the last prototype of successive evolutions originated from a traditional design (Fig. 1). The prototype marked by (a) is a classical vacuum micro-gripper characterized by a very simple but cost effective design that however may suffer from the mentioned sticking problems. A first evolution is shown in Fig. 1(b, c) which exhibits the presence of a passive automatic releasing device. A “releasing mass” that may move up and down is incorporated inside the body. A pin is embedded in the mass and inserted in the cannula. The mass (and so the pin) is sucked up when the gripper is activated by a negative pressure ΔP . When the gripper is deactivated, the mass falls down and the pin generates a releasing action on the grasped object. More details on this patent design are contained in [10]. The limit of this design is that the limited air flow does not permit the lift of a “big” releasing mass, limiting the detaching capability.

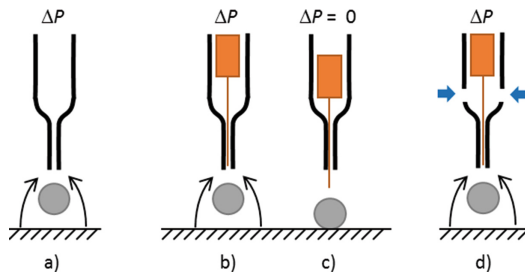


Fig. 1. Working principles of some vacuum micro-grippers: (a) traditional, (b, c) first extended design incorporating an automatic releasing system, and (d) final advanced version.

To increase the lifting capabilities some lateral holes have been added to the gripper body (two holes in the case of Fig. 1(d)). In this case, when the gripper is activated by the negative pressure, a larger air flow is generated and a larger lifting action is obtained. This allows including a bigger releasing mass able to generate a more significant detaching action, also suitable for overcoming high sticking forces. More details are described in [10, 11].

The basic equation for the gripper design (Fig. 1) is

$$F = \Delta P A_0 \geq m g \quad A_0 = \frac{\pi d_{ic}^2}{4} \quad (1)$$

which shows the dependence of the grasping force to the cross section area A_0 of the cannula and the negative pressure drop ΔP . This permitted forecasting the maximum mass m of the object that can be grasped; $g = 9.81 \text{ m/s}^2$ is the gravity acceleration and d_{ic} is the internal diameter of the cannula. If the version with the releasing mass M is considered (Fig. 1(b, c)), Eq. (1) has to be modified adding M to m . An improved model may take into account the presence of a limited airflow between the cannula and the object even when an object has been grasped, because experience shows that the

object never completely seals the cannula [10]. However, this flow is very little and difficult to model.

In the case of the prototype of Fig. 1(b, c), to overcome the sticking force F_s , the mass M of the releasing object has to satisfy the following inequality

$$Mg \geq F_s - mg$$

Moreover, for the gripper of Fig. 1(d), it has to be considered that the grasping force is the result of the difference between the pressure P_1 of the lower chamber and the outside pressure that in a standard situation is $P_0 = 100$ kPa (see Fig. 2(a))

$$F = (P_0 - P_1)A_0 \geq mg \quad (2)$$

Of course, the pressure P_1 depends on the applied negative pressure, and on the geometry of the whole system including the entity of the airflow through the lateral holes.

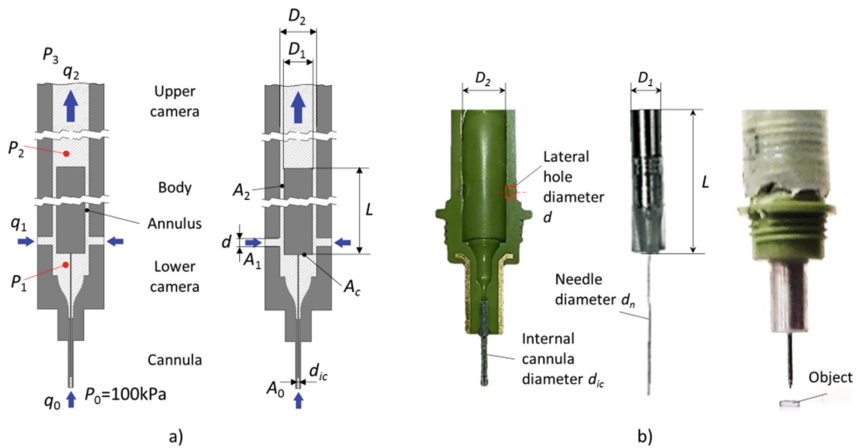


Fig. 2. Vacuum micro-gripper with additional air flows: (a) the model and the parameters used in the simulations; (b) a prototype.

Preliminary experimental tests have been performed on three different prototypes whose main characteristics are shown in Table 1 and Fig. 2(b). The tests conditions considered different pressure values and different lateral holes areas obtained by partially occluding them, then simulating different equivalent diameters. The variation of the cross section of the lateral hole proved to be an important factor greatly affecting the gripper performance: if the hole is too small, the air flow decreases significantly and the lifting force becomes insufficient to lift the releasing mass. Oppositely, a larger hole generates a too large airflow with a consistent reduction of the pressure drop $\Delta P = P_0 - P_1$ in the lower chamber, degenerating the grasping performance of the gripper. It was concluded that an optimal value of the diameter of the later holes exists and had to be

identified. In order to formulate a numerical procedure to design the micro-gripper and to identify its main characteristics, a fluid dynamic model was developed and is illustrated in the following sections.

Table 1. Main characteristics and dimensions of the micro-gripper of Fig. 2(b).

Identification code	Needle diameter d_n [μm]	Inner cannula diameter d_{ic} [μm]	Body diameter D_2 [mm]	Mass diameter D_1 [mm]	Mass length L [mm]	Mass M [mg]	Lateral hole diameter d [μm]
0.2	79	139	3.6	2.4	24.2	707	766
0.25	79	152	3.6	2.4	24.2	707	766
0.3	145	208	3.6	2.4	24.2	707	766

3 CFD Simulations

The gripper has been analyzed through a Computational Fluid Dynamics (CFD) tool, the open source CFD toolbox OpenFOAM® [12, 13], to compute the air velocity, pressure, and temperature fields inside the device. The post-processing of the computed results provides also the air mass flow rate through the cannula and the lateral holes, and the forces applied by the air on the gripper inner surfaces, such as the lifting forces on the releasing mass [14]. The aim of these simulations is to support the design of new optimized prototypes, investigating the effect of gripper geometry modifications on its performance.

The compressible steady-state solver *rhoSimpleFoam* has been used to solve the RANS (Reynolds Averaged Navier-Stokes) equations coupled with the SST turbulence model (low Reynolds number version, i.e. without wall functions). All the simulations were run in parallel on a Linux workstation (Intel Core i7 970, six cores at 3.2 GHz).

For the simulations, a simplified gripper geometry has been considered, as shown in Fig. 2(a). Table 2 reports the values of the geometric parameters (L , d , D_1 , and D_2) adopted in the simulations. Nominal values correspond to the original configuration. Modified configurations were obtained varying the parameters L , d , and D_2 , one at a time (see Table 2). 7 configurations were tested, considering three different outlet pressures P_3 (70, 80, 90 kPa) at the outlet section: 21 CFD simulations were performed.

Table 2. Geometric parameters and related values for the CFD simulations. Dimensions in [mm].

Parameter	Minimum	Nominal	Maximum
L	16.2	24.2	32.2
d	0.5	0.77	1
D_1		2.6	
D_2	3.2	3.4	3.6

The “optimal” mesh density for the simulations has been determined through a grid independence analysis. The air mass flow rate and the lifting force have been monitored on a coarse (222×10^3 cells), a medium (473×10^3 cells), and a fine (767×10^3 cells) grid, made of hexahedral and tetrahedral elements. The choice not to use wall-functions requires the size of the elements adjacent to the solid walls to be fine enough to compute the boundary layer accurately (i.e., non-dimensional thickness of the elements, y^+ , was set equal to 1 for all meshes).

The medium grid has been used for all the simulations, showing best results in term of accuracy (the relative difference with respect to the results computed on the fine grid is less than 1% for the mass flow rate, and less than 2% for the lift), and saving in computing time. All the simulations lasted about 1.5 h.

The predicted air mass flow rate through the lateral holes ranges between 4.8×10^{-5} and 28.9×10^{-5} kg/s, and the lifting force between 3.6 and 81 mN. This force is the sum of two contributions: (i) the form component, depending on the pressure difference $P_1 - P_2$, (about 85% of the total force as shown by the simulations); (ii) the skin friction component, due to the viscous stresses acting on the lateral surface of the releasing mass (about 15% of the total force).

The flow field inside the gripper is characterized by low velocities. Only the inlet zone of the cannula and of the lateral holes (see Fig. 3) are characterized by a Mach number $Ma = v/c \cong 0.5$ (with v the air velocity, and c the corresponding speed of sound), nevertheless the presence of these two zones of high velocities forced the use of a compressible solver.

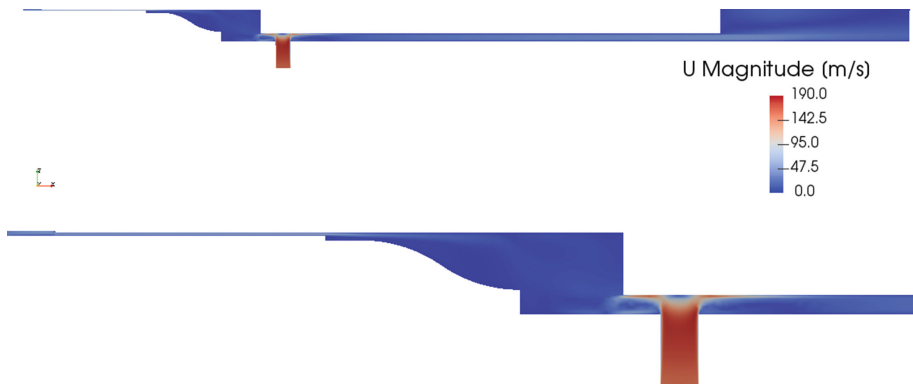


Fig. 3. Velocity field for the nominal case of Table 2, $P_3 = 80$ kPa.

Figure 4 shows the pressure contours, characterized by a fast decrease of the static pressure at the inlet zone of the cannula and of the lateral holes, and a linear decrease along the meatus from the lateral holes to the end of the releasing mass.

It was also verified that the pressure drop $\Delta P_1 = P_0 - P_1$, between the outside and the lower chamber, is much greater than the pressure drop $\Delta P_3 = P_1 - P_3$, between the lower and the upper chamber. Moreover, the zone with the lowest pressure P_2 is located in the upper chamber, just behind the releasing mass. So

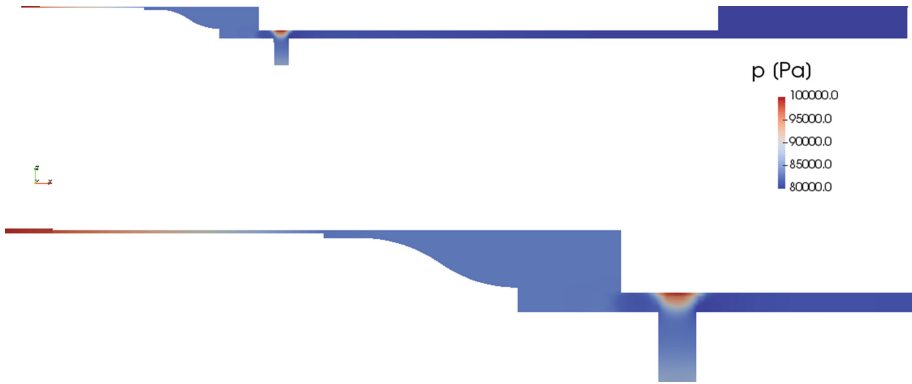


Fig. 4. Pressure field for the nominal case of Table 2, $P_3 = 80$ kPa.

$$P_0 - P_1 \gg P_1 - P_2 > P_1 - P_3 \quad P_0 > P_1 > P_3 > P_2$$

This behavior is due to the fact that the cannula cross section area is much smaller than the lateral holes area and the annulus area

$$A_0 \ll A_1 < A_2.$$

4 The Gripper Model

In order to establish a set of approximate correlations to describe the fluid dynamics of the gripper, it may be useful to refer to the following parts of the device: cannula, lower chamber, lateral holes, annulus (between the releasing mass and the body), upper chamber.

There are three air mass flow rates of interest: the one through the cannula and the lower chamber, q_0 ; the one through the lateral holes, q_1 ; and the one through the annulus and the upper chamber, q_2 , which is the sum of the other two:

$$q_2 = q_1 + q_0 \tag{3}$$

Since the cannula area is about 2% of the lateral holes area, a flow rate q_0 much smaller than the flow rate q_1 was expected. Simulations performed to compare results with and without flow through the cannula (closed cannula, $q_0 = 0$) prove that the flow rate q_0 does not affect for all practical purposes either the pressure field in the gripper or the force acting on the releasing mass: for this reason, in what follows it will be neglected

$$q_2 \cong q_1 \tag{4}$$

The flow rate q_1 and the pressure difference between the atmospheric pressure P_0 and that of the lower chamber P_1 are strongly coupled. On the basis of theory and experience, the following empirical expression was assumed:

$$P_0 - P_1 = k_a \frac{q_1^{n_a}}{d^{m_a}} \quad (5)$$

where d is the diameter of the holes, and n_a , m_a and k_a are suitable constants. The values of the constants were estimated using the least squares method to fit the computational results: these values are reported in Table 3. The pressure drop can be predicted with an average error of 3% and a maximum error of 7% (see Fig. 5(a)).

Table 3. Constants of the empirical model to predict the pressure drops as a function of the geometry and of the air mass flow rate (Eqs. (5) and (6)). Dimensions in [mm], flow rate in [kg/s], pressures in [kPa].

Subscript i	k_i	n_i	m_i
a	$2.425 \cdot 10^9$	2.295	5
1	$6.63 \cdot 10^9$	2.284	2.5
2	$1.07 \cdot 10^9$	1.898	2.5
3	$1.19 \cdot 10^7$	1.792	2.5

The pressure drop between the lower and the upper chambers is coupled to the air flow through the device. The main geometrical parameters that influence this pressure drop are the annulus area A_2 and length L . The following empirical expression was assumed to take into account a factor proportional to the annulus length L and a factor depending on the abrupt enlargement from the annulus into the upper chamber

$$P_0 - P_3 = k_1 \frac{q_2^{n_1}}{A_1^{m_1}} + k_2 \frac{q_2^{n_2}}{A_2^{m_2}} + k_3 L \frac{q_2^{n_3}}{A_2^{m_3}} \quad \text{with } A_1 = \frac{\pi}{4} d^2; A_2 = \frac{\pi}{4} (D_2^2 - D_1^2) \quad (6)$$

The values of constants k_i , m_i and n_i were estimated to fit the results of the simulations (Table 3). These coefficients allowed predicting the pressure drop $\Delta P = P_0 - P_3$ with an average relative error of 2.2% and a maximum error of 5%.

In a similar way, an empirical model was built to predict the lifting force F_{tot} which is the sum of two contributions. The first one, F_p , is proportional to the pressure difference $P_1 - P_2$ and to the cross sectional area A_c of the releasing mass. The second contribution, F_v , is due to the viscous stress exerted on the lateral surface A_l of the releasing mass by the air flow. The following empirical model was assumed

$$F_p = k' \frac{\pi}{4} D_1^2 (P_1 - P_2) \cong k_4 \frac{v^{n_4}}{(D_2 - D_1)^{m_4}} \quad F_v = k'' A_l \mu \frac{\partial v}{\partial r} = k_5 L \frac{v^{n_5}}{(D_2 - D_1)^{m_5}} \quad (7)$$

$$F_{tot} = F_p + F_v \quad F_v \cong 0.15 \times F_{tot}$$

where v is the average velocity in the annulus $v = q_2/\rho A_2$, ρ is the density which depends on the pressure $\rho = P/(R^*T)$, R^* is the gas constant, μ is the air viscosity, $\partial v/\partial r$

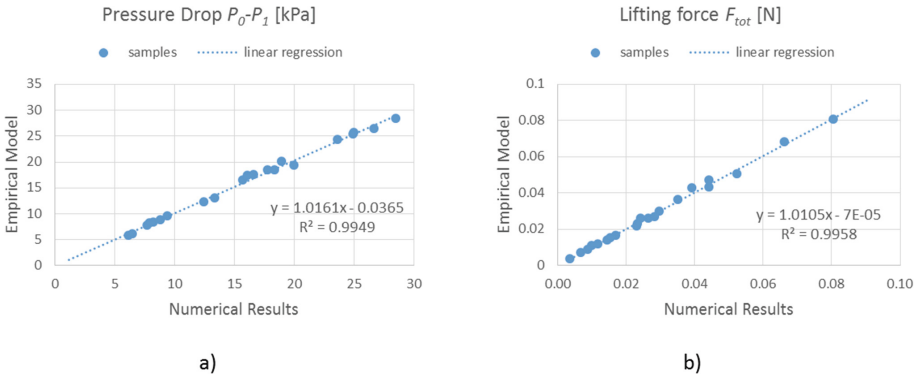


Fig. 5. Comparison of the CFD simulations with the result of the empirical model for the prediction of: (a) the pressure drop $P_0 - P_1$; (b) the lifting force. Data points, regression equation, and linear regression coefficient R .

∂r is the derivative of the velocity with respect to the radial position evaluated for $r = D_1/2$, and k_i are suitable constants. D_1 is constant in the considered simulations and its effects are included in k_4 . The value of the constants which permit predicting the lifting force with an average error of about 0.9 mN and a maximum error of 3 mN (see Fig. 5(b)) are reported in Table 4.

Table 4. Constants of the empirical model to predict the lifting force as a function of the geometry and of the air flow rate (Eq. (7)). Forces in [N].

	Subscript i	k_i	n_i	m_i
F_p	4	$3.54 \cdot 10^{-5}$	1.547	0.8180
F_v	5	$1.83 \cdot 10^{-6}$	1.454	0.2885

5 The Design Procedure

The model presented was not precise enough to be directly adopted for an optimized gripper design, however it can be used to start a recursive trial and error procedure based on finite elements fluid dynamics simulations. The model can help in choosing the parameters and reducing the required simulations. The design procedure may be composed of the following steps:

1. The object to be grasped is examined to estimate its mass m and the sticking force F_s to be overcome. Theoretical or experimental tests have to be performed for each specific situation.
2. The diameter A_0 of the cannula is chosen in function of the geometrical size of the object to be grasped. The experience suggests the rule of thumb according with the diameter of the cannula should be at least 20% of the equivalent diameter of the part [15]. The pressure value in the lower chamber is then chosen by applying Eq. (2):

$$P_0 - P_1 \geq \lambda \frac{mg}{A_0} \quad (8)$$

where $\lambda \geq 1$ is a safety factor to take into account the actual operating dynamic conditions, for instance high acceleration of the gripper when carrying an object.

3. The mass M of the releasing device is then chosen in order to generate a sufficient force to overcome the sticking force F_s :

$$M \geq \frac{F_s}{g} - m \quad (9)$$

and knowing the mass a first value for its dimensions is established.

4. The lifting force $F_r > Mg$ is then chosen and consequently the size of the releasing mass, and the value of the pressure P_2 is hypothesized according to Eq. (7) and considering

$$F_{TOT} \cong 1.2F_p$$

5. The air flow q_2 and the last geometrical dimensions are chosen according to Eq. (6).

The results can be adjusted performing few iterative adjustments. The proposed procedure permitted finding an approximate value for the main parameters of the gripper that can be used to generate a model to be analyzed by some finite element fluid dynamic model. This model can be iteratively modified to perform the final design.

6 Conclusions

The paper presents an innovative micro-gripper incorporating an automatic releasing system and its design procedure.

A prototype of this type of micro-gripper was developed and proved to reliably overcome the adhesive forces when grasping and releasing objects.

A numerical model, based on preliminary finite element fluid dynamics analysis, showed how the gripper geometry affects its performance, and was then exploited for a first design of the gripper. Indeed, Computational Fluid Dynamic- (CFD) simulations are used to identify the unknown model parameters by the least squares method in order to predict the air mass flow rates and the forces applied on the surfaces, such as the lifting forces on the releasing mass. However, at the moment, the model is not sufficiently precise to replace a detailed CFD analysis, but it is able to highlight the main characteristics of the gripper. The model will be improved considering more simulations to include combined effects of the parameters and results of experimental tests. The present results, however, confirm the first experimental results reported in [11].

Each CFD simulation is very time consuming (it requires a couple of hours of computation in addition to the time required to create the mesh and adjust all the parameters), whilst the empirical model can be solved in less than one second and the

form of the equations suggests the influence of each parameter. Although for a full detailed design procedure the model has to be validated with experimental tests, at this stage it is able to explain the behavior of the gripper and to suggest indicative values for its practical design.

Finally, the gripper design procedure, based on this empirical model, is explained step by step, in order to choose the gripper geometry and the working parameters compliant with the manipulation specifications, such as the object mass and the sticking forces.

Acknowledgments. The work has been partially supported by the project: “Cybersort” - 3AQ CNR Regione Lombardia. The authors thank Fabio Colombo for his contribution, during his Master’s thesis development, to the investigation on the presented micro-gripper.

References

1. Fearing, R.S.: Survey of sticking effects for micro parts handling. In: Proceedings of IEEE/RSJ International Conference on Intelligent Robots and Systems, Human Robot Interaction and Cooperative Robots, vol. 2, pp. 236–241. IEEE (1995)
2. Gauthier, M., Lambert, P., Régnier, S.: Microhandling and micromanipulation strategies. In: Chaillet, N., Régnier, S. (eds.) *Microrobotics for Micromanipulation*, Chap. 3, pp. 179–242. Wiley-ISTE, Great Britain (2010)
3. Fantoni, G., Porta, M.: A critical review of releasing strategies in microparts handling. In: Ratchev, S., Koelemeijer, S. (eds.) *IPAS 2008. IIFIP*, vol. 260, pp. 223–234. Springer, Boston, MA (2008). https://doi.org/10.1007/978-0-387-77405-3_21
4. Khan, S., Sabanovic, A.: Force feedback pushing scheme for micromanipulation applications. *J. Micro-Nano Mechatron.* **5**(43), 43–55 (2009)
5. Haliyo, D.S., Régnier, S., Guinot, J.C.: μ MAD, the adhesion based dynamic micro-manipulator. *Eur. J. Mech. A/Solids* **22**(6), 903–916 (2003)
6. Zesch, W., Brunner, M., Weber, A.: Vacuum tool for handling microobjects with a NanoRobot. In: Proceedings of the 1997 IEEE ICRA, vol. 2, pp. 1761–1766. IEEE (1997)
7. Prasad, R., Böhringer, K.F., MacDonald, N.C.: Design, fabrication, and characterization of single crystal silicon latching snap fasteners for micro assembly. In: Proceedings of ASME IMECE 1995, vol. 57, no. 2, pp. 917–923 (1995)
8. Bark, C., Binnenböse, T., Vögele, G., Weisener, T., Widmann, M.: Gripping with low viscosity fluids. In: Proceedings of the IEEE Eleventh Annual International Workshop on Micro Electro Mechanical Systems (MEMS 1998), pp. 301–305. IEEE (1998)
9. Haliyo, D.S., Dionnet, F., Regniér, S.: Controlled rolling of microobjects for autonomous manipulation. *J. Micromechatronics* **3**(2), 75–101 (2006)
10. Ruggeri, S., Fontana, G., Legnani, G., Fassi, I.: Design strategies for vacuum micro-grippers with integrated release system. In: Proceedings of ASME IDETC, vol. 4, pp. V004T09A022 (2017)
11. Colombo, F.: Modelization and optimization of a vacuum gripping-releasing device for micromanipulation. Master thesis in Industrial Automation Engineering, University of Brescia, Brescia, Italy (2016)
12. Weller, H.G., Tabor, G., Jasak, H., Fureby, C.: A tensorial approach to computational continuum mechanics using object-oriented techniques. *Comput. Phys.* **12** (6), 620–631 (1998)

13. OpenFOAM 4.1 Webpage. <https://openfoam.org>. Accessed 06 Dec 2017
14. Morelli, A.: Modellazione e simulazione numerica di deflussi in microdispositivi di presa ad aspirazione (Modeling and numerical simulation of flows in suction gripping microdevices). Master thesis in Mechanical Engineering, University of Brescia, Brescia, Italy (2017)
15. Fontana, G., Ruggeri, S., Fassi, I., Legnani, G.: A mini work-cell for handling and assembling microcomponents. *Assembly Autom.* **34**(1), 27–33 (2014)



Improving Rigid-Body Registration Based on Points Affected by Bias and Noise

Marek Franaszek^(✉) and Geraldine S. Cheok

National Institute of Standards and Technology, Gaithersburg, MD 20899, USA
{marek, cheok}@nist.gov

Abstract. The task of registering two coordinate frames is frequently accomplished by measuring the same set of points in both frames. Noise and possible bias in the measured locations degrade the quality of registration. It was shown that the performance of registration may be improved by filtering out noise from repeated measurements of the points, calculating small corrections to the mean locations and restoring rigid-body condition. In the current study, we investigate experimental conditions in which improvement in registration can still be achieved without cumbersome collection of repeated measurements. We show that for sufficiently small noise relative to bias, the corrections calculated from a single measurement of points can be used and still lead to the improved registration.

Keywords: Rigid-body registration · Bias · Peg-in-hole

1 Introduction

Registration is a commonly performed procedure when points measured in one coordinate frame have to be accessed in another frame. Each registration requires identification of common features with known spatial location in both frames. This may be a challenging task when spatial relations between features are not preserved, and thus non-rigid registration techniques must be used [1–4]. In many manufacturing applications (like part assembly) corresponding 3D points can be identified and rigid-body registration can be used. We call the first frame from which the points are transformed, the working frame, and the second frame the destination frame. In the ideal situation when the rigid-body condition (RBC) is satisfied, the distance between any two points (X_i, X_j) in the working frame and the distance between the same points in the destination frame (Y_i, Y_j) are equal

$$L_{i,j} = \|X_i - X_j\| - \|Y_i - Y_j\| \equiv 0 \quad (1)$$

Then, the rotation \mathbf{R} and translation $\boldsymbol{\tau}$ mapping one set of $J \geq 3$ points $\{X\}_J$ exactly on another set $\{Y\}_J$ can be determined. These common points, measured in both frames and used for registration, are called fiducials. In reality, due to noise and possible bias in the measured data, RBC does not hold (i.e., $L_{i,j} \neq 0$) and $\{X\}_J$ cannot be mapped exactly to $\{Y\}_J$. Then, the transformation $\{\mathbf{R}, \boldsymbol{\tau}\}$ can be found by minimizing the following Fiducial Registration Error

$$FRE(\mathbf{R}, \boldsymbol{\tau}) = \frac{1}{J} \sum_{j=1}^J \|\mathbf{R}\mathbf{X}_j + \boldsymbol{\tau} - \mathbf{Y}_j\|^2. \quad (2)$$

Transformation $\{\mathbf{R}, \boldsymbol{\tau}\}$ can be determined and applied to the target points $\{\mathbf{T}_X\}$ which are usually measured only in the working frame. If a corresponding set of targets $\{\mathbf{T}_Y\}$ is available in the destination frame, then the Target Registration Error $TRE(\mathbf{T}_X)$ can be calculated as

$$TRE(\mathbf{T}_X) = \|\mathbf{R}\mathbf{T}_X + \boldsymbol{\tau} - \mathbf{T}_Y\|. \quad (3)$$

The quality of the registration may be reported by providing the values of TRE for a representative set of targets measured in both frames. Thus, reduction of TRE should improve the performance of many tasks in manufacturing. For example, peg-in-hole testing (commonly used to benchmark a robot's performance [5–7] for insertion tasks) depends on the error in hole location [8–12].

Registration can be improved by obtaining repeated measurements of fiducials $\{\mathbf{X}\}_J^{(n)}$, $\{\mathbf{Y}\}_J^{(n)}$ and targets $\{\mathbf{T}_X\}^{(n)}$, $n \leq N$. Then, noise could be filtered out by using the mean locations of points and virtually noise-free registration transformation could be obtained. Subsequent use of such transformation would map the mean locations of targets from the working frame almost exactly onto the true locations of targets in the destination frame. However, removal of noise does not remove non-homogenous bias from the measured 3D points and the mean locations $\{\bar{\mathbf{X}}\}_J$ and $\{\bar{\mathbf{Y}}\}_J$ cannot satisfy RBC in (1). To deal with this problem, a method was developed which calculated bias in fiducials from their repeated measurements [13]. The method yields a set of dependent linear equations, and to solve it, a separate set of J points without bias has to be measured. This requirement severely restricts the use of the method as the location of bias-free points may not be known or available in practical applications. Another approach was developed in [14] where it was shown that the rigid-body condition can be restored for fiducials by calculating a small correction $\boldsymbol{\varepsilon}_j$ to each $\bar{\mathbf{X}}_j$. Then, the resulting transformation $\{\mathbf{R}_c, \boldsymbol{\tau}_c\}$ mapped exactly each corrected fiducial $\bar{\mathbf{X}}_j - \boldsymbol{\varepsilon}_j$ from the working frame to $\bar{\mathbf{Y}}_j$ in the destination frame and reduced FRE in (2) to zero. Correction to the mean location of target $\bar{\mathbf{T}}_X$ in the working frame was then interpolated from corrections of nearby fiducials, leading to a reduction of $TRE(\bar{\mathbf{T}}_X)$ in most cases.

It was hypothesized in [14] that repeated measurements may not be necessary if bias is the dominant cause of deviation from the rigid-body condition (i.e., the magnitude of noise is sufficiently smaller than bias). We test this hypothesis in this study: we do not use the mean of repeated measurements and instead apply the procedure directly to single measurements of fiducials and targets. Based on the outcome of our experiments we conclude that the procedure of restoration of rigid-body condition is still feasible for unfiltered, noisy data, and it can lead to improved registration when noise in the measured locations of points is sufficiently smaller (approximately three times) than bias.

2 Restoration of Rigid-Body Condition

If (1) does not hold and $L_{i,j} \neq 0$ then the corrections $\{\boldsymbol{\varepsilon}\}_J$ in locations of $\{\boldsymbol{X}\}_J$ are sought that would bring $L_{i,j}$ back to zero. Corrections are calculated in the working frame for $\{\boldsymbol{X}\}_J$ since they will be needed to estimate corrections for targets $\{\boldsymbol{T}_X\}$ which are measured in working frame. Thus, we seek for vectors $\{\boldsymbol{\varepsilon}\}_J$ such that

$$\|(\boldsymbol{X}_i - \boldsymbol{\varepsilon}_i) - (\boldsymbol{X}_j - \boldsymbol{\varepsilon}_j)\|^2 = \|\boldsymbol{Y}_i - \boldsymbol{Y}_j\|^2, \quad (4)$$

for $1 \leq i < j \leq J$. The solution $\{\boldsymbol{\varepsilon}\}_J = \{\boldsymbol{\varepsilon}'\}_J + \{\boldsymbol{\varepsilon}''\}_J$ is obtained in a two-step iterative procedure described in [14] where $\{\boldsymbol{\varepsilon}'\}_J$ and $\{\boldsymbol{\varepsilon}''\}_J$ are the corrections calculated in the first and the second iteration, respectively.

Once the corrections to fiducials are calculated, a registration between the corrected fiducial locations in the working frame $\boldsymbol{X}_j - \boldsymbol{\varepsilon}_j$ and the corresponding fiducials \boldsymbol{Y}_j in the destination frame can be performed, and the transformation $\{\boldsymbol{R}_c, \boldsymbol{\tau}_c\}$ can be determined (since the rigid-body condition is now restored for fiducials, corresponding $FRE = 0$). Then, a correction to the target \boldsymbol{T}_X in the working frame can be calculated by linear interpolation of corrections from M nearby fiducials as

$$\boldsymbol{\varepsilon}(\boldsymbol{T}_X) = \sum_{m=1}^M w_m \boldsymbol{\varepsilon}_m, \quad (5)$$

where $\boldsymbol{\varepsilon}_m$ is the correction at \boldsymbol{X}_m fiducial and w_m is a normalized weight. Corrected target locations

$$\tilde{\boldsymbol{T}}_X = \boldsymbol{T}_X - \boldsymbol{\varepsilon}(\boldsymbol{T}_X), \quad (6)$$

can now be transformed to the destination frame using $\{\boldsymbol{R}_c, \boldsymbol{\tau}_c\}$ and the transformed point is expected to be closer to the target point measured in the destination frame \boldsymbol{T}_Y .

3 Experiment

Two series of experiments were performed. In the first one, three different metrology systems were used: two motion tracking systems (A and B) and a laser tracker (LT). Registration of A to LT and B to LT were investigated. In the second set of experiments, an industrial robot operated in compliance mode was used to measure the location of the end point of its tool and robot-world registration was investigated.

In the first series of experiments, 3D fiducial points were measured by systems A, B, and LT on a semi-regular grid of $5 \times 5 \times 5$ points, placed in a work volume (approximately $3 \text{ m} \times 3 \text{ m} \times 1.8 \text{ m}$). In addition, $K = 16$ target points distributed randomly in the work volume were also acquired, as shown in Fig. 1a. Measurements of each point (fiducial and target) were repeated $N = 200$ times for System A and B; single measurement of each point was acquired with LT. However, the setting for LT was such that the average of 50 raw measurements was output (corresponding instrument noise was $1.7 \text{ }\mu\text{m}$) and therefore, for the purpose of this study, LT was considered as noise and bias free. Details of experimental set up are described in [15].

In the second set of experiments, a Six Degree of Freedom (6DOF) collaborative robot arm (RA) operated in compliance mode was used. The arm was mounted on an optical breadboard plate (600 mm \times 900 mm) firmly supported by an aluminum frame. The plate has a flatness of ± 0.15 mm and has threaded holes which form a regular grid of squares 25 mm \times 25 mm. A part of the plate accessible to the robot arm covered an area containing 17×21 holes. All available 357 holes were divided into two subsets: the first subset contained $J = 277$ points from which fiducials used in registration were selected; the second subset contained $K = 80$ target points, as shown in Fig. 1b.

A cylindrical adapter was screwed into each hole on the plate. The adapter had a hole into which a cylindrical peg, mounted to the end of the robot wrist, could be inserted. The peg was made of tool steel and had 12.67 mm diameter; the hole in the aluminum adapter had a nominal diameter of $(12.67 + 0.051)$ mm. Once the peg was inserted into the adapter, the location of the endpoint of the peg in the robot's coordinate frame was recorded. The adapter was screwed into each of 357 holes and a single measurement was acquired for each hole. For a limited number of holes randomly distributed on the plate, $N = 16$ repeated measurements were obtained. RA data contain 3D Cartesian coordinates of the endpoint of the peg and three angles defining the orientation of the peg in the robot's frame. However, for this project, the angles and z -coordinate were ignored and only 2D data (x, y) were further processed.

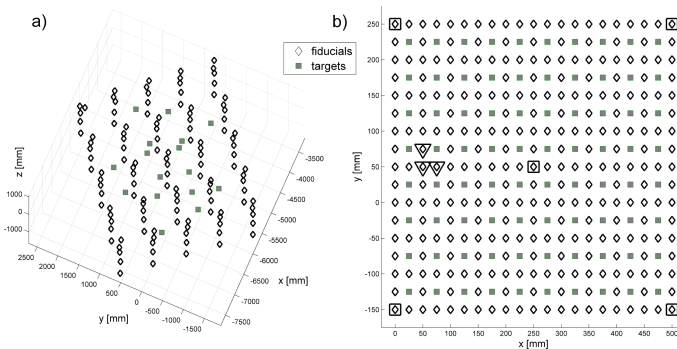


Fig. 1. (a) 3D data: locations of 125 fiducials and 16 targets plotted in coordinate frame of LT. (b) 2D data: locations of 277 fiducials and 80 targets displayed in world coordinate frame. Large squares mark locations of five fiducials used to perform the registration of original, uncorrected data. Triangles mark locations of three fiducials used to perform the registration after RBC was restored in the set of fiducials.

4 Data Processing

The differences defined in (1) were calculated for all possible pairs of fiducials (i, j) where $1 \leq i < j \leq J$. For the series of experiments using LT, the number of such pairs was $J_p = 7\,750$, for the second series using RA, $J_p = 38\,226$. For Systems A and B, the differences $L_{i,j}$ were calculated for averaged locations $\{\bar{X}\}_J$ and $L_{i,j}^{(n)}$ for each repeated

measurement of fiducials in working frame $\{\mathbf{X}\}_J^{(n)}$, $n \leq N$. For data acquired by RA, only one measurement of each point was acquired ($N = 1$). Standard deviations σ_L of differences L were calculated for instantaneous data acquired by RA and for averaged locations acquired by Systems A and B

$$\sigma_L = \sqrt{1/J_p \sum_{i=1}^{j-1} \sum_{j=2}^J (L_{i,j} - \bar{L})^2}. \quad (7)$$

Three standard deviations were calculated: σ_{L0} for the original, uncorrected locations of fiducials; σ_{L1} for the fiducials after the first step of the procedure restoring RBC; σ_{L2} after the second step when RBC was restored. In addition to the standard deviations, histograms of differences L were built for each dataset and after each iteration of the procedure restoring RBC.

Restoration of RBC was performed for 3D data for Systems A and B registered to LT and for 2D data for robot frame registered to world. Corrections $\{\boldsymbol{\varepsilon}\}_J$ were calculated for average $\{\bar{\mathbf{X}}\}_J$ and instantaneous $\{\mathbf{X}\}_J^{(n)}$ locations of the fiducials, yielding corresponding registration transformations $\{\mathbf{R}_c, \boldsymbol{\tau}_c\}$ and $\{\mathbf{R}_c^{(n)}, \boldsymbol{\tau}_c^{(n)}\}$. Once corrections to fiducials were determined, estimated corrections to average and instantaneous target $\boldsymbol{\varepsilon}(\bar{\mathbf{T}}_X)$ and $\boldsymbol{\varepsilon}(\mathbf{T}_X^{(n)})$ were determined using (5). For 3D data (Systems A and B registered to LT) corrections were interpolated from four nearby fiducials which constituted the tetrahedron containing a given target. For 2D data, correction from eight fiducials surrounding a target on a plane were used in the interpolation. Then, corrected target $\tilde{\mathbf{T}}_X$ in the working frame was calculated as in (6) and transformed to the destination frame.

Finally, two types of Target Registration Error were calculated. In the first error $TRE_u(\mathbf{T}_X)$, uncorrected target \mathbf{T}_X was transformed by $\{\mathbf{R}_u, \boldsymbol{\tau}_u\}$ derived from uncorrected locations of fiducials. In the second error $TRE_c(\tilde{\mathbf{T}}_X)$, corrected target $\tilde{\mathbf{T}}_X$ was transformed by $\{\mathbf{R}_c, \boldsymbol{\tau}_c\}$ derived from corrected locations of fiducials (after RBC was restored). For N repeated measurements, both types of errors were calculated for each dataset, i.e. $TRE_c^{(n)}(\mathbf{T}_X^{(n)})$ and $TRE_c^{(n)}(\tilde{\mathbf{T}}_X^{(n)})$, from which the corresponding median values were determined.

For each of $J = 125$ fiducials acquired by System A and B, the variance σ_j^2 was calculated from $N = 200$ repeated measurements and then the averaged variance σ^2 for all J fiducials was determined. For RA data, repeated $N = 16$ measurements were acquired only for a limited number of fiducial locations (52 out of 277) from which the average variance σ^2 was calculated.

5 Results

Table 1 contains the mean standard deviation σ , three standard deviations σ_{L0} , σ_{L1} and σ_{L2} calculated in (7), and parameter ρ for three cases. For the two registrations using LT, the differences $L_{i,j}$ and corresponding standard deviations were calculated for the average locations of fiducials $\{\bar{\mathbf{X}}\}_J$ (i.e., noise was filtered out from their locations).

Table 1. Summary of experimental results.

Registration	σ [mm]	σ_{LO} [mm]	$\rho = \sigma_{LO}/\sigma$	σ_{L1} [mm]	σ_{L2} [mm]
A to LT	0.06	2.5	41.7	4.5×10^{-3}	1.8×10^{-8}
B to LT	0.16	0.09	0.56	1.1×10^{-5}	5×10^{-13}
RA to world	0.11	0.28	2.54	2.5×10^{-4}	4×10^{-10}

For the RA data, the differences $L_{i,j}$ were calculated for instantaneous data, and the resulting standard deviations are affected by systematic bias as well as by random noise.

Histograms of the differences L calculated for data acquired by Systems A, B and LT are shown in Fig. 2; histograms for data acquired by RA are shown in Fig. 3. Target registration errors calculated in (3) for data acquired with Systems A, B and LT are shown in Fig. 4. The results in Fig. 4 were obtained for three different post-processing methods, including TRE calculated for the average as well as instantaneous locations of fiducials and targets. For data acquired with RA, only a single measurement of each fiducial or target was taken and, therefore, only two post-processing methods could be used and the results are presented in Fig. 5. The difference between both methods, i.e. $\Delta TRE = TRE_c - TRE_u$, is shown in Fig. 5b: $\Delta TRE < 0$ indicates improvement in registration.

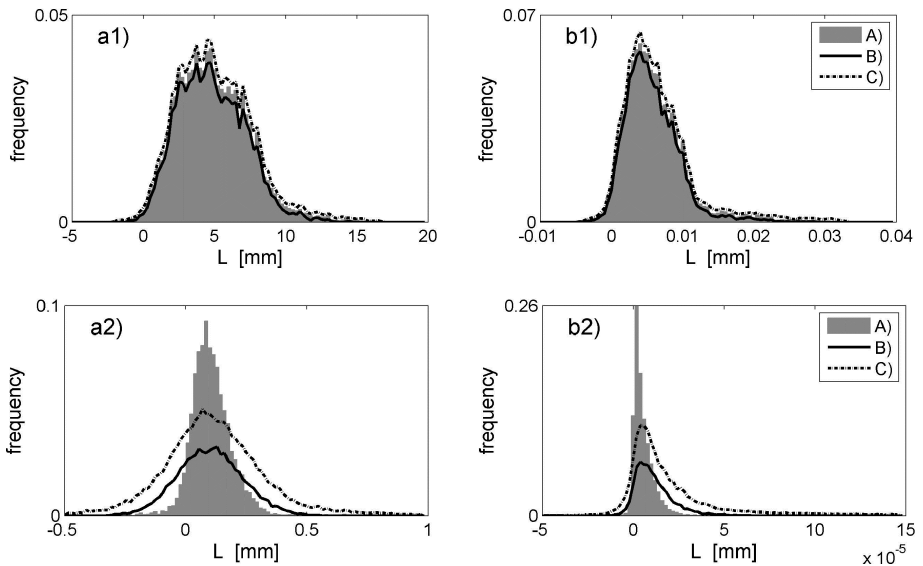


Fig. 2. Histogram of differences L evaluated from data acquired by: (1) System A and LT, (2) System B and LT; (a) based on original, uncorrected locations of fiducials; (b) based on fiducials after the first step of RBC restoration. Grey plots (A) correspond to the average locations of fiducials $\{\bar{X}\}_j$. Solid lines (B) show the lower limit of count at each bin over all N histograms from repeated data; dashed lines (C) are for upper limit of count at each bin.

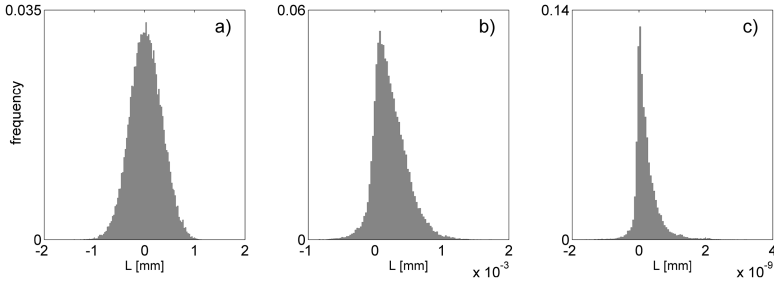


Fig. 3. Histogram of differences L evaluated from data acquired by RA on an optical breadboard plate: (a) based on original, uncorrected locations of fiducials; (b) based on fiducials after the first step of RBC restoration; (c) based on fiducials after the second, final step of RBC restoration.

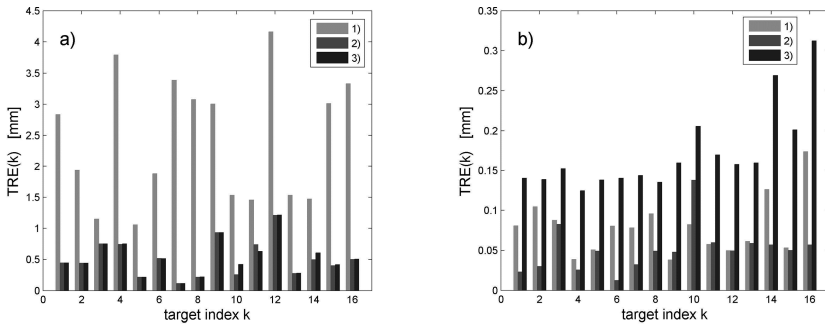


Fig. 4. Target registration error calculated using three methods: (1) $TRE_u(k)$ for uncorrected, average fiducials and targets; (2) $TRE_c(k)$ for corrected, average fiducials and targets; (3) corrected, instantaneous fiducials and targets – displayed is median of $N = 200$ instantaneous errors $TRE_c^{(n)}(k)$: (a) data acquired by System A and LT; (b) data acquired by System B and LT.

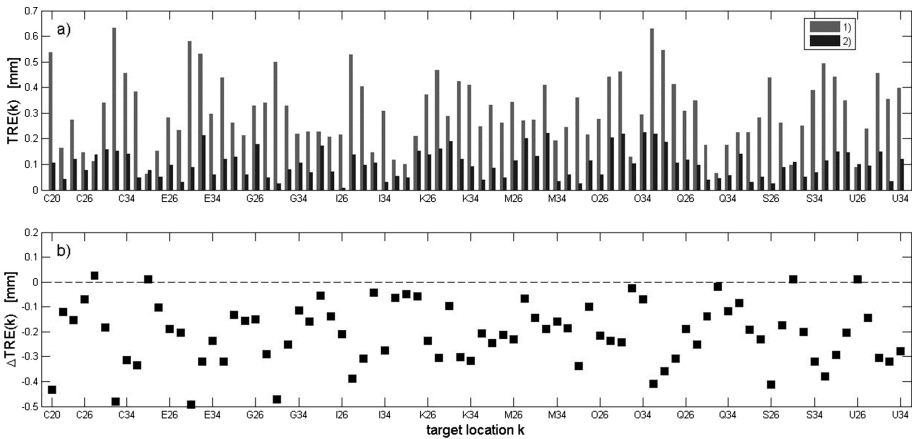


Fig. 5. (a) Target registration error calculated using two methods: (1) $TRE_u(k)$ for uncorrected, single measurement of fiducials and targets; (2) $TRE_c(k)$ for corrected, single measurement of fiducials and targets; (b) the difference ΔTRE between both methods.

6 Discussion and Conclusions

The three registrations listed in Table 1 were performed in very different experimental conditions. System A has the smallest noise σ and (when registered to LT) has the largest bias, as evidenced by σ_{L0} . System B has the largest noise and the smallest bias. The characteristics of the robot arm are between these two conditions: noise and bias of RA is between the corresponding limits of Systems A, B and LT.

Plots displayed in Figs. 2 and 3 clearly demonstrate that the two-step iterative procedure of restoring RBC in a set of fiducials converged very well. This applies to the restoration of RBC in the set of averaged fiducials $\{\bar{\mathbf{X}}\}_J$ (filled grey histograms in Fig. 2) and in instantaneous locations $\{\mathbf{X}\}_J^{(n)}$ (dashed lines in Fig. 2 and filled grey histograms in Fig. 3). The progress of the procedure to restore RBC in the fiducials can be also noted in data included in Table 1 where $\sigma_{L0} \gg \sigma_{L1} \gg \sigma_{L2} \approx 0$.

Full restoration of RBC is limited only to a set of fiducials $\{\mathbf{X}\}_J$ and for other points, like targets $\{\mathbf{T}_X\}$, only partial restoration of RBC is possible. This is because targets are measured only in the working frame and corrections for their locations are estimated by extrapolating corrections of nearby fiducials. Therefore, target errors $TRE_c(\mathbf{T}_X)$ are non-zero although fiducials error FRE equals zero. For cases where repeated measurements in the working frame are available and noise could be filtered out from fiducials and targets, the procedure investigated in this study shows substantial improvement for most targets, as shown in Fig. 4 for cases (1) and (2). For example, for targets $k = 7, 8$ in Fig. 4a, corresponding $TRE_c(k)$ are reduced by almost ten times in comparison with uncorrected $TRE_u(k)$. The overall improvement is larger for System A registered to LT (Fig. 4a) and smaller for System B registered to LT (Fig. 4b). For some targets ($k = 9, 10$ in Fig. 4b), the procedure leads to slightly increased $TRE(k)$.

For instantaneous data containing both noise and bias, the outcome of the procedure may be very different. For System B registered to LT, the median of $TRE_c^{(n)}$ (evaluated after RBC has been restored for each n -th dataset) is much larger than TRE_c calculated for average fiducials $\{\bar{\mathbf{X}}\}_J$ and targets $\{\bar{\mathbf{T}}_X\}$, see cases (3) and (2) in Fig. 4b. In fact, the median of $TRE_c^{(n)}$ is even larger than the uncorrected $TRE_u(k)$, see cases (3) and (1) in Fig. 4b. However, for System A registered to LT, there is practically no difference between the median of $TRE_c^{(n)}$ and corrected TRE_c calculated for average $\{\bar{\mathbf{X}}\}_J$ and $\{\bar{\mathbf{T}}_X\}$, see cases (3) and (2) in Fig. 4a. Similarly, for instantaneous data acquired by RA and registered to world, the procedure of restoring RBC leads to noticeable reduction in TRE_c when compared with uncorrected TRE_u , see cases (2) and (1) in Fig. 5a. In fact, in out of 80 target locations, the procedure failed only marginally in four cases, as indicated by $\Delta TRE > 0$ in Fig. 5b.

If random noise is the main cause of poor registration, reduction in $TRE(k)$ can be obtained by preplanning the placement of fiducials relative to the k -th target. This procedure is based on the fact that uncertainty propagated from fiducials via transformation $\{\mathbf{R}, \boldsymbol{\tau}\}$ to the target is anisotropic, as predicted in [16] and confirmed experimentally in [17]. Thus, optimally placed fiducials will ensure that the uncertainty propagated to a given target is the smallest. However, unlike the suppression of bias which can decrease TRE of any target point, placement of fiducials must be optimized for each target independently.

In summary, the calculation of parameter ρ as shown in Table 1 may help to determine if the procedure of restoring RBC leads to improvement in the registration of instantaneous data (i.e., data containing both noise and bias). For $\rho < 1$, the procedure should not be used as it will lead to worse performance of registration than for original, uncorrected data. For $\rho \gtrsim 2.5$, the use of the procedure is beneficial. The larger the parameter ρ , the better improvement in registration is expected and this, in turn, should improve performance of part assembly when tight tolerances are required.

References

1. Holden, M.: A review of geometric transformations for nonrigid body registration. *IEEE Trans. Med. Imaging* **27**(1), 111–128 (2008)
2. Tam, G.K.L., et al.: Registration of 3D point clouds and meshes: a survey from rigid to nonrigid. *IEEE Trans. Vis. Comput. Graph.* **19**(7), 1199–1217 (2013)
3. Wyawahare, M., Patil, P., Abhyankar, H.K.: Image registration techniques: an overview. *Int. J. Sig. Process. Image Process. Pattern Recogn.* **2**(3), 11–28 (2009)
4. Attia, M., Slama, Y., Kamoun, M.A.: On performance evaluation of registration algorithms for 3D point clouds. In: 13th International Conference on Computer Graphics, Imaging and Visualization, pp. 45–50. IEEE (2016)
5. Park, D.I., et al.: Assembly phase estimation in the square peg assembly process. In: International Conference on Control, Automation and Systems, pp. 2135–2138. IEEE (2012)
6. Park, H., et al.: Intuitive peg-in-hole assembly strategy with a compliant manipulator. In: 44th International Symposium on Robotics, pp. 1–5. IEEE (2013)
7. Liu, Z., et al.: Laser tracker based robotic assembly system for large scale peg-hole parts. In: International Conference on Cyber Technology in Automation, Control and Intelligent Systems, pp. 574–578. IEEE (2014)
8. Chhatpar, S., Branicky, M.S.: Search strategies for peg-in-hole assemblies with position uncertainty. In: IEEE/RSJ International Conference on Intelligent Robots and Systems IROS, pp. 1465–1470. IEEE (2001)
9. Chhatpar, S., Branicky, M.S.: Localization for robotic assemblies with position uncertainty. In: IEEE/RSJ International Conference on Intelligent Robots and Systems IROS, pp. 2534–2540. IEEE (2003)
10. Kim, J.Y., Kim, W.S., Cho, H.S.: Misalignment estimation and compensation for robotic assembly with uncertainty. *Robotica* **23**(03), 355–364 (2005)
11. Usubamatov, R., Adam, S.A., Harun, A.: Analyzing the jamming of parts on the shaft in assembly processes. *Assem. Autom.* **32**(4), 340–346 (2012)
12. Usubamatov, R., Leong, K.W.: Analyses of peg-hole jamming in automatic assembly machines. *Assem. Autom.* **31**(4), 358–362 (2011)
13. Moghari, M.H., Abolmaesumi, P.: Understanding the effect of bias in fiducial localization error on point-based rigid-body registration. *IEEE Trans. Med. Imaging* **29**(10), 1730–1738 (2010)
14. Franaszek, M., Cheok, G.: Method to improve point-based registration by restoring rigid-body condition. National Institute of Standards and Technology Report NISTIR-8180 (2017)
15. Franaszek, M., Cheok, G.S.: Optimization of registration performance metrics. National Institute of Standards and Technology Report NISTIR-8111 (2016)
16. Wiles, A.D., et al.: A statistical model for point-based target registration error with anisotropic fiducial localizer error. *IEEE Trans. Med. Imaging* **27**(3), 378–390 (2008)
17. Franaszek, M., Cheok, G.S.: Orientation uncertainty characteristics of some pose measuring systems. *Math. Prob. Eng.* **2017**, 1–13 (2017)

Author Index

- Alemão, Duarte 49
- Bacharoudis, Konstantinos 103
- Barata, José 49
- Baumann, Valentin 3
- Blankemeyer, Sebastian 72
- Bointon, Patrick 145
- Changizi, Alireza 82
- Chaplin, Jack C. 15, 40
- Cheok, Geraldine S. 226
- Clévy, Cédric 201
- Crivelli, Francesco 3
- Crossley, Richard 92, 158
- D'Urso, Mark 3
- de Silva, Lavindra 134
- Drouot, Adrien 92, 169
- Fassi, Irene 114, 214
- Feng, Xiaobing 145
- Fontana, Gianmauro 114, 214
- Franaszek, Marek 226
- Ghidoni, Antonio 214
- Göke, Joshua 72
- Griffin, Joseph 92
- Grimm, Tobias 72
- Irving, Lucas 169
- Järvenpää, Eeva 29
- Jones, Mark 183
- Kolditz, Torge 63
- Komati, Bilal 201
- Lanz, Minna 29, 82
- Lawes, Simon 145
- Leach, Richard 145
- Legnani, Giovanni 214
- Lezzi, Adriano Maria 214
- Lutz, Philippe 201
- Meier, Benedikt 72
- Morelli, Alessandro 214
- Murray, Gavin 183
- Parreira-Rocha, Mafalda 49
- Piano, Samanta 145
- Popov, Atanas 103
- Raatz, Annika 63, 72
- Ratchev, Svetan 15, 40, 92, 103, 134, 158, 169
- Ruggeri, Serena 114, 214
- Sanderson, David 40
- Schmid, Philipp 3
- Schmidt, Marek 124
- Senin, Nicola 145
- Siltala, Niko 29
- Sims-Waterhouse, Danny 145
- Stavroulakis, Petros 145
- Steinecker, Alexander 3
- Steiner, Markus 3
- Su, Rong 145
- Syam, Wahyudin 145
- Terrazas, German 134
- Thomas, Matthew 145
- Turner, Thomas 103
- Wittsock, Volker 124
- Wolff, Julius 63
- Zarzycki, Leszek 183
- Zhao, Ran 92, 169